Structural modification of CNG channels during activation

Thesis submitted for the degree of

"Doctor Philosophiae"

S.I.S.S.A

Neurobiology Sector

October 2007

CANDIDATE

Anilkumar V. Nair

SUPERVISOR

Prof. Vincent Torre

SISSA - Via Beirut 2-4 - 34014 Trieste - ITALY

to my mother

Declaration

The work described in this thesis was carried out at the International School for Advanced Studies, Trieste, between November 2003 and August 2007. All work reported arise from my own experiments and also in collaboration with *Monica Mazzolini*. The site directed mutagenesis, other than during 2004 and beginning of 2005 was done by Monica. The experiments shown in the article other than Nair et al.2006 was done partly by Monica. Some of the mutant channels were prepared also by Paolo Codega during 2004.

Molecular modeling was done partly by the help of Alejandro Giorgetti and Claudio Anselmi. This thesis is composed of the following published and unpublished work,
the already published articles

Giorgetti,A., **Nair,A.V.**, Codega,P., Torre, V., and Carloni.P (2005). Structural basis of gating of CNG channels. *FEBS Lett* **579**:1968-1972.

Nair,A.V., M.Mazzolini, P.Codega, A.Giorgetti, V.Torre (2006) Locking CNGA1 channels in the open and closed state. *Biophys J* **90**:3599-3607.

the under review articles

Monica Mazzolini, **Anil V. Nair**, Claudio Anselmi and Vincent Torre.
Movements of native C505 during channel gating in CNGA1 channels.

Monica Mazzolini, **Anil V. Nair** and Vincent Torre. A comparison of electrophysiological properties of the CNGA1, CNGA1$_{tandem}$ and CNGA1$_{cys-free}$channels

and the following in preparation

Monica Mazzolini[1], , **Anil V. Nair**[1], Alejandro Giorgetti[*] and Vincent Torre.
Conformational rearrangements in the S6 domain during gating in CNGA1 channels

Contents

Abbreviations

ATP	Adenosine Triphosphate
CaM	Calmodulin
cAMP	cyclic 3′, 5′-Adenosine Monophosphate
CAP	Catabolite Activator Protein
cGMP	cyclic 3′, 5′-Guanosine Monophosphate
CNBD	Cyclic Nucleotide-Binding Domain
CNG	Cyclic Nucleotide-Gated
CuP	Cpper Phenantroline
DAG	Diacylglycerol
DTT	Dithiothreitol
GARP	Glutamic-Acid-Rich Protein
GDP	3′, 5′-guanosine diphosphate
GMP	3′, 5′-guanosine monophosphate
GTP	3′, 5′-guanosine triphosphate
HCN	Hyperpolarization-activated and Cyclic Nucleotide–gated channel
HEPES	(N-2-hydroxyethyl)piperazine-N′-(2-ethanesulphonicacid)
IP$_3$	Inositol 1,4,5-triphosphate
KNF	Koshland-Nemethy-Filmer
LG	Ligand–Gated
M-2-M	1,2-Ethanediyl bismethanethiosulfonate;
MTS	Methane Thiosulfonate
MTSEA	2-aminoethylmethane thiosulfonate
MTSES	2-sulfonatoethyl methane thiosulfonate
MTSET	2-(Trimethylammonium)ethyl methanethiosulfonate
MTSPT	3-(Trimethylammonium)propyl methanethiosulfonate
MTS-PtrEA	3-(Triethylammonium)propyl methanthiosulfonate
MWC	Monod- Wyman- Changeux
NO	Nitric Oxide
OSN	Olfactory Sensory Neurons
PDE	Phosphodiesterase
PIP2	Phosphatidylinositol-4′,5′-biphosphate
PKA	Protein kinase A
PLC	Phospholipase C
PsTX	Pseudechetoxin
ROS	Rod Outer Segment
SCAM	Substituted-Cysteine Accessibility Method
TEA	Tetra Ethyl Amonium
TRP	Transient Receptor Potential
TTX	Tetrodotoxin
VG	Voltage–Gated
VNO	Vomero Nasal Organ

Abstract

Cyclic nucleotide-gated ion channels are distributed most widely in the neuronal and non-neuronal cell. Great progress has been made in molecular mechanisms of CNG channel gating in recent years since their discovery in 1985(Fesenko et al., 1985). Results of many experiments have indicated that the stoichiometry and assembly of CNG channel subunit affect their property and gating. The substituted cysteine accessibility method (SCAM) has been a very powerful tool in understanding many of the molecular mechanisms underlying their functions. Cite directed mutagenesis has been a great help in elucidating the possible mechanism behind the ligand discrimination among channels expressed in different cell types. In the recent years the advance in computer technology has provided tremendous help in understanding the three dimensional arrangement of proteins by virtue of molecular biology. Most probably this is the perfect time in which molecular biology, biochemistry and computational science has come together to provide some amazing view of membrane proteins. Still crystallography has its own limitations, and electrophysiology serves as an adequate substitute. Most of our understanding about the CNG channels arises from the study of these channels expressed in sensory neurons, viz photoreceptors and olfactory sensory neurons. In my work I have used heterologously expressed homologous CNGA1 subunit from bovine rod receptors as a target. The expression system used was *Xenopus leavis* oocytes. Though the homologous channels thus expressed vary in several aspects provides a very good tool in studying the structure function relationship of these channels. In the preliminary part of the study an extensive site directed mutagenesis from residue F375 to V424, one at a time, has been performed (SCAM). I have then probed these mutant channels with divalent cations such as Cd^{2+} and Ni^{2+} and several methane thiosulfonate compounds to study their accessibility and interaction. The residues from F375 until S399 does not show much effect to these externally applied compounds with few exceptions. One remarkable exception is F380C, which is found to be potentiated by Cd^{2+} when applied in the open state of the channel inhibited when applied in the closed. Further studies have revealed a locking effect of the channel and thus some insight into the proximity of residues and possible molecular rearrangement while channel passing from closed to open. Another study has revealed the interaction of native Cys505 residues with several other residues in the C-linker domain when are mutated into cysteine. This study has helped to propose a molecular model of C-linker domain. Also it provided some knowledge in the possible rearrangement of C-linker region while channel opens. One another course of study has revealed that the residues from 390 to 400 come closer in the closed state than in the open. The following stretch of residues, from 410 to 420, on the contrary comes closer in the open state than in the closed. My studies suggest that the channel while passing from close to open does not undergo a major translational movement of residues near the S6. Probably the coupled movement of of S6 with pore helix provides enough energy to open the gate.
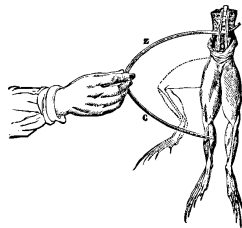
Chapter 1

Introduction

1.1 Early biophysics

Figure 1.1: *Luigi Galvani and his Frog muscle twitch experiment*

A precious moment in the history of science has brought us the understanding of electricity and with it a revolution in human life. From the frog leg twitch experiments of **Galvani** in 1791 we have progressed to telegraphs, telephones, internet and super computers. In the same period the ubiquitous role of electricity in life has become clear. As early as 1817, the great Swedish chemist **Berzelius** suggested that electric eel's current was *"elicited by an organic chemical process"*. Italian physicist **Leopoldo Nobili** was the first to measure the current in a frog muscle using an *astatic galvanometer*. Following up on Nobili's work **Carlo Matteucci** (1838) measured current, which leaking out of injured muscle, formed the basis of the important concept of resting potential. He went on to discover that muscle cells, after stimulation by a nerve, produce a current by their own. Matteucci also discovered that altering the pH of the solution surrounding the muscle fiber brings a contraction to it. It was becoming more and more clear that the phenomenon underlying muscle and nerve cell excitation was chemical in nature.

By the late 1800s the chemical mechanism underlying nerve and muscle tissue messaging was still a mystery. **Ludimar Hermann**, in 1872, was remarkably able to suggest that muscle and nerve cells were capable of exhibiting a *"self-propagating wave of negative charge which advances in steps along the tissue"*. In 1905 he described the passive spread of potentials in axons and muscles by a theory for a *leaky* telegraph cable *(Herman Cable theory)*. In the 1880s **Sidney Ringer** has discovered that sodium, potassium and calcium salts are necessary for the isolated frog heart to continue beating. Into this void of current understanding, **Julius Bernstein**, a famous physicist made the first real theoretical contribution. He postulated the ionic theory, the Nernst equation and the assumption of a semi-permeable membrane surrounding nerve and muscle cells that could help explain the mounting physiological data of the past century. According to him the difference in K^+ concentration in the inside and outside of the

cell could explain the origin of membrane potential. British physiologist **John N. Langley**, in 1907, put forward the concept of receptor molecules on the surface of the muscle and nerve cells in order to explain effect of chemicals and tetanus toxin on them. In 1923, **Kenneth.S. Cole** with **H.J. Curtis** began

to study the membrane properties by measuring the electrical impedance of cell suspension and of single cell. These careful studies concluded that each cell has a high-conductance cytoplasm, with an electrical conductivity $30 - 60\%$ that of the bathing saline, surrounded be a membrane of low conductance and an electrical capacitance of $1 \ \mu\text{F/cm}^2$.

The period from 1935 to 1952 was heroic in the history of membrane biophysics. **John Z. Young**, in 1936, was the first one to use squid giant axons for studying the ionic current. For the first time, **Hodgkin**

Figure 1.2: *A.L. Hodgkin and Huxley H.F : Nobel Prize in Physiology or Medicine 1963.*

and **Huxley** (1939, 1945) and **Curtis** and **Cole** (1940, 1942) were able to measure the full action potential of an axon with an intracellular micro pipette. In 1949 Cole found that by placing two glass electrodes inside the cell one can hold the potential of the interior of the cell. Later by Cole (1949), Marmont (1949) and Hodgkin, Huxley and Katz (1949, 1952) developed a new experimental procedure known as "*voltage clamp*" which has been the best biophysical technique for the study of ion channels for over 50 years. A great milestone during this period was the definitive description of electrical signaling in axon membrane in 1952 by Hodgkin and Huxley (1952d,a,c,b). After their great work there were three main questions remaining. (a) How do ions get through membrane? (b) How does the membrane distinguish between Na^+ and K^+? (c) How does the membrane change its electrical resistance and ion selectivity in a fraction of second? Until the beginning of 1970s channels were a less popular idea because selectivity seemed harder to explain for a channel. Some guesses were even wild. One of those was that the conduction path in a membrane was formed of lipid with protein as the insulator. By early 1970s **Bertil Hille** and **Clay Armstrong** each concluded separately with experiments using tetrodotoxin (TTX^+) and TEA^+ respectively that the Na^+ and K^+ passage should be through separate aqueous pores. They ruled out the chance of transport based on a carrier because of its slow nature.
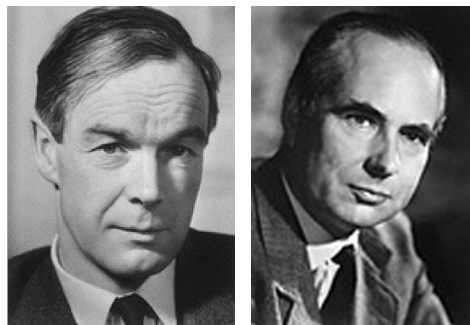

Figure 1.3: *Erwin Neher and Bert Sakmann:The Nobel Prize in Physiology or Medicine 1991, for the invention of patch clamp method.*

In 1971 Hille and in 1972 **Bezanilla** and Armstrong proposed models of discrimination between ions by channels. They attributed this discrimination on the unfavorable energetics of stripping water from the ions and providing favorable interaction by the channel pore walls in return. By 1980, it seemed probable that the channels are made of proteins, which lead Armstrong (1981) to propose that the activation charge mentioned by Hodgkin and Huxley were in fact charged membrane helices – specifically, a negatively charged helix moves inward with respect to a positively charged helix, yielding a lot of charge movement, and hence voltage sensitivity relative to small physical motion. When the Na^+ channel was cloned few years later the positively

charged helix – the now called *S4 segment* – was immediately visible and the expected negatively charged helix doesn't exist.

One of the 20th century revolutions in biophysics was the development of patch clamp method by **Erwin Neher** and **Bert Sakmaan** in 1970s. An improvement in the patch clamp method called "*gigaseal formation*" occurred serendipitously in 1980. The final proof that channels are made of proteins was made possible by Hamill et al. (1981) through single channel patch clamp experiments. 1984 saw the first clone of an ion channel. **Noda**(Noda et al., 1984) and co–workers succeeded in isolating, cloning and sequencing first voltage–gated Na^+ channel from electric eel. In 1998, the first crystal structure of an ion channel the KcsA from bacteria was reported by the **Mackinnon**'s lab (Doyle et al., 1998). While this achievement provided a great deal of information about what a channel "*looks*" like, the next step will be to produce a series of structures of an ion channel in all various modes of operation to determine what it "*acts*" like, basically a motion picture of a protein in action.

Figure 1.4: *Roderick Mackinnnon: The Nobel Prize in Chemistry 2003, for solving the K^+ channel crystal structure.*

1.2 Ion channels

Ion channels are membrane protein complexes and their function is to facilitate the diffusion of ions across biological membranes or phospholipid bilayers. The bilayers that are electrical insulators, build a hydrophobic, low dielectric barrier to hydrophilic and charged molecules. Ion channels provide a high conducting, energetically less expensive hydrophilic pathway across the interior of the membrane. Ion channels are broadly classified into voltage-gated (VG) channels and ligand-gated (LG) channels (Hille, 2001). Some of the major ubiquitous ion channels are K^+, Na^+, Ca^{2+}, TRP, Cl^- etc. For an overview refer (Armstrong and Hille, 1998; Armstrong, 2007; Hille, 2001)

1.2.1 K^+ channels

Potassium channels, originally identified as the molecular entities mediating flows of potassium ions across nerve membrane in action potential generation, are now known in virtually all types of cells in all organisms, where they are involved in a multitude of physiological functions. All fully sequenced genomes – eukaryotic, eubacterial and archaeal – contain at least one type K^+ channel making them the most ubiquitous. K^+ channels are the founding member of the 'S4–superfamily' of ion channels dedicated to electrical signaling, which, apart from the K^+ channels, are found exclusively in eukaryotes (Miller, 2000). The cyclic nucleotide–gated channels evolved from K^+ channels via acquisition of a cyclic nucleotide–binding domain near the carboxyl terminus; the Ca^{2+} and Na^+ channels, each of which is a monomer containing four repeats, evolved from K^+ channels via two gene duplications, with the Ca^{2+} channel appearing in unicellular organisms and Na^+ channels arising with the appearance of neurons in multicellular organisms (Miller, 2000).

There are two broad classes of K^+ channels defined by the transmembrane topology, as reflected from the primary sequence: the six–transmembrane(S1, S2, S3, S4, S5 & S6)–helix, voltage–gated (K_v) and the two–transmembrane–helix(M1 & M2) inward rectifier (K_{ir}) subtypes. All K^+ channels

display a *'signature sequence'* between the most carboxy–terminal transmembrane helices which reads–TMxTVGYG(Heginbotham et al., 1994). All K_v–type channels have an S4 helix sequence with a lysine or arginine repeating every third or fourth position in an otherwise hydrophobic stretch. This makes them voltage sensitive and helps in the channel activation. Some variations are known such as Ca^{2+} activated K^+ channels, 2P channels, Cyclic Nucleotide–Gated(CNG) channels etc, they posses the sequence similarity but no voltage sensitivity. K^+ channels are formed as tetramers of similar or identical subunits arranged in four fold symmetry around a water filled K^+ conduction pathway (except 2P channels, which are presumably dimer of dimers).

In 1998 Roderick Mackinnon's group solved the crystal structure of a non–voltage gated (Ca^{2+} gated), two–transmembrane spanning K^+ channel from the bacteria *Streptomyces lividans* (KcsA K^+ channel) at 3.2 Å resolution (in this crystal structure the amino acids from 126 to 158 at the carboxy terminal end have been cleaved off)(Doyle et al., 1998). They subsequently determined the crystal structure of Ca^{2+} gated MthK, a complete K^+ channel from *Methanobacterium thermoautotropicus* (Jiang et al., 2002a,b). They went on to solve the more difficult voltage–dependent K^+ channel K_vAP from the thermophilic Archea *Aeropyrum pernix* (Jiang et al., 2003). The crystal structures of these proteins tremendously improved our knowledge about protein structure: four subunits surround a central water filled ion pathway in the shape of an inverted "**tepee**" across the membrane, near the center of the membrane the pathway is very wide, the GYG sequence forms the selectivity filter close to the extracellular side of the membrane and so on. The selectivity, voltage sensitivity and desensitization of channels will be described in a separate following section.

1.2.2 Na^+ channels

Voltage–gated sodium channels play an essential role in the initiation and propagation of action potentials in neurons and other electrically excitable cells such as myocytes and endocrine cells (Hille, 2001). When the cell membrane is depolarized by a few millivolts, sodium channels activate and inactivate within milliseconds. Influx of sodium ions through the integral membrane proteins comprising the channel depolarizes the membrane further and initiates the rising phase of the action potential. The voltage-gated sodium channel is a large, multimeric complex, composed of an α subunit (260 kDa complex) and one or more ($\beta1$, $\beta2$ and/or $\beta3$) smaller β subunits (33 - 36 kDa) (Catterall, 2000a; Catterall et al., 2005a). The ion–conducting aqueous pore is contained entirely within the α subunit, and the essential elements of sodium–channel function – channel opening, ion selectivity and rapid inactivation – can be demonstrated when α subunits are expressed alone in heterologous cells. Coexpression of the α subunit is required for full reconstitution of the properties of native sodium channels, as these auxiliary subunits modify the kinetics and voltage–dependence of the gating (that is, opening and closing) of the channel. Nine α subunits ($Na_v1.1$-$Na_v1.9$) have been functionally characterized and a tenth related isoform (Na_x) may also function as a Na^+ channel. The primary sequence predicts that the sodium channel α subunit folds into four domains (I-IV), which are similar to one another and contain six α – helical transmembrane segments (S1-S6). Each domain contains a voltage sensitive helix S4 just like in K^+ channels. A re–entrant loop between helices S5 and S6 is embedded into the transmembrane region of the channel to form the narrow, ion-selective filter at the extracellular end of the pore.

Sodium channels were the first members of the ion channel superfamily to be discovered. But in evolution, the sodium channel family is the most recent of the voltage–gated ion channels to have arisen. They might have been evolved from similarly structured Ca^{2+} channels that contain four homologous

domains. Because of their fundamental importance, much of the early work on ion channels involved characterizing the electrophysiological and biochemical properties of sodium channels. In recent years, however, the rapidly expanding number and diversity of potassium and calcium channels has overshadowed the field of sodium channel research, particularly given the fact that all voltage–gated sodium channels are relatively similar. Recent identification that minor changes in the properties of specific isoforms are responsible for several heart (long Q-T syndrome, Brugada syndrome), muscle (epilepsy, myotonia) and nervous system (hyperexcitability) diseases, bringing them back to the main research.

1.2.3 Ca^{2+} channels

There are several different signals that controls cellular Ca^{2+}, such as voltage changes, neurotransmitters, hormones, sensory inputs etc(Catterall, 2000b). Here in this session I introduce the voltage–gated Ca^{2+} channels. They mediate calcium influx in response to membrane depolarization and regulate intracellular processes such as contraction, secretion, neurotransmission, and gene expression. Their activity is essential to couple electrical signals in the cell surface to physiological events in cells. The calcium channels that have been characterised biochemically, are complex proteins composed of four or five distinct subunits, which are encoded by multiple genes. The α_1 subunit of 190-250 kDa is the largest subunit and it incorporates the conduction pore, the voltage sensor and gating apparatus, and the known sites of channel regulation by second messengers, drugs, and toxins. The composition and organisation of α subunits is like that of Na^+ channels (infact Na^+ channel is supposed to be evolved from Ca^{2+} channel). An intracellular β subunit and a transmembrane, disulfide–linked $\alpha_2\delta$ subunit complex are components of most types of calcium channels. A γ subunit has also been found in skeletal muscle calcium channels and related subunits are expressed in heart and brain. Although these auxiliary subunits modulate the properties of the channel complex, the pharmacological and electrophysiological diversity of calcium channels arises primarily from the existence of multiple α_1 subunits.

According to different physiological and pharmacological properties there are several distinct classes of Ca^{2+} currents. L-type calcium currents require a strong depolarization for activation, are long-lasting, and are blocked by the organic L-type calcium channel antagonists. They are the main calcium currents recorded in muscle and endocrine cells, where they initiate contraction and secretion. N–type, P/Q–type, and R–type calcium currents also require strong depolarization for activation. They are relatively unaffected by L–type calcium channel antagonist drugs but are blocked by specific polypeptide toxins from snail and spider venoms. They are expressed primarily in neurons, where they initiate neurotransmission at most fast synapses and also mediate calcium entry into cell bodies and dendrites. T–type calcium currents are activated by weak depolarization and are transient. They are resistant to both organic antagonists and to the snake and spider toxins. They are expressed in a wide variety of cell types, where they are involved in shaping the action potential and controlling patterns of repetitive firing. Different type of channel subfamily α subunits modulates afore said Ca^{2+} currents. The Ca_v1 subfamily ($Ca_v1.1$ to $Ca_v1.4$) includes channels containing α_{1S}, α_{1C}, α_{1D} and α_{1F}, which mediate L–type Ca^{2+} currents. The Ca_v2 subfamily ($Ca_v2.1$ to $Ca_v2.3$) includes channels containing α_{1A}, α_{1B}, and α_{1E}, which mediate P/Q-type, N-type, and R-type Ca^{2+} currents, respectively. The Ca_v3 subfamily ($Ca_v3.1$ to $Ca_v3.3$) includes channels containing α_{1G}, α_{1H}, and α_{1I}, which mediate T-type Ca^{2+} currents (channel names are according to the nomenclature adapted in 2005(Catterall et al., 2005b)).

1.2.4   TRP channels

In the ion channel research field the mammalian TRP channels are the latest arrivals (first time reported in 1995(Wes et al., 1995)). Since then six protein families have been identified with many members in each family. All TRP channels have putative six–transmembrane polypeptide subunits that assemble as tetramers to form a cation permeable channel pore like the voltage–gated channel super family(Ramsey et al., 2006). Though they have similar folding architecture like the voltage–gated channel family, there is no sequence similarity. They are either modulated by store–operated calcium (Clapham et al., 2005)(a theoretical description related to a poorly understood phenomenon) or by receptors or in some cases by hormones (TRPM5 is modulated by Klotho(Chang et al., 2005)). TRP channels are the vanguard of our sensory systems responding to temperature, touch, pain, osmolarity, taste hearing and other stimuli. But their role is much broader than classical sensory transduction. This make them ubiquitously expressed with many splice variants. So most cells have number of TRP proteins. The subfamilies are TRPC (canonical TRP, with TRPC1 being the first ever reported), TRPV (vanilloid receptor), TRPM (melastatin), TRPP (polycystin) and TRPML (mucolipin). The TRPMs are responsible for the renal Ca^{2+} absorption and the recently identified TRPM6 is supposed to be playing a role in cellular Mg^{2+} maintenance.

The gnawing mystery of TRP channels are their elusive mechanism of gating. Only few studies have been conducted at their physiological environment or at physiological temperature. Attempts to understand TRP channel activation have given rise to several theories such as receptor–operated theory, store-operated Ca^{2+} entry hypothesis, vesicle fusion hypothesis and cell sensory hypothesis. The future work should indeed need to display whether really they are activated by the above said mechanisms or there is any other common mechanism of activation like the recently identified hormone activation (Klotho) of TRPM5 proteins.

1.2.5 Cl^- channels

For more than 50 years the study of these ion channels has been dominated by their neuronal function: initiating action potentials at synapses, propagating signal along axons and dendrites etc. Electrical signalling in neurons almost exclusively use cations (Na^+, K^+, Ca^{2+}, H^+) as current carriers. On the other hand Cl^- channels were supposed to be maintaining the house keeping acts such as epithelial secretion of mucus, saliva, digestive and reproductive effluvia etc. In the past decade, however, Cl^- channels started enjoying the attention mainly because of the realisation that they are a large molecular family expressed almost in all cell type (showing their functional importance) and their electrophysiological characters are much different from the cation–conducting channels(Nilius and Droogmans, 2003).

The first ClC channel was identified from the electric organ of *Torpedo californica* (White and Miller, 1979) and subsequently cloned in 1990(Jentsch et al., 1990). In 2002 the first CLC-ec1 (bacterial chloride channel) channel crystal structure was reported (Dutzler et al., 2002). Until now nine mammalian Cl^- channels have been identified (CLC-1 to 7, CLC-K$_a$ and CLC-K$_b$). A unique feature of CLC channel is their dimeric architecture in which each subunit forms a proper pore. The single channel activity of this channel shows a common gate to both subunits and an individual gate to each of them. Another interesting feature is that the single subunit can function by itself leaving behind the question, why they are together? In striking contrast to structures of familiar ion channels, CLC-ec1 lacks transmembrane pore. Later in 2004 it was understood that this feature is because CLC-ec1 is not

a channel but a transporter (Accardi and Miller, 2004). Later in 2005 (Picollo and Pusch, 2005) the mammalian analogues of this channel (CLC-4 and CLC-5) were also proved to be Cl^-/H^+ exchanger. At the moment it is supposed to be the CLC-1 & 2 and CLC-K_a & K_b express on the cell plasma membrane and help in the stabilization of the membrane potential and trans epithelial transport. The other members of the family, CLC-3 to 7, express on the membrane of intracellular organelles where they help in the acidification of intra–organellar compartment.

Some of the basic characteristics of all membrane proteins such as selectivity, activation and inactivation are briefly introduced in the following session.

1.2.6   Selectivity

How does a channel distinguish divalent and monovalent cation? How do they distinguish between a Na^+ and K^+ ion? This question was quite satisfactorily, theoretically tackled in the beginning of 1970s by Hille (1971a,b) and Bezanilla and Armstrong (1972). Hille's working hypothesis for the selectivity of Na^+ over K^+ for sodium channel was that, the ions passing through the pore are partially hydrated and are stabilized by the compensatory direct interaction with the negative charge in the selectivity filter. In this view the small cations such as Na^+ and Li^+ are well stabilized in the negatively charged pore but the bigger cations such as K^+ and Rb^+ are not stabilized.

Figure 1.5: *A theory for K^+ selectivity. K^+ and Na^+ are shown in water and in a carbonyl-lined filter environment. Na^+ has very high energy in filter compared to K^+. Modified from (Armstrong, 2007)*

The discrimination between divalent and monovalent cations can be more easily understood. The Na^+ and Ca^{2+} channel have two rings of charge encircling the pore, each containing four residues. The outer ring is entirely negative and the inner ring is composed of the amino acids Asp Glu Lys Ala in the Na^+ channel and Glu Glu Glu Glu in Ca^{2+} channel. From this channel conducting Ca^{2+} has more negative charge to bind the calcium more tightly compared to Na^+ channel. Once the Ca^{2+} is bound to the negatively charged pore it interferes with the Na^+ passage and stops its permeability. By keeping this fact in mind Heinemann et al. (1992) successfully converted a Na^+ channel into a Ca^{2+} preferring channel by site directed mutagenesis.

The high resolution crystal structure of KcsA (2 Å (Jiang et al., 2002a) from Mackinnon's lab has given an experimental demonstration of the ion discrimination by K^+ channels and the necessity for a signature sequence for highly selective channels. The TVGYG (signature sequence of K^+ channels (Heginbotham et al., 1992)) amino acids have all their carbonyl oxygen atom pointing in one direction towards ions along the pore. The alternating glycine amino acids permits the required dihedral angles, the threonine hydroxy oxygen atom coordinates to a K^+ ion and the side-chains of valine and tyrosine directed into the pore core surrounding the filter to impose geometric constraint. The result when all subunits come together is a narrow tube consisting four equally spaced K^+ binding sites. The oxygen atoms in the filter mimic the water molecules of the hydrated K^+ ion compensating the dehydration energy. It has been shown that two ions can occupy the pore at the same time and the electrostatic
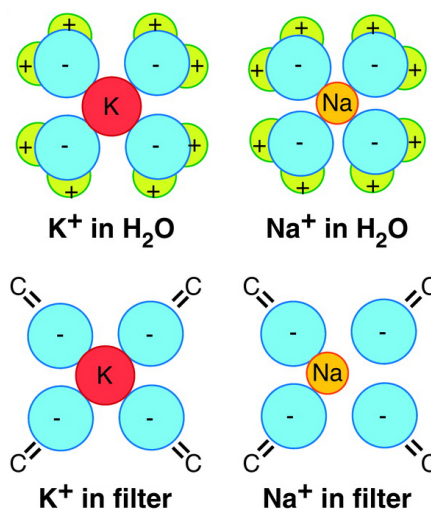
repulsion between the occupied ion helps in the high throughput (10^7 - 10^8 ions/s) of the highly selective channel.

1.2.7 Activation gating

There are several ways of activation gating in ion channels: voltage, ligand, pressure, temperature etc. Among them activation process of the Voltage gated channels are vigorously studied and may be the most understood. Voltage gated channels are exquisitely sensitive to small changes in membrane potential. Decades ago Hodgkin and Huxley realised that Na^+ and K^+ channel opening or activation must result from movement of charges within the membrane. They predicted the "gating current", which is now recognised as a positively charged helix, the S4. The idea that the gating current is a helix came from the work of Armstrong (1981): he predicted the counter movement of charged helices (positive and negative) yielding a lot of charge movement and hence voltage sensitivity. The cloning of Na^+ channel (Noda et al., 1984, 1986) revealed the existence of the positively charged helix (the now called S4) but the expected negatively charged helix was not visible. The S4 is coupled to the gate and its movement bring the conformational change to open the gate (or close?) leading the permeation of ions across channel through the pore. The actual movement of S4 and its coupling with the gate is under controversy (Bezanilla, 2005; Ahern and Horn, 2004; Cuello et al., 2004; Jiang et al., 2003; Chanda et al., 2005; Mackinnon, 2004). There are several predicted models for the S4 movement with respect to the membrane voltage. The simplest are the 1) zipper model, 2) its helical screw variant and 3) the paddle model. All three models have problems. The negative counter charges suggested by the first and second models have never been identified in sufficient number. The energetic cost to put the charged arginines in the lipid membrane stirs up a controversy strengthened by the proof that S4 undergoes limited translational movement ($\sim$ 2 Å) verses the large (>15 Å) translational movement suggested by the paddle model.

The coupling of S4 to the gate is still not understood completely. Do the S4 pull the gate open when they are activated? Or do they lock the gate shut when they are deactivated? Or both? Though the second idea gains some support from the crystal structure of $K_v1.2$, it is premature to establish unanimously the action of S4 on gate–opening. Another peculiarity of the gate–opening is that, it is all or none, i.e., all S4s must be activated for the gate to open. This is clear from the single–channel records in which the opening is a single jump

Figure 1.6: *First panel: Cartoon model of an ion channel in 1977. Second, 15 years later: notice the S4 helix and increased intra–and extra– cellualr masses compared to the previous. (adapted from Hille(2001))*

that cannot be resolved into smaller jump. Why all four S4s must be activated to open the gate? A possible answer is that the gate region's hydrophobic lining must be pulled in all four directions to effectively break the hydrophobic bonds that almost certainly help to hold it closed. One factor almost
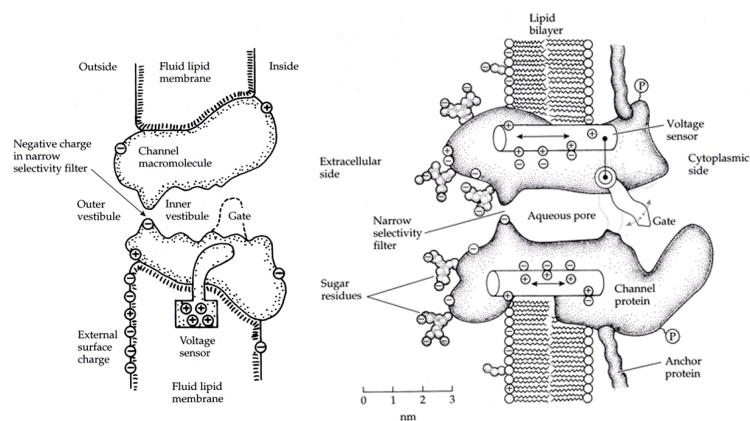
surely is that the gate region is either large enough to admit a dehydrated K^+ ion, or it is not. In the case of CNG channels there are proofs that the channel can have partially conducting states.

1.2.8   Inactivation gating

Sodium channels open in response to depolarization admitting Na^+ and driving the membrane potential more positive during the upstroke of an action potential. They then inactivate spontaneously (stop conducting), making it easy for the K^+ channels to restore its membrane potential to rest. This inactivation gating in Na^+ channel and some of the K^+ channel are mechanistically simpler than the activation gate. Experiments during 1970s show that a cytoplasmically located portion of the channel peptide diffuses into the mouth of the inner vestibule of the pore and blocks conduction. Cutting off this part of the protein with pronase removes the inactivation of the channel. These observations led to the proposal of ball and chain model (Bezanilla and Armstrong, 1977), in which an inactivation ball attached to the inner surface of the protein by a peptide chain diffuses into the pore and blocks the permeation. The movement of this peptide is relatively slow allowing the average Na^+ channel to complete the rising phase of the action potential. The apparent voltage sensitivity of the inactivation gating is derived from the voltage dependence of activation that precedes it rather than utilising a highly charged dedicated voltage sensor. Unlike that of the activation gate the inactivation gate is not all or none. The experiments by Aldrich and colleagues (Hoshi et al., 1990, 1991; Zagotta et al., 1990) suggest that one "ball peptide" from any of the subunit is enough for inactivation and four of them increase the probability of finding the pore and thus speed up the inactivation. Who get first in the pore is a matter of chance (Armstrong and Hille, 1998).

1.3   Cyclic Nucleotide Gated channels

Cyclic nucleotide gated channels underlie sensory transduction in vertebrate photoreceptors and in olfactory sensory neurons. To open, they require cyclic nucleotides such as cAMP or cGMP (Fesenko et al., 1985; Zimmerman et al., 1985; Nakamura and Gold, 1987; Kaupp et al., 1989; Zagotta and Siegelbaum, 1996; Biel et al., 1999; Kaupp and Seifert, 2002; Craven and Zagotta, 2006). They are relatively recent arrivals in the world of ion channels. The search for the intracellular messenger that mediates photoresponse in retinal photoreceptors paved the way for their discovery. Since the late 1960s Ca^{2+} and cGMP (cyclic $3'$, $5'$ – Guanosine Mono Phosphate) were considered to be the most probable candidates to control the light–sensitive conductance in the outer segment of rod photoreceptors. It was believed that cyclic nucleotides control the activity of proteins through phosphorylation mediated by cyclic nucleotide dependent kinases. It was a surprise when Fesenko et al. (1985) reported that cGMP can directly activate light–dependent channel of rods. Since then, in a relatively short period, similar channels were identified in cone photoreceptors, olfactory sensory neurons, pineal gland etc.

1.3.1   Family of CNG channels

CNG channels belong to a heterogeneous gene superfamily of ion channels that share a common trans–membrane topology, pore structure and a Cyclic Nucleotide Binding Domain (CNBD). Other members of this family are the Hyperpolarization–activated and Cyclic Nucleotide–gated (HCN) channels (Kaupp and Seifert, 2002; Craven and Zagotta, 2006), the *ether–à–go–go*(EAG) and human eag–

related gene (HERG) family of voltage activated K^+ channels(Ganetsky et al., 1999) and several plant K^+ channels (KAT, KST and AKT)(Schachtman, 2000).

1.3.2 Physiological roles of CNG channels

CNG channels have been identified and described in a variety of cell types there they play a fundamental role in variety of physiological processes. They were first discovered in the plasma membrane of the outer segment of vertebrate photoreceptors, there it take part in a critical role of phototransduction (Fesenko et al., 1985). Most of what we know about how CNG channels work has come from the extensive studies of rod and olfactory channels. CNG channels mediate the final step of enzymatic cascade in sensory cells of the olfactory and visual systems (Kaupp and Seifert, 2002).
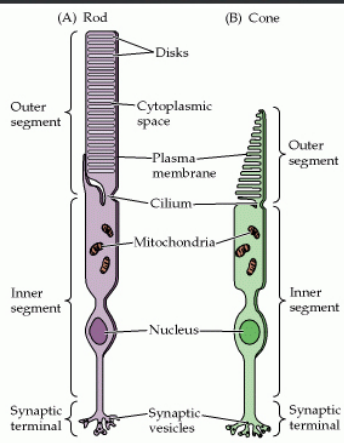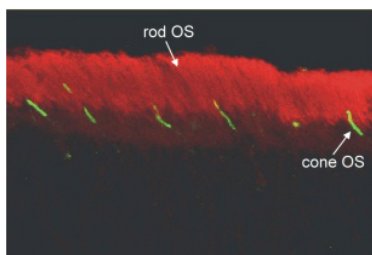
CNG channels in photoreceptors

The vertebrate photoreceptors are ciliary type, whereas the invertebrate photoreceptors fall into two different subtypes: rhabdomeric photoreceptors with a microvilli–derived photosensitive structure and ciliary photoreceptors (Kaupp and Seifert, 2002). The ciliary type photoreceptors use cGMP–signalling pathways. The targets of these signalling pathways are CNG channels that either open or close in response to light. The signalling mechanism in the rhabdomeric receptors is not yet clear.

Phototransduction in vertebrate rod photoreceptors

Phototransduction is the process by which photons of light generate an electrical response in retinal rod and cone photoreceptors, thereby initiating vision (Arshavsky et al., 2002; Fain et al., 2001).

Figure 1.7: *Comparison between vertebrate rod and cone photoreceptors.*

Photoisomerization: Visual detection begins with the absorption of a photon by the photopigment rhodopsin. In the darkness rhodopsin is bound to a small molecular weight chromophore, 11–cis–retinal, that regulates its activity. This preattached ligand of visual pigment is photoisomerized to all–cis–retinal by the captured photon. Within a millisecond rhodopsin undergoes a series of intra–molecular transitions leading to a conformational state called metarhodopsin II (R^* of activating the photoreceptor-specific G protein, transducin).

Transducin Activation: R^* interact with the GDP–bound form of the transducin $\alpha\beta\gamma$ trimer; i.e., with $G\alpha_t$ – GDP – $G\beta\gamma_t$. R^* activates the transducin by triggering rapid exchange of bound GDP for GTP on the $G\alpha_t$; this is followed very rapidly by dissociation of the transducin from the R^*, as well by dissociation of the active $G\alpha_t$ – GTP (or G^*) from $G\beta\gamma_t$.

Phosphodiesterase Activation: At the next step of the cascade $G\alpha_t$ – GTP stimulates the activity of its effector enzyme, the cGMP phosphodiesterase (PDE). The PDE is a heterotetramer consisting of two identical or nearly identical catalytic subunits ($\alpha\beta$ in rods, $\alpha\alpha$ in cones) and two identical regulatory γ subunits (PDEγ), which serve as protein inhibitors of PDE activity and responsible for maintaining the activity in the non activated state at it's very low basal level. Activation of the PDE results from the binding of $G\alpha_t$ to the γ subunit, thereby removing the inhibitory constraint that the PDEγ had imposed on the catalytic site of the PDE α or β subunit.

cGMP reduction and CNG channel closure: In the dark the binding of cGMP to CNG channels keep them open, allowing Na^+ and Ca^{2+} to flow into the cell. This flow of inward current, the dark current, depolarizes the outer segments. The activation of PDE causes the reduction in cytoplasmic concentration of the cGMP by hydrolyzing them to $5'$– GMP. The CNG channels in the plasma membrane close in direct response to this decrease in cGMP, inhibiting the dark current, and hence hyperpolarizing the outer segments. This hyperpolarization is transmitted to the inner segments and ultimately causes a decrease in the ionic release of the neurotransmitter glutamate from the presynaptic terminal. The CNG channel is crucially important for the control of the Ca^{2+} concentration in the outer segment of the rod cells because it is the only source for Ca^{2+} influx.

Termination of Phototransduction: In rods between 10 and 18 % of the dark current is carried by the Ca^{2+}. The entry of Ca^{2+} through open CNG channels is balanced by its extrusion though a Na^+/Ca^{2+}–K^+ exchange mechanism. In light, when CNG channels close, the exchanger continues to clear Ca^{2+} from the cystol, and the Ca^{2+} balance is disturbed. This decrease in Ca^{2+} controls at least three mechanisms. First, it activates guanylyl cyclase (GC) that synthesizes cGMP. The Ca^{2+} sensitivity of the GC is relayed by two Ca^{2+} binding proteins (GCAP1 and GCAP2). In dark (at rest), when Ca^{2+} is $\sim 300 – 500$ nM GCAPs prevail in the inactive form with Ca^{2+} bound. In light when Ca^{2+} is lowered to 50 to 100 nM, Ca^{2+} dissociates from GCAPs; this Ca^{2+} free form stimulates GC activity. Second, the life time of active PDE is shortened through the phosphorylation of light–activated rhodopsin

Figure 1.8: *Photo transduction mechanism. Refer text for more details(Modified from www.mcw.edu))*

(R^*) by the rhodopsin kinase. This reaction is mediated by another Ca^{2+} binding protein, recoverin (Koch, 1992). Finally, the ligand sensitivity of CNG channels increases as Ca^{2+} concentration decreases. The regulation of ligand sensitivity by Ca^{2+} is mediated by a third Ca^{2+}– dependent protein calmodulin (CaM) (Hsu and Molday, 1993). All three reactions in various degrees help to restore the dark state and to adjust the light sensitivity of the cell.

The light activated rhodopsin (R^*) is inactivated by two sequential processes: first the phosphorylation of rhodopsin and then the binding of arrestin to the phosphorylated photopigment (Fain et al.,
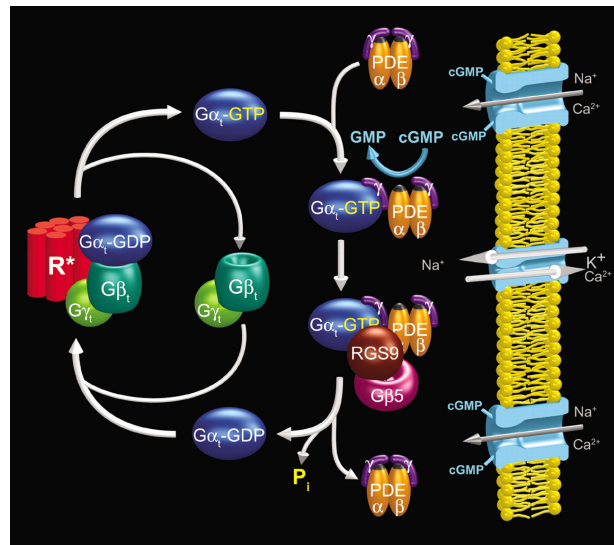
2001). Phosphorylation of rhodopsin can, itself, reduce the ability of R* to activate the transduction cascade. However, a complete inactivation of R* is achieved by the binding of arrestin. After this inactivation process the photopigment must be regenerated before a new photon can be absorbed. This is a multi step process, in which the chromophore all–trans–retinol must be converted back to 11–cis–retinal. The retinal in the outer segment is reduced to all–trans–retinol by a membrane associated dehydrogenase. This chromophore is then transported to an adjacent retinal pigment epithelium and it is isomerised to 11–cis–isomer. It is then retransported back to the photoreceptor and combined with de–phosphorylated opsin. This cycle is often called the visual cycle.

A similar phototransduction cascade exists also in cone photoreceptors and both receptors utilize similar protein isoforms of the enzyme cascade. However, the light sensitivity of cones is 30– to 100– fold lower than that of rods and they adapt over a wider range of light intensity. The cGMP sensitivity, its modulation by intracellular Ca^{2+} and the Ca^{2+} permeation are profoundly different in CNG channels of rods and cones.

CNG channels in chemosensory transduction

Chemosensory cells of vertebrates can be subdivided into three major subgroups: olfactory sensory neurons, neurons of the vomeronasal organ and taste receptor cells. The involvement of CNG channel in signal transduction in all these three system has been proposed. Chemosensory transduction in invertebrates is far less well understood, possibly due to the fact that a single system is not involved in the work. In this section I will describe the involvement of CNG channels in olfactory sensory transduction.
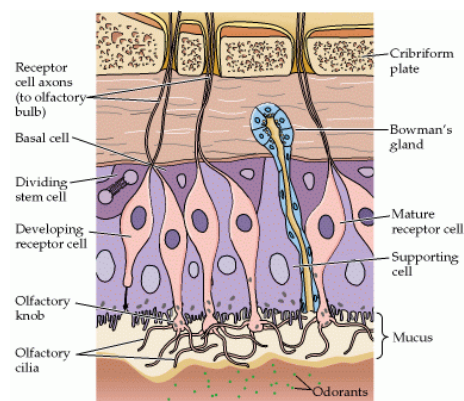
Signal transduction in vertebrate olfactory sensory neurons

Figure 1.9: *Cross-section of an olfactory epithelium*

The olfactory epithelium is made of mainly three different types of cells: olfactory receptor neurons and their cilia, sustentacular cells (that detoxify potentially dangerous chemicals), and basal cells(Firestein, 2001) (for reviews see (Menini, 1999; Buck, 2000; Schild and Restrepo, 1998; Menini et al., 1999)). Olfactory receptor neurons are generated continuously from basal cells. The cellular and molecular machinery for olfactory transduction is located in the olfactory cilia. Although two possible transduction cascades have previously been proposed, involving the production of cAMP or IP3 (inositol–1, 4, 5-triphosphate), there is converging evidence for only the cAMP pathway of intracellular signaling.

Odorant transduction begins with odorant binding to specific receptors on the external surface of cilia. Once the receptor has bound an odour molecule, a cascade of events is initiated that transforms the chemical energy of binding into a neural signal. Binding may occur directly, or by way of proteins in the mucus (called odorant binding proteins) that sequester the odorant and shuttle it to the receptor. The olfactory receptor neurons contain an olfactory–specific G–protein (G_{olf}), which activates an olfactory–specific adenylyl cyclase (ACIII). The cyclase converts the abundant intracellular molecule ATP in to cyclic AMP.

This cAMP binds to the intracellular face of a CNG channel (closely related to that found in photoreceptors) and opens. The opening up of CNG channel permits Na^+ and Ca^{2+} entry (mostly Ca^{2+}), increasing the resting potential of the plasma membrane towards positive. This depolarization amplified by a Ca^{2+}–activated Cl^- current, is conducted passively from the cilia to the axon hillock region of the olfactory receptor neuron, where action potentials are generated and transmitted to the olfactory bulb.

The second–messenger cascade of enzymes provide amplification and integration to odour–binding events. One membrane receptor activated by a bound odour can in turn activate tens of G–proteins, each of which will activate a cyclase molecule capable of producing thousands of cAMP molecules per second. It seems that one odour molecule can produce measurable electrical event in an olfactory sensory neuron (OSN), and just few channels opening simultaneously could pass sufficient current to induce an action potential.

Another amplification mechanism is controlled by the Ca^{2+} entering through the CNG channels. The Ca^{2+} thus entering are able to activate another ion channel permeable to negatively charged chloride ion. At rest OSNs maintain an unusually high concentration of intracellular Cl^- ions, presumably by the action of a membrane pump. Once the Ca^{2+} dependent chloride channels are open the Cl^- ions rush out from the cell throwing up the membrane potential more positive that further depolarizes the

cell. The Ca^{2+} ions entering through the CNG channels are also important in response adaptation through a negative feedback pathway involving the ion channel (Kurahashi and Menini, 1997). The intracellular increase of Ca^{2+} during the odour response decreases the sensitivity of the CNG channel towards cAMP, (probably through calmodulin) thereby requiring stronger odour stimulus to produce sufficient cAMP to activate the channel. One another mechanism by which OSN adapt to odour stimulus is through RGS protein (regulator of G–protein signalling). Apparently this protein acts on

Figure 1.10: *Olfactory sensory transduction cascade(Adapted from Firestein (2001)).*

the adenylyl cyclase to decrease its activity (Sinnarajah et al., 2001). Another by a kinase that phosphorylates activated receptors to a desensitised state.
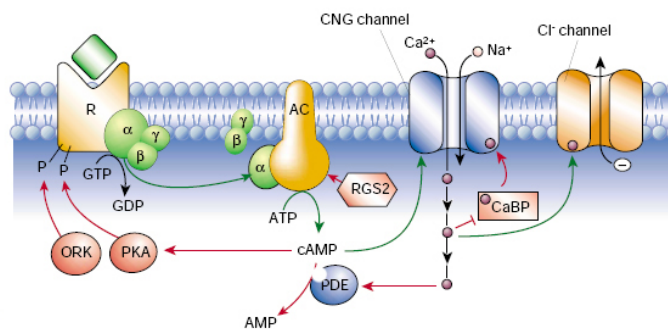
Olfactory receptor neurons are especially efficient in extracting a signal from chemosensory noise. Fluctuations in the cAMP concentration in an olfactory receptor neuron could, in theory, cause the receptor cell to be activated in the absence of odorants. Such nonspecific responses do not occur, however, because the cAMP–gated channels are blocked at the resting potential by the high Ca^{2+} and Mg^{2+} concentrations in mucus. To overcome this voltage–dependent block, several channels must be opened at once. This requirement ensures that olfactory receptor neurons fire only in response to stimulation by odorants. Moreover, changes in the odorant concentration change the latency of response, the duration of the response, and/or the firing frequency of individual neurons, each of which provides additional information about the environmental circumstances to the central stations in the system.

Other chemosensory signal transduction:

     The vomeronasal organ (VNO) is a chemoreceptor organ enclosed in a cartilaginous capsule and separated from the main olfactory epithelium. The vomeronasal neurons have two distinct types of receptor that differ from each other and from the large family of odorant receptors. In situ hybridization studies revealed that a modualtory CNG channel subunit that is also found in OSNs is reportedly expressed in these neurons. But the principal CNGA2 (see nomenclature in sect. 1.3.4) subunit of OSNs is lacking (Berghard et al., 1996). The CNGA4 subunit by itself does not form functional channels (Liman and Buck, 1994) or they become activated by an unknown ligand. The significance of this finding is unclear; because recent findings suggest that the signaling in VNO is mediated by inositol 1,4,5–trisphosphate pathway and TRP channels as opposed to cAMP pathway (Liman et al., 1999; Zufall and Munger, 2001; Keverne, 1999).

1.3.3   Hyperpolarization–activated and cyclic nucleotide–gated channels

     HCN channels are another important member of the Cyclic Nucleotide activated ion channel family (for review see (Craven and Zagotta, 2006)). They have a very different physiological role from that of CNG channels. They regulate neuronal and cardiac firing rate. Unlike CNG channels they are activated by membrane hyperpolarization also, and are weakly K^+ selective. One area in which it is described extensively is the cardiac sinoatrial node, which is the pacemaker region of the heart. HCN channel also mediate pacemaker activity in nervous system by a similar mechanism as in the heart, but the neuronal action potentials are much faster than cardiac action potentials. Besides acting as a pacemaker, HCN current also functions as a regulator of resting potential and membrane resistance. Moreover, they regulate synaptic transmission and nervous system development. The adenosine $3'$, $5'$ – cyclic monophosphate (cAMP) speeds up the activation kinetics and maximal current levels of HCN channels in the cardiac pacemakers. In the nervous system they influence the neuronal firing rate.

1.3.4   The subunit gene family and molecular cloning

     In vertebrates, six members of the gene family expressing CNG channels have been identified. These genes are grouped according to sequence similarity into two subtypes, CNGA and CNGB (Bradley et al., 2001). The first subfamily consists of four members namely, CNGA1, CNGA2, CNGA3, CNGA4. Except CNGA4 all others form functional homomeric channels. The second family comprises two members called CNGB1 and CNGB3 (Refer table 1.1). Additional genes coding for CNG channels have been identified from *Drosophila melanogaster* and *Caenorhabditis elegans.*

     After the physiological observation of a cGMP gated channel (Fesenko et al., 1985), it was subsequently identified through protein purification by Cook at al (1987). The first cDNA clone for a subunit of a CNG channel (CNGA1) was islotaed from bovine retina by Kaupp et al. (1989). This 63 kDa CNGA1 subunit was expressed in rod photoreceptors and produced functional channels when expressed exogenously. Later in 1993 Chen and co–workers (Chen et al., 1993) cloned a second subunit of the CNG channel. This subunit appeared to exist in two different forms one 70 kDa and one 120 kDa. None of these proteins were found in retina. Two years later another polypeptide of 240 kDa, the now known CNGB1, was identified by Korschen et al. (1995). CNGB1 subunits expressed alone do not produce functional CNG channels, but co–expression of CNGA1 and CNGB1 yields functional channels with physiological properties very similar to that of native channels (See CNGB1 subunit in 1.3.1) (Chen et al., 1993; Korschen et al., 1995).

Nomenclature for CNG subunits	
Adopted	Previous designations
CNGA1	Rod CNG Channel CNGA1 /CNGα1 /RCNC1
CNGA2	olfactory CNG channels CNG2,CNGα3,OCNC1
CNGA3	Cone CNG channel CNG3,CNGα2,CCNC1
CNGA4	Second/modulatory subunit of olfactory CNG channels CNG5, CNGB2, CNGα4, OCNC2
CNGB1	Second/modulatory subunit of rod CNG channel CNG4,CNGβ1
CNGB3	modulatory subunit of cone CNG channel CNG6, CNGβ1

Table 1.1: *The newly adopted subunit nomenclature of cyclic–nucleotide gated channels. (From Bradely et al.(2001))*

CNGA2 and CNGA3 than the two CNGB subunits (Kaupp, 1995).

CNG channels from cone photoreceptors are composed of two other subunits, CNGA3 and CNGB3 that are cloned (Matulef and Zagotta, 2003)(Bonigk et al 1993, Gerstner et al 2000).

The first subunit of the olfactory CNG channel, CNGA2, was cloned in 1990 (Dhallan et al., 1990; Ludwig et al., 1990). A second subunit, CNGA4, was found to be expressed in olfactory epithelium in 1994 (Liman and Buck, 1994). Also an alternatively spliced form of CNGB1 (CNGB1b) is found in olfactory epithelium (Bonigk et al., 1999; Picco et al., 2001; Matulef and Zagotta, 2003; Sautter et al., 1998). The CNGA2 subunits alone form functional channels when heterologously expressed. The CNGA4 subunits, similar to CNGB, do not form functional channels by its own when expressed. They have many similar characters of CNGB subunits than the CNGA. However, based on the overall sequence similarity and functional sequence motifs, it is closer to CNGA1,

1.3.5 The Stoichiometry of subunits

The first indication that CNG channels are built from several distinct subunit came from the functional characterization of heterologously expressed CNGA1 subunit of rod photoreceptors. Though these recombinant channels maintained many key properties of the native CNG channels, they deviated in some aspects. The native channel in rods consists of two types of subunits CNGA1 and CNGB1a. When coexpressed they produce channels that exhibit most, if not all, of the key properties of the native channel. One strategy taken to examine the stoichiometry of subunits was by coex-

Figure 1.11: *The subunit stoichiometry of CNG channels from rods, cones and two population of olfactory sensory neurons*

pressing wild–type and mutant subunits and studying their change in characteristics thereby *"report"* the number and arrangement of individual subunits (Liu et al., 1996; Bucossi et al., 1997).

Shammat and Gordon (1999) coexpressed CNGA1 and CNGB1 subunits either with constructed or mutated (destructed) Ni^{2+} potentiating site and from the obtained results they concluded with an AABB (CNGA1 CNGA1 CNGB1 CNGB1) arrangement. This view was challenged by He et al. (2000b), and by using Ni^{2+} potentiation experiments they suggested an ABAB stoichiometry. Interestingly

their experiments using the blockage of L–cis–diltiazem and cAMP activation properties of coexpressed tandem constructs did not provide evidence against an AAAB or BBBA arrangement. Kaupp and Seifert (2002) without providing experimental proof suggested an AAAB stoichiometry. Later in the same year, from Kaupp's and other two groups, the proof came that CNGA channel has an AAAB stoichiometry (Zhong et al., 2002; Weitz et al., 2002; Zheng et al., 2002).

Although CNG channels from cones has not been extensively studied as in rods, it likely is composed of CNGA3 and CNGB3 subunits similar to rod CNG channels (Bonigk et al., 1996). CNG channels in the OSNs consist of three different subunits: CNGA2, CNGA4, CNGB1b (Bonigk et al., 1999)(Figure 1.11).

1.3.6   Structural and Functional domains

The CNG channel subunits all share the same basic architectural plan. Though they are activated by ligands, according to the sequence similarity they are classified as members of the voltage – dependent K^+ channels (Jan and Jan, 1990). The CNG channels form a tetrameric assembly of several homologous subunits (Chen et al., 1994; Korschen et al., 1995; Shammat and Gordon, 1999; Zhong et al., 2002; Zheng et al., 2002; Kaupp and Seifert, 2002; Weitz et al., 2002). In this section I will discuss the structural and functional domains formed by CNGA1 homologous channels unless specified. The primary amino acid sequence of CNGA1 channel from bovine rods is composed of 690 residues (Kaupp et al., 1989). They share a significant sequence homology with K^+ channels (Zagotta and Siegelbaum, 1996; Biel et al., 1999) and have been considered to share same 3D topology and gating mechanism. Each subunit contain six transmembrane segments (S1–S6), a re–entrant pore–loop, and intracellular amino and carboxy–terminal regions (Kaupp et al., 1989; Liu et al., 1996; Molday et al., 1991).

Voltage sensor motif, the S4

In voltage gated channels the fourth transmembrane helix is a voltage sensor, characterized by repeating arginine or leucine at every third amino acid position (refer section 1.2.7 *Activation gating*). The CNG channels also contain this domain, but their net charge is neutralised by the presence of negative charges making the CNG channels voltage independent.

The pore

Another similar structural region shared by the K^+ and CNG channel is the pore. Sun and co–workers (Sun et al., 1996) by using SCAM (Substituted Cysteine Accessibility Method (Akabas et al., 1992)) proposed that, P–region of the CNG tetramer should extend towards the axis of the pore, forming the blades of an iris like structure. The presence of the pore–helix in CNGA1 was shown by the pattern of reaction to modification by extracellular MTSEA ((2–amino ethyl) methane thiosulfonate), in which every third or fourth position is modified, consistent with the presence of an alpha helical structure at the beginning of the P–loop (Liu et al., 1996). By SCAM method the pore helix has been probed with cysteine modifying reagents MTSEA and MTSET (2-((Trimethylammonium) ethyl) methane thiosulfonate) to determine the accessibility (Sun et al., 1996; Becchetti et al., 1999; Liu and Siegelbaum, 2000). The first crystal structure of a K^+ channel was obtained in 1998 (Doyle et al., 1998) and it described the pore organization like an inverted tepee. The pore of CNG channel consists of a stretch of 20 amino acids and exhibit approximately 30% sequence similarity with K^+ channels. The

pore of K^+ selective channels consist a signature sequence (Heginbotham et al., 1992) of GYG (glycine - tyrosine - glycine) and are responsible for the higher selectivity of these channels. In CNG channels this signature sequence is absent it is replaced with a G − − ET(glycine − − glutame threonine) sequence. It has been shown that when the conserved residues from the pore of shaker channels are deleted, they become non–selective ion channel (Heginbotham et al., 1994). Though the filter in K^+ channels is rigid it has been shown that in CNG the selectivity filter moves during channel activation, leading to the speculation that it might act as a gate(Becchetti et al., 1999; Sesti et al., 1995; Bucossi et al., 1996; Fodor et al., 1997b).
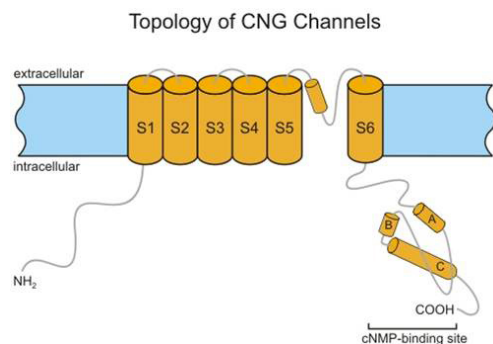
The inner helix (S6)

Figure 1.12: *The putative secondary structure of CNGA1 subunit, where the six transmembrane helices, pore forming region, CNBD are depicted(adapted from (Kaupp and Seifert, 2002)).*

In KcsA the inner helix lines the inner vestibule. Recent studies have shown that the analogous structure in CNG, the S6 segment, serves a very similar role (Flynn and Zagotta, 2001; Flynn et al., 2001; Jiang et al., 2002a; Johnson and Zagotta, 2001). Using sequence alignment between CNGA1 and KcsA (Doyle et al., 1998) Zagotta and co–workers constructed a homology model to represent the putative pore structure of CNG channels. A conformational change occurs in the CNGA1 helix bundle during activation. It has been shown that S399C residues, located near the cytoplasmic end of S6, forms spontaneous disulfide bonds in the closed state, but not in the open (Flynn and Zagotta, 2001). Further proof for the conformational change comes from the state dependent block of V391C, a residue situated in the inner vestibule of the channel, which is modified by MTSET faster in the open state than in the closed (Flynn and Zagotta, 2001). All these results show that the helix–bundle undergoes a conformational change during activation. However, Ag^+ enters the inner vestibule of the channel both in the open and closed state. This shows that the helix bundle cannot act as a gate (Flynn and Zagotta, 2001): which strengthens the observation that the gate is situated in the pore itself.

N–terminal

Nearly 150 amino acid residues compose the N–terminal region of the CNGA1 subunit of the rod CNG channel. An interaction between the amino and carboxy terminal of the same or different subunit of the channel was shown by electrophysiological and biochemical methods (Gordon et al., 1997; Rosenbaum and Gordon, 2002). It was shown that a disulfide bond formation between the C481 of different subunits can take place and C35 can form a disulfide bond with the C481 of the same subunit or with the C481 of the adjacent subunit. These results show that in functional channels the C–linker regions of different subunits lie in close proximity and the N–terminal can contact the C–linker of the same and that of the adjacent subunit(Rosenbaum and Gordon, 2002). In the closed state C481 residue is not accessible, this shows a conformational change in this region during activation (Brown et al., 2000; Gordon et al., 1997; Zheng and Zagotta, 2000). The involvement of amino terminal region in determining the allosteric gating transition and spontaneous opening has been proved (Tibbs et al.,

1997).

The C–linker

In CNG the region between the S6 and CNBD (Cyclic Nucleotide Binding–Domain) is known as the C–linker. Throughout this region the residues are shown to have state dependent modification, and mutations are shown to have large effect on gating (Gordon and Zagotta, 1995b,a; Broillet and Firestein, 1996; Johnson and Zagotta, 2001). It has been shown that the H420 residue from neighbouring subunits in CNGA1 channels create a Ni^{2+} binding site at the interface between subunits and a histidine at 396 in CNGA2 support Ni^{2+} coordination (Gordon and Zagotta, 1995a,b). Histidine substitution experiments in the C–linker region showed that Ni^{2+} preferentially binds to residues 409, 413 and 417 in the closed state and 416 and 420 in the open state of CNGA1 channel (Johnson and Zagotta, 2001). By considering what is known about KcsA and putting these results together the authors suggested a homology model. Some of these findings are in disagreement with the results shown by Hua and Gordon (2005).

The Cyclic Nucleotide–Binding Domain

The CNBDs of CNG channels share significant sequence similarity with other cyclic nucleotide–binding proteins including cGMP– and cAMP– dependent protein kinases (PKG and PKA respectively) and the *Escherichia coli* catabolite gene activator protein (CAP). The crystal structures of CAP and PKA have been solved (Su et al., 1995; Weber et al., 1987) and are very similar. Although the over all sequence identity among the CNBDs of these cyclic nucleotide–binding proteins is only $\sim$ 20 %, the residues that make important contacts with the bound cAMP or occur at turns between adjacent β strands are conserved. Hence the structure of the CNBD of CAP is used as a model for the ligand–binding domain of CNG channels. The cAMP–binding site of CAP comprises three α–helices (A, B and C) and eight β–strands (β1 - β8). The CNBD of CNGA1 is considered to be formed by eight–stranded antiparallel β–rolls flanked by a short amino–terminal α–helix (A helix) and two C–terminal α–helices (B and C helices).

Functional roles

CNG channels exhibit a very high degree of cyclic nucleotide specificity. The cGMP, cIMP (Inosine $3'$, $5'$– cyclic monophosphate) and cAMP differ by only three positions on their purine rings. All three ligands can bind to CNBD of bovine CNGA1 channel subunits. However bound nucleotides promote allosteric opening transition differently. The free energy of opening in CNGA1 channel with cGMP is the lowest, intermediate with cIMP and highest with cAMP. In the case of CNGA2 channel the current can be activated by saturating concentrations of both cGMP and cAMP. They have a lower free energy of opening with cGMP than with cAMP (Dhallan et al., 1990), though cAMP is the specific physiological ligand. It is tacitly assumed that the differential interaction with the purine rings (Matulef and Zagotta, 2003)(figure 1.13) of the ligands control the selectivity.

By probing with a photoaffinity radioactive analogue of the cGMP that is able to label specifically CNGA1 and CNGB1 subunits of the bovine rod CNG channel, Brown and co–workers localised the cGMP binding site and identified the residues lining the binding pocket (Brown et al., 1995). Apparently it became evident that there are at least two important positions in the CNBD which are responsible for the ligand specificity. The first is a threonine in the β roll corresponding to T560 in CNGA1 channels.

The mutation at this position decreases the apparent affinity for cGMP but has little effect on the affinity for cAMP (Altenhofen et al., 1991). Molecular modeling studies suggest that this threonine forms an important hydrogen bond with amino group attached to C2 on the guanine ring (figure 1.13) of cGMP (Scott et al., 1996; Weber et al., 1989). This hydrogen bond formation would require the cGMP to bind in the *syn* configuration. Whereas cAMP was found in the *anti* configuration in the crystal structure of CAP (Weber et al., 1987) and *syn* configuration of that of PKA (Su et al., 1995). Since all CNG channel sequences identified has a threonine at this position, T560 alone cannot account for the ligand discrimination.

The second residue involved in the ligand specificity is in the C-helix (Goulding at al 1994). The mutation of a single residue in this region, D604, found to dramatically alter the ligand specificity (Varnum et al., 1995). In fact, the D604Q mutation (the equivalent residue in fish olfactory channels), altered the specificity to cGMP $\geq$ cAMP > clMP. Substitution of D604 with methionine (the amino acid present at this position in rat olfactory CNGA2), completely inverted the relative agonist efficacy of the expressed channels, such that I_{max} for cAMP > clMP $\geq$ cGMP. The purine ring of cGMP has amino group at N1 and N2 positions, cIMP has at N1 and cAMP has none. The carboxylic acid side chain of D604 can hydrogen bond with the H of the amino group of cGMP. The unavailability of an H to bond with D604 leaves out cAMP as the poorest agonist of CNGA1 channels (Varnum et al., 1995; Matulef and Zagotta, 2003).

Recently, the crystal structure of the C–terminal of HCN2 channel was solved (Zagotta et al., 2003), shedding light on the binding of ligand and the activation of this channel. The sequence alignment of these domains in HCN2 and bovine CNGA1 channels indicates a sequence identity of 32 %. Several important residues such as K472, E502 and D542 known to form salt bridges in HCN2 channels (Craven and Zagotta, 2004) are conserved also in CNG channels (Zagotta et al., 2003) and the charged residues R590 and E617 forming

Figure 1.13: *Chemical structure of nucleotides: from top to bottom, cGMP, cIMP and cAMP respectively. Notice the decrease in available H in the purine ring while passing from cGMP to cAMP*

inter–subunit bonds between the proximal HCN2 CNB domains (Zagotta et al., 2003) are also conserved in CNG channels. This indicates that the overall folding of the C–linker domain of HCN2 and CNGA1 channels could be similar. Several experiments failed to verify the validity of this model to be homologous to that of the CNGA1, leaving the speculation that the crystallized ligand bound state of the HCN2 C–linker might represent the resting configuration of homologous region of CNGA1 channels (Hua and Gordon, 2005; Islas and Zagotta, 2006).

CNGB1 subunit

Native rod CNG channels are oligomeric proteins composed of CNGA1 and CNGAB1 subunits. As mentioned earlier the CNGB1 cannot form functional channels by itself. When coexpressed with
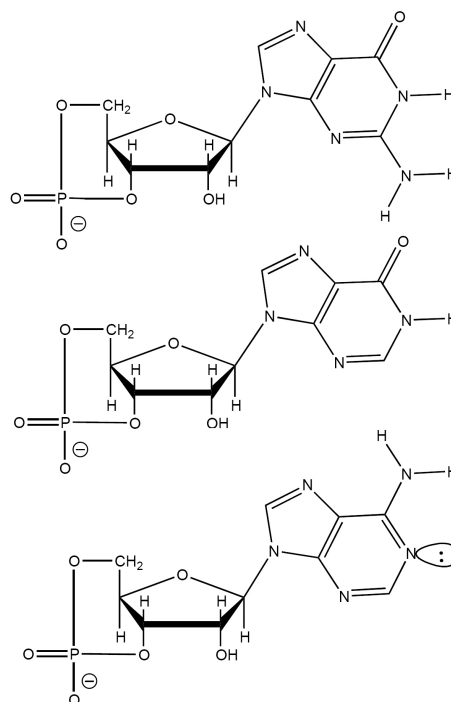
CNGA1 subunit they form functional channels with identical properties of the native rod CNG channels (Korschen et al., 1995; Biel et al., 1999; Kaupp and Seifert, 2002): apparent affinity for cGMP, sensitivity

to L-cis-diltiazem, fast single channel gating, inhibition by Ca^{2+}/CaM. Since they serve to modulate the function of the native CNG channels they are also called modulatory subunits. The earlier cloning studies suggested that there are two alternatively spliced forms of the

Figure 1.14: *The putative secondary structure of CNGB1 subunit, where the six trans-membrane helices, pore forming region, CNBD, the C^{a2+} binding CaM and GARP region are depicted*

CNGB1 subunit, which differ only in length. The shorter one has a predicted molecular mass of $\sim$ 70 kDa and the longer one with an additional N–terminus and has a molecular mass of $\sim$ 102 kDa. However polypeptide of this mass range was not detected in the purified rod channel preparations (Molday et al., 1990; Chen et al., 1994), instead they showed distinct 63 or 240 kDa polypeptides. The 63 kDa corresponds to the CNGA1 (Kaupp et al., 1989; Molday et al., 1991) and the 240 kDa was shown to bind calmodulin and to contain partial amino acid sequence of the human CNGB1 (Hsu and Molday, 1993; Chen et al., 1994). In 1995 the 240 kDa subunit from bovine rod was cloned (Korschen et al., 1995) and shown that it has a unique bipartite structure. The C–terminal region, from 572 – 1394, with a voltage–sensor like motif, a pore region, the cGMP binding domain and the calmodulin–binding site. The hydrophilic N–terminal part, from amino acid 1–571, contains a bovine retina specific glutamic acid – and proline – rich protein (GARP, cloned earlier (Sugimoto et al., 1991). Electrophysiological properties of the native CNG channel were not influenced
by the GARP–part.

Quaternary structure

  Most of the crystallographic studies on mammalian membrane proteins are often hindered by difficulty in obtaining enough quantity of purified proteins. In 2002 Kaupp and co–workers (Higgins et al., 2002) purified the heteromeric CNG channels and studied that by electron microscopy and image processing of single particles. The resultant 35 Å resolution structure shows three distinct domains. The larger domain has a width $\sim$100 Å, thickness $\sim$50 Å and four corners, similar to the putative membrane spanning domain of the shaker K^+ channels (Sokolova et al., 2001). Two smaller domains each with 40×40×50 Å dimension (two fold symmetry) are attached to this by two narrow linkers. They suggested this as the cytoplasmic end of the four C–terminal and N–terminal part of the protein. The authors proposed a "hanging gondola" structure, similar to some K^+ channel structures, for the ligand–binding domains that hang below the transmembrane part by taking into account of the electron density distribution. The cytoplasmic regions that hang below the transmembrane

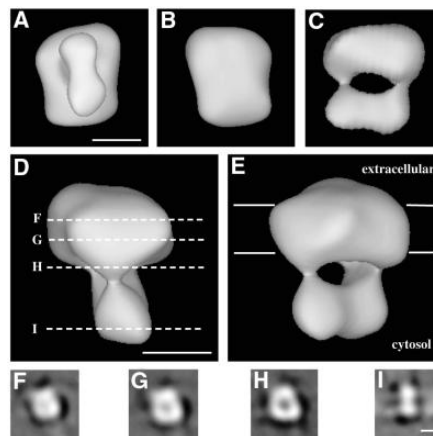**Figure 1.15:** *Surface representation of CNG channel at a contour level that includes the mass of four subunits. **A** is viewed from the cytosolic side of the membrane, **B** is viewed from the extracellular side **C,D,** and **E** are viewed from a direction parallel to the membrane. **F-I** sections through the electron density along the lines indicated in **D** (refer Higgins et al. (2002))*

part seem to have two–fold symmetry instead of four fold. The gating properties of CNG channels also indicate that the subunits are arranged as two functional dimers (Liu et al., 1998).

1.3.7   Properties of CNG channels

Ionic permeation

The pore–forming region of membrane protein is known to be the major determinant of ion permeation in voltage–as well as ligand–gated ion channels(Heginbotham et al., 1994; Goulding et al., 1993; Yang et al., 1993). Native CNG channels are permeable to monovalent cations, such as Na^+, Li^+, K^+, Rb^+, Cs^+ and Ti^+ but do not discriminate much between them (Capovilla et al., 1983; Nakatani and Yau, 1988; Yau and Nakatani, 1984). It has been shown also in the excised patches (Fesenko et al., 1985; Nunn, 1987; Menini, 1990; Colamartino et al., 1991) Ca^{2+} is also permeable but at the same time acts as a voltage–dependent blocker of monovalent cations (as does Mg^{2+}, Ba^{2+}, Sr^{2+}, Mn^{2+}) (photo receptors: see (Yau and Nakatani, 1984; Zimmerman and Baylor, 1992; Colamartino et al., 1991) for olfactory receptors: see (Zufall and Firestein, 1993; Zufall et al., 1994). This reduces the single–channel conductance from between 20 and 45 pS in the absence of divalent cations to less than 1 pS under physiological conditions. The first attempt to record a single channel activity was a failure (Fesenko et al., 1985). The low single channel conductance is of physiological significance because the gating of a large number of low conductance channels is associated with less current noise than that of a few high conductance channels. This facilitates the reliable detection of small changes in current and thus enhances sensitivity, to detect even a change in single photon. CNG channels are also sensitive to external proton concentration: a subconductance state due to a blocking effect observed with decreasing pH (Goulding et al., 1992; Zufall and Firestein, 1993).

The selectivity of CNG channels for monovalent cations was determined from relative ion permeabilties recorded under bionic conditions in excised patches. The following selectivity and permeability ratio was obtained for the excised salamander rod photoreceptors; $Li^+ > Na^+ \sim K^+ > Rb^+ > Cs^+$ $= 1.14 : 1 : 0.98 : 0.84 : 0.58$ (Menini, 1990). Similar ratios were also determined from frog rods (Fesenko et al., 1985), mammalian rods (Luhring et al., 1990), and lizard parietal eye (Finn et al., 1997, 1998). The recombinant CNGA1 channels of rod photoreceptor shows similar selectivity and permeability ratio except Na^+ is more permeable than Li^+ (Kaupp et al., 1989), which is due to the lack of CNGB1 subunit. The permeability of CNG channel was probed with large organic cations and estimated the narrowest part of the pore to be 3.8 Å× 5 Å rectangle(Picco and Menini, 1993). This estimated size suggests that the pore of CNG channels is bigger than the ones of Na^+ and K^+ channels but smaller than the one of the Ca^{2+} channel of skeletal muscle. This conclusion is in accordance with the estimation obtained by Laio and Torre(Laio and Torre, 1999). The ion selectivity of CNG channel of cone is similar to that of rod: $K^+ > Na^+ \sim Li^+ \sim Rb^+ > Cs^+$ $= 1.11 : 1.0 : 0.99 : 0.96 : 0.8$ (Picones and Korenbrot, 1992).

Role of conserved pore glutamate in permeation

Ca^{2+} binds to a site inside the pore for permeation and thereby block the current carried by monovalent cations (Refer section selectivity). A glutamate residue in the P loop (E363 in CNGA1) of the CNG channels (CNGA1 to CNGA3 subunits) has been identified as an important structural element of Ca^{2+} binding. When this glutamate is replaced with a neutral residue, the Ca^{2+} blockage is almost abolished (Eismann et al., 1994; Gavazzo et al., 2000; Park and Mackinnon, 1995; Root and MacKinnon, 1993). Experiments either enhance or diminish the net negative charge of this residue increased or

decreased respectively the $K_{1/2}$ of blockage, showing that the net negative charge of this residue is an important determinant in deciding the blockage. The CNGB1 subunit has a glycine at the equivalent position of glutamate. This explains the reduced Ca^{2+} blockage in the native channel compared to the heterologously expressed homologous CNGA1 channels (Korschen et al., 1995). Recently it was shown that the S5–pore–S6 module, by providing a characteristic electrostatic environment, determines the protonation state of pore glutamates and thereby controls Ca^{2+} affinity and permeation in different channel type (Seifert et al., 1999). This glutamate was also shown to be responsible for the multi–ion nature of the pore of CNG channels (Sesti et al., 1995). Another interesting observation regarding E363 of CNGA1 was made regarding channel gating (Bucossi et al., 1996). By mutating E363 into an alanine, a serine or an asparagine, a current decline reminiscent of the desensitisation of ligand gated channels was observed for the CNG channel suggesting that glutamate 363 is involved in the gating in addition to be a part of the selectivity filter. In the same study, it was demonstrated that the mutant E363S was permeable to dimethylammonium; replacing the glutamate with a smaller residue led larger organic cations to permeate suggested that E363 was located close to the narrowest part of the pore. The findings in this article also lead to the conclusion that probably the gate is situated in the pore it self (Bucossi et al., 1996).

Single channel properties

Single channel properties of CNG channels from different preparations vary significantly. The CNGA2 channels from catfish olfactory sensory neuron have three open states with a conductance of 25, 50 and 80 pS (Goulding et al., 1992; Root and MacKinnon, 1993). The CNGA1 from bovine rod has only one resolvable open state with a conductance of about 28 pS (Kaupp et al., 1989; Nizzari et al., 1993) CNGA2 from bovine olfactory sensory neuron has a single–channel conductance of about 40 pS. The single–channel openings of the native CNG channels from vertebrate rods are peculiarly characterized by rapid flickering (Sesti et al., 1994) in the total absence of divalent cations, and its mean open time is not more than 40 μs. Because of this rapid flickering the determination of single channel conductance is controversial. Single channel conductance measured from patches containing many channels suggested a conductance of 50 pS (Sesti et al., 1994), but the measurement based on patches with single channel showed a conductance of 25 pS (Taylor and Baylor, 1995). In contrast the native channels from olfactory sensory neurons have well resolved openings with mean open time larger than 1 ms.

Bucossi et al. (1997) addressed the phenomenon of rapid flickering observed in the native rod photoreceptor cells. They studied heterologously expressed hetero–multimeric channels and arrived at two important findings. First, at least three types of channels with different properties were observed, first with stable single channel openings at the positive potential and multiple openings at the negative potential; second with a low apparent conductance (5–25 pS) and third with a high apparent conductance (25–45). This difference may arise due to different stoichiometry of channel subunits, or different spatial arrangement of subunits or due to posttranslational modifications. The second finding was that the rapid flickering appears to be an intrinsic property of the channel and not caused by rapid proton blockage.

Several groups reported that CNG channel can open occasionally to subconducting states (Zimmerman and Baylor, 1986; Hanke et al., 1988; Taylor and Baylor, 1995; Bucossi et al., 1997). Ruiz and Karpen (1997) have used an elegant approach to show that CNG channels have multiple sub–conducting opening states. They succeeded to covalently tether a cGMP photoaffinity analog to the CNGA1 chan-

nel and thereby permanently activate the channel. The technique allowed them to lock exactly one, two, three or four cGMP molecule to the channel. By single channel analysis they found that channels occupied by four ligands are open most of the time; unliganded channels and channels with one ligand open with a probability $P_o \sim 10^{-5}$. When two or three ligands were locked in place the probability is 0.01 and 0.33, respectively. Though the approach was elegant the finding is not unequivocal. Several others found either less subconducting states or none (Liu et al., 1998; Sunderman and Zagotta, 1999; Ildefonse and Bennett, 1991; Benndorf et al., 1999). A more qualitative description and comparison will be given in one of the following section (see Kinetic modeling in sec. 1.3.7).
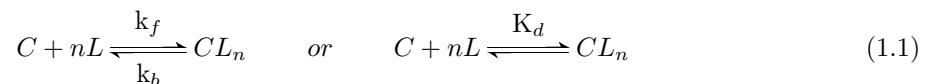
Macroscopic currents

Most ligand gated channels eventually close even in the continued presence of agonist (see Inactivation gating in sec. 1.2.8). The CNG channel, however, display little desensitisation, thus eliminates technical and analytical complications. The CNG channels involved in phototransduction responds immediately to the ligand (cGMP) variation, whereas those of olfactory have slow activation kinetics (Zufall et al., 1993). These differences certainly account for the different requirement of the two modes of sensory transduction. After macro patch excision, for several minutes, there is a run up in the fractional activation of cGMP induced current, and has been previously shown to represent dephosphorylation of the channels by endogenous patch–associated phosphatases (Gordon et al., 1992; Molokanova et al., 1997) (also see *Phosphorylation/dephosphorylation* in section 1.3.8). A small outward rectification is shown by CNG channels of the photoreceptors. It is ascribed to the decreased open probability at negative voltages (Sesti et al., 1994).

Kinetic models

A protein whose shape is changed when it binds a particular molecule is called allosteric proteins. The term "allostery" means "*other sites.*"

In studying ligand–gated channels, many experimenters have measured the fraction of open channels in response to varied concentration of agonist. In a very common finding this dose-response relation shows an S – shape rather than a rectangular hyperbola (in a linear scale plot). The Hill equation was used to explain these type of data. A.V. Hill in 1910 applied this equation to describe the binding of oxygen to hemoglobin (Hill, 1910), and subsequently has been widely used in biochemistry, physiology, and pharmacology to analyze the binding equilibria in ligand–receptor interactions(Weiss, 1997).

The Hill equation is readily derived from a binding reaction scheme in which n molecules of ligand (L) bind to a receptor (C), i.e.,

$$C + nL \underset{\mathrm{k}_b}{\overset{\mathrm{k}_f}{\rightleftharpoons}} CL_n \qquad or \qquad C + nL \overset{\mathrm{K}_d}{\rightleftharpoons} CL_n \tag{1.1}$$

where, $\mathrm{K}_d = \mathrm{k}_f / \mathrm{k}_b$. At equilibrium, the ratio of bound to total receptors is given by a familiar form of the Hill equation

$$P = \frac{P_{max}}{1 + (K_{0.5}/[L])^n} \tag{1.2}$$

Where P is the response(ratio of bound to total ligand), P_{max} is the maximum response, $K_{0.5}$ is the [L] at which half of the receptors are bound, and is equivalent to n^{th} root of K_d

Dose–response data of CNG channels have almost always shown an S–shaped curve with a Hill coefficient n∼3. The physical origin of this S–shaped curve and an n∼3 is the following: the channel is most likely to open with a presence of multiple bound agonist molecule than single bound agonist, probably with a minimum of 3 molecules.
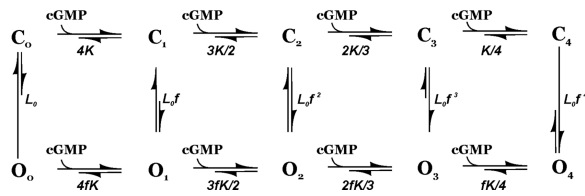

Figure 1.16: *The WMC model for CNG channel with four equivalent binding cites.C_o–C_4 are closed states; O_o–O_4 are corresponding open states. K, microscopic equilibrium associating constant of the closed state; L_o, equilibrium constant between closed and open state in the abscense of ligand; f, the multiplicative factor with which each binding displaces the closed–open equilibrium.(Monod et al., 1965), scheme adapted from Li et al. (1997)*

However, for a receptor with more than one ligand binding site, the Hill equation does not reflect a physically possible reaction scheme; only under the very specific condition of marked positive cooperativity does the Hill coefficient accurately estimate the number of binding sites(Li et al., 1997; Weiss, 1997). For example, when n=2 simultaneous interaction of three molecules with no intermediate state RL occurs between the R and RL_2 state. In real ligand–receptor interactions the intermediate states have to occur. The Hill coefficient is best thought of as an "*interaction*" coefficient, reflecting the extent of cooperativity among multiple ligand binding sites (the sigmoidicity of the S curve).

The mechanistic limitations of the Hill equation have led to interpret the channel behavior by using kinetic models. One of the most widely used models based on the "binding–then–gating" hypothesis, contains a linear series of binding steps leading to a final conformational change (figure 1.16). After the importance of conformational changes was recognized, two different theories of the cooperative mechanism were postulated in 1960s. One was the theory of Monod, Wyman, and Changeux (MWC model also called as the "symmetry" model, "concerted" model, or "the two–state" model) (Monod et al., 1965), and the other was the theory of Koshland, Nemethy, and Filmer (KNF model; often called as the "induced fit" model or the "sequential" model) (Koshland et al., 1966).

The MWC model assumes that the two structures, one named T, for tense, and the other R, for relaxed, are in equilibrium at whatever ligation state due to the concerted transition of the protomers from one structure to the other. In the absence of ligand, the equilibrium is governed by the allosteric constant, $L = [T_0] / [R_0]$, where the subscript indicates zero ligand. The homotropic ligand binds the molecules in the T structure with low affinity (K_T) and binds to those in the R structure with high affinity (K_R). The model is translated into an equation the ratio between the bound sites and the total number of sites, with the ligand concentration, which takes the form of a sigmoid curve. Such a curve indicates that the sites of the homotropic ligand cooperate positively in binding. (figure 1.16)

The KNF model, does not assume equilibrium of quaternary structures. The switch from the T to the R structure occurs progressively through intermediate structures induced by the homotropic ligand binding. The structural pathways for the transition depend on the specific protein case. This model can describe positive and negative cooperative interactions.

The MWC model has had a major impact on the understanding of cooperativity because of the universality of the equilibrium concept and the simplicity of the formulation, which is capable of describing the behavior of many allosteric proteins with good accuracy by using only three parameters. In contrast, to formulate the mechanism of the allosteric protein the KNF model requires a detailed

knowledge of the functional/structural properties of all of the intermediates, in addition to the end states, a prerequisite that in most cases is too difficult to fulfill.

The MWC model has three predictions. Ligand independent channel opening, every liganded state has unique opening and the equilibrium constant therefore the open probability should increase by a constant factor. The first prediction is satisfied. In fact it is shown that CNG channels show ligand independent openings (Kleen, 2000; Picones and Korenbrot, 1992; Ruiz and Karpen, 1997, 1999; Tibbs et al., 1997). The spontaneous open probability is significantly lower for CNGA1 than CNGA2 channels (spontaneous open probability $P_{sp} = 1.5 \times 10^{-5}$ for CNGA1(Ruiz and Karpen, 1997) and $P_{sp} = 2.25 \times 10^{-3}$ for CNGA2 (Tibbs et al., 1997). The amino terminal domain determines differences in both ligand gating and spontaneous openings between rod and olfactory CNG channels, and that channel activation occurs by a cyclic allosteric mechanism and not by linear reaction steps where ligand binding is obligatory before channel opening. Another significant step in checking the allosteric model was the work by Ruiz and Karpen (1997) (see *Single channel properties* in sec. 1.3.7). The P_o (open probability) values predicted by MWC are not in accordance with the experimentally obtained values of Ruiz and Karpen (1997). More interestingly when less than four ligands are bound the opening events show smaller subconductance states, as if the flipping of each subunit opens the channel into a particular open state. These observations are inconsistent with the MWC model. An alternative model taken by Liu et al. (1998) also shows the inadequacy of MWC model to explain the allosteric activation of CNG channels. To check the validity of the model the authors constructed channels with constrained number of binding sites. Their results quantitatively differed from that of Ruiz and Karpen but qualitatively agreed and went on to propose an interesting variation of MWC model: coupled dimer model (CD). In this model each dimer binds to ligand independently and undergo an allosteric conformational change to open and each dimer make this transition independently.

1.3.8   Modulation of CNG channels

Modulation by calmodulin

Native olfactory and rod CNG channels are inhibited by nano molar levels of CaM in a Ca^{2+} and time dependent way (Chen and Yau, 1994; Hsu and Molday, 1993). For both channels Ca^{2+}/CaM decreases the apparent affinity for cyclic nucleotides. One way for this to occur is if Ca^{2+}/CaM destabilizes the opening allosteric transition as proposed (Chen and Yau, 1994). The time course of adaptation to either pulses of odorant or to photolysis of caged compound are the same suggesting that adaptation work through olfactory CNG channels. Adapted channels and Ca^{2+}/CaM inhibited channels have a similar apparent affinity for cAMP suggesting that odorant adaptation is due to Ca^{2+}/CaM dependent inhibition of CNG channels.

Unlike in the case of olfactory neurons the physiological role of CaM modulation in rod photoreceptors are not yet clear. Speculatively the interaction of Ca^{2+}/CaM with CNG induces a negative feedback loop in native rods. In the dark, in high levels of Ca^{2+} and cGMP, Ca^{2+}/CaM bound channels would be inhibited, thereby having a lower apparent affinity for cGMP. Once light hit the receptors, Ca^{2+} and cGMP levels drop, Ca^{2+}/CaM would not be bound, the channel increases the apparent affinity for cGMP. However, such a mechanism is under scrutiny as CaM alters the apparent affinity of rod channels by two fold, which is a relatively small change compared with the 1000–fold range in intensity over which visual adaptation occurs (Koutalos et al., 1995; Koutalos and Yau, 1996; Nakatani et al., 1995).

The cone CNG channels in excised patches from some species are weakly modulated by CaM (Bonigk et al., 1996), cones from other species found to be insensitive to CaM: native catfish (Haynes and Stotz, 1997). Bewilderingly, the A3 subunit of cone CNG channels comprises in its amino terminal region fairly conserved CaM target motif that, in various binding assays, shows CaM binding. Most probably the cGMP sensitivity of cone CNG channels are controlled by some another Ca^{2+} binding protein and CaM acts a partial modifier. Rebrik and Korenbrot (1998) have experimentally supported this hypothesis. The detached patch supplemented with Ca^{2+}/CaM does not mimic the same ligand sensitivity in a cellular environment.

The molecular mechanism underlying the Ca^{2+}/CaM inhibition of olfactory and rod channels are broadly the same. Olfactory CNGA2 subunits contain a site in their NH_2–terminal region that is necessary and sufficient to bind Ca^{2+}/CaM (Chen and Yau, 1994). Deletion of this site in CNGA2 results insensitiveness to Ca^{2+}/CaM (Chen and Yau, 1994). The CNGA4 and CNGB1b subunits of OSNs work as modualtory subunit in determining the kinetics of Ca^{2+}/CaM action. Even though CNGA4 does not bind directly to CaM, the olfactory CNG channels with out these subunit shows 200 fold slower on-rate on modulation by Ca^{2+}/CaM. CNGA4 subunit allows for a state–independent association of Ca^{2+}/CaM with the CNGA2/CNGA4/CNGB1b channel complex. The Ca^{2+}/CaM modulation is independent on the open probability of channel; this enables channels with high open probability to be inhibited.

Rod CNGA1 subunit does not contain CaM binding site; however, CNGB1 subunit has an N–terminal site for CaM binding which modulates the channel activity in the intact cells. Co–expression of CNGA1 and CNGB1, where the CaM binding site is deleted from the later, results in a functional channel that are insensitive to Ca^{2+}/CaM. How ever, the CNGB1 is unconventional as in the C–terminal region it has another CaM binding location that binds to Ca^{2+}/CaM in biochemical assays. The functional significance of this site is unclear because when deleted, channels retain wild–type Ca^{2+}/CaM dependence (Weitz et al., 1998; Trudeau and Zagotta, 2002b).

In CNGA2 channels, the N–terminal regions forms an interaction with the C–terminal. This interaction may promote channel opening by helping to stabilize conformations of the C–linker and CNBD (Varnum and Zagotta, 1997). The cytoplasmic N– and C– terminal of CNGA1/CNGB1 channel also interact (Trudeau and Zagotta, 2002b,a). The Ca^{2+}/CaM binding site of the CNGB1 interact with the short C–terminal end of CNGA1; unlike the olfactory channels the CNBD and C–linker of CNGA1 are not involved in this interaction. The Ca^{2+}/CaM disrupts the N– and C– terminal interactions in both olfactory CNGA2 and rod CNGA1/CNGB1 channels (Varnum and Zagotta, 1997; Trudeau and Zagotta, 2002b). This explains the possible mechanism for inhibition in both channels. In CNGA2 channel the CaM binding region serves as an autoexcitatory site upon interaction with C–terminal (Chen et al., 1994; Varnum and Zagotta, 1997). The disruption of this interaction upon Ca^{2+}/CaM binding inhibits the channel response. This autoexcitatory mechanism is not present in rod CNG channels, suggesting some different unknown mechanism.

Phosphorylation/dephosphorylation

Studies suggest that CNG channels can be modulated by changes in phosphorylation state catalyzed by serine/threonine protein kinases and phosphatases (Gordon et al., 1992) and, more recently, by protein tyrosine kinases (PTKs) and phosphatases (PTPs) (Molokanova et al., 1997). Repeated measurement of the dose-response curve of channel activation in excised patches of ROS membranes disclosed a slow increase in cGMP sensitivity over time (Gordon et al., 1992). The decrease in $K_{0.5}$

was usually 2– to 3– fold but could be as large as 10– fold. The enhancement of ligand sensitivity was slowed down by both ATP and inhibitors of Ser/Thr phosphatases and was accelerated by purified type 1 phosphatase, suggesting that phosphorylation might control the conversion of channels between states of high and low ligand sensitivity(Kramer and Molokanova, 2001).

Heterologously expressed (Xenopus oocytes expression system) CNGA1 subunit displays a seemingly similar decrease in $K_{0.5}$ after patch excision, attributable to changes in tyrosine phosphorylation state (Molokanova et al., 1997, 1999). Unlike native channels, orthovanadate and pervanadate (inhibitors of phosphotyrosine phosphatase (PTP)) slowed down the progressive sensitivity enhancement (Molokanova et al., 1997, 1999). The effect is reduced by Y498F mutation, consistent with the idea that this residue is phosphorylated by a protein tyrosine kinase (PTK) in oocytes. Studies on homomeric rod CNG channels containing CNGA1–subunits show that the channel can only be dephosphorylated when it is opened with cGMP and can only be phosphorylated when it is closed by removing cGMP. Application of cAMP weakly alters the ability of PTP to modulate the channel, supporting the notion that channel opening, rather than ligand occupancy of the cyclic–nucleotide–binding site, is responsible for the activity–dependent effects of cyclic nucleotides (Molokanova et al., 1999).

Regulation by nitric oxide

Nitric oxide (NO) is an important signaling molecule in the retina. The major target for NO in most cell types is soluble guanylate cyclase, which, by synthesizing cGMP, can lead to activation of CNG channels. In some olfactory neurons, NO can directly activate CNG channels even in the absence of cyclic nucleotides (Broillet and Firestein, 1996), but there is no evidence that NO has a direct affect on photoreceptor CNG channels (Trivedi and Kramer, 1998). One crucial locus for NO action appears to be a cysteine residue (C460) in the CNGA2–subunit of the olfactory channel (Broillet, 2000), a residue that is also conserved in the olfactory CNGB3– subunit and in the rod CNGA1– and CNGB1– subunits. Why the rod channels are unaffected by NO remains a mystery. It was shown that the homomeric CNGA4 (modualtory subunit of OSNs) channel can function when activated by NO (Broillet and Firestein, 1997; Cudeiro and Rivadulla, 1999).

Regulation by lipid metabolites

Recent studies have shown that certain lipid metabolites, including diacylglycerol (DAG), modulate native and expressed rod CNG channels (Gordon et al., 1995; Crary et al., 2000). Even though DAG is an activator of protein kinase C (PKC), the effect of DAG on CNG channels does not require the catalytic activity of protein kinases (Gordon et al., 1995). Invertebrate phototransduction is thought to be mediated by phospholipase C (PLC) (Ranganathan et al., 1995), and DAG metabolites have been implicated in activating the light–sensitive ion channels in Drosophila melanogaster photoreceptors (Chyb et al., 1999).

Divalent cations

The sensitivity of CNG channels can also be altered by transition metals, such as Ni^{2+} and Zn^{2+} (Karpen et al., 1993; Gordon and Zagotta, 1995c). Like other divalent cations (Ca^{2+}, Mg^{2+}, Mn^{2+} and Cd^{2+}), at sufficiently high (Gordon and Zagotta, 1995c) concentrations these ions induce a voltage–dependent block by binding to sites within the permeation pathway of the CNG channel (see also *Ionic*

permeation in sec. 1.3.7). However, Ni^{2+} and Zn^{2+} have an additional effect on channel gating (see *The C–linker* in section 1.3.6). Ni^{2+} coordination by His420 of CNGA1 channel can potentiate the channel activation, and His396 in CNGA2 can inhibit channel activation (Gordon and Zagotta, 1995b). From a functional perspective, there is the intriguing possibility that Zn^{2+} might play a physiological role in rod CNG channel regulation. Free or loosely bound Zn^{2+} can be detected in rods and cones (Wu et al., 1993; Kaneda et al., 2000), and Zn^{2+} is tightly bound to rhodopsin (Shuster et al., 1996) and phosphodiesterase, where it is essential for enzymatic function (He et al., 2000a). Exposure to light results a dramatic redistribution of chelatable Zn^{2+} in rods (Ugarte and Osborne, 1999), raising the possibility that Zn^{2+} plays a dynamic role in phototransduction, perhaps with CNG channels as an important target.

pH

In the catfish olfactory neurons, pH titration combined with mutagenesis studies of Glu363 (the conserved glutamate involved in the block by divalent cations) have suggested that this pore residue is also involved in proton binding and subsequent channel block (Tanaka, 1993; Root and MacKinnon, 1994). Protonation of D604 in the rod CNG channel may enhance the interaction between the binding site and the cyclic–nucleotide triggering the allosteric changes that lead to channel opening (Varnum et al., 1995; Gordon et al., 1996) (see also *The cyclic nucleotide Binding Domain* in sec. 1.3.6).

Pseudechetoxin

Recently, a peptide blocker that can be used as a pharmacological tool has been extracted and purified from the venom of the australian king brown snake (Brown et al., 1999). This protein (PsTX, 24 kDa) blocks the cGMP dependent current in CNGA2 channel, when applied extracellularly. The block is independent of voltage and requires only a single molecule of toxin. PsTx also blocks CNGA1 homologous channel with an apparent affinity of 100 nM. The Heteromeric rod photoreceptor CNG channels have the lowest affinity ($K_i \sim 3.5 \ \mu M$).

Tetracaine

Tetracaine is a local anaesthetic which has been shown to block the bovine rod but not the rat olfactory CNG channel (Fodor et al., 1997b,a). It is a state–dependent and a voltage dependent blocker. Tetracaine blocks preferentially in the closed state, by binding to the pore E363. Mutating this residue abolishes the blockage. Widening of the pore in the open state might be destabilising this conformation, or alternatively, the electrostatic repulsion by permeating cations and the positively charged amine group of tetracaine leads to low affinity binding in the open state.

Dequalinium

Dequalinium is an organic divalent cation which suppresses the rat small conductance Ca^{2+}– activated K^+-channel 2 (rSK2) and the activity of protein kinase C (Rosenbaum et al., 2003). Dequalinium blocks CNGA1 intracellulary, with a $K_{0.5} \approx$ 190 nM and CNGA1+CNGB1 channels with a $K_{0.5} \approx$ 385 nM, at 0 mV. The blockage is state independent, but it is voltage dependent. Single channel recordings indicate that dequalinium acts as a slow blocker. It promotes the appearance of long closed

states (with no change in unitary conductance) rather than promoting "flickering" between the closed and open states which would be characteristic of a fast (low affinity) blocker (Hille, 2001).

Calcium channel blockers

L-cis-diltiazem, the inactive isomer of a calcium channel blocker was the first blocker of CNG channels discovered (Koch and Kaupp, 1985). In the rod channel, the efficiency of this block depends on the CNGB1 subunit (Chen et al., 1993). The concentration dependence of block showed that one molecule of the blocker is sufficient to block the channel (Haynes, 1992). The blockage in CNG channels of rods, cones and olfactory neurons is voltage–dependent (Haynes, 1992; McLatchie and Matthews, 1992). Pimozide blocks the cyclic GMP–activated current with half–maximal suppression at a concentration of about 0.8 μM and nearly complete suppression at 10 μM. The block produced by pimozide is voltage and time independent (Nicol, 1993). D–600, amiloride Frings et al. (1992) and nifedipine (Zufall and Firestein, 1993) act on the olfactory CNG channels.

Nicotine

Nicotine has been reported to stabilise the closed conformation of the rod CNG channel (McGeoch et al., 1995). Calcium lowers the $K_{0.5}$ of blockage and cGMP increases it, giving a range of $K_{0.5}$ between 10^{-11} and 10^{-8} M.

Polyamines

Polyamines have been shown to block the pore of inward rectifier K^+ channels as well as some glutamate–gated channels. Three polyamines (putrescine, spermidine and spermine) effectively block the CNG channel from both sides of the membrane. Among them, spermine has the greatest potency (Lu and Ding, 1999). Extracellular spermine blocks the channel as a permeant blocker, whereas intracellular spermine appears to block the channel in two conformations –one permeant, and the other non– (or much less) permeant. Since polyamines exist in both the intracellular and extracellular media, blockade of the CNG channel by polyamines may play an important role in suppressing noise in the signal transduction system in rods.

Quaternary ammonium

In potassium channels, the blockade by TEA ions has provided tremendous insight into the structure and function of this class of channels. The idea that K^+ – and Na^+ – permeation occur through two different physical pathways came from studies using the TEA^+ blocker (also due partly by the studies using TTX by Hille (1975))(Armstrong and Binstock, 1965; Armstrong, 1971) as well. The quaternary ammonium (QA) derivatives block the permeation pathway of CNG channels in concentration–and voltage – dependent manner. With the increase in number of tail methylene group the binding affinity increases (Contreras and Holmgren, 2006). In CNG channels QA derivatives can bind to both open and closed state. In the open state blockage decreases the mean open time of channel rather than decreasing the unitary conductance. The state independent blockage in CNG channels show that the permeation pathway in these channels is different from that of K_v channels, where QA derivatives bind preferentially to the open state.

1.4   Aim of the study

The identification of ion channels opened up several puzzles which were experimentally and theoretically addressed during the past three decades. In the beginning one of the major problem was to explain the selectivity of ion channels. The theoretical models of the 1970s waited until 1998 for experimental conformations. Still many more questions are open. How does a voltage sensor move in a voltage gated channel to open the gate? Or how does the binding of ligand transfer energy to open the gate in a ligand gated channel etc. The movement of the voltage sensor in K^+ channel has been studied in detail for the last couple of years with controversial results coming from different groups.

The energy of ligand binding in a ligand-gated channel can be transmitted tens of angstroms through the structure of a protein to open the channel. It is not well understood how this energy transfer can open the gate. The simplicity in function and lack of desensitization makes CNG channels a favorite target in studying the structure function relation ship of ligand-gated ion channels. Previous studies suggested several possible rearrangements in the pore forming region of CNG channels associated with the binding of ligand in the CNBD. Still the transmission of energy (as a result of ligand binding) from CNBD toward the gate through the C-linker is largely unclear. Even though the crystal structures can give amazing insight into the structural details, at the moment, it lacks the potential to decipher the modulation of channels during its activation. Electrophysiology can improve substantially our knowledge about channel rearrangement during closed to open transition. Electrophysiology combined with molecular biology with the help of homology modeling can be a powerful tool to address this problem.

In order to understand the aforesaid structure-function relationship of CNG channels, I addressed the molecular rearrangement of these channels during channel activation. The substituted cysteine accessibility method developed by Akabas et al. (1992) is a widely used strategy in studying this kind of problems. The amino acid of interest can be specifically mutated to a cysteine and challenged with different thiol modifying reagents. The change in the cGMP evoked current before and after application of the thiol modifying reagents in the closed state or in the open state can provide information regarding the rearrangement or proximity of those homologous residues from different subunits. The information, thus, achieved can be used as spatial restraints in refining the homology model of the channel.

To achieve my goal I aimed, first of all, to substitute all residues in the pore region one by one with a cysteine and to challenge with thiol specific reagents with a hope to obtain spatial restrain to refine the CNG channel model. It is widely believed that the recently obtained KcsA crystal structure is a good homology template for CNG channel. My second aim was to check this hypothesis. The crystal structure of CNBD of HCN channel is supposed to be a good model for the CNBD of CNG channel also. Checking whether this structure is a possible template for the CNBD of CNG channel was my third aim.

In the current study I have used excised inside-out patch clamp method as the electrophysiological tool. *Xenopus leavis* oocyte was used as the expression system for the heterologous expression of the homologous CNGA1 channel. The ease of handling and the readiness in patching make *Xenopus leavis* oocytes advantageous over other expression systems. The simplicity to modify (mutate) and the native (heterologous CNG channel) like physiological characters (most–if not all) of homologous CNGA1 channel make them a very good tool to study the structure – function relationship of ligand gated channels.

Chapter 2

Materials and Methods

See the enclosed articles

Chapter 3

Results

See the enclosed articles

Structural basis of gating of CNG channels

Alejandro Giorgetti[1], **Anil V. Nair**[1], Paolo Codega, Vincent Torre, Paolo Carloni*

Istituto Nazionale per la Fisica della Materia (INFM DEMOCRITOS Modeling Center for Research

In aTOmistic Simulation) and International School for Advanced Studies (SISSA)

International School for Advanced Studies

via Beirut 2-4 I-34014 Trieste, Italy

Structural basis of gating of CNG channels

Alejandro Giorgetti[1], Anil V. Nair, Paolo Codega, Vincent Torre, Paolo Carloni*

Istituto Nazionale per la Fisica della Materia (INFM – DEMOCRITOS Modeling Center for Research In aTOmistic Simulation) and International School for Advanced Studies (SISSA), Via Beirut 4, 34014 Trieste, Italy

Abstract Cyclic nucleotide-gated (CNG) ion channels, underlying sensory transduction in vertebrate photoreceptors and olfactory sensory neurons, require cyclic nucleotides to open. Here, we present structural models of the tetrameric CNG channel pore from *bovine rod* in both open and closed states, as obtained by combining homology modeling-based techniques, experimentally derived spatial constraints and structural patterns present in the PDB database. Gating is initiated by an anticlockwise rotation of the N-terminal region of the C-linker, which is then, transmitted through the S6 transmembrane helices to the P-helix, and in turn from this to the pore lumen, which opens up from 2 to 5 Å thus allowing for ion permeation. The approach, here presented, is expected to provide a general methodology for model ion channels and their gating when structural templates are available and an extensive electrophysiological analysis has been performed.
© 2005 Federation of European Biochemical Societies. Published by Elsevier B.V. All rights reserved.

Ion channels are membrane spanning proteins that allow ions, such as K^+, Na^+, Ca^{2+} and Cl^-, to cross the hydrophobic core of the cell membrane [1]. Because of the well-known difficulties in obtaining high resolution 3D structures by X-ray crystallography of ion channels, alternative strategies based on computational biology tools are currently used to investigate their biophysical properties (for reviews on ion channel modelling see: [2–4]).

Here, we present a computational structural study on the widely characterized homotetrameric cyclic nucleotide-gated channel (CNG), from *bovine rod*, composed by the subunit CNGA1 [5], which forms functional assemblies with the same selectivity and gating properties as the native channels, which are instead heteromeric tetramers. Each subunit consists of two domains: (i) a transmembrane domain formed by six transmembrane helices (S1–S6) and a pore helix (P-helix) with the same topology of voltage-gated K^+ channels [6,7]. (ii) A cytoplasmic domain formed by the cyclic nucleotide binding domain (CNBD) which is linked to the transmembrane domain through the so called C-linker region. The pore, unselective for Na^+ and K^+, is believed to gate via a conformational change of S6 transmembrane helix (TMH) initiated by the

binding of cyclic nucleotides to the binding domains. This conformational change is transduced to the pore via coupling with the four P-helices [8,9].

Here, we provide a molecular basis to this proposal by constructing models of the transmembrane region of the CNGA1 channel from *bovine rod*, which includes S6, P-helix-loop (P-helix + pore wall or filter), along with the C-linker N-terminal section, for which there exist a great amount of experimental data. Models of P-helix-loop and S6 are based on the KcsA X-ray structure [10,11], whose topology has been suggested to be similar to that of CNG channels [6]. The C-linker domain was modeled using the C-linker of the HCN (from *mouse*) channel in ligand bound state, for which the X-ray structure has been recently solved [12]. This template shares a high sequence identity (>30%) with CNG channels in this particular region. Finally, the obtained models refer to residues from Arg345 to Arg422 of the CNGA1 channel.

The models, obtained based on the alignments shown in Fig. 1A, were refined by the inclusion of an extensive dataset of spatial constraints inferred by electrophysiological measurements on cysteine mutants (Fig. 1B and C). A large set (about 50) of structural constraints among $C\alpha$ atoms are inferred from measurements in the presence of metal ions (Table 1) [6,13–20]: (i) Cd^{2+}, which can block the channel [21] when it binds to, at least, two cysteine residues (see Table 1). Estimates obtained by a calculation of residue–residue distribution function based on the RCSB Protein Data Bank [22] suggest that the $C\alpha$ of these cysteines are located at about 11–13 Å (Fig. 1D and the Note in the figure caption) [23]. (ii) Mild-oxidizing agent copper phenanthroline (CuP) favors disulfide bridge formation between two cysteines separated by a distance going from 6 to 11 Å (see Fig. 1D and the Note in the figure caption).

A smaller set of data (about 20) provide information on solvent accessibilities, inferred from measurements in the presence of three differently sized and charged sulfhydryl specific reagents such as $MTSET^+$, $MTSEA^+$ and $MTSES^-$. Indeed, these compounds may react with solvent accessible cysteines [24] (Table 1) [25].

In the S6 TMH and in the N-terminal portion of the C-linker, Cd^{2+} blockage is almost absent for residues upstream Gly395 in both open and closed states, whilst it is strongly state dependent for residues downstream Asn400 (Table 1 and Fig. 1C). As a result, in the open state, the N-terminal section of the C-linker is bent around a hinge located approximately between Val391 and Gly395, and it is also rotated in the anticlockwise sense by about 60° (around the helix axis) related to the closed conformation, assuming a configuration similar to that of the template (Fig. 2). These conformational changes resemble somehow that proposed for the Shaker K^+ channel [26], in

*Corresponding author.
E-mail address:* carloni@sissa.it (P. Carloni).

[1] Present address: Department of Biochemical Sciences, University of Rome "La Sapienza".
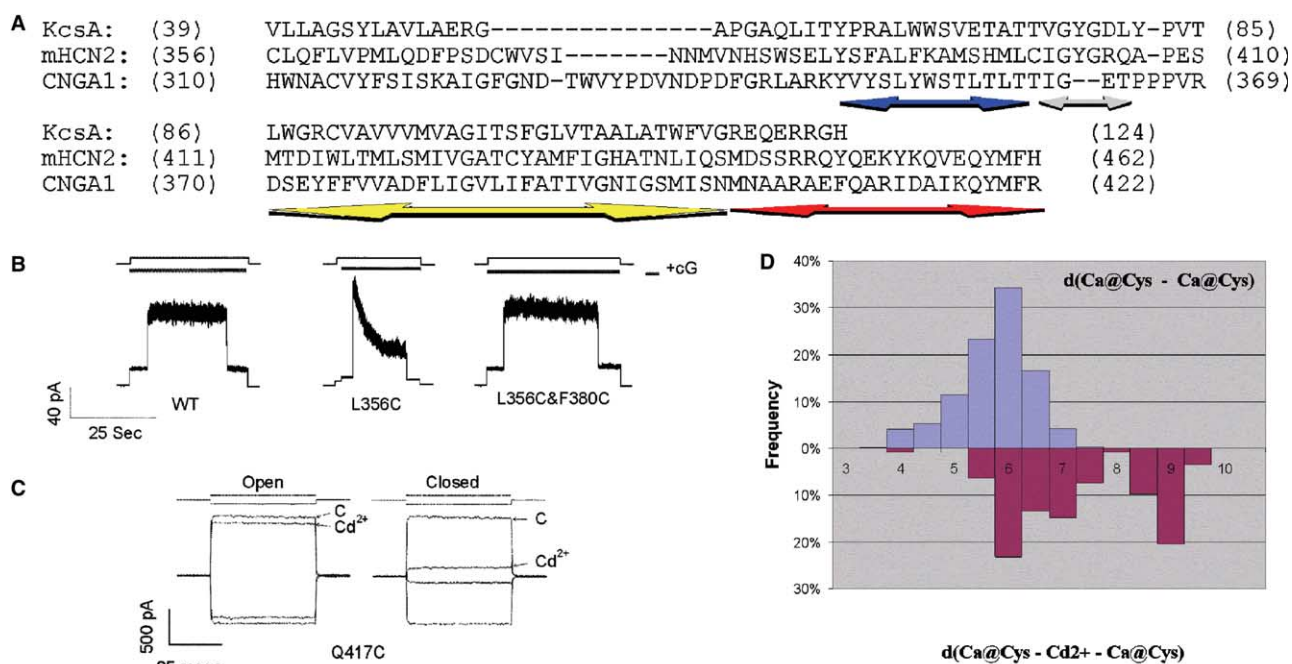
Fig. 1. (A) Sequence alignment of the CNGA1 channel from bovine rod used for building up the structure by homology modelling. The templates are: KcsA K$^+$ channel from *Streptommyces lividans* [11,30] for P-helix-loop and TM2/S6, and HCN from *mouse* for the C-linker [12]. Colour coding (for all figures): Gray: pore walls (filter). Blue: P-helix. Yellow: S6 transmembrane helix. Red: C-linker N-terminal section. Selected experiments taken from [18,19]: (B) Current response for wild type (wt), mutant L356C and double mutant L356C & F380C in the presence of 1 mM cGMP (cG). L356C desensitise while double mutant shows similar response like wt. (C) Effect of 100 μM Cd^{2+} in the open and closed states of mutant Q417C (C: control current; Cd^{2+} is the current after cadmium application for 5 min). (D) Distances between Cα of cysteines forming disulfide bridges or coordinating to Cd^{2+} ions (blue and red, respectively). Distributions were obtained by screening of the PDB data bank [22]. For the latter distance, note that there are two distributions (from 4 to 7.5 and 8.5–10 Å) associated to complexes involving two adjacent and opposite cysteine residues, respectively. Note: In the used distance restraints (see text and Table 1) an average of 2.5–3 Å was added, in order to consider thermal fluctuations.

which the S6 TMH bends around a valine residue (Val374). This residue is in correspondence to CNG's Val391, suggesting a common mechanism in the gating of a variety of ion channels.

In the P-helix-loop region, formed by the P-helix and the putative filter region (known also as the pore walls), the following structural features can be established.

In the P-helix, L356 forms hydrophobic interactions with F380@S6. In fact, L356C desensitizes and F380C shows locking effects, whilst L356C & F380C double mutant (Table 1 and Fig. 1B) behaves as wt, suggesting that in the latter case the hydrophobic interactions are substituted by an S–S bridge (Fig. 2). In addition, this helix changes its location in space on passing from closed to open form. Indeed, Thr355 and Leu358 of the P-helix are accessible to extracellular solvent only in the closed state, whilst Val348 and Leu351 are accessible in both states (Table 1).

For the filter, we notice that: (i) the homology of the sequences here is very low (Fig. 1). (ii) The filter GYG motif for K$^+$ channels is *not* conserved in CNG channels (Fig. 1), as the Tyr residue and one Gly residue have been lost during evolution. Thus, there must be two gaps on passing from the K$^+$ channel sequence to that of the CNG channel. As a result, the accuracy in this region is clearly very low and the only structural information should come from experimental data [13]. Specifically, it is found that Thr360 is solvent accessible in both states and this residue exhibits different conformation in the open and closed conformation, as shown by the differences in response upon Cd^{2+} addition (Table 1): In the open state, the channel is blocked by Cd^{2+}, and thus the distance be-

tween the T360C's Cα should be of about 11–13 Å (Table 1), whilst in the closed state it is not blocked, so this distance should be larger than 14 Å. The experimental data on Thr360 have immediate consequences on the conformation of the adjacent residues Ile361 and Gly362: in both cases, the distances between Cα belonging to opposite subunits increase in passing from the closed to the open conformation (e.g. distance between opposite Gly362 Cα increases from 3 to about 6 Å, Fig. 2), making the pore lumen to increase upon opening, till a diameter of about 5 Å. Although the difficulties in modelling and the low accuracy found in this region, this result, and in particular the variation of the pore lumen obtained in the models (Fig. 2), is corroborated by measurements based on the permeability of the channel to large organic cations (such as NH$_4^+$, CH$_3$NH$_3^+$, (CH$_3$)$_2$NH$_2^+$, (CH$_3$)$_3$NH$^+$ and CH$_2$CH$_3$NH$_3^+$) [27–29]: using permeability information, it was possible to estimate that the diameter of the narrowest part of bovine CNG channel pores in the open configuration measures between 4 and 6 Å [27–29].

On the basis of these findings, we propose that gating occurs by bending and an anticlockwise rotation by about 60° (around the helix axis and seen from the extracellular side of the membrane) of the C-linker N-terminal section (Fig. 2). This rotation is transmitted upwards, making the upper part of S6 to rotate anticlockwise by about 30° (around the helix axis). Due to the direct interaction of S6 with the P-helix, this motion is transmitted to the latter, which rearranges so as its terminal Thr360 residues and therefore, the lower part of the pore wall, leading to the opening of the pore lumen.

Table 1
Spatial constraints involving P-helix-loop, S6 and N-term@C-linker of CNGA1 channels from bovine rod, based on experimental data on cysteine mutants

Mutant	Cd^{2+}		MTS		Restraint
	Open	Closed	Open	Closed	
V348C	Block-E NoEff-I [20]	Block-E NoEff-I [20]	Block-MTSET-E [6,13]	Block-MTSET-E [6,20]	Accessible from outside open/closed state
	–	–	NoEff-MTSET-E [13]	NoEff-MTSET-E [13]	
S350C	NoEff E&I [16]	NoEff E&I [16]	NoEffMTSET-E [13]	NoEff-MTSET-E [13]	
L351C	–	–	**NoEff-MTSET-E** [20]	**Block-MTSET-E** [20]	Accessible from outside closed state
Y352C	–	–	NoEff-MTSET-E [6]	NoEff-MTSET-E [13]	
W353C	–	–	NoEff-NTSET-E [6]	NoEff-MTSET-E [13]	
S354C	–	–	NoEff-MTSET-E [6]	NoEff-MTSET-E [13]	
T355C	–	–	**NoEff-MTSET-E** [6]	**Block-MTSET-E** [13]	Accessible from outside closed state
L356C	–	–	NoEff-MTSET-E [6]	NoEff-MTSET-E [13]	
T357C	–	–	NoEff-MTSET-E [6]	NoEff-MTSET-E [13]	
L358C	–	–	**NoEff-MTSET-E** [20]	**Block-MTSET-E** [13]	Accessible from outside closed state
T359C			NoEff-MTSET-E [13]	NoEff-MTSET-E [13]	
T360C	**Block-I** [20]	**NoEff-I** [20]	Poten-MTSES-I [18]	Poten-MTSES- I [18]	$D(C\alpha–C\alpha) \approx 11$ Å (open) $D(C\alpha–C\alpha) > 14$ Å (closed) Accessible from inside
I361C	Block-I [20]	Block-I [20]	NoEff-MTSET-E [13]	NoEff-MTSET-E [13]	Accessible from inside
G362C	–	–	NoEff-MTSET-E [13]	NoEff-MTSET-E [13]	
E363C	–	–	Block-MTSET-E [13]	Block-MTSET-E [13]	Accessible from outside open/closed-state
T364C	Block-E NoEff-I [20]	Block-E NoEff-I [20]	Block-MTSET-E NoEff-MTSET-I [6,13]	Block-MTSET-E NoEff-MTSET-I [6,13]	Accessible from outside open/closed-state
P365C	–	–	NoEff-MTSET-E,I [6]	NoEff-MTSET-E,I [6]	
P366C	Block-E NoEff-I [20]	Block-E NoEff-I [20]	Block-MTSET-E NoEff-MTSET-I [6,13]	Block-MTSET-E NoEff-MTSET-I [6,13]	Accessible from outside open/closed-state
F375C	NoEff-I [19]	NoEff-I [19]	–	–	$D(C\alpha–C\alpha) > 14$ Å
V376C	NoEff-I [19]	NoEff-I [19]	–	–	$D(C\alpha–C\alpha) > 14$ Å
V377C	NoEff-I [19]	NoEff-I [19]	–	–	$D(C\alpha–C\alpha) > 14$ Å
A378C	NoEff-I [19]	NoEff-I [19]	–	–	$D(C\alpha–C\alpha) > 14$ Å
D379C	NoEff-I [19]	NoEff-I [19]	–	–	$D(C\alpha–C\alpha) > 14$ Å
F380	Poten-I [19]	Block-I [19]	–	–	$D(F380C\alpha–C314C\alpha) < 8$ Å **CuP**: Disulfide bridge
F380C–L356C	NoEff-I [19]	NoEff-I [19]	–	–	$D(F380C\alpha–L356C\alpha) \approx 6$ Å Disulphide bridge formation
I381C	NoEff-I [19]	NoEff-I [19]	–	–	$D(C\alpha–C\alpha) > 14$ Å
I382C	NoEff-I [19]	NoEff-I [19]	–	–	$D(C\alpha–C\alpha) > 14$ Å
I383C	NoEff-I [19]	NoEff-I [19]	–	–	$D(C\alpha–C\alpha) > 14$ Å
V384C	NoEff-I [19]	NoEff-I [19]	Block-MTSEA-I [15]		$D(C\alpha–C\alpha) > 14$ Å Face central pore
L385C	NoEff-I [19]	NoEff-I [19]	NoEff-MTSEA-I [15]		$D(C\alpha–C\alpha) > 14$ Å
I386C	NoEff-I [19]	NoEff-I [19]	NoEff-MTSEA-I [15]		$D(C\alpha–C\alpha) > 14$ Å
F387C	NoEff-I [19]	NoEff-I [19]	Block-MTSEA-I [15]		$D(C\alpha–C\alpha) > 14$ Å Face central pore
A388C	NoEff-I [19]	NoEff-I [19]	Block-MTSEA-I [15]		$D(C\alpha–C\alpha) > 14$ Å Face central pore
T389C	NoEff-I [19]	NoEff-I [19]	Block-MTSEA-I [15]		$D(C\alpha–C\alpha) > 14$ Å
I390C	NoEff-I [19]	NoEff-I [19]	NoEff-MTSEA-I [15]		$D(C\alpha–C\alpha) > 14$ Å
V391C	Block-I [19]	Block-I [19]	Block-MTSET- I [16] Block-MTSEA-I [16]	NoEff MTSET-I [16] BlockMTSEA-I [16]	$D(C\alpha–C\alpha) < 14$ Å Face central pore
G392C	NoEff-I [19]	NoEff-I [19]	Block-MTSET-I [16] Block-MTSEA-I [15]		$D(C\alpha–C\alpha) > 14$ Å Face central pore
N393C	NoEff-I [19]	NoEff-I [19]	Block-MTSET-I [16] NoEff-MTSEA-I [15]⁻		$D(C\alpha–C\alpha) > 14$ Å
I394C	NoEff-I [19]	NoEff-I [19]	Block-MTSET-I [16]⁻ Block-MTSEA-I [15]	NoEff-MTSET-I [16]	$D(C\alpha–C\alpha) > 14$ Å Face central pore
G395C	Block-I [19]	Block-I [19]	Block-MTSET-I [16]⁻ Block-MTSEA-I [15]		$D(C\alpha–C\alpha) < 14$ Å Face central pore
S396C	NoEff-I [19]	Block-I [19]	Block-MTSET-I [16]⁻ Block-MTSEA-I [15]	Block-MTSET-I [16]	$D(C\alpha–C\alpha) < 14$ Å
S397C			NoEff-MTSET-I [16]⁻ NoEff-MTSEA-I [15]	–	$D(C\alpha–C\alpha) < 14$ Å
I398C	NoEff-I [19]	NoEff-I [19]	Block-MTSET-I [16] NoEff-MTSEA-I [15]	–	$D(C\alpha–C\alpha) > 14$ Å (open) $D(C\alpha–C\alpha) \approx 11$ Å (closed)
S399C	Block-I [19]	BlockI [19]	Block-MTSET-I [16] Block-MTSEA-I [15]	Block-MTSET-I [16]	$D(C\alpha–C\alpha) < 14$ Å Face central pore
N400C	**NoEff-I** [19]	**Block-I** [19]	–	–	$D(C\alpha–C\alpha) > 14$ Å (open) $D(C\alpha–C\alpha) \approx 11$ Å (closed)

Table 1 (*continued*)

Mutant	Cd²⁺		MTS		Restraint
	Open	Closed	Open	Closed	
M401C	NoEff-I [19]	NoEff-I [19]	–	–	$D(C\alpha–C\alpha) > 14$ Å
N402C	**NoEff-I** [19]	**Block-I** [19]	–	–	$D(C\alpha–C\alpha) > 14$ Å (open)
					$D(C\alpha–C\alpha) \approx 11$ Å (closed)
A403C	**NoEff-I** [19]	**Block-I** [19]	–	–	$D(C\alpha–C\alpha) > 14$ Å (open)
					$D(C\alpha–C\alpha) \approx 11$ Å (closed)
A404C	**NoEf- I** [19]	**Block-I** [19]	–	–	$D(C\alpha–C\alpha) > 14$ Å (open)
					$D(C\alpha–C\alpha) \approx 11$ Å (closed)
R405C	NoEff-I [19]	NoEff-I [19]	–	–	$D(C\alpha–C\alpha) > 14$ Å
A406C	**NoEff-I** [19]	**Block-I** [19]	–	–	$D(C\alpha–C\alpha) > 14$ Å (open)
					$D(C\alpha–C\alpha) \approx 11$ Å (closed)
D407C	**NoEff-I** [19]	**Block-I** [19]	–	–	$D(C\alpha–C\alpha) > 14$ Å (open)
					$D(C\alpha–C\alpha) \approx 11$ Å (closed)
F408C	**NoEff-I** [19]	**Block-I** [19]	–	–	$D(C\alpha–C\alpha) > 14$ Å (open)
					$D(C\alpha–C\alpha) \approx 11$ Å (closed)
Q409C	**NoEff-I** [19]	**Block-I** [19]	–	–	$D(C\alpha–C\alpha) > 14$ Å (open)
					$D(C\alpha–C\alpha) \approx 11$ Å (closed)
A410C	NoEff-I [19]	NoEff-I [19]			$D(C\alpha–C\alpha) > 14$ Å
I412C	NoEff-I [19]	NoEff-I [19]	–	–	$D(C\alpha–C\alpha) > 14$ Å
A413C	**Block-I** [19]	**Poten-I** [19]			$D(C\alpha–C\alpha) > 14$ Å
A414C	**NoEff-I** [19]	**Block-I** [19]	–	–	$D(C\alpha–C\alpha) > 14$ Å (open)
					$D(C\alpha–C\alpha) \approx 11$ Å (closed)
I415C	NoEff-I [19]	NoEff-I [19]	–	–	$D(C\alpha–C\alpha) > 14$ Å
L416C	NoEff-I [19]	NoEff-I [19]	–	–	$D(C\alpha–C\alpha) > 14$ Å
Q417C	**NoEff-I** [19]	**Block-I** [19]			$D(C\alpha–C\alpha) > 14$ Å (open)
					$D(C\alpha–C\alpha) \approx 11$ Å (closed)
Y418C	Block-I [19]	Block-I [19]	–	–	$D(C\alpha–C\alpha) > 14$ Å (open)
					$D(C\alpha–C\alpha) \approx 11$ Å (closed)
M419C	NoEff-I [19]	NoEff-I [19]	–	–	$D(C\alpha–C\alpha) > 14$ Å
H420C	NoEff-I [19]	NoEff-I [19]			$D(C\alpha–C\alpha) > 14$ Å
F421C	NoEff-I [19]	NoEff-I [19]	–	–	$D(C\alpha–C\alpha) > 14$ Å
R422C	**NoEff-I** [19]	**Block-I** [19]	–	–	$D(C\alpha–C\alpha) > 14$ Å (open)
					$D(C\alpha–C\alpha) \approx 11$ Å (closed)

Distance restraints always refer to opposite Cα in the tetramer, unless specified. Accessibilities patterns were used to constraint the P-helix orientation in agreement with [13]. The first, second, third and fourth bracket refer to the blue, gray, yellow and red color coding in the figures. Abbreviation details: No Eff: no effect; Block: irreversible blockage of the current; E and I: measurements carried out with the reagents in the extracellular and intracellular sides of the membrane, respectively; Poten: current potentiation; MTS: methylsulfonate agents – MTSET, MTSEA, MTSES – (see text). Experimental information: The CNGA1 channel contained native cysteines [6]; experiments performed in tandem construct of CNGA1 (with native cysteines) channels where cysteine mutants were introduced in only one of the tandem component [13]; experiments performed in a cysteine-free CNGA1 channel from bovine rods [15,16]; the CNGA1 channel contained native cysteines [18–20].
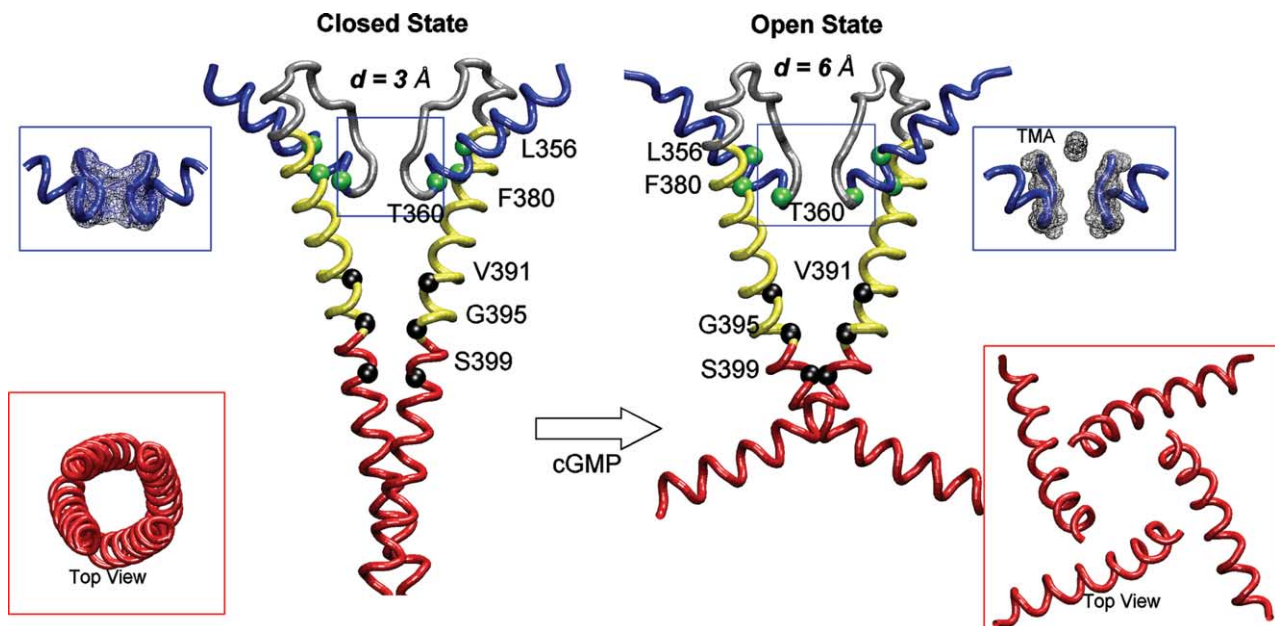

Fig. 2. Structural models [31] of S6, the P loop of the transmembrane domain along with the N-term@C-linker in the closed and open states. Only two opposite subunits are shown for the sake of clarity. The structures were obtained by homology modelling (see Fig. 1B) by using Modeller6v2 [32] with the inclusion of the spatial constraints in Table 1. Selected residues's Cα are shown. *d* is the shortest distance between opposite Cα's in the pore. Insets: (i) Detail of the central P-Helix-Loop region (able to permeate trimethylammonium ion (TMA⁺) only in the open conformation) (Blue). Also here only two opposite subunits are shown. (ii) Top view of the N-term@C-linker (Red).

In conclusion, the initial event of cyclic nucleotide binding is transmitted to the pore walls by a remarkable and sophisticated coupling of conformational changes spanning throughout the entire cytoplasmic and transmembrane domains of the channel.

References

[1] Hille, B. (2001) Ionic Channels of Excitable Membranes, Sinaver Associate, Sunderland, MA.

[2] Giorgetti, A. and Carloni, P. (2003) Molecular modelling of ion chanels: structural predictions. Curr. Opin. Chem. Biol. 7 (1), 150–156.

[3] Capener, C.E, Kim, H.J., Arinaminpathy, Y. and Sansom, M.S. (2002) Ion channels: structural bioinformatics and modelling. Hum. Mol. Genet. 11 (20), 2425–2433.

[4] Simoes, M., Garneau, L., Klein, H., Banderali, U., Hobeila, F., Roux, B., Parent, L. and Sauve, R. (2002) Cysteine mutagenesis and computer modeling of the S6 region of an intermediate conductance IKCa channels. J. Gen. Physiol. 120 (1), 99–116.

[5] Kaupp, U.B., Niidome, T., Tanabe, T., Terada, S., Bonigk, W., Stuhmer, W., Cook, N.J., Kangawa, K., Matsuo, H. and Hirose, T. (1989) Primary structure and functional expression from complementary DNA of the rod photoreceptor cyclic GMP-gated channel. Nature 342, 762–766.

[6] Becchetti, A., Gamel, K. and Torre, V. (1999) Cyclic nucleotide-gated channels. Pore topology studied through the accessibility of reporter cysteines. J. Gen. Physiol. 114, 377–392.

[7] Sesti, F., Eismann, E., Kaupp, U.B., Nizzari, M. and Torre, V. (1995) The multi-ion nature of the cGMP-gated channel from vertebrate rods. J. Physiol. 487 (Pt. 1), 17–36.

[8] Johnson, J. and Zagotta, W.N. (2001) Rotation movement during cyclic nucleotide-gated channel opening. Nature 412, 917–921.

[9] Matulef, K., Flynn, G.E. and Zagotta, W.N. (1999) Molecular rearrangements in the ligand-binding domain of cyclic nucleotide-gated channels. Neuron 24, 443–452.

[10] Jiang, Y., Lee, A., Chen, J., Cadene, M., Chait, B.T. and MacKinnon, R. (2002) The open pore conformation of potassium channels. Nature 417, 523–526.

[11] Zhou, Y., Morais-Cabral, J.H., Kaufman, A. and MacKinnon, R. (2001) Chemistry of ion coordination and hydration revealed by a K+ channel-Fab complex at 2.0 Å resolution. Nature 414, 43–48.

[12] Zagotta, W.N., Olivier, N.B., Black, K.D., Young, E.C., Olson, R. and Gouaux, E. (2003) Stuctural basis for modulation and agonist specificity of HCN pacemakers channels. Nature 425, 200–205.

[13] Liu, J. and Siegelbaum, S.A. (2000) Change of pore helix conformational state upon opening of cyclic nucleotide-gated channels. Neuron 28, 899–909.

[14] Flynn, G.E. and Zagotta, W.N. (2001) Conformational changes in S6 coupled to the opening of cyclic nucleotide-gated channels. Neuron 30, 689–698.

[15] Flynn, G.E. and Zagotta, W.N. (2001) A cysteine scan of the inner vestibule of cyclic nucleotide-gated channels reveals architecture and rearrangement of the pore. J. Gen. Physiol 121, 563–582.

[16] Flynn, G.E., Johnson, J.P. and Zagotta, W.N. (2001) Cyclic nucleotide-gated channels: shedding light on the opening of a channel pore. Nat. Rev. Neurosci. 2, 643–651.

[17] Johnson, J.P. and Zagotta, W.N. (2001) Rotational movement during cyclic nucleotide-gated channel opening. Nature 412, 917–921.

[18] Mazzolini, M., Codega, P., Nair, A.V, Giorgetti, A., Torre, V. Conformational changes in the S6 domain of CNGA1 channels probed by intracellular Cd(II), J. Gen. Physiol., submitted.

[19] Nair, A.V., Mazzolini, M., Codega, P., Giorgetti, A., Torre, V. Conformational changes in the pore of CNGA1 channels during gating, revealed by electrophysiological experiments with mutant channels, J. Gen. Physiol., submitted.

[20] Becchetti, A. and Roncaglia, P. (2000) Cyclic nucleotide-gated channels: intra and extracellular accessibility to Cd^{2+} of substituted cysteine residues within the P-loop. Pflugers Arch. 440, 556–565.

[21] Rothberg, B., Shin, K., Phale, P. and Yellen, G. (2002) Voltage-controlled gating at the intracellular entrance to a hyperpolarization-activated cation channel. J. Gen. Physiol. 119 (2002), 83–91.

[22] Berman, H.M., Westbrook, J., Feng, Z., Gilliland, G., Bhat, T.N., Weissig, H., Shindyalov, I.N. and Bourne, P.E. (2000) The Protein Data Bank. Nucleic Acids Res. 28, 235–242.

[23] The hypothesis that the presence of a close proximity between opposite H420 residues, as inferred in [8] by Ni^{2+} binding, is not consistent with the whole set of (about 22 experiments) data on the C-linker from N400C to R442C and it is therefore not included here.

[24] Akabas, M.H., Stauffer, D.A., Xu, M. and Karlin, A. (1992) Acetylcholine receptor channel structure probed in cysteine-substitution mutants. Science 258, 307–310.

[25] Because the topology of MthK is similar to that of KcsA, we have attempted using the former as a template for the open configuration. The MthK based constructs from Cd^{2+} adducts (Table 1) resulted in extremely large rearrangements (more than 10 Å), while causing relatively small rearrangements (overall RMSD of 3 Å) (Fig. 2) in the KcsA-based model. Thus, MthK was not considered any further.

[26] Webster, S.M., del Camino, D., Dekker, J.P. and Yellen, G. (2004) Intracellular gate opening in Shaker K+ channels defined by high-affinity metal bridges. Nature 428, 864–868.

[27] Goulding, E.H., Tibbs, G.R., Liu, D. and Siegelbaum, S.A. (1993) Role of H5 domain in determining pore diameter and ion permeation through cyclic nucleotide-gated channels. Nature 364, 61–64.

[28] Bucossi, G., Eismann, E., Sesti, F., Nizzari, M., Seri, M., Kaupp, U.B. and Torre, V. (1996) Time-dependent current decline in cyclic GMP-gated bovine channels caused by point mutations in the pore region expressed in *Xenopus* oocytes. J. Physiol. 493 (Pt. 2), 409–418.

[29] Laio, A. and Torre, V. (1999) Physical origin of selectivity in ionic channels of biological membranes. Biophys. J. 76, 129–148.

[30] Doyle, D.A., Morais-Cabral, J., Pfuetzner, R.A., Kuo, A., Gulbis, J.M., Cohen, S.L., Chait, B.T. and MacKinnon, R. (1998) The structure of the potassium channel: molecular basis of K+ conduction and selectivity. Science 280, 69–77.

[31] The final models can be found in the following web address: www.sissa.it/sbp/web/research/biomolecular_simula-tions/pdbfiles/.

[32] Sanchez, R. and Sali, A. (1997) Advances in comparative protein-structure modelling. Curr. Opin. Struct. Biol. 7, 206–214.

Locking CNGA1 Channels in the Open and Closed State

textbf*Anil V. Nair*[1], Monica Mazzolini, Paolo Codega, Alejandro Giorgetti, Vincent Torre

International School for Advanced Studies and Instituto Nazionale Fisica della Materia, I-34014

Trieste, Italy

Alejandro Giorgetti's present address is Biocomputing Department of Biochemical Sciences, University

of Rome "La Sapienza" P.le Aldo Moro, 5 00185 Rome, Italy.

Locking CNGA1 Channels in the Open and Closed State

Anil V. Nair, Monica Mazzolini, Paolo Codega, Alejandro Giorgetti, and Vincent Torre
International School for Advanced Studies and Instituto Nazionale Fisica della Materia, I-34014 Trieste, Italy

ABSTRACT   With the aim of understanding the relation between structure and gating of CNGA1 channels from bovine rod, an extensive cysteine scanning mutagenesis was performed. Each residue from Phe-375 to Val-424 was mutated into a cysteine one at a time and the modification caused by various sulfhydryl reagents was analyzed. The addition of the mild oxidizing agent copper phenanthroline (CuP) in the open (presence of 1 mM cGMP) or closed state locked the channel in the respective states. A subsequent treatment with the reducing agent DTT restored normal gating fully in the open state and partially in the closed state. This action of CuP was not observed when F380 was mutated into a cysteine in the cysteine-free CNGA1 channel and in the double mutant C314S&F380C. These observations suggest that these effects are mediated by the formation of a disulfide bond (S-S) between F380C and the endogenous Cys-314 in the S5 segment. It can be rationalized by supposing that during gating the S6 segment rotates anticlockwise—when viewed from the extracellular side—by $\sim$30°.

INTRODUCTION

CNG channels play a major role in sensory transduction of vertebrate photoreceptors and olfactory sensory neurons. They require cyclic nucleotides to open (1–7). Native CNG channels are heterotetramers composed of distinct subunit referred to as CNGA and CNGB (8,9). Homotetrameric CNGA1 channels from bovine rods when heterologously expressed give rise to functional channels with properties similar but not identical to those of native CNG channels (4). Each subunit is composed of 690 residues (4) encoding for a cyclic nucleotide-binding (CNB) domain made of $\sim$125 amino acids in the cytoplasmic C-terminal end (5,7).

The amino acid sequences of CNG and K^+ channels have a significant homology and both channels are members of the superfamily of voltage-gated channels (5). Therefore, it is highly possible that CNG and K^+ channels share the same gross three-dimensional (3D) topology. The 3D structure of several K^+ channels has been solved recently: the bacterial KcsA from *Streptomyces lividans* in the closed state (10,11), the bacterial MthK from *Methanobacterium thermautotrophicum* in the open state (12,13), and the KirBac 1.1 in the closed state (14). In all these K^+ channels the pore domain includes four identical subunits comprising two transmembrane helices, S5 and S6 (referred to as TM1 and TM2 in KcsA and MthK channels), a loop forming the filter region, and an additional small helix, not spanning the lipid membrane referred to as the P-helix (Fig. 1). S6 is involved in the gating of K^+ channels, whereas the loop forming the filter region does not change its conformation upon gating. In K^+ channels, the major structural difference on passing from the

closed to open conformation is the bending of S6 helix by 30° toward the lipid phase, around a glycine hinge (12,13).

In CNGA1 channels the gate is believed to be located in the pore itself (15–18) and a model of possible conformational changes in the pore region has been proposed (19). These conformational changes are initiated by the binding of cGMP in the CNB domain (4–7,18,20,21). This initial event must be transmitted to the pore region by conformational changes spanning throughout the entire cytoplasmic domain of the channel. As the S6 helix is connected to the C-linker and CNB domain, a signal must be transmitted to the pore region through S6.

With the aim of understanding the nature of this signal an extensive site-directed cysteine scanning mutagenesis was performed. Each residue—one by one—from Phe-375 to Val-424 was mutated into a cysteine and the modification produced by various sulfhydryl reagents was analyzed. During this analysis, we observed that mutant channel F380C was blocked by Cd^{2+} ions in the closed state but was potentiated in the open state. The irreversible potentiation of the mutant F380C caused by the addition of Cd^{2+} in the open state suggests some major changes in the gating of the mutant channel and we asked whether it was possible to lock the channel in the open state, in a way similar to that observed in the spHCN channel (22,23). Therefore we explored properties of the mutant channel F380C in more detail. The application of the mild oxidizing agent CuP in the presence of cGMP locked the channel in the open state. The addition of CuP in the closed state locked the channel in the closed state. The application of CuP did not lock the mutant channel F380C in a cysteine-free CNGA1 channel (24) neither in the open nor in the closed state. Similarly, application of CuP to the double mutant channel F380C&C314S did not have any significant effect. These results suggest the formation of disulfide bonds (S-S) between exogenous cysteines introduced in position 380 and endogenous Cys-314 in the S5 segment were responsible for the effect observed in the mutant channel F380C. These results provide clues for understanding

---
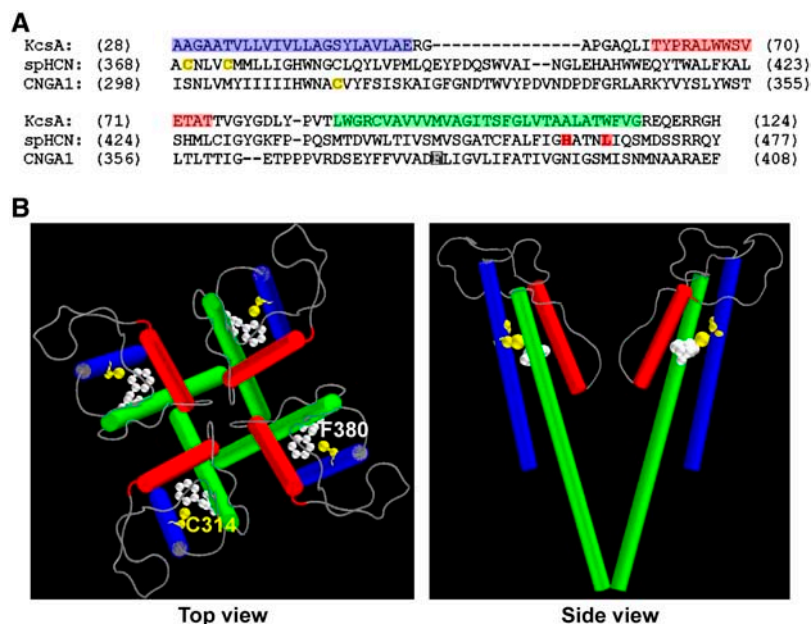
FIGURE 1 Sequence alignment of the KcsA, CNGA1, and spHCN channels. (A) Sequence alignments between the KcsA (K$^+$ channel from *Streptomyces lividans*), the CNGA1, and the spHCN channel (HCN channel from sea urchin sperm). Residues in blue, red, and green boxes of the KcsA channel indicate the S5, the P-helix, and the S6 domain, known to have an α-helical conformation. Yellow indicates cysteine residues. Residues involved in locking the spHCN channel in the open state (22) are shown in red boxes and Phe-380 of the CNGA1 channel is shown in a black box. (B) Homology model of CNGA1 channel showing the location of Cys-314 (in *yellow*) in the S5 domain flanking Phe-380 (in *white*) in the S6 domain. The homology model was obtained using the 3D structure of the KcsA channel as template with the sequence alignment shown in panel A. A top view of the homology model is shown on the left panel and a side view on the right. Colored cylinders indicate α-helices; blue, red, and green indicate the S5, the P-helix, and the S6 presumed domains.

conformational changes in the upper part of the S6 domain, which leads to channel opening (19).

MATERIALS AND METHODS

Molecular biology

The clone of the BROD CNGA1 channel, consisting of 690 residues, was mutated using the Quick Change Site-Directed Mutagenesis kit (Stratagene, La Jolla, CA). The DNA was sequenced with the sequencer LI-COR (4000L) to verify whether the mutation was correct. The selected residues were replaced by introducing a cysteine in the wild-type (WT) and cysteine-free WT as described (16,24). The double mutants were constructed by insertion of an additional mutation into the DNA with a single mutation. The RNAs were synthesized in vitro by using the mCAP RNA Capping kit (Stratagene).

Oocyte preparation and chemicals

The WT or mutant channel cRNAs were injected into *Xenopus laevis* oocytes (''Rettili'' Dr. Rainer Schneider, Varese, Italy). Oocytes were prepared as described (25). Injected eggs were maintained at 19°C in a Barth solution supplemented with 50 μg/ml gentamycin sulfate and containing (in mM): 88 NaCl, 1 KCl, 0.82 MgSO$_4$, 0.33 Ca(NO$_3$)$_2$, 0.41 CaCl$_2$, 2.4 NaHCO$_3$, 5 TRIS-HCl, pH 7.4 (buffered with NaOH). During the experiments, oocytes were kept in a Ringer solution containing (in mM): 150 NaCl, 2.5 KCl, 1 CaCl$_2$, 1.6 MgCl$_2$, 10 HEPES-NaOH, pH 7.4 (buffered with NaOH). All chemicals were purchased from Sigma Chemicals (St. Louis, MO).

Recording apparatus

cGMP-gated currents from excised patches were recorded with a patch-clamp amplifier (Axopatch 200B, Axon Instruments, Foster City, CA), 2–6 days after RNA injection, at room temperature (20–24°C). The perfusion system was as described (26) and allowed a complete solution change in <200 ms. Borosilicate glass pipettes had resistances of 3–5 MΩ in symmetrical standard solution. The standard solution on both sides of the membrane consisted of (in mM) NaCl, 110; HEPES, 10; and EDTA, 0.2 (pH 7.4). The membrane potential was usually stepped from 0 to ±60 mV. We used Clampex 8.0, Clampfit, and Matlab for data acquisition and analysis. Currents were low-pass filtered at 2 kHz and acquired digitally at 5 kHz.

Application of sulfhydryl-specific reagents

In the inside-out patch-clamp configuration, soon after patch excision, the cytoplasmic face of the plasma membrane was perfused with the same pipette-filling solution and then with the same solution containing 1 mM cGMP. The Cd^{2+} effect was tested by perfusing the intracellular side of the membrane with a standard solution without EDTA (to avoid partial Cd^{2+} chelation), supplemented with 100 μM CdCl$_2$ for variable time course, to study the effect in the closed state. For the open state we applied the above solution in the presence of 1 mM cGMP. CuP was prepared by mixing cupric sulfate and phenanthroline in a 1:3 ratio to a final concentration of 1 (or 10) μM of CuSO$_4$ in the standard solution without EDTA. Phenanthroline was dissolved in ethanol and cupric sulfate in water. DTT (5 mM) was dissolved in the standard solution without EDTA. CuP and DTT was freshly prepared everyday. DTT was used for a maximum of 5 h. Current traces illustrated in the figures were obtained by subtracting the current measured in the absence of cGMP before application of CuP and DTT to the current measured after the ionic manipulations (addition and removal of CuP, DTT, or cGMP) of the intracellular medium. Therefore, the current measured at the beginning of the experiment in the absence of cGMP is shown as zero (see *straight line* in panels A of Figs. 4–8).

Sequence alignment

Sequence alignments were performed using ClustalW multiple alignment program (27). Three-dimensional models of the S5, the P-helix, and the S6 domain of CNGA1 were constructed using a homology modeling approach as implemented in the program Modeller 6.2 (28,29). The molecular models in Figs. 1and 9 are prepared with VMD 1.8.2. visualization software.

RESULTS

CNG and K$^+$ channels belong to the same superfamily of voltage-gated ionic channels (30) and are most likely to share the common molecular architecture. Therefore, the structure of KcsA (10,11) is a possible template for the 3D structure of the pore, S5, and S6 domains of CNG channels (18). Fig. 1 A illustrates the sequence alignment between residues from Ala-28 to His-124 of the KcsA channel and from Iso-298 to Phe-408 of the CNGA1 channel and Ala-368–Tyr-477 of

spHCN channels (the hyperpolarization and cyclic nucleotide controlled channels from sea urchin sperm (31)). The S5, S6 domains and the P-helix of the KcsA channel are indicated in Fig. 1 *A* and it is believed that the aligned amino acids of the CNGA1 and spHCN channels have an α-helical configuration with a similar orientation in space.

With the aim of understanding the relation between structure and gating in CNGA1 channels an extensive site-directed cysteine scanning mutagenesis was performed in the S6 and C-linker domain of the CNGA1 channel and the effect of 100 μM Cd^{2+} added to the intracellular side of the membrane patch was investigated.

The mutant and WT constructs were expressed in *Xenopus laevis* oocytes and studied with the patch-clamp method in the excised inside-out patch configuration. The effect of the addition of 100 μM Cd^{2+} on the WT CNGA1 channel is illustrated in Fig. 2, *A–C*. Brief voltage pulses from -100 to $+100$ mV in step of 20 mV were alternated, while changing the medium bathing the intracellular side of the membrane patch. When Cd^{2+} ions were added in the presence of 1 mM cGMP (Fig. 2 *B*), the cGMP-activated current (Fig. 2 *A*) was reduced in a voltage-dependent way, presumably by binding to Glu-363 in the pore region (26,32). At higher negative voltages (below -40 mV; see also Becchetti and Roncaglia (15)), 100 μM Cd^{2+} did not block but potentiated the cGMP-activated current. This potentiation is similar to that observed in the presence of Ni^{2+} ions, known to be mediated by His-420 in the C-linker (33–35). Blockage at positive voltages and potentiation at higher negative voltages caused

by 100 μM Cd^{2+} in the WT CNGA1 channel were fully reversible when Cd^{2+} ions were removed from the bathing medium (Fig. 2 *C*). Similarly, exposures to 100 μM Cd^{2+} in the absence of cGMP did not cause any significant alteration of the cGMP-activated current measured after removing Cd^{2+} ions. The current voltage relation of the cGMP activated current in the presence of 1 mM cGMP and with (*open symbols*) and without 100 μM Cd^{2+} (*solid symbols*) are shown in panel *D*: Cd^{2+} ions potentiate the cGMP-activated current at negative voltages and block the current at positive voltages. Very similar results were obtained with a cysteine-free CNGA1 channel, here referred as $WT_{cys-free}$ kindly provided by William Zagotta (24). These observations provide a rationale to distinguish the action of Cd^{2+} ions mediated by the binding to exogenously introduced cysteines: significant changes of the cGMP-activated current (i.e., >20%), observed after exposure to 100 μM Cd^{2+} can be attributed to exogenously introduced cysteines.

During the cysteine scanning analysis of residues from Phe-375 to Val-424 the exposure of the intracellular side of the membrane to 100 μM Cd^{2+} ions for 5 min either had a negligible effect or blocked in an irreversible way the cGMP evoked current. The remarkable exception was mutant channel F380C; as shown in Fig. 2 *D*, when the mutant channel was exposed for 5 min to 100 μM Cd^{2+} ions in the presence of 1 mM cGMP, the cGMP-activated current was permanently activated by $37 \pm 15\%$ ($n = 7$) both at positive and negative voltages for at least 15 min after removal of Cd^{2+} ions from the intracellular medium. On the contrary, when Cd^{2+} ions were
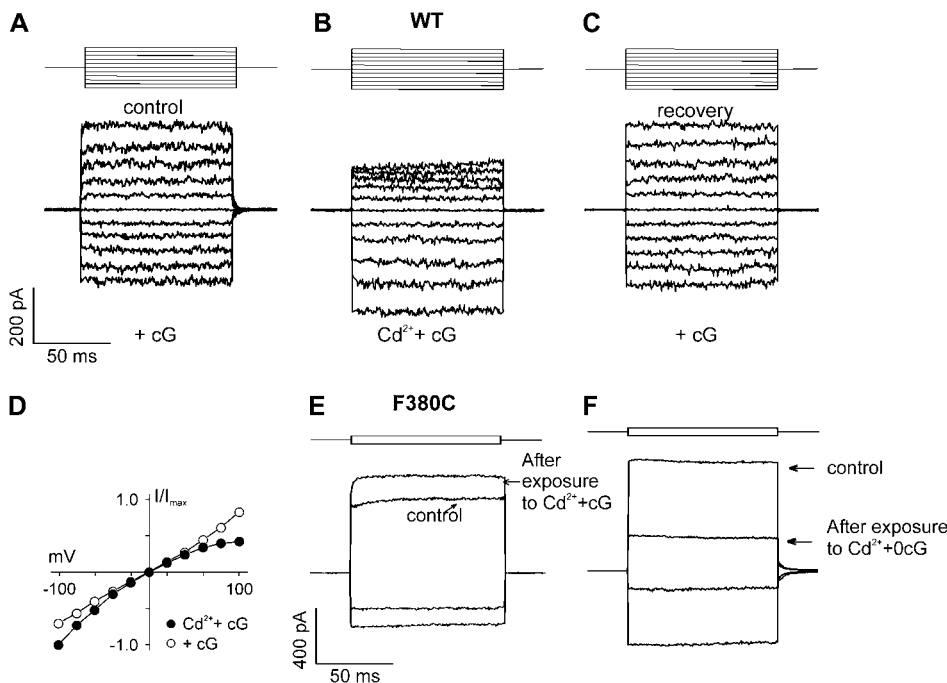

FIGURE 2 The effect of Cd^{2+} on the WT CNGA1 and mutant channel F380C. (*A–C*) Current recordings (average of three trials) at membrane voltages from -100 to 100 mV in 20 mV steps from the WT in control conditions (*A*), in the presence of 100 μM Cd^{2+} (*B*), and after removal of Cd^{2+} ions (*C*). No permanent modification in the cGMP-activated current after removal of Cd^{2+} ions was observed. (*D*) I/V relation of the WT. CNGA1 channel in control conditions (*open symbols*) and in the presence of 100 μM Cd^{2+} (*solid symbols*). (*E* and *F*) Permanent modification of the cGMP-activated current in mutant F380C after exposure to 100 μM Cd^{2+} ions in the presence and absence of 1 mM cGMP, respectively. In panels *D* and *E*, Cd^{2+} ions were applied for 5 min and the cGMP-activated current at ±60 mV was measured before application of Cd^{2+} ions (*traces labeled control*) and after removal of Cd^{2+} ions (*traces labeled after exposure* to Cd^{2+} + cG and Cd^{2+} + 0 cG) from the bathing solution. The cGMP-gated current was obtained as the difference of the current in the presence and in the absence of 1 mM cGMP. The current traces shown in panels *D* and *E* are the average of 10 individual trials. Thin horizontal lines represent the applied membrane potential.

added in the absence of cGMP, the cGMP-activated current was blocked both at positive and negative voltages for at least 15 min after Cd^{2+} removal (Fig. 2 *E*). Therefore we decided to investigate the mutant channel F380C in more detail.

Fig. 3 illustrates current recordings obtained from the WT (*A*), the mutant F380C (*B*), the $WT_{cys-free}$ (*C*), and the mutant channel $F380C_{cys-free}$ in a $WT_{cys-free}$ background (*D*), when the membrane voltage was applied from -100 to $+100$ mV in 20 mV steps. The mutant channel F380C either in the WT or in the $WT_{cys-free}$ background had a significant rectification: the ratio of the cGMP-activated current at -100 mV and at $+100$ mV in mutant channel F380C was $39 \pm 19\%$ ($n = 32$) and in the $WT_{cys-free}$ was $37 \pm 22\%$ ($n = 24$).

The irreversible potentiation of the mutant F380C (Fig. 2 *D*) caused by the addition of Cd^{2+} in the open state suggests some major changes in the gating of the mutant channel and we asked whether it was possible to lock the channel in the open state, in a way similar to that observed in the spHCN channel (22). Indeed, in the spHCN mutant channel L466C, nanomolar quantities of Cd^{2+} ions greatly slow down its closure once opened at negative voltages (22). In the presence of Cd^{2+} ions, the double mutant channel H462C&L466C once opened remains locked in the open configuration. This locking in the open state could be caused by the formation of disulfide bonds between exogenous cysteines and endogenous cysteines (Cys-373 and Cys-369 shown in *yellow* in Fig. 1 *A*) becoming close in the open state as suggested by Giorgetti et al. (23). Phe-380 (*white*) of the CNGA1 channel and His-462 and Leu-466 (*red*) of the spHCN channel are located in the S6 domain (Fig. 1 *A*), which presumably moves during channel gating. The yellow boxes in Fig. 1 *A* show the endogenous cysteines present in the S5 of the CNGA1 and spHCN channels. Fig. 1 *B* illustrates a top and side view of the molecular model of S5, pore, and S6 domains of the CNGA1 channel based on the homology with the KcsA channel and the sequence alignment of Fig. 1 *A*. According to this model, Cys-314 (shown in *yellow*) in the S5 domain is at a short distance from Phe-380 (shown in *white*) of the S6 domain. Therefore the endogenous Cys-314 could form S-S bonds with the exogenous sulfur atoms of mutant channel F380C. This interaction could be responsible for the locking of mutant channel F380C in the open and closed state, which will be described in the coming sections.

Locking of mutant channel F380C in the open state

When mutant channel F380C in the presence of 1 mM cGMP was exposed to the mild oxidizing agent CuP (1 or 10 μM) for some tens of seconds the amplitude of the cGMP-activated current increased significantly. After an exposure for several minutes to CuP in the presence of 1 mM cGMP, the cGMP-activated current persisted even after cGMP was removed from the solution bathing the intracellular side of the patch (Fig. 4, *A* and *B*). After exposure to CuP (1 or 10 μM) in the presence of 1 mM cGMP for at least 3 min, the current measured in the absence of cGMP significantly increased: data collected from 26 patches indicate that the current measured in the absence of cGMP was $68 \pm 25\%$ of that measured in the presence of 1 mM cGMP before CuP with cGMP application. This behavior could be either due to the locking of the channel in the open state (locked open) or due to an increase in the leak current caused by the deterioration of the patch. Two reasons suggest that the channels were locked in the open state. Firstly, as shown in Fig. 4, *E* and *F*, the I/V relations of the current flowing through the patch after CuP treatment had the same degree of rectification as the cGMP-activated current before CuP treatment; indeed the ratio of the cGMP-activated current at -100 mV and at $+100$ mV in mutant channel F380C was $39 \pm 19\%$ ($n = 32$) before exposure to CuP and after treatment of CuP in the presence of 1 mM cGMP. The same ratio of currents of CuP treatment in the absence of cGMP was $35 \pm 23\%$ ($n = 15$). Secondly, 100 μM Cd^{2+} blocked the current measured in the absence of cGMP of locked-open channel (Fig. 4, *D* and *F*) with the same voltage-dependent way as the current measured in the presence of 1 mM cGMP before CuP application (Fig. 4, *C* and *E*); the current at positive voltage is blocked more powerfully than the current at negative voltages. In addition, as shown in Fig. 4, *C* and *D*, a clear potentiation of the cGMP-activated current at higher negative voltages was observed, as observed in the WT CNGA1 channel (see Fig. 2). The blocking effect of Cd^{2+} ions of the cGMP-activated current at positive voltages was significantly larger in the mutant F380C than in the WT channel (compare Figs. 2 and 4), as shown from the current voltage relations shown in Fig. 4, *E* and *F*.

Perfusing mutant channels F380C locked in the open state with the standard solution without cGMP for several minutes
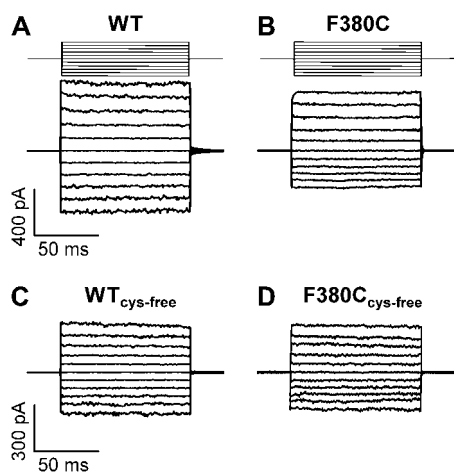

FIGURE 3 Comparison of the I/V relations in the WT (*A*), mutant F380C (*B*), $WT_{cys-free}$ (*C*), and mutant channel $F380C_{cys-free}$ in the $WT_{cys-free}$ background (*D*); current recordings at membrane voltages from -100 to 100 mV in 20 mV steps are shown. Each trace was obtained as an average of five individual trials. The cGMP-gated current was obtained as the difference of the current in the presence and in the absence of 1 mM cGMP. Thin horizontal lines represent the applied membrane potential.
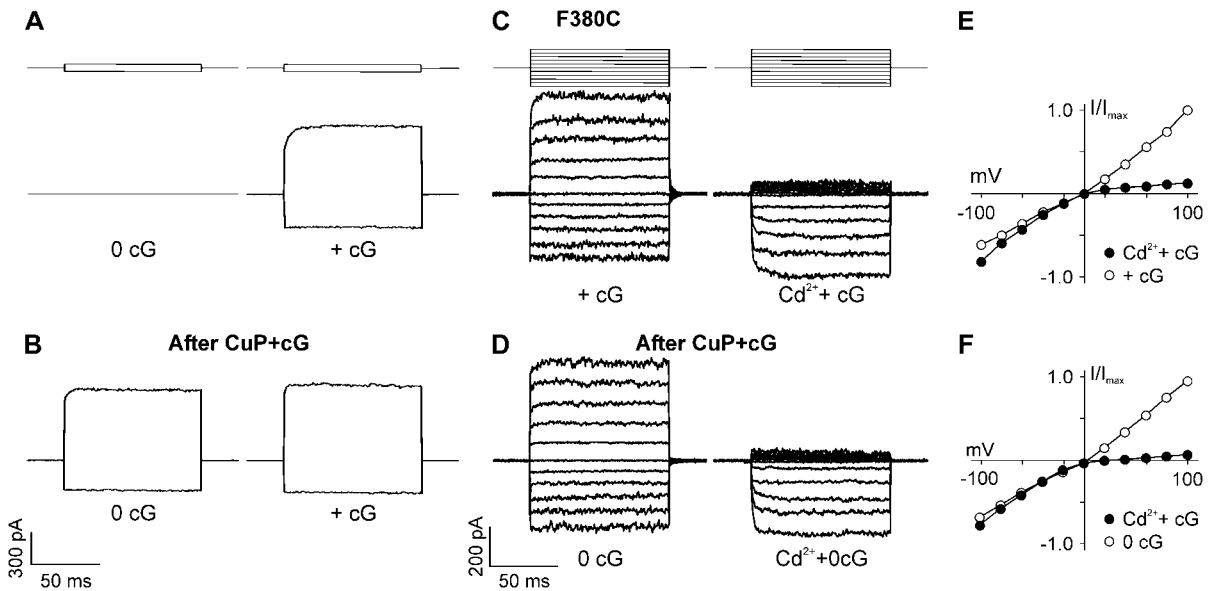
FIGURE 4   CuP in the presence of 1 mM cGMP locks the mutant channel F380C in the open state. (A) Currents recorded in the absence of cGMP (0 cG) and in the presence of 1 mM cGMP (+ cG) in mutant channels F380C. (B) The effect of exposure to 1 μM CuP for 5 min in the presence of 1 mM cGMP on the currents recorded in the absence of cGMP (0 cG) and in the presence of 1 mM cGMP (+ cG). In panels A and B, current recordings were obtained at ± 60 mV by averaging 10 individual trials. (C) The blockage of cGMP-activated current (+ cG) by 100 μM Cd^{2+} added to the medium bathing the intracellular side of the membrane patch (Cd^{2+} + cG) before CuP treatment. (D) Blockage by 100 μM Cd^{2+} (Cd^{2+} + 0 cG) of the current persistent (0 cG) in a locked-open channel after exposure to CuP + 1 mM cGMP. (E) I/V relation of the mutant F380C channel in control conditions (open symbols) and in the presence of 100 μM Cd^{2+} (solid symbols). (F) I/V relation of the current persistent in a locked-open channel (open symbols) and in the presence of 100 μM Cd^{2+} (solid symbols). In panels A and C the cGMP-activated current was obtained by subtracting the current measured in the absence of cGMP from the current measured in the presence of 1 mM cGMP. In panels B and D the current was obtained by subtracting the current measured in the absence of cGMP before CuP exposure from the current measured after CuP exposure. In panels C and D current recordings were obtained by averaging three individual trials each obtained at voltages from -100 to $+100$ mV in steps of 20 mV. Thin horizontal lines represent the applied membrane potential.

did not unlock mutant channels. The locking of the channel in the open state could be caused by the formation of disulfide bonds between the sulfur atoms of exogenous cysteines and endogenous cysteines (Fig. 1). In this case treatment with the reducing agent DTT is expected to break these disulfide bonds and unlock the channel from the open configuration. CuP could also overoxidize cysteines and this modification is not reverted by DTT (36).

After treatment with 5 mM DTT for 5 min the amplitude of the current recorded in the absence of cGMP (Fig. 5 B) in the locked-open mutant channel F380C decreased and approached the amplitude of current observed before CuP treatment (gray trace in Fig. 5 A). The amplitude of the current observed in the presence of cGMP was almost unaffected by treatment with DTT (compare Fig. 5, A and B). Collected data from six patches showed that DTT reduced the current measured in the absence of cGMP in the locked-open channel by 70 $\pm$ 25%.

Locking of mutant channel F380C in the closed state

Next we addressed the question: what would happen if mutant channels F380C were treated with CuP in the absence of cGMP? When the patch was treated with CuP in the closed

state—i.e., in the absence of cGMP—the cGMP-activated current (Fig. 6 A) was abolished, as shown in Fig. 6 B. Indeed the current measured in the presence and absence of cGMP did not show any rectification and had amplitude similar to
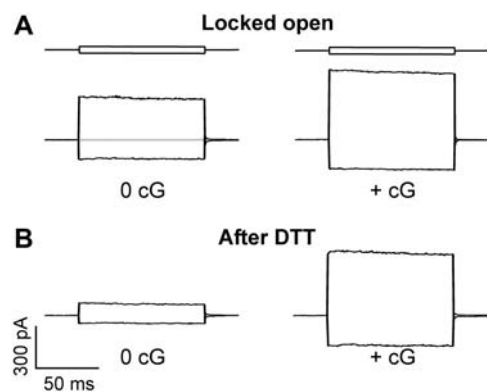

FIGURE 5   The locking of mutant F380C in the open state is reverted by DTT. (A) The current measured in the absence (0 cG) and in the presence of 1 mM cGMP (+ cG) after exposure to CuP in the presence of 1 mM cGMP for 5 min. The gray trace in the first column indicates the current measured under the same conditions before CuP exposure. (B) Same as in panel A, but after removal of CuP and exposure to 5 mM DTT for 5 min in the absence of cGMP. Current traces shown are obtained as in Fig. 4 B. Thin horizontal lines represent the applied membrane potential.
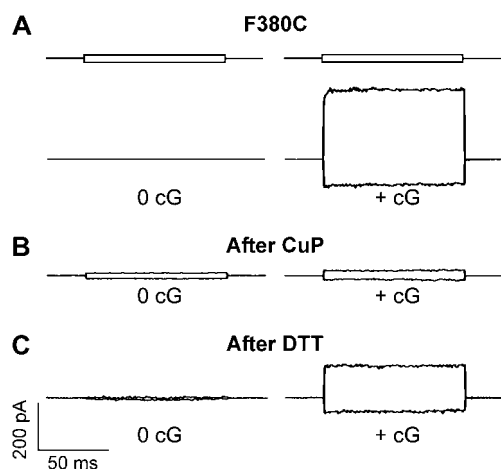
FIGURE 6 Locking of mutant channel F380C by CuP in the absence of cGMP. (*A*) Currents recorded in the absence of cGMP (0 cG) and in the presence of 1 mM cGMP (+ cG) before CuP exposure. (*B*) Same as in panel *A* but after exposure to 1 μM CuP for 5 min in the absence of cGMP. (*C*) Same as in panel *B* but after removal of CuP and exposure to 5 mM DTT in the absence of cGMP for 5 min. Current traces shown are obtained as in Fig. 4 *B*. Thin horizontal lines represent the applied membrane potential.

that observed in the absence of cGMP before CuP treatment. In all 19 patches examined, the exposure to CuP in the absence of cGMP for longer than 5 min invariably led to an almost complete blockage of the cGMP-activated current (locked closed). When mutant channels F380C were locked in

the closed state by treatment with CuP (Fig. 6 *B*), a subsequent treatment with DTT unlocked (Fig. 6 *C*) these channels to some extent. DTT treatment (5 mM) for 5 min restored 46 $\pm$ 24% (six patches) of the current initially observed in the presence of 1 mM cGMP before CuP treatment.

Mutant channel F380C in a cysteine-free background and the double mutant channel F380C&C314S

The homology modeling of Fig. 1 *B* suggest that the exogenous cysteines introduced in the position 380 are far apart to form intersubunit disulfide bonds. To investigate the possible formation of disulfide bonds between endogenous and exogenous cysteines, we repeated the mutation F380C in a cysteine-free CNGA1 channel (F380C$_{\text{cys-free}}$) kindly provided by Matulef et al. (24). Data obtained from different patches show that treatment with CuP for 5 min in the open (seven patches) or closed (six patches) state did not lock the channel in either states (Fig. 7, *A* and *B*).

Sequence alignment of the CNGA1 and KcsA channel (Fig. 1 *A*) and the homology model with the 3D structure of the KcsA channel (Fig. 1 *B*) show that in the S5 domain of CNGA1 there is a native cysteine at position 314 that could form a disulfide bond with the exogenous cysteine at position 380, responsible for the effects described in Figs. 4–6. To test this possibility the mutant channel F380C&C314S was constructed. Incubation of patch in CuP for 5 min in the presence
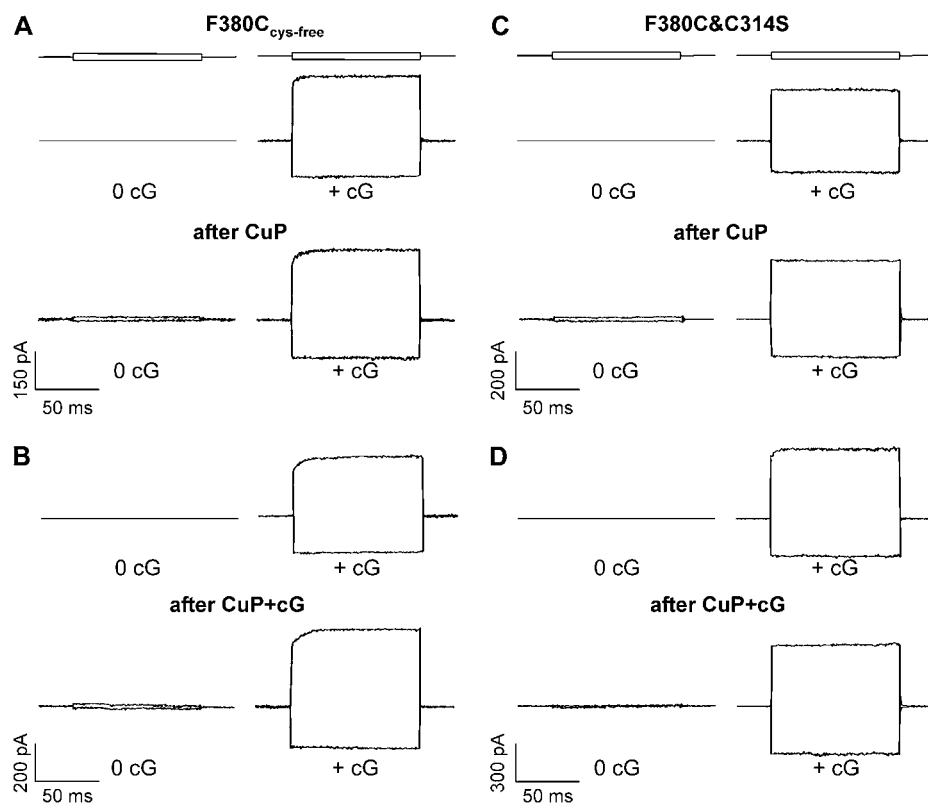

FIGURE 7 CuP has no effect on the mutants F380C$_{\text{cys-free}}$ and double mutant F380C&C314S. (*A* and *B*) The effect of exposure to 1 μM CuP for 5 min in the absence of cGMP (*A*) and in its presence (*B*) on the mutant F380C in the cysteine-free WT (F380C$_{\text{cys-free}}$). (*C* and *D*) The effect of the exposure for 5 min to 1 μM CuP in the absence of 1 mM cGMP (*C*) and in its presence (*D*) on the double mutant F380C&C314S. 0 cG represents the current measured in the absence of cGMP and + cG represents the current measured in the presence of 1 mM cGMP. Current traces shown are obtained as in Fig. 4 *B*. Thin horizontal lines represent the applied membrane potential.

or in the absence of cGMP did not lock the channel in both conformations (Fig. 7, *C* and *D*). Similar results were observed in four different patches excised from two different oocytes.

To verify whether the locking of the channel in the open and closed state described in Figs. 3–6 was caused primarily and uniquely by the formation of disulfide bonds between cysteines in positions 380 and 314, cysteines were introduced at positions 380 and 314 in the cysteine-free CNGA1 background. CuP was able to lock—to some extent—also this mutant channel (Fig. 8, *A* and *B*) in the closed and open state as observed in the mutant F380C. After CuP application in the closed state the cGMP-activated current was reduced by 49 $\pm$ 23% ($n = 7$). After application of CuP in the presence of 1 mM cGMP the current measured in the absence of cGMP was 51 $\pm$ 28% ($n = 6$) of the current measured in the presence of cGMP. Therefore the effect of CuP on the mutant F380C is similar but not identical to that observed on the mutant F380C&C314$_{cys-free}$ constructed on the WT$_{cys-free}$ background.

All these results show that the mechanism responsible for locking the channel in the open and closed state is indeed due to the formation of disulfide bonds between cysteines in positions 380 and 314.

DISCUSSION

Upon binding of cyclic nucleotide, CNG channels undergo a sequence of conformational changes leading to channel opening (1). As the binding domain is located in the cytoplasm (4) and the gate is presumably located in the pore itself (15–18) a signal must be transmitted to the S6 domain and finally to the pore. The nature of this signal is unknown and constitutes the molecular basis of channel gating. Locking CNG channels in the open and closed state provides useful information on conformational changes that occur during gating. Our results show that in mutant channel F380C, the addition of the oxidizing agent CuP in the open and closed state locks CNGA1 channels in the respective states. Moreover

DTT, a reducing agent, unlocks the channels from their locked configuration. These results suggest that the observed locking effect was mediated by the formation of disulfide bridges. When a cysteine at position 380 was introduced in the cysteine-free CNGA1 wild-type channel (24) CuP could not lock the channel in either state. Also in the double mutant F380C&C314S CuP could not lock the channel in open or closed states. Two cysteines were introduced at positions 380 and 314 in the cysteine-free CNGA1 background for the conformation of this observation. CuP was able to lock—to some extent—also this mutant channel (Fig. 8, *A* and *B*) in the closed and open state. These results indicate the formation of disulfide bridges between the exogenous cysteine introduced at position 380 and the endogenous cysteine at position 314.

These experimental observations can be used to hypothesize the signal originating from the cyclic nucleotide-binding domain and sent to the pore through the S6 domain. As suggested by our experiments Cys-314 of S5 and the exogenous cysteine in position 380 are near each other, both in the open and closed state so that in both states they can form a disulfide bond. Inspection of the Protein Data Bank (PDB) indicates that the distance between the C$_{\alpha}$ of cysteines forming a S-S bond is between 6 and 9 Å. Therefore, the distance between the C$_{\alpha}$ of the exogenous cysteine of mutant F380C and the endogenous Cys-314 must be within this range in both states. As a consequence, the conformational rearrangement that occurs during gating in the upper part of S6—where Phe-380 is located—does not involve large molecular motions but a subtle displacement; likely just a few Angstroms are enough to lead a major functional change.

A possible motion compatible with these experimental constraints is a rotation of the S6 domain around its helical axis by $\sim$30° (Fig. 9). In the closed state the F380C and Cys-314 of each subunit can form an S-S bond, locking the channel in the closed state, as illustrated in Fig. 9.

In the open state (Fig. 9) the upper portion of S6 rotates anticlockwise by $\sim$30°, when viewed from the extracellular side. Also in this configuration F380C and Cys-314 can form
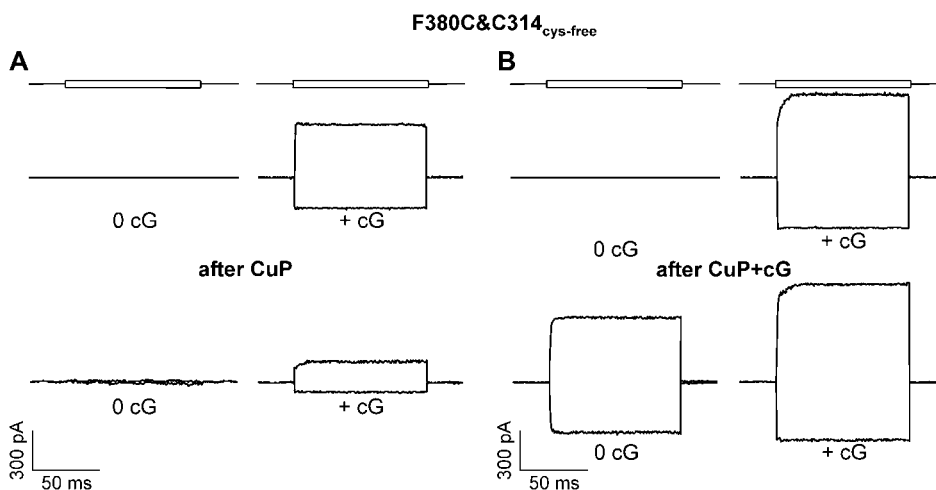
F380C&C314$_{cys-free}$

FIGURE 8 The effect of CuP in the absence and in the presence of 1 mM cGMP on the mutant channel F380C&C314$_{cys-free}$ constructed in the WT$_{cys-free}$ background. (*A* and *B*) Same as in Fig. 7, *A* and *B*. Current traces obtained as in Fig. 7. Thin horizontal lines represent the applied membrane potential.
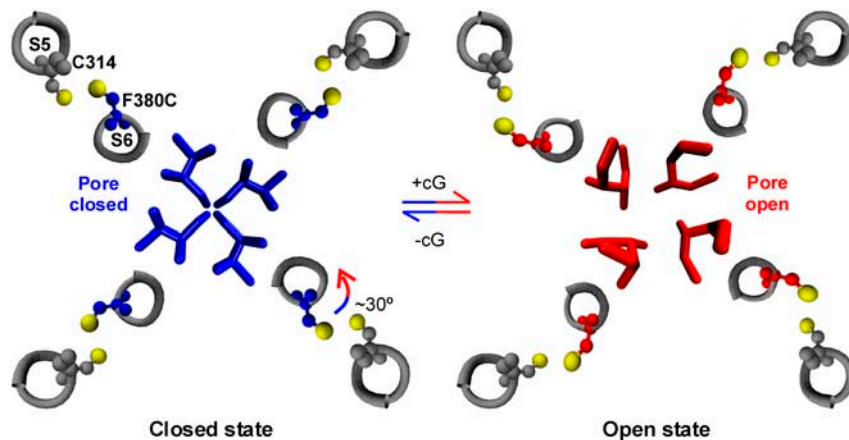
FIGURE 9 A model of the conformational changes during gating in the upper portion of S6 and the locking of mutant channel F380C in the closed and open state. Locking is mediated by the formation of disulfide bonds between the exogenous cysteines of mutant F380C and the endogenous cysteine Cys-314. The blue and red residues in the center show the narrowest region of the pore in the closed state and open state, respectively. In the open state the upper portion of S6 rotates anticlockwise—when viewed from the extracellular side of the membrane—by ~30°. This anticlockwise rotation, by a suitable coupling between the P-helix and S6 causes a small displacement of residues forming the narrowest portion of the pore leading to channel opening (see red residues). The position of the F380 has been slightly displaced from the analogous position of the corresponding residue (Met-96) of the KcsA structure (11), which points toward the selectivity filter.

an S-S bond but this time locking the channel in the open configuration. This anticlockwise rotation, by a suitable coupling between the P-helix and S6 causes a small displacement of residues that are forming the narrowest portion of the pore, leading to channel opening as hypothesized and shown in Fig. 9. The notion that channel gating is mediated by an anticlockwise rotation of the S6 domain was already proposed (37) on the basis of a histidine scanning of the S6 domain. An anticlockwise rotation of ~30° of the upper portion of S6 (19) may be the molecular signal underlying gating in the pore of CNGA1 channels. In this view we speculate that in the WT CNGA1 channel Phe-380 by interacting also with hydrophobic residues such as those comprised between Leu-351 and Leu-356 in the P-helix is part of the molecular coupling between the P-helix and S6.

The model described in Fig. 9 providing a molecular explanation of the locking of the channel in the open and closed state is certainly not unique and other mechanisms could be envisaged. For instance it is possible that in the closed state, blockage is mediated by the formation of disulfide bonds between cysteines within the same subunit and in the open state by the formation of disulfide bonds between cysteines in neighboring subunits or vice versa. This mechanism, however, requires large conformational changes of the pore topology between the open and closed state, which do not appear to be supported by the available experimental evidence. The fact that the mutant channels F380C&C314S and F380C$_{cys-free}$ did not lock the channels in either states by the application of CuP also strengthens the current notion. Indeed, the pattern of accessibility of residues in the pore region are very similar in the open and closed states (16,17) indicating that only minor and subtle conformational changes of the pore mediate the transition between the open and closed state. The model in Fig. 9 is certainly consistent with the experimental results described in this article and requires only small conformational changes for gating. The results obtained from different laboratories also support this model.

REFERENCES

1. Fesenko, E. E., S. S. Kolesnikov, and A. L. Lyubarsky. 1985. Induction by cyclic GMP of cationic conductance in plasma membrane of retinal rod outer segment. *Nature*. 313:310–313.

2. Zimmerman, A. L., G. Yamanaka, F. Eckstein, D. A. Baylor, and L. Stryer. 1985. Interaction of hydrolysis-resistant analogs of cyclic GMP with the phosphodiesterase and light-sensitive channel of retinal rod outer segments. *Proc. Natl. Acad. Sci. USA*. 82:8813–8817.

3. Nakamura, T., and G. H. Gold. 1987. A cyclic nucleotide-gated conductance in olfactory receptor cilia. *Nature*. 325:442–444.

4. Kaupp, U. B., T. Niidome, T. Tanabe, S. Terada, W. Bönig, W. Stühmer, N. J. Cook, K. Kangawa, H. Matsuo, T. Hirose, T. Miyata, and S. Numa. 1989. Primary structure and functional expression from complementary DNA of the rod photoreceptor cyclic GMP-gated channel. *Nature*. 342:762–766.

5. Zagotta, W. N., and S. A. Siegelbaum. 1996. Structure and function of cyclic nucleotide-gated channels. *Annu. Rev. Neurosci*. 19:235–263.

6. Biel, M., X. Zong, F. A. Ludwing, A. Sautter, and F. Hofmann. 1999. Structure and function of cyclic nucleotide-gated channels. *Rev. Physiol. Biochem. Pharmacol*. 135:151–171.

7. Kaupp, U. B., and R. Seifert. 2002. Cyclic nucleotide gated channels. *Physiol. Rev*. 82:769–824.

8. Shammat, I. M., and S. E. Gordon. 1999. Stoichiometry and arrangement of subunits in rod cyclic nucleotide-gated channels. *Neuron*. 23:809–819.

9. He, Y., M. Ruiz, and J. W. Karpen. 2000. Constraining the subunit order of rod cyclic nucleotide-gated channels reveals a diagonal arrangement of like subunits. *Proc. Natl. Acad. Sci. USA*. 97:895–900.

10. Doyle, D. A., J. M. Cabral, R. A. Pfuetzner, A. Kuo, J. M. Gulbis, S. L. Cohen, B. T. Chait, and R. MacKinnon. 1998. The structure of the potassium channel: molecular basis of K^+ conduction and selectivity. *Science*. 280:69–77.

11. Zhou, Y., J. H. Morais-Cabral, A. Kaufman, and R. MacKinnon. 2001. Chemistry of ion coordination and hydration revealed by a K^+ channel-Fab complex at 2.0 Å resolution. *Nature*. 414:43–48.

12. Jiang, Y., A. Lee, J. Chen, M. Cadene, B. T. Chait, and R. MacKinnon. 2002. Crystal structure and mechanism of calcium gated potassium channel. *Nature*. 417:515–522.

13. Jiang, Y., A. Lee, J. Chen, M. Cadene, B. T. Chait, and R. MacKinnon. 2002. The open pore conformation of potassium channels. *Nature*. 417:523–526.

14. Kuo, A., J. M. Gulbis, J. Antcliff, T. Rahman, E. Lowe, J. Zimmer, J. Cuthbertson, F. M. Ashcroft, T. Ezaki, and D. A. Doyle. 2003. Crystal structure of the potassium channel KirBac1.1 in the closed state. *Science*. 3000:1922–1926.

15. Becchetti, A., and P. Roncaglia. 2000. Cyclic nucleotide-gated channels: intra- and extracellular accessibility to Cd^{2+} of substituted cysteine residues within the P-loop. *Pflugers Arch*. 440:556–565.

16. Becchetti, A., K. Gamel, and V. Torre. 1999. Cyclic nucleotide-gated channels pore topology studied through the accessibility of reporter cysteines. *J. Gen. Physiol*. 114:377–392.

17. Liu, J., and S. A. Siegelbaum. 2000. Change of pore helix conformational state upon opening of cyclic nucleotide gated channels. *Neuron*. 28:899–909.

18. Flynn, G. E., and W. N. Zagotta. 2003. A cysteine scan of the inner vestibule of cyclic nucleotide gated channels reveals architecture and rearrangement of the pore. *J. Gen. Physiol*. 121:563–582.

19. Giorgetti, A., A. V. Nair, P. Codega, V. Torre, and P. Carloni. 2005. Structural basis of gating of CNG channels. *FEBS Lett*. 579:1968–1972.

20. Flynn, G. E., and W. N. Zagotta. 2001. Conformational changes in s6 coupled to the opening of cyclic neucleotide-gated channels. *Neuron*. 30:689–698.

21. Mazzolini, M., M. Punta, and V. Torre. 2002. Movement of the C-helix during the gating of cyclic nucleotide gated channels. *Biophys. J*. 83:3283–3295.

22. Rothberg, B., K. Shin, and G. Yellen. 2003. Movements near the gate of a hyperpolarization-activated cation channel. *J. Gen. Physiol*. 122:501–510.

23. Giorgetti, A., P. Carloni, P. Mistrik, and V. Torre. 2005. A homology model of the pore region of HCN channels. *Biophys. J*. 89:932–944.

24. Matulef, K., G. E. Flynn, and W. N. Zagotta. 1999. Molecular rearrangements in the ligand-binding domain of cyclic nucleotide-gated channels. *Neuron*. 24:443–452.

25. Nizzari, M., F. Sesti, M. T. Giraudo, C. Virginio, A. Cattaneo, and V. Torre. 1993. Single-channel properties of cloned cGMP-activated channels from retinal rods. *Proc. Biol. Sci*. 254:69–74.

26. Sesti, F., E. Eismann, U. B. Kaupp, M. Nizzari, and V. Torre. 1995. The multi-ion nature of the cGMP-gated channel from vertebrate rods. *J. Physiol*. (*Lond*.). 487:17–36.

27. Thompson, J. D., D. G. Higgins, and T. J. Gibson. 1994. CLUSTAL W: improving the sensitivity of progressive multiple sequence alignment through sequence weighting, position-specific gap penalties and weight matrix choice. *Nucleic Acids Res*. 22:4673–4680.

28. Šali, A., and T. L. Blundell. 1993. Comparative protein modeling by satisfaction of spatial restraints. *J. Mol. Biol*. 234:779–815.

29. Sánchez, R., and A. Šali. 1997. Advances in comparative protein-structure modeling. *Curr. Opin. Struct. Biol*. 7:206–214.

30. Jan, L. Y., and Y. N. Jan. 1990. A superfamily of ion channels. *Nature*. 345:672.

31. Gauss, R., R. Seifert, and U. B. Kaupp. 1998. Molecular identification of a hyperpolarization-activated channel in sea urchin sperm. *Nature*. 393:583–587.

32. Root, M. J., and R. MacKinnon. 1993. Identification of an external divalent binding site in the pore of a cGMP-activated channel. *Neuron*. 11:459–466.

33. Gordon, S. E., and W. N. Zagotta. 1995. A histidine residue associated with the gate of the cyclic nucleotide-activated channels in rod photoreceptors. *Neuron*. 14:177–183.

34. Gordon, S. E., and W. N. Zagotta. 1995. Localization of regions affecting an allosteric transition in cyclic nucleotide-activated channels. *Neuron*. 14:857–864.

35. Gordon, S. E., and W. N. Zagotta. 1995. Subunit interactions in coordination of Ni^{2+} in cyclic nucleotide-gated channels. *Proc. Natl. Acad. Sci. USA*. 92:10222–10226.

36. Hua, L., and S. E. Gordon. 2005. Functional interaction between A′ helices in the C-linker of open CNG channels. *J. Gen. Physiol*. 125:335–344.

37. Johnson, J. P., and W. N. Zagotta. 2001. Rotational movement during cyclic nucleotide-gated channel opening. *Nature*. 412:917–921.

A comparison of electrophysiological properties of the CNGA1, CNGA1$_{tandem}$ and CNGA1$_{cys-free}$ channels

Monica Mazzolini, **Anil V. Nair** and Vincent Torre[#]

International School for Advanced Studies

via Beirut 2-4 I-34014 Trieste, Italy

[#]Corresponding author: Vincent Torre

Scuola Superiore di Studi Avanzati (SISSA)

Area Science Park, SS 14 Km 163.5, Edificio Q1,

34012 Basovizza (TS), Italy

Tel/Fax: +39-040-3756513   e-mail: torre@sissa.it ;

Abstract:

Three constructs are used for the analysis of biophysical properties of CNGA1 channels: the CNGA1 channel, a CNGA1 channel where all endogenous cysteines were removed (CNGA1$_{cys-free}$) and a construct composed of two CNGA1 subunits connected by a small linker (CNGA1$_{tandem}$). So far, it has been assumed, but not proven, that the molecular structure of these ionic channels is almost identical. The I/V relations, ionic selectivity to alkali monovalent cations, blockage by tetracaine and TMA$^+$ were not significantly different. The cGMP dose response and blockage by TEA$^+$ and Cd^{2+} were instead significantly different in CNGA1 and CNGA1$_{cys-free}$ channels, but not in CNGA1 and CNGA1$_{tandem}$ channels. Cd^{2+} blocked irreversibly the mutant channel A406C in the absence of cGMP. By contrast, Cd^{2+} did not block the mutant channel A406C in the CNGA1$_{cys-free}$ background (A406C$_{cys-free}$), but an irreversible and almost complete blockage was observed in the presence of the cross-linker M-4-M. Results from the application of different MTS cross-linkers and reagents suggest that the 3D structure of the CNGA1$_{cys-free}$ differs from that of the CNGA1 channel by several Angstroms and the distance between homologous residues at position 406 in CNGA1$_{cys-free}$ is 3-4 Angstroms longer than in the CNGA1.

Introduction:

Cyclic nucleotide gated (CNG) channels mediate sensory transduction in photoreceptors and olfactory sensory neurons (Fesenko et al., 1985). In these cells, sensory transduction requires the binding of cyclic nucleotides (cGMP for photoreceptor and cAMP for olfactory receptor) to CNG channels in order for the latter to open (Craven and Zagotta, 2006; Kaupp et al., 1989; Kaupp and Seifert, 2002; Matulef and Zagotta, 2003; Zagotta and Siegelbaum, 1996). Native CNG channels are heterotetramers and have distinct subunits usually referred to as CNGA and CNGB (Bradley et al., 2001). Native CNG channels from bovine rod photoreceptors are composed of 3 CNGA1 and 1 CNGB1 subunits (Weitz et al., 2002; Zheng et al., 2002; Zhong et al., 2002). The CNGA1 subunit from bovine rod is composed of 690 amino acids encoding for a cyclic nucleotide-binding (CNB) domain composed of about 125 amino acids in the cytoplasmic C terminal end (Biel et al., 1999; Zagotta and Siegelbaum, 1996). The analysis of the amino acid sequence of the CNGA1 subunit indicates the existence of six transmembrane segments, usually referred to as S1, S2, S3, S4, S5 and S6 helices. Between the S5 and S6 helices there is a pore region, from Val348 to Pro367, that shows a significant sequence homology with the pore region of K$^+$ channels (Becchetti et al., 1999; Liu and Siegelbaum, 2000). The overall architecture places CNG channels in the superfamily of voltage - gated ionic channels, rather than in the superfamily of ligand gated channels (Jan and Jan, 1990). Homotetrameric CNGA1 channels from bovine rods, when heterologously expressed in *Xenopus leavis* oocytes, give rise to functional channels with properties similar - but not identical - to those of native CNG channels (Kaupp et al., 1989).

In order to understand the relation between structure and function of ionic channels, residues were mutated and electrophysiological properties of mutant channels were investigated. A common strategy is to substitute native residues with exogenous cysteines and to analyze the effect of compounds known to react with the sulfur (S) atom of cysteines. This procedure usually known as cysteine scanning mutagenesis (CSM) (Akabas et al., 1992; Karlin and Akabas, 1998) analyses the formation of S-S bridges, spontaneously occurring or induced by appropriate cross-linking reagents, such as copper phenanthro-

line, Cd^{2+} ions or MTS-MTS compounds (Glusker, 1991; Hastrup et al., 2001; Loo and Clarke, 2001; Ren et al., 2006). As native ionic channels have endogenous cysteines, it is not easy to distinguish between the formation of S-S bridges between a pair of exogenous cysteines and between exogenous and endogenous cysteines. This issue is particularly relevant in studies aiming at establishing distances between homologous residues. (Matulef et al., 1999) have engineered a CNGA1 channel ($CNGA1_{cys-free}$) where all endogenous cysteines were replaced with other residues not bearing a S atom. When exogenous cysteines are introduced in the $CNGA1_{cys-free}$ any effect mediated by agents reacting with thiol groups can be ascribed to exogenous cysteines.

Another very useful construct is the $CNGA1_{tandem}$ where two CNGA1 subunits are joined together by a small linker composed of some tens of residues (Flynn and Zagotta, 2003; Matulef and Zagotta, 2002; Rosenbaum and Gordon, 2002; Rothberg et al., 2002). By introducing a mutation in only one subunit of the tandem it is possible to study the effect caused by the mutations in only two subunits out of the four composing the channel. In this way, a mutation that does not lead to functional channels when performed in all four subunits, may lead to functional channels when performed in only two subunits. This enabled an extensive CSM in the pore region of CNGA1 channels (Liu and Siegelbaum, 2000) extending the analysis to mutant channels otherwise not functional (Becchetti and Gamel, 1999; Sun et al., 1996).

All these constructs are very useful if the molecular structure of the CNGA1, $CNGA1_{cys-free}$ and $CNGA1_{tandem}$ is always the same or, if not, it is very similar.(Matulef et al., 1999) observed that the concentration of tetracaine blocking half of the maximal cGMP activated current in $CNGA1_{cys-free}$ and in CNGA1 was 10.5 and 8.9 μM respectively. They also reported that the cGMP concentration activating half of the maximal cGMP activated current in $CNGA1_{cys-free}$ and the CNGA1 was 8.56 and 75.1 μM respectively. On the basis of these two observations, (Matulef et al., 1999) concluded that mutating the endogenous cysteines did not greatly alter the structure of the channel, without providing any quantitative estimation of the similarity between the 3D structure of the $CNGA1_{cys-free}$ and CNGA1 channels.

In order to verify this hypothesis, physiological properties of these channels were extensively compared by performing electrophysiological experiments where experimental variations were minimized. Ionic selectivity, cGMP dependency and blockage by a variety of compounds were investigated. Our results indicate that the electrophysiological properties of the CNGA1 and $CNGA1_{tandem}$ are not significantly different. By contrast, differences between several electrophysiological properties of CNGA1 and $CNGA1_{cys-free}$ are statistically significant. In addition, we show that Cd^{2+} ions in the absence of cGMP block irreversibly, the mutant channel A406C in the CNGA1 background, as well when near endogenous Cys481 and Cys505 are replaced with alanine and threonine respectively. By contrast, Cd^{2+} ions did not block the mutant channel A406C constructed in the $CNGA1_{cys-free}$, but an irreversible blockage was observed in the closed state by the application of the cross-linker (Loo and Clarke, 2001) M-4-M. Blockage of mutant channel $A406C_{cys-free}$ was not observed in the presence of non cross-linking MTS derivatives with the same length and a volume larger than that of M-4-M. These results indicate that homologous residues at position 406 in the $CNGA1_{cys-free}$ are approximately 3-4 Å more distant than in the CNGA1 channel. Functional differences between native and cysteine free proteins have already been reported and investigated (Kato et al., 1988; Kohler et al., 2003; Taylor et al., 2001), but

their structural differences were rarely quantified. The present manuscript quantifies these differences.

Materials and Methods:

Molecular Biology

Three different bovine rod channel constructs were used. The CNGA1 channel, consisting of 690 residues, the CNGA1$_{\text{tandem}}$, a tandem dimer construct and - a gift from William Zagotta - the CNGA1$_{cys-free}$ channel (Matulef et al., 1999). Selected residues were replaced by introducing a cysteine in the CNGA1 and CNGA1$_{cys-free}$ as previously described (Becchetti et al., 1999; Matulef et al., 1999) with the use of a Quick Change Site-Directed Mutagenesis kit (Stratagene). Point mutations were confirmed by sequencing them with the sequencer LI-COR (4000L). cDNAs were linearized and was transcribed to cRNA in vitro using the mMessage mMachine kit (Ambion, Austin, TX).

The tandem dimer construct was generated by the insertion of one copy of the CNGA1 DNA into a vector pGEMHE already containing another copy of CNGA1 DNA. At the end of cloning two copies of the CNGA1 DNA, they were connected by a 10-amino acid linker GSGGTELGST (Rothberg et al., 2002) joining the C-terminus of the first CNGA1 with the N - terminus of the second one. This second subunit was made by replacing the ApaI restriction site 'GGGCCC' at the end of the CNGA1 DNA without changing the amino acid 'GGTCCC' and adding at the start codon a new ApaI restriction site followed by a linker, using a PCR reaction. Subunits were linked after HindIII/ApaI cut.

Oocyte preparation and chemicals

Mutant channel cRNAs were injected into *Xenopus laevis* oocytes ("Xenopus express" Ancienne Ecole de Vernassal, Le Bourg 43270, Vernassal, Haute-Loire, France). Oocytes were prepared as already described (Nizzari et al., 1993). Injected eggs were maintained at 18°C in a Barth solution supplemented with 50 μg/ml gentamycin sulfate and containing (in mM): 88 NaCl, 1 KCl, 0.82 MgSO$_4$, 0.33 Ca(NO$_3$)$_2$, 0.41 CaCl$_2$, 2.4 NaHCO$_3$, 5 TRIS-HCl, pH 7.4 (buffered with NaOH). During the experiments, oocytes were kept in a Ringer solution containing (in mM): 110 NaCl, 2.5 KCl, 1 CaCl$_2$, 1.6 MgCl$_2$, 10 HEPES-NaOH, pH 7.4 (buffered with NaOH). Usual salts and reagents were purchased from Sigma Chemicals (St. Louis, MO, USA), and MTS compounds (MTSET, MTSEA, MTSPT, MTSPtrEA and cross-linkers) were purchased from TRC (Toronto Research Chemicals, Canada). Cross-linker compounds such as M-2-M (1,2-Ethanediyl bismethanethiosulfonate), M-4-M (1,4-Butanediyl bismethanethiosulfonate), M-6-M (1,6-Hexanediyl bismethanethiosulfonate), M-8-M (3,6-Dioxaoctane-1,8-diyl bismethanethiosulfonate) and M-11-M (3,6,9-Trioxaundecan-1,11-diyl bismethanethiosulfonate) had different maximum cross-linking span - i.e.: the longest distance between the S atoms of the cross-linker reacting with the S atoms of cysteine and forming S-S bonds (see Fig.3.3.1) (Loo and Clarke, 2001).

The cross-linker M-2-M has a cross-linking span of 5.2 Å and an actual volume of 139 Å^3. When M-2-M reacts with a S atom it loses one SO$_2$CH$_3$ group and when it cross-links with two S atoms its effective volume becomes 73.8 Å^3. Longer cross-linkers, such as M-4-M, M-6-M, M-8-M and M-11-M can exist in different configurations, i.e. they have several rotamers illustrated in the first column of Fig.3.3.1.
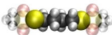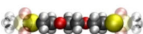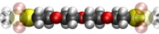
MTS cross-linkers	Maximum cross-linking span (Å)	Actual Volume (Å³)	Effective Volume (Å³)
M-2-M	5.2	139.0	73.80
M-4-M	7.8	166.4	101.2
M-4-M$_{rot1}$	4.9	160.7	99.2
M-4-M$_{rot2}$	6.5	174.2	102.5
M-6-M	10.4	200.3	133.6
M-6-M$_{rot1}$	5.7	193.9	132.8
M-6-M$_{rot2}$	6.7	201.2	131.9
M-8-O$_2$M	13	182.0	130.4
M-8-O$_2$M$_{rot1}$	3.9	183.3	110.9
M-8-O$_2$M$_{rot2}$	9.3	189.4	106.2
M-11-O$_3$M	16.9	224.6	157.6
M-11-O$_3$M$_{rot1}$	3.8	223.7	159.1
M-11-O$_3$M$_{rot2}$	12.1	225.2	163.7

Figure 3.3.1: *Properties of cross-linkers with handles of increasing length. The first column shows the chemical structure and some representative rotamers. The spheres shown in yellow represent Sulfurs, Oxygens are in red, Carbons are in grey and Hydrogens are in white. The suffixes rot1 and rot2 show two representative rotamers of a minimum and intermediate spacer arm length. The cross linking span of the M-X-M is calculated by the estimated chemical bond size (Loo and Clarke, 2001) and the rotamers' cross-linking span was calculated by using the VMD visualization software(Humphrey et al., 1996) (second column). The actual volume is the volume with the SO_2CH_3 (shown as transparent objects) group at both ends (third column). The effective volume is the volume when the cross-linker loses its SO_2CH_3 groups to form bonds with the sulfur of cysteines (fourth column). The volumes are calculated using the program steric v1.12 (White et al., 1993)*

Recording apparatus

cGMP-gated currents from excised patches were recorded with a patch-clamp amplifier (Axopatch 200B, Axon Instruments Inc., Foster City, CA, USA), 2-6 days after RNA injection, at room temperature (20-24°C). The perfusion system was as described (Sesti et al., 1995) and allowed a complete solution change in less than 1 s. Borosilicate glass pipettes had resistances of 3-5 MΩ in symmetrical standard solution. The standard solution on both sides of the membrane consisted of (in mM) NaCl, 110; HEPES, 10; and EDTA, 0.2 (pH 7.4). The membrane potential was usually stepped from 0 to ± 100 mV in 20 mV steps or ± 60 mV. We used Clampex 8.0, Clampfit, and Matlab for data acquisition and analysis. Currents were low-pass filtered at 2 kHz and acquired digitally at 5 kHz.

Application of sulfhydryl-specific reagents

In the inside-out patch-clamp configuration, soon after patch excision, the cytoplasmic face of the plasma membrane was perfused with the same pipette-filling solution and then by adding 1 mM cGMP to it. The effect of divalent cations was tested by perfusing the intracellular side of the membrane

with a standard solution without EDTA (to avoid partial divalent cation chelation), supplemented with variable concentrations of $CdCl_2$ or 1mM $CaCl_2$ for different periods of time to study their effect in the closed state. In order to study the open state effect we applied these solutions in the presence of 1mM cGMP.

Cross-linker compounds were dissolved in dimethyl sulfoxide (DMSO) and diluted in standard solution to a final concentration of 100 μM. The final concentration of DMSO was 0.1%. We checked that this concentration of DMSO did not affect the cGMP activated current. Solutions containing cross-linker compounds were prepared immediately before the application (typically <5 min) to prevent degradation, as these reagents dissociate rapidly in aqueous solution. They were not used for more then 45 minutes after dissolving in aqueous solution. The cross-linkers of different length were used to determine the distance between exogenously introduced cysteines (Loo and Clarke, 2001; Ren et al., 2006)

Comparison of electrophysiological properties

In order to reduce the sources of variability in the comparison of electrophysiological properties, several precautions were taken. Solutions from the same stock were used to fill the patch pipette or to perfuse the intracellular side of the membrane in all three channels. In all experiments the mRNA of the three channels were injected in oocytes harvested from the same animal. Each experiment was repeated at least three times in the same experimental session. Statistical significance of different properties between two channels was analyzed using Student's t-test. For every data set, the current measured after a given chemical manipulation (Y_{iA} (i=1, n)) was normalized ($A_i = Y_{iA}/ X_{iA}$) to the current measured in control condition (X_{iA} (i=1, n)). We used the Shapiro-Wilk test (Shapiro and Wilk, 1965) to verify that normalized data had a Gaussian distribution: if the value of W was greater than 0.5 we assumed that the data had a Gaussian distribution. Variance comparison of normalized data were evaluated using the one sided F variance ratio method. The upper critical value for hypothesis rejection was compared with 5% significance ($\alpha = 0.05$) level value (Snedecor and Cochran, 1989). After verifying that both hypotheses were satisfied, we checked the statistical significance using Student's t-test. The level of statistical difference was assumed to be very high when ***p<0.001, medium when **p<0.01 and marginal when *p<0.05

Results:

The membrane topology of a single subunit of the CNGA1 channel from bovine rod is shown in Fig.3.3.2.A where the presumed transmembrane segments S1, S2, S3, S4, S5 and S6 are indicated by vertical cylinders. The CNGA1 channel contains 7 native cysteines: Cys35, Cys169, Cys186, Cys314, Cys481, Cys505 and Cys573 encircled in Fig.3.3.2.A.

Cys35 is located near the N-terminal of the CNGA1 channel at the cytoplasmic side (Brown et al., 1998; Molday et al., 1991) and it is thought to interact with Cys481 in the open state, but not in the closed state (Gordon et al., 1997; Rosenbaum and Gordon, 2002). Cys169 and Cys186 are presumably located in S1 and their functional and/or structural role has not been studied in detail. Cys314 in the S5 transmembrane segment can interact with residues at position 380 in the S6 domain (Nair et al.,

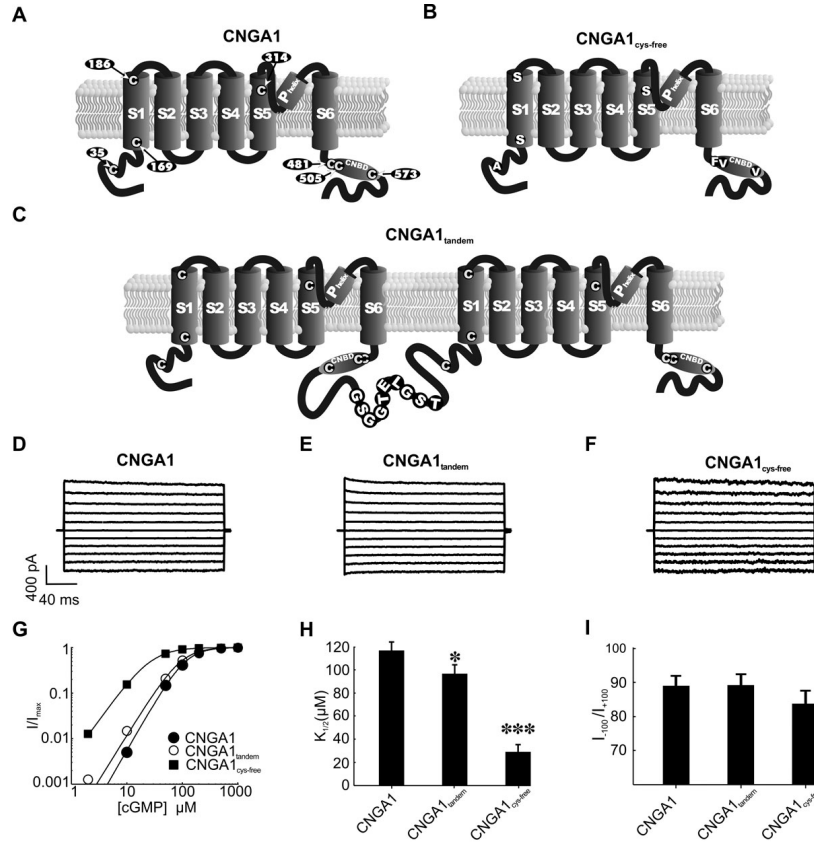2006). Cys481 is located in the C-linker region (Brown et al., 1998) and its role in channel function has

Figure 3.3.2: *The three channels under comparison. **A:** the CNGA1 channel. **B:** the CNGA1$_{cys-free}$. **C:** the CNGA1$_{tandem}$. In yellow are indicated the locations of the endogenous cysteines- Cys35, Cys169, Cys186, Cys314, Cys481, Cys505, Cys573 - which are absent in the CNGA1$_{cys-free}$ channel. Residues substituted with cysteines are shown in the corresponding circles in panel B. **D:**, **E:** and **F:** recordings of the cGMP activated current in voltage clamp experiments when the membrane voltage was stepped from -100 to +100 mV in 20 mV steps for the CNGA1, CNGA1$_{tandem}$ and CNGA1$_{cys-free}$ channels respectively. Each trace was the average of 5 individual traces and the current was obtained as the difference between current recordings in the presence of 1mM cGMP and current recordings obtained in the absence of cGMP. **G:** the dose-response curve of cGMP activation at +60 mV for CNGA1 (closed circle), CNGA1$_{tandem}$ (open circle) and CNGA1$_{cys-free}$ (closed square) channels respectively. The smooth curves are the fit to the equation $\frac{I}{I_{max}} = \frac{[cGMP]^2}{[cGMP]^2 + [K_{1/2}]^2}$. Where I_{max} is the maximum current elicited in the presence of 1mM cGMP and $K_{1/2}$ is the concentration of the cGMP producing half maximal current. **H:** bar plot for the $K_{1/2}$ of the three channels. Statistical significance for differences of $K_{1/2}$ of CNGA1$_{tandem}$ and CNGA1$_{cys-free}$ to CNGA1 was checked by using Student's t-test (see material and methods). The difference in $K_{1/2}$ between CNGA1$_{tandem}$ and CNGA1 channels has a marginal significance (*p<0.05). The difference of $K_{1/2}$ between CNGA1$_{cys-free}$ and CNGA1 channels has very high significance (***p <0.0001). **I:** bar plot for the ratio of the current elicited at -100 mV and at +100 mV in the presence of 1mM cGMP. In CNGA1, CNGA1$_{tandem}$ and CNGA1$_{cys-free}$ this ratio was 89.4 ± 2.5 %, 89.6 ± 2.6% and 84.7 ± 2.9% respectively. No statistically significant difference was observed.*

been extensively studied. Modification of Cys481 in the open state with sulfhydryl reagents potentiates CNGA1 channels (Brown et al., 1998). Cys505 in the CNB domain is accessible to sulfhydryl reagents in the closed state but not in the open state (Matulef et al., 1999; Sun et al., 1996). Finally, Cys573 is located near the C-terminus of the channel. Cys505 and Cys573 do not contribute to the potentiation observed by the application of compounds promoting the formation of disulfide bonds (Gordon et al., 1997), whereas Cys35 in the open state can form a disulfide bond with Cys481 (Gordon et al., 1997).

In the CNGA1$_{cys-free}$ (Fig.3.3.2.B) the 7 native cysteines Cys35, Cys169, Cys186, Cys314, Cys481,

Cys505, and Cys573 were replaced by alanine, serine, serine, serine, phenylalanine, valine and valine respectively (Matulef et al., 1999). In CNGA1$_{\text{tandem}}$ channels, the N-terminal of the CNGA1 channel is linked to the C-terminal of another copy of the CNGA1 channel by the linker shown in Fig.3.3.2.C (Flynn and Zagotta, 2003; Gordon and Zagotta, 1995; Liu and Siegelbaum, 2000; Rosenbaum and Gordon, 2002; Varnum and Zagotta, 1996).

In what follows, an extensive comparison of physiological properties of the CNGA1, CNGA1$_{\text{tandem}}$ and CNGA1$_{cys-free}$ channels will be presented. The cGMP activated current here analyzed is the current measured in the presence of a given amount of cGMP minus the current measured in its absence (leak current). When the cGMP dose response and blockage were compared in the three channels, the same solutions were used either to fill the patch pipette or to perfuse the intracellular side of the membrane. For every set of comparison experiment the mRNA of three channels were injected in oocytes harvested from the same animal.

I/V relations and cGMP dose response

cGMP activated currents from CNGA1 and CNGA1$_{\text{tandem}}$ channels were recorded within one or two days after mRNA injection, but one or two additional days were necessary to obtain a comparable current from CNGA1$_{cys-free}$ channels. As shown in Fig.3.3.2.D, E and F current recordings elicited in voltage clamp mode from membrane patches excised from oocytes injected with the mRNA of the three channels were very similar. In all three channels, when the voltage was stepped from 0 mV to $\pm$ 100 in 20 mV steps, the current reached its steady value within 2-4 ms. No time dependent relaxation of the cGMP activated current was observed.

The dose response, i.e. the relation between fractional activated current ($I_{[cGMP]}/I_{[cGMPsat]}$) and cGMP concentration in the medium bathing the intracellular side of the membrane patch is shown in Fig.3.3.2.G for the CNGA1 (filled circle), CNGA1$_{\text{tandem}}$ (open circle) and CNGA1$_{cys-free}$ (filled square) channels. The cGMP concentration activating a half maximal current ($K_{1/2}$) was 116.9 ± 7.2 (N = 7 patches), 96.6 ± 7.7 (N = 5) and $27.5 \pm 6.1 \mu$M (N = 6) for the three channels respectively. In agreement with (Matulef et al., 1999), the CNGA1$_{cys-free}$ channel has higher cGMP affinity than CNGA1 channel. The Student's t-test indicated that the difference between the $K_{1/2}$ of CNGA1$_{cys-free}$ and CNGA1 channels is highly significant (***p<0.0001) and the difference between the $K_{1/2}$ of CNGA1$_{\text{tandem}}$ and CNGA1 channels is only marginal (*p<0.05) (Fig.3.3.2.H). As shown in Fig.3.3.2.I, the ratio of the current flowing at -100 and + 100 mV ($I_{-100/100}$) for the three channels, was rather similar: indeed it was 89.4 ± 2.5 % (N =10), 89.6 ± 2.6% (N =10), 85.7 ± 2.9% (N =10) for the CNGA1, CNGA1$_{\text{tandem}}$ and CNGA1$_{cys-free}$ channels respectively. The difference between the value of $I_{-100/100}$ for the CNGA1 and the CNGA1$_{cys-free}$ was not significant.

Ionic selectivity

CNG channels differ from the other members of the superfamily of voltage gated channels (Jan and Jan, 1990; Kaupp et al., 1989; Zagotta and Siegelbaum, 1996) for their poor selectivity among monovalent alkali cations. The permeability ratio in the native CNG channels from rod photoreceptors (Menini, 1990) is

$$\text{Li } (1.14) > \text{Na } (1) > \text{K } (0.98) > \text{Rb } (0.84) > \text{Cs } (0.58)$$

where the number in parenthesis indicates the selectivity ratio between the tested alkali monovalent cation and Na^+. This permeability ratio differs from that of the homomeric CNGA1 channel (Kaupp et al., 1989; Nizzari et al., 1993):

$$\text{Na } (1) > \text{K } (0.96) > \text{Li } (0.75) > \text{Rb } (0.73) > \text{Cs } (0.36)$$

The presence of the CNGB1 subunit makes the native CNG channel more permeable to Li^+ than to Na^+ (Kaupp et al., 1989; Korschen et al., 1995). In this analysis, the selectivity to monovalent alkali cations was estimated by measuring V_{rev} in bi-ionic conditions, in saturating cGMP. The pipette always contained 110 mM NaCl, while the equimolar monovalent alkali cationic solutions were changed at the intracellular side of the patch. Currents were elicited by applying $\pm$ 40 mV in step of 2 mV across the patch membrane. A comparison of the measured V_{rev} among the three channels is shown in Table 3.3.1: the three channels had similar values of V_{rev} within the experimental variability. No statistically significant difference was observed.

Table.3.3.1: *Reversal potentials (V_{rev}) X^+/Na^+*

	Li^+ (mV)	K^+(mV)	Rb^+(mV)	Cs^+(mV)
CNGA1	7.5±2.0	1.0±0.6	8.2±2.4	26.3±4
CNGA1$_{tandem}$	7.3±2.8	-0.2±1.4	12.5±2.4	34±6.3
CNGA1$_{cys-free}$	10.8±3.4	-0.4±1.7	11.5±2.6	26.8±7.5

The effect of Cd^{2+} ions

Having compared the I/V relations, the cGMP dose response and ionic selectivity, we compared blockage by different compounds added at the intracellular side of the membrane. Blockage by divalent cations (Colamartino et al., 1991), TEA, TMA (Menini, 1990; Picco and Menini, 1993) and tetracaine (Fodor et al., 1997b; Fodor et al., 1997a) was analyzed. These compounds have a different size and blocking mechanism and therefore their blockage can be used to probe the molecular environment of the intracellular side of the channel. The CNGA1 channel does not have any cysteine residue in the pore region and therefore any effect of Cd^{2+} ions on the inner pore of CNGA1 channels cannot be ascribed to interactions with thiol groups.

The I-V relations of the current recordings obtained from the three channels in the absence (black symbols) and in the presence of 100 μM Cd^{2+} (grey symbols) at the intracellular side of the membrane patch are shown in Fig.3.3.3.A, B and C. In all channels Cd^{2+} ions potentiated the amplitude of the cGMP activated current at negative voltages, as shown in Fig.3.3.3. Indeed, at voltages lower than -60 mV, 100 μM Cd^{2+} ions potentiated the cGMP activated current by about 15% in all the three channels. Cd^{2+} potentiation is expected to have the same molecular origin as that observed in the presence of Ni^{2+} (Gordon and Zagotta, 1995), which depends on His420, present in the three channels. However, at +100 mV we consistently observed a lower blockage in CNGA1$_{cys-free}$ channels: in fact, at this voltage, the residual cGMP activated current in the presence of 100 M Cd^{2+} was 67.1 $\pm$ 8.7% (N=6), 41.8±5.9% (N=6) and 36.7±5.1% (N=4) in CNGA1$_{cys-free}$, CNGA1 and CNGA1$_{tandem}$ channels respectively.
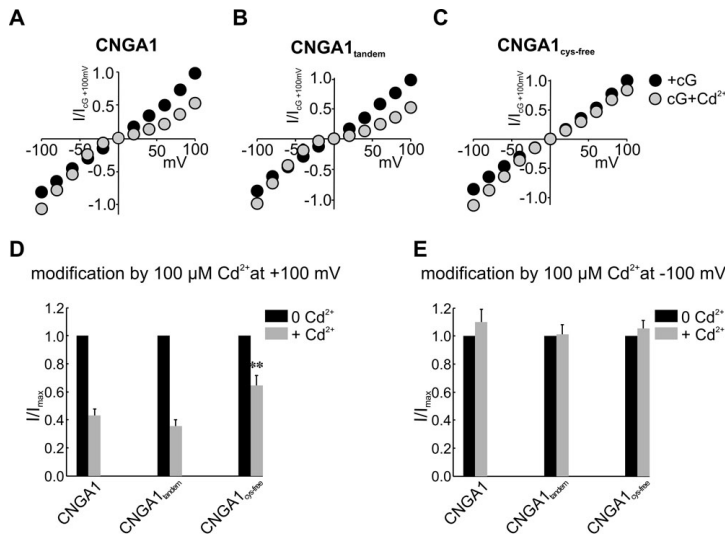
Figure 3.3.3: *Comparison of Cd^{2+} blockage. A, B, C: I/V relation in control conditions (black symbols) and in the presence of 100 μM Cd^{2+} (grey symbols) in the CNGA1, CNGA1$_{tandem}$ and CNGA1$_{cys-free}$ respectively. D: bar plot showing the ratio of current measured at +100 mV in the presence of 1mM cGMP with Cd^{2+} (+ Cd^{2+}) and the current measured with out Cd^{2+} (0 Cd^{2+}). At +100 mV presence of Cd^{2+} has reduced the cGMP current to 41.8 $\pm$ 5.9% in CNGA1, to 36.7 $\pm$ 5.1% in CNGA1$_{tandem}$ and to 67.1 $\pm$ 8.7% in the CNGA1$_{cys-free}$ channels. Difference in Cd^{2+} blockage at +100 mV between CNGA1$_{cys-free}$ and CNGA1 channels was significant (**p<0.001), but CNGA1$_{tandem}$ did not show an important difference compared to CNGA1 channels. E: same as in D but at -100mV. No statistically significant difference was observed.*

The different blockage at +100 mV observed in the CNGA1$_{cys-free}$ was statistically significant (t-test provides a value of **p <0.001). Potentiation at negative voltages and blockage at positive voltages caused by the addition of Cd^{2+} ions were both quickly and entirely reversible as soon as Cd^{2+} ions were removed from the bathing medium.

The effect of Ca^{2+} ions

It is well known that Ca^{2+} ions permeate through CNG channels but also block the current carried by Na^+ ions (Colamartino et al., 1991). Ca^{2+} ions block CNG channels from the extracellular side rather powerfully and the concentration of Ca^{2+} blocking half of the maximal current is voltage dependent and is 288 μM at + 80 mV and 2.3 μM at -30 mV (Eismann et al., 1994). At the intracellular side Ca^{2+} ions block CNGA1 channels less powerfully and the Ca^{2+} concentration blocking half of the maximal cGMP activated current is 2.3 mM at + 80 mV and 6.9 mM at -80 mV. Ca^{2+} blockage is partly mediated by Glu363 at the extracellular mouth of the inner pore (Root and MacKinnon, 1993). In none of the three channels under investigation, Ca^{2+} ions potentiated the cGMP current at negative voltages, as observed in the presence of Cd^{2+} ions. Similar to Cd^{2+} ions, at positive voltages Ca^{2+} ions potently blocked the cGMP activated current in a voltage dependent way. When data from all patches were considered for a statistical analysis, Ca^{2+} blockage in CNGA1$_{cys-free}$, CNGA1$_{tandem}$ and in the CNGA1 channels was not significantly different.

The effect of TEA^+ and TMA^+ ions

Organic compounds such as TMA and TEA added at the intracellular side of the membrane block the flux of alkali monovalent cations from both sides (Picco and Menini, 1993) in a reversible way. The blockage of CNG channel by organic cations requires a concentration of the order of 10^{-2} M and therefore their blockage is less potent compared to Ca^{2+} and Cd^{2+} requiring concentrations 10 and 100 times lower. We analyzed blockage by TMA^+ and TEA^+ when 110 mM Na^+ was present on both sides of the membrane and 25, 50 and 75% of Na^+ in the intracellular medium was replaced by TMA^+ or TEA^+. When Na^+ ions were replaced by TMA^+ differences among the CNGA1, CNGA1$_{tandem}$ and CNGA1$_{cys-free}$ channels were not statistically significant.
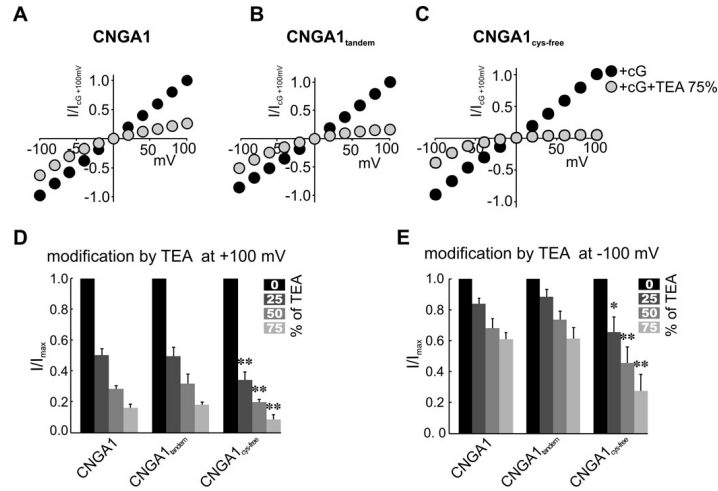
Figure 3.3.4: *Blockage of Na^+ flux by TEA^+ ions. A, B, C: I/V relations in control conditions and in the presence of TEA^+. Black symbol shows the I/V relation in control conditions and grey symbol shows the I/V relation in the presence of 75 % TEA^+ + 25 % Na^+. D: bar plot showing the modification of the Na^+ flux by TEA^+ at +100 mV. Bars are indicated in different grey levels indicating the percentage of TEA^+/Na^+ replacement: 0% indicates 110 mM NaCl, 25% is 87.5 mM NaCl + 27.5 mM TEACl, 50% is 55 mM NaCl+55 mM TEACl and 75 % is 27.5 mM NaCl + 87.5 mM TEACl. The replacement of Na^+ ions with TEA^+ ions by 25, 50 & 75% decreased the cGMP current to 49.7 ± 5.0%, 31.1 ± 5.3%, 18.1 ± 5.7% in CNGA1 channel, to 51.3 ± 16.1%, 29.7 ± 8.6%, 15.5 ± 4.5% in $CNGA1_{tandem}$ and to 32.5 ± 7.1%, 14.4 ± 6.7%, 7.9 ± 3.2% in the $CNGA1_{cys-free}$ channel respectively. Blockage in $CNGA1_{tandem}$ was not significantly different from that observed in CNGA1 channels. TEA^+ blockage in $CNGA1_{cys-free}$ channels was statistically different from that observed in CNGA1 channels with a significance of **p<0.01. E: TEA^+ blocks the $CNGA1_{cys-free}$ channel significantly also at -100 mV. The presence of 27.5, 55 and 82.5 mM TEA^+ at the intracellular side of the membrane reduced the Na^+ influx to 82.3 ± 7.0%, 68.0 ± 6.2%, 58.2 ± 7.6% in CNGA1 channels, to 80.7 ± 11.7%, 64.5 ± 14.6%, 50.7 ± 17.6% in $CNGA1_{tandem}$ channels and to 56.6 ± 22.2%, 43.0 ± 14.1%, 24.5 ± 12.9% in $CNGA1_{cys-free}$ channels . No significant differences were observed between $CNGA1_{tandem}$ and CNGA1 channels. Blockage in $CNGA1_{cys-free}$ was different from that observed in CNGA1 channels with a statistical significance of *p<0.05 in the presence of 25% TEA^+ and of **p<0.01 in the presence of 50 and 75% TEA^+.*

TEA^+ is a larger organic cation compared to TMA^+ and its blocking effect on the current carried by Na^+ ions in CNG channels is more effective.(Menini, 1990; Picco and Menini, 1993) Fig.3.3.4 illustrates results of experiments showing the effect of TEA^+ on the three channels under investigation, with the same style and format used in Fig.3.3.3.

In contrast to what observed with TMA^+ blockage, TEA^+ blocked the cGMP activated current more potently in the $CNGA1_{cys-free}$ channels than in CNGA1 and $CNGA1_{tandem}$ channels, as shown in Fig.3.3.4.A-C. At positive voltages replacing the concentration of intracellular Na^+ ions with TEA^+ by 25, 50 and 75%, it decreased the cGMP current to 49.7 ± 5.0%, 31.1 ± 5.3%, 18.1 ± 5.7% in CNGA1 channels (N=7), to 51.3 ± 16.1%, 29.7 ± 8.6%, 15.5 ± 4.5% in $CNGA1_{tandem}$ (N=4) and to 32.5 ± 7.1%, 14.4 ± 6.7%, 7.9 ± 3.2% in $CNGA1_{cys-free}$ (N=6) channels (see Fig.3.3.4.D), indicating that TEA^+ ions block more effectively. Differences between CNGA1 and $CNGA1_{tandem}$ channels were not statistically significant, but the differences of $CNGA1_{cys-free}$ with CNGA1 channels were important: in fact the significance was **p<0.01 in all three cases. At negative voltages, i.e. at -100 mV the presence of 27.5, 55 and 82.5 mM TEA^+ at the intracellular side of the membrane reduced the Na^+ influx to 82.3 ± 7.0%, 68.0 ± 6.2%, 58.2 ± 7.6% the cGMP current in CNGA1 channels (N=7), to 80.7 ± 11.7%, 64.5 ± 14.6%, 50.7 ± 17.6% in $CNGA_{tandem}$ (N=4) channels and to 56.6 ± 22.2%, 43.0 ± 14.1%, 24.5 ± 12.9% in $CNGA1_{cys-free}$ (N=6) channels (see Fig.3.3.4.E). Similarly to what observed at +100 mV differences between the CNGA1 and $CNGA1_{tandem}$ channels were not statistically significant

but differences with the CNGA1$_{cys-free}$ channel were significant with *p<0.05 in the presence of 25% TEA$^+$ and **p<0.01 in the presence of 50 and 75% of TEA$^+$. TEA$^+$ effect was analyzed in the presence of a saturating cGMP concentration and therefore the different blockage observed in the CNGA1 and CNGA1$_{cys-free}$ channels cannot be ascribed to their different sensitivity to cGMP, as in the presence of 1 mM cGMP both channels have an open probability about 0.9.

Tetracaine blockage

Tetracaine at micromolar concentrations added to the intracellular side of the membrane blocks the CNGA1 channels (Fodor et al., 1997b) and is therefore a more potent blocker of CNGA1 channels than divalent cations, TMA$^+$ and TEA$^+$. In the light of this, we have compared tetracaine blockage in the three channels under investigation. The blockage was measured at the end of voltage pulses lasting 100 ms. In the presence of 1 mM cGMP, the tetracaine concentration blocking half of the cGMP activated current T$_{1/2}$ at +80 mV was 5.34 $\pm$ 2.35 (N=6), 4.17 $\pm$ 0.97 (N=5) and 4.25 $\pm$ 0.86 (N=6) μM for the CNGA1, CNGA1$_{cys-free}$ and CNGA1$_{tandem}$ channels respectively. At -80 mV the values of T$_{1/2}$ was 11.77 $\pm$ 4.38, 10.32 $\pm$ 4.31 and 8.88 $\pm$ 1.35 M respectively for the three channels. In agreement with a previous report (Fodor et al., 1997b) blockage by tetracaine in the presence of a lower cGMP concentration was stronger in all three channels. These results do not highlight any difference in tetracaine blockage in the three channels.

Irreversible Cd^{2+} blockage in cysteine mutants in CNGA1 and CNGA1$_{cys-free}$ channels

The comparison of physiological properties described in the previous sections has not identified any significant difference between the CNGA1 and CNGA1$_{tandem}$ channels, but has indicated statistically significant differences between the CNGA1 and CNGA1$_{cys-free}$ channels.

In the following session we will attempt to quantify structural differences between these two channels. The distance between residues in homologous subunits can be estimated by studying which cross-linking reagents, among those shown in Fig.3.3.1, is able to cross-link the mutant channel obtained when these residues are mutated into cysteines. The existence of a residue cross-linked by reagents with different cross-linking span in the CNGA1 and CNGA1$_{cys-free}$ channels provides a quantification of the structural difference between the two channels, at least for that residue. With this rationale we have scanned several residues in the C-linker domain of CNGA1 channels and we found that Ala406 was the suitable residue. Therefore we have studied the irreversible blockage of the cGMP activated current after a 5 minute application of 200 μM Cd^{2+} to the intracellular side of the membrane patch in the closed state in mutant channels A406C and A406C$_{cys-free}$.

As shown in Fig.3.3.5.A, the cGMP activated current observed in control conditions (left panel in Figs 3.3.5.A and B) was irreversibly blocked by Cd^{2+} ions in the mutant channel A406C (right panel of Fig.3.3.5.A), but not in the mutant channel A406C$_{cys-free}$ (right panel of Fig.3.3.5.B). This different blocking effect of Cd^{2+} ions can be produced by two different mechanisms or by their combination. Cd^{2+} blockage of the cysteine mutant in the CNGA1 background illustrated in Fig.3.3.5.A can originate from Cd^{2+} coordination to the exogenous cysteine with endogenous cysteines and in particular with Cys481 and/or Cys505 (Mechanism 1) which are part of the C-linker domain (Brown et al., 1998). An alternative
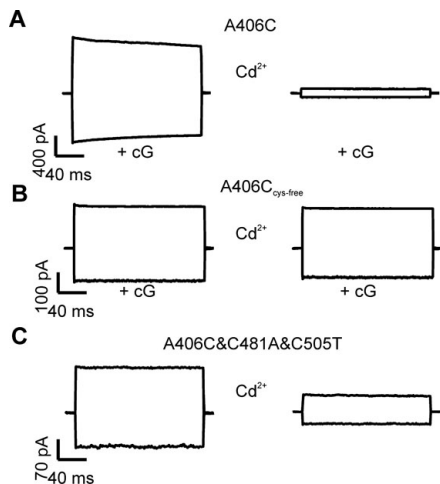
Figure 3.3.5: *In the closed state, Cd^{2+} blocks irreversibly A406C and A406C & C481A & C505T but not $A406C_{cys-free}$. A, B and C: The effect of 200 μM Cd^{2+} added for 5 minutes in mutant channel A406C (A), in mutant channel $A406C_{cys-free}$ (B) and in mutant channel A406C&4C481A&C505T (C). Cd^{2+} ions were added to the medium bathing the intracellular side of the membrane patch in the absence of cGMP. The left and right traces in A and B illustrate the current activated by 1 mM cGMP at $\pm$ 60 mV in control conditions and after exposure to Cd^{2+} ions respectively. In the mutant channel A406C the irreversible blockage induced by 200 μM Cd^{2+} ions was 93 $\pm$ 6 % (N= 5), and in the triple mutant it was 65 $\pm$ 18 % (N= 2).*

explanation is that the 3D structure of $CNGA1_{cys-free}$ channels differs by some Å from CNGA1 channels (Mechanism 2), so that Cd^{2+} can coordinate exogenous cysteines introduced in the CNGA1 channels but not in the $CNGA1_{cys-free}$ channels. In order to resolve this issue we studied in detail mutant channel A406C and we performed two series of experiments. In the first series of experiments we analysed Cd^{2+} blockage in cysteine mutant channels where the two endogenous cysteines Cys481 and Cys505 were replaced by residues not reacting with S atoms, such as alanine or threonine. In the second series of experiments the effect of cross-linkers of different length in mutant channel $A406C_{cys-free}$ was examined. Copper phenanthroline is the shortest cross-linker as it promotes the formation of disulfide bonds among neighboring cysteines but being an oxidizing reagent it has multiple effects. Cd^{2+} ion cross-links cysteines when the distance between their C_α are at a maximum of $\sim$11 Å. The recently synthesized MTS cross-linkers (Loo and Clarke, 2001) have a thiol group at both ends with a linker of variable length. (see Fig.3.3.1). The existence of MTS cross-linkers able to irreversibly between their C_α are at a maximum of $\sim$11 Å. The recently synthesized MTS cross-linkers (Loo and Clarke, 2001) have a thiol group at both ends with a linker of variable length. (see Fig.3.3.1). The existence of MTS cross-linkers able to irreversibly block the mutant channel $A406C_{cys-free}$ in the closed state will support Mechanism 2.

We investigated the mechanism of the irreversible Cd^{2+} blockage observed in the closed state illustrated in Fig.3.3.5.A in mutant channel A406C by removing Cys481 and Cys505. Membrane patches were exposed to 200 μM Cd^{2+} ions for 5 minutes in the absence of cGMP and the current recorded after Cd^{2+} removal and in the presence of a saturating cGMP concentration was measured. As shown in Fig.3.3.5.C Cd^{2+} blockage although slightly reduced is still observed in the triple mutant channel A406C&C481A&C505T. In the mutant channel A406C the irreversible blockage induced by 200 μM Cd^{2+} ions was 93 $\pm$ 6 % (N= 5) and in the triple mutant it was 65 $\pm$ 18 % (N= 2).

The effect of MTS cross-linkers on mutant channel $A406C_{cys-free}$

Cd^{2+} ions in the absence of cGMP powerfully blocked mutant channel A406C but not mutant channel $A406C_{cys-free}$ (see Fig.3.3.5.A, B). The data presented in Fig.3.3.5.C indicate also that Cd^{2+} blockage in mutant channel A406C does not depend significantly on the presence of endogenous cys-

teines at location 481 and 505 and therefore the observed Cd^{2+} blockage is likely to be caused by its coordination to the ring of exogenously introduced cysteines at position 406. In this view, the absence of Cd^{2+} blockage observed in mutant channel $A406C_{cys-free}$ is caused by a different 3D structure of the CNGA1 and $CNGA1_{cys-free}$ channels, whereby in the $CNGA1_{cys-free}$ channel residues at position 406 are at a

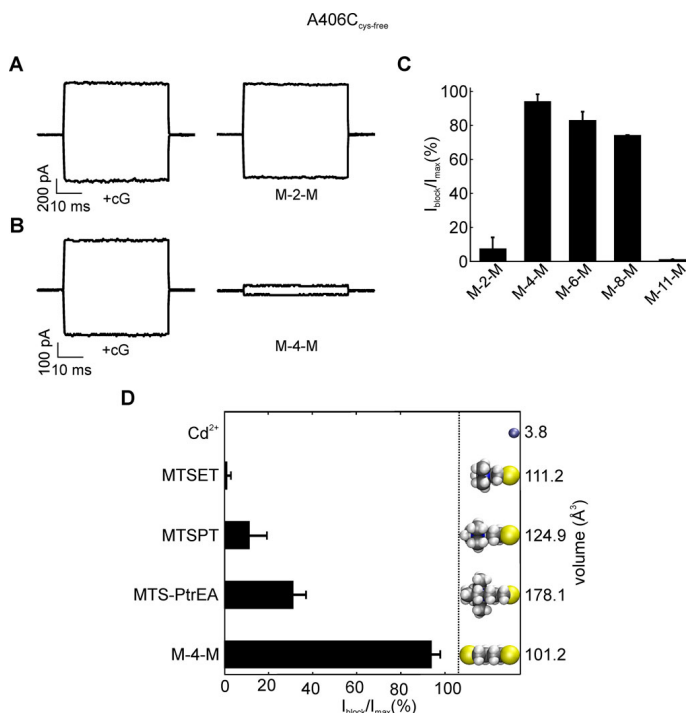**Figure 3.3.6:** *The sulfhydryl specific MTS cross-linkers block the $A406C_{cys-free}$ channel. A, B: represents the current traces in the control condition and after the application of cross-linkers. The current recordings shown are the response to ± 60 mV holding potential in the inside-out patch configuration. In A: the first panel shows the control current from $A406C_{cys-free}$ channels and the second after the application of M-2-M cross linker. In B: as in A but after the application of M-4-M cross-linker. In $A406C_{cys-free}$ 93.9 ± 4.3 % of the control current was blocked by M-4-M. C: bar plot showing the percent of blockage of the channel $A406C_{cys-free}$ after the application of cross-linkers of varying length in the closed state. D: blockage of $A406C_{cys-free}$ by different sulfhydryl reagents. On the right hand side of the panel the effective volumes of the reagents are shown with their 3D molecular structures.*

different distance not allowing the coordination of Cd^{2+} ions by exogenous cysteines. In order to test this possibility, we investigated blockage by thiol cross-linkers M-X-M with an increasing length of the linker. 100 μM of the cross-linker M-2-M, with a linker of 5.2 Å did not block mutant channel $406C_{cys-free}$ (N = 5), as shown in Fig.3.3.6.A, C. In contrast, the same concentration of the reagent M-4-M (N = 6) with a linker of 7.8 Å powerfully blocked mutant channel $A406C_{cys-free}$ (see Fig.3.3.6.B, C).

We have also analyzed blockage of the cGMP current in mutant $A406C_{cys-free}$ by cross-linkers of increasing length. As shown in Fig.3.3.6.C, cross-linkers M-2-M (N=5) and M-11-M (N=5) did not block significantly mutant channel $A406C_{cys-free}$, while cross-linkers M-4-M (N=6), M-6-M (N=4) and M-8-M (N=6) all blocked the mutant channel $A406C_{cys-free}$, with cross-linker M-4-M being the most potent blocker. M-2-M did not block the mutant channel $A406C_{cys-free}$ probably because of its shorter cross-linking span. M-6-M and M-8-M cross-linkers exist in several rotamers (see Fig.3.3.1) so that they can have an effective cross-linking span similar to that of M-4-M. We examined the effect of the M-2-M and M-4-M cross-linkers applied in the closed state of the mutant channels A406C and A406C&C481A&C505T. 100 M M-2-M did not block either the mutant channel A406C (10.4 ± 9.4 %; N= 5) or the triple mutant channel A406C&C481A&C505T (12 ± 10 %; N= 4). Blockage by 100 μM M-4-M was also low with 13 ± 9.7 % (N=5) of the A406C channel and 5 ± 4.5 % (N=4) blockage of the triple mutant channel A406C&C481A&C505T.

The observed blockage of mutant channel $406C_{cys-free}$ by the cross-linker M-4-M could be caused by a simple steric occlusion and not by the cross-linking of the two exogenous cysteines. In order to investigate this possibility, we analyzed the effect of MTS compounds with an increasing volume. During the formation of an S-S bond, MTS compounds react and lose one SO_2CH_3 group. In this way the effective volume of MTS compounds reacting with a cysteine decreases by about 30 $Å^3$. M-X-M cross linkers lose two SO_2CH_3 groups reducing their effective volume by about 60 $Å^3$ (see Fig.3.3.1). We then compared the blocking effect of 100 μM of different MTS compounds such as MTSET (N=6), M-4-M (N=6), MTSPT (N=4) and MTSPtrEA (N=8) (see Fig.3.3.6.D). MTSET is the shortest of the four compounds and MTS-PtrEA is the bulkiest. As shown in Fig.3.3.6.D, MTSET is shorter than M-4-M; in contrast, MTSPT and MTS-PtrEA have the same effective length of M-4-M but have a larger volume. If M-4-M is sterically occluding the pore, rather than cross-linking two exogenous cysteines, bulkier MTS compounds are expected to block more intensely the mutant channel $A406C_{cys-free}$. But as shown in Fig.3.3.6.D neither 100 μM MTSET (N =5) nor the same concentration of MTSPT blocked the mutant $A406C_{cys-free}$ (N = 4) and the same concentration of the much bulkier compound MTSPtrEA blocked $\sim$30% (N = 8) of the current observed in the control condition (see Fig.3.3.6.D). These results show that the blockage observed by the M-4-M is not caused by steric occlusion, but by the cross-linking of exogenous cysteines. The absence of Cd^{2+} blockage in mutant channel $A406C_{cys-free}$ is ascribed to the fact that the 3D structure of the CNGA1 and $CNGA1_{cys-free}$ is different and in particular residues at position 406 of the $CNGA1_{cys-free}$ are at a reciprocal distance not compatible with Cd^{2+} coordination but compatible with the coordination by the cross-linker M-4-M. In the A406C mutant channel residues at position 406 are at a compatible reciprocal distance to coordinate with Cd^{2+}, but not with the longer cross-linkers M-2-M and M-4-M.

Discussion:

Two constructs derived from the CNGA1 channels from bovine rods have been recently proposed as useful tools for the investigation of the relation between structure and function in CNGA1 channels. The first construct is the $CNGA1_{cys-free}$ channels (Matulef et al., 1999), where all endogenous cysteines were replaced with other residues not bearing a S atom. The second construct is the $CNGA1_{tandem}$ where two CNGA1 subunits are joined together by a small linker composed of some tens of residues (Flynn and Zagotta, 2003; Liu and Siegelbaum, 2000; Matulef and Zagotta, 2002; Rosenbaum and Gordon, 2002; Rothberg et al., 2002). However, it has not been proven that ionic channels formed by these constructs have a 3D structure identical or very similar to that of the CNGA1 channel. On the basis of their experimental investigation regarding the physiological properties of CNGA1 and $CNGA1_{cys-free}$ channels, (Matulef et al. 1999) concluded that mutation of all endogenous cysteines led to functional channels which were gated by cGMP in a way not too different from what observed in the CNGA1 channel. However, the degree of structural similarity between the $CNGA1_{cys-free}$ and CNGA1 was not established. The investigation of electrophysiological properties of CNGA1, $CNGA1_{tandem}$ and $CNGA1_{cys-free}$ channels here presented, does not show any statistically significant difference between the CNGA1 and $CNGA1_{tandem}$ channels. The CNGA1 and $CNGA1_{cys-free}$ channels have also very similar qualitative properties, such as ionic selectivity, I/V relations, blockage by divalent cations, organic compounds and tetracaine instead differ in some quantitative features which are statistically significant. Given the crucial role of cysteine residues in protein structure it is not surprising that functional properties of CNGA1 and $CNGA_{cys-free}$ channels are different and it is important to quantify

their structural difference.

Electrophysiological differences between the CNGA1 and CNGA1$_{\text{tandem}}$ channels

As shown in Figs.3.3.2-4 and Table 1 the I/V relations, ionic selectivity, dose response of the cGMP activated current and blockage in CNGA1$_{\text{tandem}}$ and CNGA1 channels are not different in a statistically significant way. Since there is no electrophysiological difference between these two channels, we can then deduct that their 3 D structure is very similar even though we cannot provide a precise estimate of this similarity.

Electrophysiological differences between the CNGA1 and CNGA1$_{cys-free}$ channels

Three quantitative differences were observed in the electrophysiological properties of the CNGA1 and CNGA1$_{cys-free}$ channels. Firstly, as shown in Fig.3.3.2 the concentration of cGMP activating half of the maximal current K$_{1/2}$ was 116.9 $\pm$ 7.2 and 27.5 $\pm$ 6.1 for the CNGA1 and CNGA1$_{cys-free}$ channels respectively, in agreement with what already observed by (Matulef et al 1999). Secondly, as shown in Fig.3.3.3, at +100 mV 100 μM Cd^{2+} ions added to the intracellular side of the membrane blocked CNGA1$_{cys-free}$ to a lower extent than CNGA1 channels. Thirdly, as shown in Fig.3.3.4 and discussed in the text when Na$^+$ ions were replaced with TEA$^+$, the cGMP activated current at both +100 and - 100 mV decreased more in CNGA1$_{cys-free}$ than in CNGA1 channels. These differences were statistically significant. Blockage by Ca^{2+} ions and by the organic compound TMA$^+$ was not significantly different in CNGA1 and CNGA1$_{cys-free}$ channels.

Structural differences between the CNGA1 and CNGA1$_{cys-free}$ channels

From the observed electrophysiological differences it is not possible to determine at which extent the 3D structures of the CNGA1 and CNGA1$_{cys-free}$ channel differ. Indeed blockage of an ionic channel can be modulated by the position and properties of a single residue (Bucossi et al., 1996; Gordon and Zagotta, 1995) and significant functional differences can originate from very small structural changes often of the order of just 1 Å or less. For instance, single channel properties of the CNGA1 channel change when the length of the side chain at position 363 is reduced by 1 Å in the mutant E363D (Bucossi et al., 1997).

In order to quantify differences in the 3D structure of CNGA1 and CNGA1$_{cys-free}$ channels, we looked for a residue of the CNGA1 channel, which, when mutated into a cysteine, could cross-link with another cysteine at the same position but from a different subunit. The length of the cross-linker is a good indicator of the distance between homologous residues in different subunits: if Cd^{2+} ion is the cross-linking reagent, the distance between the C$_\alpha$ of the homologous residues is between 8 and 11 Å. The reagents M-2-M, M-4-M and M-6-M are molecules with a S atom at both ends separated by a handle of variable lengths (Loo and Clarke, 2001). If the same residue in the CNGA1$_{cys-free}$ channel is not cross-linked by a Cd^{2+} ion but by a M-X-M reagent, the length of the handle provides an estimate of the different distance between homologous residues in the CNGA1 and CNGA1$_{cys-free}$ channels. Given the presence of several endogenous cysteines in the CNGA1 channel (see Fig.3.3.1) it is difficult to distinguish between the formation of S-S bridges between a pair of exogenous cysteines
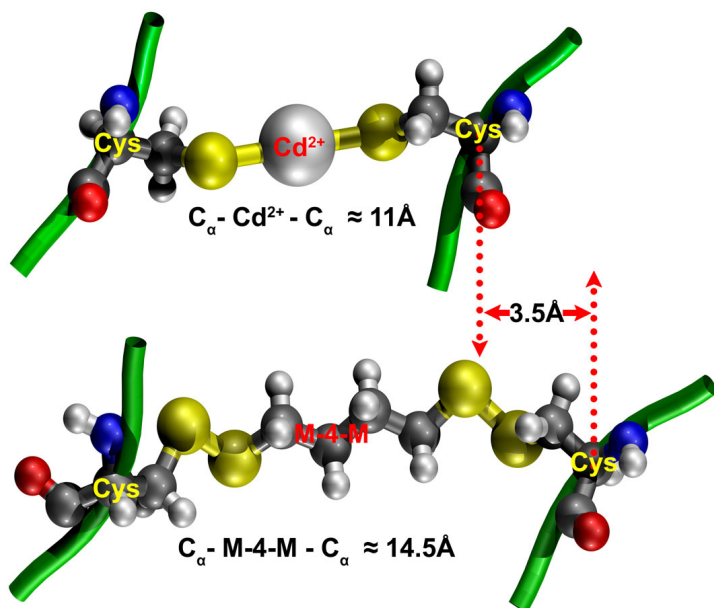
Figure 3.3.7: *The distance between homologous residues at position 406 in the CNGA1 and CNGA1$_{cys-free}$ channels. A and B: a model of the binding of Cd^{2+} and M-4-M to CNGA1 and CNGA1$_{cys-free}$ channels respectively. The green tube represents part of S6 helix where the mutated A406C is positioned. The sulfur atom of cysteine is shown as yellow spheres, coordinating with a Cd^{2+} in the CNGA1 channel and cross-links with the sulfur atoms from both ends of M-4-M in the CNGA1$_{cys-free}$ channel. The difference in the distance between the C$_\alpha$ of the two channels is about 3.5 Å.*

and between one exogenous and one endogenous cysteine. As shown in Fig.3.3.5 in the absence of cGMP Cd^{2+} ions powerfully block in an irreversible way the mutant channel A406C. In the triple mutant channel A406C&C481A&C505T Cd^{2+} blockage was still present. These results indicate that the observed irreversible Cd^{2+} blockage in mutant channel A406C can be ascribed to a cross-linking reaction between exogenous cysteines in homologous positions. By contrast, the mutant channel A406C$_{cys-free}$ in the absence of cGMP is not blocked by Cd^{2+} ions but is blocked by 100 μM of the cross-linker M-4-M (see Fig.3.3.6). Mutant channel A406C$_{cys-free}$ is not blocked by 100 μM MTSET, which has a slightly higher volume than M-4-M. Further more two other MTS derivatives MTSPT (Sullivan and Cohen, 2000) and MTS-PtrEA (Contreras and Holmgren, 2006) with same length as M-4-M but with much higher volume (see Fig.3.3.6.D) did not block the channel. Therefore blockage of the mutant channel A406C$_{cys-free}$ in the absence of cGMP by M-4-M is ascribed to the cross-linkage of exogenous cysteines in two subunits. These results are summarized in Fig.3.3.7.A and B.

The C$_\alpha$ of residues at position 406 of the CNGA1 are at distance of about 8-11 Å, but the same residues in the CNGA1$_{cys-free}$ channel are at a distance about 3-4 Å longer, so that one Cd^{2+} cross-links homologous residues in the CNGA1 channel but not in the CNGA1$_{cys-free}$ channel. In the CNGA1$_{cys-free}$ channel the reagent M-4-M is necessary to cross-link the same homologous residues, so that the distance between their C$_\alpha$ is 14.5Å, i.e. 3-4 Å more than in the CNGA1 channel. As the strength and nature of chemical interactions change drastically when distances are increased by 3-4 Å, the way in which the CNGA1 and CNGA1$_{cys-free}$ channels interact with chemical probes can be completely different. This conclusion is not surprising, as when all cysteines are removed from a protein the overall 3D structure can change quite significantly. Indeed we have previously shown that it was possible to lock the mutant channel F380C channel in the open and closed state, but *only to some extent* when Phe380 is replaced with a cysteine in the CNGA1$_{cys-free}$ channel (Nair et al., 2006).

Functional differences between native and cysteine free proteins have already been reported and investigated. The catalytic activity of the cysteine free B Glutathione Synthetase from *Escherichia coli* reduced to 26% compared to that measured in the w.t. (Kato et al., 1988). The different catalytic

activity was ascribed to a perturbation in the tertiary structure of the enzyme. The effect of drugs on the cysteine free P-glycoprotein is significantly different from that observed on the wild type protein (Taylor et al., 2001): the action of nicardipine on the catalytic cycle of P-glycoprotein is clearly modulated by cysteine substitution. The removal of all 12 native cysteines from the rat renal Na^+/Pi cotransporter led to a non functional protein (Kohler et al., 2003).

References

Akabas,M.H., D.A.Stauffer, M.Xu, A.Karlin (1992) Acetylcoline receptor channel structure probed in cysteine-substitution mutants. *Science* **258**:307-310.

Becchetti,A., K.Gamel, V.Torre (1999) Cyclic Nucleotide-gated Channels Pore topology studied through the Accessibility of Reporter Cysteins. *J Gen Physiol* **114**:377-392.

Becchetti,A., K.Gamel (1999) The properties of cysteine mutants in the pore region of cyclic-nucleotide-gated channels. *Pflugers Arch* **438**:587-596.

Biel,M., X.Zong, F.A.Ludwing, A.Sautter, F.Hofmann (1999) Structure and function of cyclic nucleotide-gated channels. *Rev Physiol Biochem Pharmacol* **135**:151-171.

Bradley,J., S.Frings, K.W.Yau, R.Reed (2001) Nomenclature for ion channel subunits. *Science* **294**:2095-2096.

Brown,R.L., S.D.Snow, T.L.Haley (1998) Movement of gating machinery during activation of rod cyclic nucleotide-gated channels. *Biophys J* **75**:825-833.

Bucossi,G., E.Eismann, F.Sesti, M.Nizzari, M.Seri, U.B.Kaupp, V.Torre (1996) Time-dependent current decline in cyclic GMP-gated bovine channels caused by point mutations in the pore region expressed in Xenopus oocytes. *J Physiol (Lond)* **493**:409-418.

Bucossi,G., M.Nizzari, V.Torre (1997) Single-channel properties of ionic channels gated by cyclic nucleotides. *Biophys J* **72**:1165-1181.

Colamartino,G., A.Menini, V.Torre (1991) Blockage and permeation of divalent cations through the cyclic GMP-activated channel from tiger salamander retinal rods. *J Physiol* **440**:189-206.

Contreras,J.E., M.Holmgren (2006) Access of quaternary ammonium blockers to the internal pore of cyclic nucleotide-gated channels: implications for the location of the gate. *J Gen Physiol* **127**:481-494.

Craven,K.B., W.N.Zagotta (2006) CNG and HCN channels: two peas, one pod. *Annu Rev Physiol* **68**:375-401.

Eismann,E., F.Muller, S.H.Heinemann, U.B.Kaupp (1994) A single negative charge within the pore region of a cGMP-gated channel controls rectification, Ca^{2+} blockage, and ionic selectivity. *Proc Natl Acad Sci USA* **91**:1109-1113.

Fesenko,E.E., S.S.Kolesnikov, A.L.Lyubarsky (1985) Induction by cyclic GMP of cationic conductance in plasma membrane of retinal rod outer segment. *Nature* **313**:310-313.

Flynn,G.E., W.N.Zagotta (2003) A Cysteine scan of the inner Vestibule of Cyclic Nucleotide gated channels Reveals Architecture and Rearrangement of the Pore. *J Gen Physiol* **121**:563-582.

Fodor,A.A., K.D.Black, W.N.Zagotta (1997a) Tetracaine reports a conformational change in the pore of cyclic nucleotide-gated channels. *J Gen Physiol* **110**:591-600.

Fodor,A.A., S.E.Gordon, W.N.Zagotta (1997b) Mechanism of tetracaine block of cyclic nucleotide-gated channels. *J Gen Physiol* **109**:3-14.

Glusker,J.P. (1991) Structural aspects of metal liganding to functional groups in proteins. *Adv Protein Chem* **42**:1-76.

Gordon,S.E., M.D.Varnum, W.N.Zagotta (1997) Direct interaction between amino- and carboxyl-terminal domains of cyclic nucleotide-gated channels. *Neuron* **19**:431-441.

Gordon,S.E., W.N.Zagotta (1995) Subunit interactions in coordination of Ni^{2+} in cyclic nucleotide-gated channels. *Proc Natl Acad Sci U S A* **92**:10222-10226.

Hastrup,H., A.Karlin, J.A.Javitch (2001) Symmetrical dimer of the human dopamine transporter revealed by cross-linking Cys-306 at the extracellular end of the sixth transmembrane segment. *Proc Natl Acad Sci U S A* **98**:10055-10060.

Humphrey,W., A.Dalke, K.Schulten (1996) VMD: visual molecular dynamics. *J Mol Graph* **14**:33-38.

Jan,L.Y., Y.N.Jan (1990) A superfamily of ion channels. *Nature* **345**:672.

Karlin,A., M.H.Akabas (1998) Substituted-cysteine accessibility method. *In Methods in Enzimology.* P.M. Conn, Editor. Academic Press, San Diego:123-145.

Kato,H., T.Tanaka, T.Nishioka, A.Kimura, J.Oda (1988) Role of cysteine residues in glutathione synthetase from Escherichia coli B. Chemical modification and oligonucleotide site-directed mutagenesis. *J Biol Chem* **263**:11646-11651.

Kaupp,U.B., T.Niidome, T.Tanabe, S.Terada, W.Bonigk, W.Stuhmer, N.J.Cook, K.Kangawa, H.Matsuo, T.Hirose, T.Miyata, S.Numa (1989) Primary structure and functional expression from complementary DNA of the rod photoreceptor cyclic GMP-gated channel. *Nature* **342**:762-766.

Kaupp,U.B., R.Seifert (2002) Cyclic nucleotide gated channels. *Physiol Rev* **82**:769-824.

Kohler,K., I.C.Forster, G.Stange, J.Biber, H.Murer (2003) Essential cysteine residues of the type IIa Na^+/Pi cotransporter. *Pflugers Arch* **446**:203-210.

Korschen,H.G., M.Illing, R.Seifert, F.Sesti, A.Willams, S.Gotzes, C.Colville, F.Mller, A.Dos, M.Godde

(1995) A 240 kDa protein represents the complete beta subunit of the cyclic nucleotide-gated channel from rod photoreceptor. *Neuron* **15**:627-636.

Liu,J., S.A.Siegelbaum (2000) Change of pore helix conformational state upon opening of cyclic nucleotide gated channels. *Neuron* **28**:899-909.

Loo,T.W., D.M.Clarke (2001) Determining the dimensions of the drug-binding domain of human P-glycoprotein using thiol cross-linking compounds as molecular rulers. *J Biol Chem* **276**:36877-36880.

Matulef,K., W.N.Zagotta (2003) Cyclic nucleotide-gated ion channels. *Annu Rev Cell Dev Biol* **19**:23-44.

Matulef,K., G.E.Flynn, W.N.Zagotta (1999) Molecular rearrangements in the ligand-binding domain of cyclic nucleotide-gated channels. *Neuron* **24**:443-452.

Matulef,K., W.Zagotta (2002) Multimerization of the ligand binding domains of cyclic nucleotide-gated channels. *Neuron* **36**:93-103.

Menini,A. (1990) Currents carried by monovalent cations through cyclic GMP-activated channels in excised patches from salamander rods. *J Physiol* **424**:167-185.

Molday,R.S., L.L.Molday, A.Dose, I.Clark-Lewis, M.Illing, N.J.Cook, E.Eismann, U.B.Kaupp (1991) The cGMP-gated channel of the rod photoreceptor cell characterization and orientation of the amino terminus. *J Biol Chem* **266**:21917-21922.

Nair,A.V., M.Mazzolini, P.Codega, A.Giorgetti, V.Torre (2006) Locking CNGA1 channels in the open and closed state. *Biophys J* **90**:3599-3607.

Nizzari,M., F.Sesti, M.T.Giraudo, C.Virginio, A.Cattaneo, V.Torre (1993) Single-channel properties of cloned cGMP-activated channels from retinal rods. *Proc R Soc Lond* **254**:69-74.

Picco,C., A.Menini (1993) The permeability of the cGMP-activated channel to organic cations in retinal rods of the tiger salamander. *J Physiol* **460**:741-758.

Ren,X., D.A.Nicoll, K.D.Philipson (2006) Helix packing of the cardiac Na^+-Ca^{2+} exchanger: proximity of transmembrane segments 1, 2, and 6. *J Biol Chem* **281**:22808-22814.

Root,M.J., R.MacKinnon (1993) Identification of an external divalent binding site in the pore of a cGMP-activated channel. *Neuron* **11**:459-466.

Rosenbaum,T., S.E.Gordon (2002) Dissecting intersubunit contacts in cyclic nucleotide-gated ion channels. *Neuron* **33**:703-713.

Rothberg,B., K.Shin, P.Phale, G.Yellen (2002) Voltage-controlled gating at the intracellular entrance to a hyperpolarization-activated cation channel. *J Gen Physiol* **119**:83-91.

Sesti,F., E.Eismann, U.B.Kaupp, M.Nizzari, V.Torre (1995) The multi-ion nature of the cGMP-gated channel from vertebrate rods. *J Physiol (Lond)* **487**:17-36.

Shapiro,S.S., M.B.Wilk (1965) An analysis of variance test for normality (complete samples). *Biometrika*

52 :591-611.

Snedecor,G.W. and W.G.Cochran. 1989. *Statistical Methods*. 8th ed. Blackwell Publishing Company, 98-99 pp.

Sullivan,D.A., J.B.Cohen (2000) Mapping the agonist binding site of the nicotinic acetylcholine receptor. Orientation requirements for activation by covalent agonist. *J Biol Chem* **275**:12651-12660.

Sun,Z.P., M.H.Akabas, E.H.Goulding, A.Karlin, S.A.Siegelbaum (1996) Exposure of residues in the cyclic nucleotide-gated channel pore: P region structure and function in gating. *Neuron* **16**:141-149.

Taylor,A.M., J.Storm, L.Soceneantu, K.J.Linton, M.Gabriel, C.Martin, J.Woodhouse, E.Blott, C.F.Higgins, R.Callaghan (2001) Detailed characterization of cysteine-less P-glycoprotein reveals subtle pharmacological differences in function from wild-type protein. *Br J Pharmacol* **134**:1609-1618.

Varnum,M.D., W.N.Zagotta (1996) Subunit interactions in the activation of cyclic nucleotide-gated ion channels. *Biophys J* **70**:2667-2679.

Weitz,D., N.Ficek, E.Kremmer, P.J.Bauer, U.B.Kaupp (2002) Subunit stoichiometry of the CNG channel of rod photoreceptors. *Neuron* **36**:881-889.

White,D., C.B.Taverner, P.G.L.Leach, N.J.Coville (1993) Quantification of substituent and ligand size by the use of solid angles. *J Comp Chem* **14**:1042-1049.

Zagotta,W.N., S.A.Siegelbaum (1996) Structure and function of cyclic nucleotide-gated channels. *Annu Rev Neurosci* **19**:235-263.

Zheng,J., M.C.Trudeau, W.N.Zagotta (2002) Rod cyclic nucleotide gated channels have a stoichiometry of three CNGA1 subunits and one CNGB1 subunit. *Neuron* **36**:891-896.

Zhong,H., L.L.Molday, R.S.Molday, K.W.Yau (2002) The heteromeric cyclic nucleotide-gated channel adopts a 3A:1B stoichiometry. *Nature* **420**:193-198.

Movements of native C505 during channel gating in CNGA1 channels

Monica Mazzolini, **Anil V. Nair***, Claudio Anselmi and Vincent Torre*[#]

International School for Advanced Studies and INFM section

via Beirut 2-4 I-34014 Trieste, Italy

[#]Corresponding author: Vincent Torre

Scuola Superiore di Studi Avanzati (SISSA)

Area Science Park, SS 14 Km 163.5, Edificio Q1,

34012 Basovizza (TS), Italy

Tel/Fax: +39-040-3756513   e-mail: torre@sissa.it ;

Condensed Title: C505 during gating of CNGA1 channels

Monica Mazzolini, Anil V. Nair, Claudio Anselmi and Vincent Torre.

Abstract:

We have investigated conformational changes occurring in the C-linker and cyclic nucleotide-binding (CNB) domain of CNGA1 channels from bovine rod photoreceptors, by analyzing the inhibition induced by thiol specific reagents in mutant channels Q409C and A414C in the open and closed state. 200 μM Cd^{2+} inhibited irreversibly mutant channels Q409C and A414C in the closed but not in the open state. Cd^{2+} inhibition was abolished in the double mutant A414C&C505T and in the tandem construct A414C&C505T+w.t$_{tandem}$. The cross-linker reagent M-2-M inhibited mutant channel Q409C in the open state. M-2-M inhibition in the open state was abolished in the double mutant Q409C&C505T and in the tandem construct Q409C&C505T+ w.t$_{tandem}$. These results show that the C_α of C505 in the closed state is located at a distance of approximately 8 Å from the C_α of A414 of the same subunit, but in the open state it moves towards Q409 of the same subunit between 10 and 13 Å from the C_α of this residue. These results are not consistent with a 3-D structure of the CNGA1 channel homologous to that of HCN2 channels neither in the open nor in the closed state.

Abbreviations used in this article:

CNG, Cyclic nucleotide-gated; CNBD, Cyclic nucleotide-binding domain; CSM, Cysteine scanning mutagenesis; MTS, Methanethiosulfonate; MTSET, 2-(Trimethylammonium)ethyl methanethiosulfonate bromide; MTSPT, 3- (Trimethylammonium) propyl methanethiosulfonate bromide; MTS-PtrEA, 3-(Triethylammonium)propyl methanthiosulfonate bromide; M-2-M, 1,2-Ethanediyl bismethanethiosulfonate; M-4-M, 1,4-Butanediyl bismethanethiosulfonate.

Introduction:

Cyclic nucleotide gated (CNG) channels underlie sensory transduction in vertebrate photoreceptors and in olfactory sensory neurons. To open, they require cyclic nucleotides such as cAMP or cGMP (Fesenko et al., 1985; Zimmerman et al., 1985; Nakamura and Gold, 1987; Kaupp et al., 1989; Zagotta and Siegelbaum, 1996; Biel et al., 1999; Kaupp and Seifert, 2002; Craven and Zagotta, 2006). Contrarily to the usual N^+ and K^+ channels, CNG channels are cation selective, but poorly selective among monovalent alkali cations (Zimmerman and Baylor, 1986; Kaupp et al., 1989; Menini, 1990; Picco and Menini, 1993; Craven and Zagotta, 2006). They also form a tetrameric assembly of several homologous subunits (Chen et al., 1994; Korschen et al., 1995; Shammat and Gordon, 1999; Zheng et al., 2002; Zhong et al., 2002; Craven and Zagotta, 2006), referred to as CNGA and CNGB (Bradley et al., 2001). The CNGA1 channel from bovine rods (BROD) is composed of 690 residues (Kaupp et al., 1989) and each subunit encodes for a cyclic nucleotide-binding (CNB) domain consisting of about 125 amino acids in the cytoplasmic C terminal (Kaupp et al., 1989; Zagotta and Siegelbaum, 1996). The CNB domain connects to the transmembrane domain of CNG channels through another domain composed of about 77 amino acids referred to as the C-linker.

The amino acid sequence of CNG and K^+ channels share a significant homology and both channels are members of the superfamily of voltage-gated channels (Zagotta and Siegelbaum, 1996; Biel et al., 1999). They also have a significant homology with the family of Hyperpolarization-activated and Cyclic

Nucleotide-gated (HCN) channels (Anselmi et al., 2007), composed of four isoforms called HCN1, HCN2, HCN3 and HCN4 (Hofmann et al., 2005). All these channels open when the membrane potential is hyperpolarized and their activation properties can be modulated, to some extent, by cyclic nucleotides. It is known that the 3-D structure of the C-linker and CNB domains of murine HCN2 channels has been solved (Zagotta et al., 2003); and that the sequence alignment of these domains in HCN2 and bovine CNGA1 channels indicates a sequence identity of 32 %. Several important residues such as K472, E502 and D542 known to form salt bridges in HCN2 channels (Craven and Zagotta, 2004) are conserved also in CNG channels (Zagotta et al., 2003) and the charged residues R590 and E617 forming inter-subunit bonds between the proximal HCN2 CNB domains (Zagotta et al., 2003) are also conserved in CNG channels. This indicates that the overall folding of the C-linker domain of HCN2 and CNGA1 channels could be similar.

The purpose of the present manuscript is to obtain experimental constraints on the relative distance between amino acids to test the hypothesis that the 3D structure of the C-linker in CNGA1 channels is homologous to that of HCN2 channels. Here we show that in the closed state C505 is near to A414 of the same subunit but in the open state it moves close to Q409 of the same subunit. These results are not consistent with a 3-D structure of the CNGA1 channel, homologous to that of HCN2 channels neither in the open nor in the closed state.

Materials and Methods:

Molecular Biology

Three different channel constructs from bovine rods were used: the CNGA1 channel consisting of 690 residues, the tandem dimer construct and the CNGA1$_{cys-free}$ channel (Matulef et al., 1999). Selected residues were replaced by introducing a cysteine in the three channels as described (Becchetti and Gamel, 1999; Matulef et al., 1999) using the Quick Change Site-Directed Mutagenesis kit (Stratagene). Point mutations were confirmed by sequencing, using the sequencer LI-COR (4000L). cDNAs were linearized and were transcribed to cRNA in vitro using the mMessage mMachine kit (Ambion, Austin, TX).

The tandem dimer construct was generated by the insertion of one copy of the CNGA1 DNA into a vector pGEMHE already containing another copy of CNGA1 DNA. At the end of cloning, two copies of the CNGA1 DNA were connected by a 10-amino acid linker GSGGTELGST(Rothberg et al., 2002) joining the C-terminus of the first CNGA1 with the N- terminus of the second one. This second subunit was made by replacing the ApaI restriction site 'GGGCCC' at the end of the CNGA1 DNA without changing the aminoacid 'GGTCCC' and adding to the start codon a new ApaI restriction site followed by a linker using a PCR reaction. Subunits were linked after HindIII/ApaI cut.

Oocyte preparation and chemicals

Mutant channel cRNAs were injected into *Xenopus laevis* oocytes ("Xenopus express" Ancienne Ecole de Vernassal, Le Bourg 43270, Vernassal, Haute-Loire, France). Oocytes were prepared as described (Nizzari et al., 1993). Injected eggs were maintained at 18°C in a Barth solution supplemented

with 50 μg/ml of gentamycin sulfate and containing (in mM): 88 NaCl, 1 KCl, 0.82 MgSO$_4$, 0.33 Ca(NO$_3$)$_2$, 0.41 CaCl$_2$, 2.4 NaHCO$_3$, 5 TRIS-HCl, pH 7.4 (buffered with NaOH). During the experiments, oocytes were kept in a Ringer solution containing (in mM): 110 NaCl, 2.5 KCl, 1 CaCl$_2$, 1.6 MgCl$_2$, 10 HEPES-NaOH, pH 7.4 (buffered with NaOH). Usual salts and reagents were purchased from Sigma Chemicals (St. Louis, MO, USA) and MTS cross-linkers (M-2-M and M-4-M) were purchased from TRC (Toronto Research Chemicals, Canada).

Recording apparatus

cGMP-gated currents from excised patches were recorded with a patch-clamp amplifier (Axopatch 200B, Axon Instruments Inc., Foster City, CA, USA), 2-6 days after RNA injection, at room temperature (20-24°C). The perfusion system was as described (Sesti et al., 1995) and allowed a complete solution change in less than 1 s. Borosilicate glass pipettes had resistances of 3-10 MΩ in symmetrical standard solution. The standard solution on both sides of the membrane consisted of (in mM) NaCl, 110; HEPES, 10; and EDTA, 0.2 (pH 7.4). The membrane potential was usually stepped from 0 to $\pm$ 60 mV. We used Clampex 8.0, Clampfit, and Matlab for data acquisition and analysis. Currents were low-pass filtered at 2 kHz and acquired digitally at 5 kHz.

Application of sulfhydryl-specific reagents

In the inside-out patch-clamp configuration, soon after patch excision, the cytoplasmic face of the plasma membrane was perfused with the same pipette-filling solution. The effect of Cd^{2+} was tested by perfusing the intracellular side of the membrane with a standard solution without EDTA (to avoid partial Cd^{2+} chelation), supplemented with variable amounts (from 10 to 500 μM) of CdCl$_2$ for different times. The time course of Cd^{2+} inhibition of mutants Q409C and A414C was determined by applying 100 and 200 μM of the reagent in the closed state (i.e. in the absence of cGMP) for variable time periods and by measuring the current observed after Cd removal in the presence of 1 mM cGMP. Fig.4.3.1.A and B show data collected from 7 patches containing the mutant channel Q409C exposed for variable times to 100 and 200 μM Cd^{2+} respectively. Data were normalized to the cGMP current activated at + 60 mV before Cd^{2+} treatment. The solid line through the experimental points was obtained from the equation y $= exp(-\tau/t)$ where τ is the time constant of Cd^{2+} inhibition. Fig.4.3.1.C and D show similar data but for the mutant channel A414C.

Therefore, we analysed Cd^{2+} inhibition in the closed state by exposing patches to 200 μM Cd^{2+} for 5 minutes. In some constructs, such as Q409C+C505T and Q409C+C481A, with this procedure an inhibition between 30 and 70 % was observed. The partial inhibition observed after 5 minutes of Cd^{2+} exposure could be due to a slower inhibition rate of Cd^{2+} ions and therefore we investigated the effect of longer exposures to Cd^{2+} ions. To study Cd^{2+} inhibition in the open state, we applied 200 μM Cd^{2+} in the presence of 1mM cGMP for 5 minutes or longer, during which the amplitude of the cGMP activated current was continuously monitored.

Cross-linker compounds were dissolved in dimethyl sulfoxide (DMSO) and diluted in standard solution to a final concentration of 100 μM. The final concentration of DMSO was 0.1%. We checked that this concentration of DMSO did not affect the cGMP activated current. Solutions containing
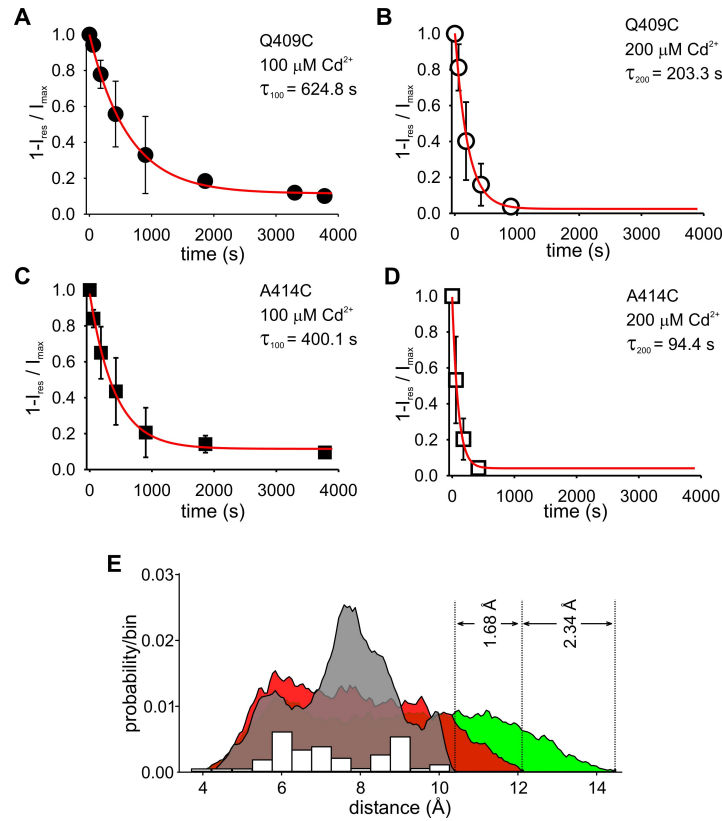
Figure 3.4.1: *Time course of inhibition by Cd^{2+} on mutant channels Q409C and A414C. **A,B:** Inhibition of Q409C by 100 and 200 μM Cd^{2+} respectively in the closed state. Values are shown as mean $\pm$ SD. The solid red line through the data is the fit to equation $y = exp(-\tau/t)$, where τ is the time constant of Cd^{2+} inhibition. The τ for mutant Q409C by 100 μM Cd^{2+} is 624.8 s and 203.3 s by 200 μM Cd^{2+}. **C,D:** the data shown are obtained as of panel A and B, but for mutant channel A414C. The time course of inhibition is 400.1 s by 100 μM Cd^{2+} and 94.4 s by 200 μM Cd^{2+}. **E:** Distribution of the distance between the C_α of cysteines coordinating one Cd^{2+} ion (grey), M-2-M (red) and M-4-M (green) calculated with AMBER package (see methods). White bars indicate distances between C_α of cysteines coordinating one Cd^{2+} ion obtained from inspection of the PBD (Giorgetti et al., 2005)*

cross-linker compounds were prepared immediately before the application (typically < 5 min) to prevent degradation, as these reagents dissociate rapidly in aqueous solution. They were never used for more then 45 minutes after dissolving in aqueous solution. The cross-linkers of different length were used to determine the distance between exogenously introduced cysteines (Loo and Clarke, 2001; Ren et al., 2006).

Estimation of the distance between C_α of coordinating cysteines

The distance between the C_α of cysteines coordinating Cd^{2+} ions or cross-linkers such as M-2-M and M-4-M was estimated by inspection of the 3D structure of proteins contained in the Protein Data Bank (PDB) and by molecular dynamical simulations. Inspection of PDB shows that distance between C_α of cysteines that Cd^{2+} coordinates ranges between 5 and 10 Å(see white bars in Fig.3.4.1.E) (Giorgetti et al., 2005). The cross-linkers M-2-M and M-4-M can coordinate cysteines at a larger distance. As no crystal structure of a protein coordinating either M-2-M or M-4-M is available, a direct evaluation of the distance between C_α of cysteines cross-linking these compounds cannot be obtained from the PDB. For this reason we used molecular dynamics: first we calculated the distribution of distances between

C_α of cysteines coordinating one Cd^{2+} ion by molecular dynamics simulation using AMBER package (see grey area in Fig.3.4.1.E). The distribution of the C_α - C_α distance obtained by molecular dynamics provides similar results as those obtained by the direct inspection of the 3D structures in the PDB. We then performed similar molecular dynamics simulations of two cysteines cross-linked by M-2-M and M-4-M (red and green areas in Fig.3.4.4.E). As shown in Fig.3.4.1.E, M-2-M can coordinate two cysteines when the distance between their C_α is between 4 and 12 Å and M-4-M when the distance between their C_α is between 4 and 15 Å. These results indicate that if Cd^{2+} inhibits the channel by coordinating to two cysteines, the distance between the C_α of coordinating cysteines is $\leq$10.5 Å. If channel inhibition is observed with M-2-M but not Cd^{2+} then the distance between the C_α of coordinating cysteines is between 10 and 13 Å. Similarly, if the inhibition is caused by M-4-M and not by Cd^{2+} and M-2-M, the distance of the C_α of coordinating cysteines is between 12 and 14.5 Å.

Results:

A common tool for the investigation of functional and structural properties of ionic channels is Scanning Cysteine Mutagenesis (SCM) in which residues in a given region of the ionic channel are mutated one by one into a cysteine and the action of reagents able to interact with the sulfur atom of the cysteine is investigated. With this rationale we scanned several residues in the C-linker domain of CNGA1 channels from Phe375 to His420. In these mutated channels we studied the effect on cGMP activated current induced by 200 μM Cd^{2+} added for 5 minutes to the bathing medium in the presence (open state) or in the absence (closed state) of 1 mM cGMP. Exposure of CNGA1 channel for 5 minutes to 200 μM Cd^{2+} induced a very small permanent change in the cGMP activated current (9.4 $\pm$ 6 %, N = 7) (Nair et al., 2006). During this extensive SCM we found that many mutant channels were irreversibly inhibited by Cd^{2+} ions.

In the present manuscript, we analyze in detail the molecular mechanisms underlying inhibition by Cd^{2+} and longer cross-linkers such as M-2-M and M-4-M in mutant channels Q409C and A414C by using the following rationale. Inspection of the three dimensional (3D) structure of proteins in the Protein Data Bank(Berman et al., 2000) shows that one Cd^{2+} ion coordinate with two cysteines when the distance between their C_α varies between 4 and 10.5 Å. Therefore, if we can prove that Cd^{2+} inhibition is caused by its coordination with the exogenous cysteine inserted at position 414 (414C) and with the native C505 of the same subunit, we obtain a good estimate of the distance between the C_α of A414 and C505 in that specific subunit. The newly synthesized MTS cross-linkers (Loo and Clarke, 2001) can coordinate a pair of cysteines which are at a longer distance: indeed the two ends of these compounds have a S atom - which can react with the cysteines' S atom - separated by a handle or a spanning distance of increasing length, which for the cross-linkers M-2-M and M-4-M are 5 and 8 Å respectively. As discussed in the Methods section, a inhibition by M-2-M and not by Cd^{2+} indicates a slightly larger distance for the C_α of coordinating cysteines varying between 10.5 and 12.5 Å, and the inhibition by M-4-M (and not by Cd^{2+} and by M-2-M) reports a distance between the C_α of coordinating cysteines varying from 12 to 14.5 Å. This analysis provides valuable information for the understanding of the molecular structure of CNGA1 channels in the open and closed state.

Cd^{2+} inhibition of mutant channel A414C

The CNGA1 channel is composed of four subunits each containing 6 transmembrane helices indicated by grey cylinders in the insets of Fig.3.4.2. Each subunit contains 7 native cysteines indicated by a yellow C: C35, C169, C186, C314, C481, C505 and C573. When the CNGA1 channel from bovine rod is exposed for some minutes to an intracellular medium containing 200 μM Cd^{2+} in the open or closed state, the cGMP activated current measured after Cd^{2+} removal is not significantly modified, as shown in Fig.3.4.2.A (see also (Becchetti and Roncaglia, 2000; Nair et al., 2006)). The absence of any irreversible effect indicates that in the CNGA1 either Cd^{2+} ions cannot coordinate with multiple cysteines or such coordination does not modify the channel gating. A different behaviour was observed when a cysteine was introduced at position 414. In fact, as shown in Fig.3.4.2.B, the mutant channel A414C was irreversibly inhibited by exposure to Cd^{2+} ions in the closed state. The irreversible inhibition of the mutant channel A414C by 200 μM Cd^{2+} was 96.4 $\pm$ 2.7 % (N = 7). As shown in Fig.3.4.2.C, mutant channel A414C was not inhibited by Cd^{2+} in the open state (2.6 $\pm$ 2 %, N =4), and neither the cross-linker M-2-M nor M-4-M inhibited the mutant channel A414C in the open state (data not shown). These results suggest that in the open state 414C of different subunits are far from each other and they are also distant from endogenous C481 and C505. Irreversible inhibition (10.1 $\pm$ 2.1 %, N =2) in the closed state was not observed, even when A414 was substituted by a cysteine in the cysteine free CNGA1 channel (Matulef et al., 1999), as shown in Fig.3.4.2.D.
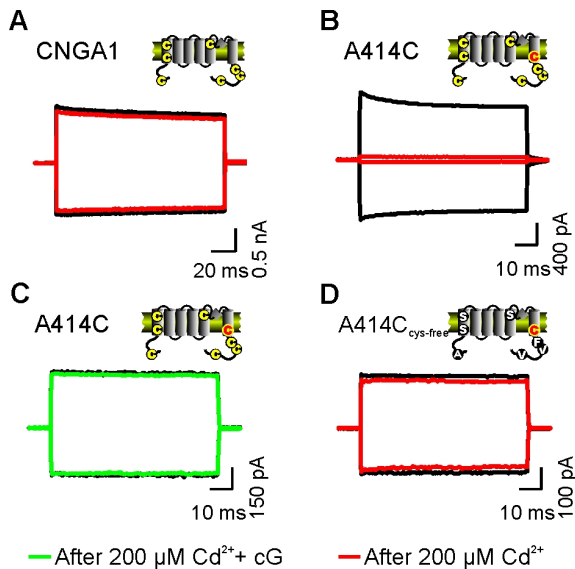

Figure 3.4.2: *Effect of Cd^{2+} on the CNGA1 and mutant channels. **A**: effect of 200 μM Cd^{2+} on the CNGA1 channel in the closed state. **B** & **C**: Effects of 200 μM Cd^{2+} on mutant channel A414C in the closed and open state respectively. Cd^{2+} irreversibly inhibits the mutant channel A414C (B red trace) in the closed state but not in the open state (C green trace). **D**: effect of 200 M Cd^{2+} on the mutant $Q409C_{cys-free}$ (mutation in the cysteine free background) in the closed state. Location of endogenous and exogenous cysteines introduced in mutant channels are shown superimposed to the presumed topology of an individual subunit at the upper right portion of each panel. Currents were measured in the presence of 1mM cGMP before and after a 5 min exposure to 200 M Cd^{2+}. Current traces were obtained by stepping the membrane voltage from 0 mV to 60 mV. Black traces were obtained in control conditions, before the application of Cd^{2+}, and red traces after the application of Cd^{2+} in the closed state - absence of cGMP. Green traces were obtained after the application of Cd^{2+} in the open state - presence of 1 mM cGMP.*

The different blocking effect of Cd^{2+} ions in the closed state observed in mutant channels A414C and A414C$_{cys-free}$ can be produced either by two different mechanisms or by their combination. Cd^{2+} inhibition of cysteine mutants in the CNGA1 background can originate from Cd^{2+} coordination with endogenous cysteines and particularly with C481 and C505 which are known to be part of the C-linker domain and are involved in the gating machinery of CNGA1 channels (Brown et al., 1998). An alternative explanation is that the 3-D structure of CNGA1$_{cys-free}$ channels differs by few Å from that of CNGA1 channels, so that Cd^{2+} can coordinate exogenous cysteines introduced in the CNGA1 channels but not in the CNGA1$_{cys-free}$ channels. Matulef et al (1999) have shown that tetracaine blocks in a very similar way both the CNGA1 and CNGA1$_{cys-free}$ channels, but also that the concentration of CNG activating half of the maximal current is different in the two channels. Therefore, some physiological properties of the CNGA1$_{cys-free}$ are very similar to those of the CNGA1 channels, but the degree of

similarity of the 3D structure of the CNGA1 and CNGA1$_{cys-free}$ has not been established. Experiments from our lab show that removal of all cysteines from the CNGA1 channels perturbs the position in space of several residues and that, for some aminoacids, the relative distance between homologous residues in different subunits is different by some Angstrom in the two channels (Mazzolini et. al, unpublished data). Given the major structural role of cysteines in protein structure it is expected that the exact 3D structure of a native protein is to be different at some extent from its cys-free version. Therefore, we decided to analyse Cd^{2+} inhibition in mutant channels Q409C and A414C when the least number of endogenous cysteines. Given their likely proximity to Gln409 and Ala414 we concentrated our attention to the two endogenous Cys481 and Cys505 and we investigated the mechanism of the irreversible Cd^{2+} inhibition observed in the closed state of mutant channel A414C by comparing Cd^{2+} inhibition whilst C481 was replaced with an alanine and C505 was replaced with a threonine. The inhibition caused by the exposure to 200 μM Cd^{2+} in A414C was not significantly affected in the double mutant A414C&C481A (Fig.3.4.3.A) but was drastically reduced in the double mutant A414C&C505T (Fig.3.4.3.B).
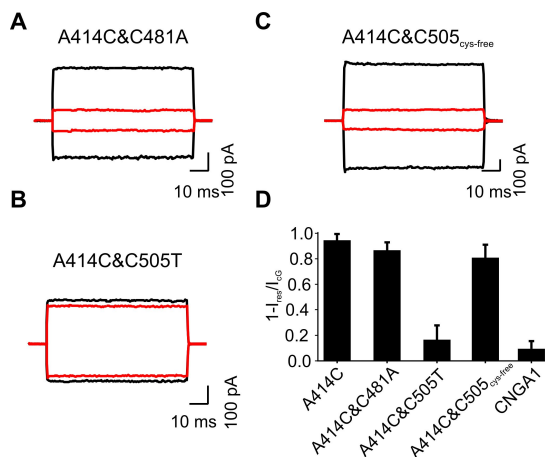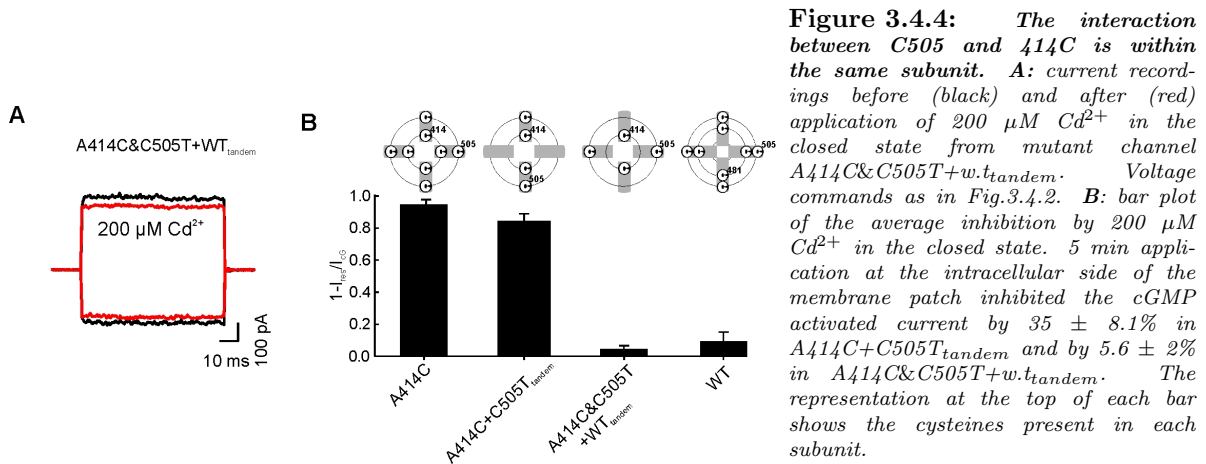

Figure 3.4.3: *Closed state inhibition of mutant channel A414C depends on C505. A, B and C: current recordings of cGMP activated current before (black) and after (red) application of 200 μM Cd^{2+} in the closed state from mutant channels A414C&C481A, A414C&C505T and A414C&C505$_{cys-free}$ respectively. Voltage commands as in Fig.3.4.2. B: bar plot of the average block by 200 μM Cd^{2+} of mutant channels in the closed state. Cd^{2+} was applied for 15 min in the CNGA1, A414C&C505T and A414C&C505$_{cys-free}$ channels and for 5 min in the A414C and A414C&C481A mutant channels.*

As shown in Fig.3.4.3.C, 200 μM Cd^{2+} ions inhibited the mutant channel A414C by 96.4 $\pm$ 2.7 % (N = 7), the double mutant channel A414C&C481A by 86 $\pm$ 6.2 % (N =5) and the mutant channel A414C&C505$_{cys-free}$ by 81.3 $\pm$ 11.1 % (N =4). In contrast, Cd^{2+} inhibition was drastically reduced and almost eliminated in the double mutant A414C&C505T (25$\pm$ 7.2%, N = 3). We report that in CNGA1 inhibition by the same concentraion of Cd^{2+} is 9.4 $\pm$ 6 %, (N = 7). These results strongly indicate that Cd^{2+} inhibition in the closed state in A414C mutant channels was generated by its coordination with 414C and C505.

The interaction between C505 and exogenous cysteine A414C is within the same subunit

In order to establish whether Cd^{2+} inhibition - observed in the closed state in mutant A414C - was a consequence of a cross-linkage between two cysteines from the same subunit or from neighboring subunits, two tandems were constructed: the tandem A414C & C505T+w.t$_{tandem}$ where each subunit contained either an exogenous cysteine at 414 or the native cysteine 505; and the tandem A414C + C505T$_{tandem}$ where two subunits have 414C as well as C505. As shown in Fig.3.4.4.A, 200 μM Cd^{2+} in the absence of cGMP inhibited poorly the tandem construct A414C&C505T+w.t$_{tandem}$ and Cd^{2+} inhibition was very similar to what observed in the CNGA1 channel.

The tandem A414C&C505T+w.t$_{tandem}$ has a very low expression rate. In 6 macro patches obtained

A

A414C&C505T+WT$_{tandem}$

200 μM Cd^{2+}

10 ms | 100 pA

B

Figure 3.4.4: *The interaction between C505 and 414C is within the same subunit.* **A:** *current recordings before (black) and after (red) application of 200 μM Cd^{2+} in the closed state from mutant channel A414C&C505T+w.t$_{tandem}$. Voltage commands as in Fig.3.4.2.* **B:** *bar plot of the average inhibition by 200 μM Cd^{2+} in the closed state. 5 min application at the intracellular side of the membrane patch inhibited the cGMP activated current by 35 ± 8.1% in A414C+C505T$_{tandem}$ and by 5.6 ± 2% in A414C&C505T+w.t$_{tandem}$. The representation at the top of each bar shows the cysteines present in each subunit.*

we have seen an intermediate inhibition between A414C and A414C&C505T+w.t$_{tandem}$. But subjected to prolonged (ranging between 600 and 900 s) application of Cd^{2+},the current in A414C & C505T +w.t$_{tandem}$ was completely inhibited. As summarized in fig.3.4.4.B, while 200 μM Cd^{2+} ions inhibited almost completely the cGMP activated current in mutant channel A414C, it did not block significantly the tandem A414C&C505T+w.t$_{tandem}$ (5.6 ± 2 %, N = 4). In contrast, Cd^{2+} inhibition in the A414C + C505T$_{tandem}$ channel was intermediate between the inhibition observed in mutant channels A414C and A414C & C505T+w.t$_{tandem}$. From these results, we conclude that the inhibition in mutant channel A414C in the closed state, by Cd^{2+}, is caused by its cross-linkage between C505 and 414C of the same subunit.

Open state inhibition of mutant channel Q409C

During the SCM analysis in the C-linker region we found that a majority of mutant channels in the open state were not inhibited by thiol specific reagents. Neither Cd^{2+} nor long cross-linkers such as those of the M-X-M family produced any significant permanent inhibition of the cGMP activated current. A remarkable exception was mutant channel Q409C, which was permanently inhibited by 100 μM M-2-M. But, exposure to 200 μM Cd^{2+} ions in the open state poorly inhibited (16 ± 2.1%, N = 4) the cGMP activated current in mutant channel Q409C (see Fig.3.4.5.A).

In contrast, as shown in Fig.3.4.5.B, when 100 μM M-2-M was added in the open state, the cGMP activated current recorded from the mutant channel Q409C was permanently inhibited. Inhibition persisted even after the patch was washed for 10 minutes or longer with a medium not containing thiol reagents. During the exposure to M-2-M, the cGMP activated current declined within 4 to 6 minutes with an average time constant of about 255 seconds (panel C). In order to identify the molecular mechanisms underlying this open state inhibition, we analyzed the effect of 100 μM M-2-M on mutant channel Q409C when C505 was replaced with a threonine. As shown in Fig.3.4.5.D, the compound M-2-M did not block the double mutant channel Q409C&C505T (10 ± 7 %, N =4). Therefore, inhibition of Q409C in the open state by the compound M-2-M is caused by its cross-linking to 409C and C505. In order to establish whether the inhibition was a consequence of cross-linkage of two cysteines from the same subunit or from neighboring subunits, M-2-M inhibition in the open state was analyzed in the tandem Q409C&C505T+w.t$_{tandem}$. In this tandem construct, each subunit contained either 409C or

C505 and this demonstrates that the cross-linkage between 409C and the C505 can occur only between different subunits. As shown in Fig.3.4.5.E, M-2-M in the open state did not block the tandem construct Q409C&C505T+w.t.$_{tandem}$.
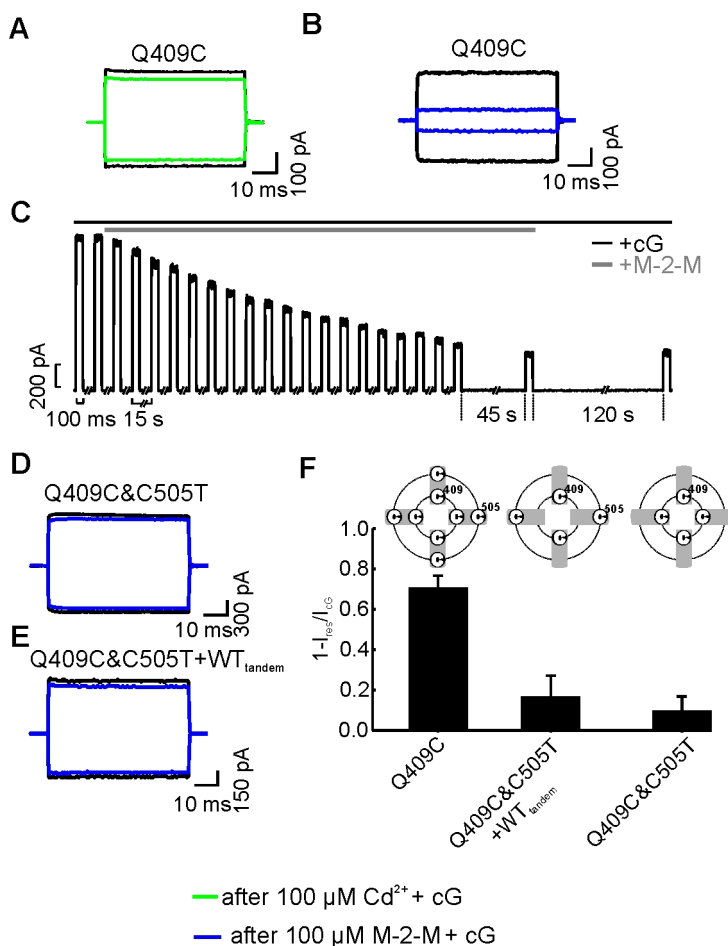

Figure 3.4.5: *409C is inhibited by M-2-M in the open state.* **A**: *Current recordings obtained in the presence of 1mM cGMP before (black) and after (green) exposure to 200 μ M Cd^{2+} in the open state.* **B**: *Current recordings obtained in the presence of 1 mM cGMP before (black) and after (blue) exposure to M-2-M in the open state.* **C**: *Plot of time course of inhibition by M-2-M in the open state. Recordings done every 15 s for 100 ms at +60 mV holding potential.* **D** and **E**: *Effect of M-2-M in the open state on Q409C&C505T and Q409C&C505T+w.t.t$_{tandem}$ channels respectively. Colors of current recordings have the same meaning as in panel B. Voltage commands as in Fig.3.4.2.* **F**: *bar plot of average inhibition by 100 μM M-2-M in the open state. 5 min application at the intracellular side of the membrane patch inhibited the cGMP activated current by 71 ± 6 % in Q409C, by 17 ± 10.5% in Q409C&C505T+w.t.tandem and by 10 ± 7 % in Q409C&C505T. The representation at the top of each bar shows the cysteines present in each subunit.*

As summarized in Fig.3.4.5.F, 100 μM M-2-M in the open state inhibited 71 ± 6 % (N =5) of the cGMP activated current in mutant channel Q409C, but only 10 ± 7 % (N = 4) in the double mutant Q409C&C505T and 17 ± 10.5% (N = 4) in the tandem construct Q409C&C505T+w.t.$_{tandem}$. Therefore, inhibition of mutant channel Q409C by the compound M-2-M in the open state is caused by the cross-linkage of C505 with 409C of the same subunit.

Cd^{2+} inhibition of mutant channel Q409C in the closed state

Mutant channel Q409C was permanently inhibited by the exposure to 200 μM Cd^{2+} ions also in the closed state, as shown in Fig.3.4.6.A. The irreversible inhibition observed in the closed state was not seen when Q409 was substituted with a cysteine in the CNGA1$_{cys-free}$ (see Fig.3.4.6.B).

To understand the molecular mechanisms underlying Cd^{2+} inhibition in the closed state in mutant channel Q409C, we analyzed inhibition when C481 was replaced with an alanine and C505 was replaced with a threonine. As shown in Fig.3.4.6.C and D, exposure to 200 μM Cd^{2+} for 5 minutes inhibited the cGMP activated current in the double mutant channels Q409C&C481A and Q409C&C505T between

30 and 50 % . When membrane patches were exposed to 200 μM Cd^{2+} for at least 15 minutes an almost complete blockage of the cGMP activated current was observed (see traces indicated by arrows in Fig.3.4.6.C and D).
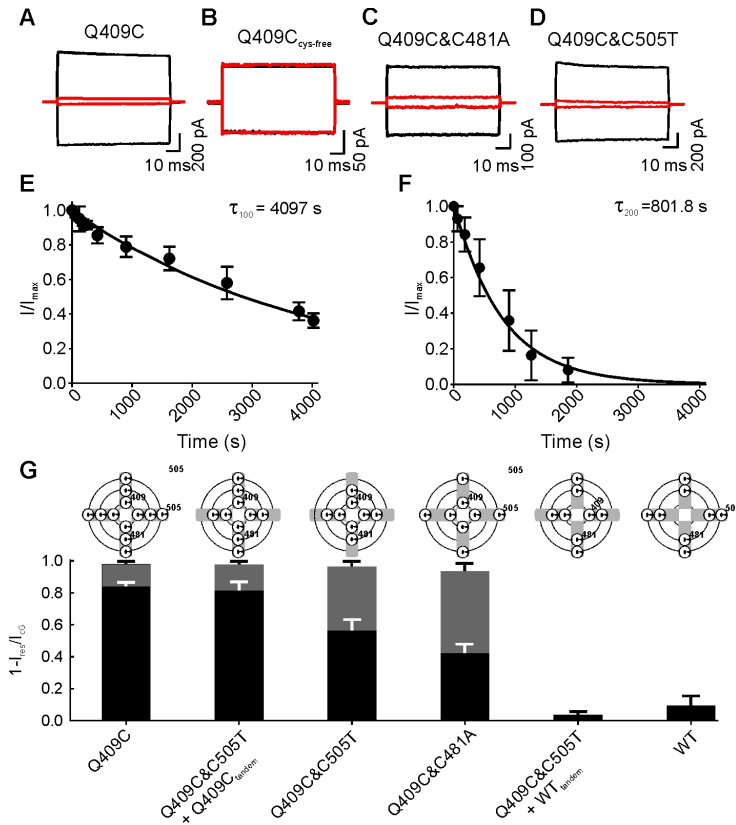

Figure 3.4.6: *Closed state inhibition of Q409C by Cd^{2+} depends on C505 and C481. **A**, **B**, **C** and **D**: current recordings of cGMP activated current before (black) and after (red) closed state application of 200 μM Cd^{2+} on mutant channels Q409C, $Q409C_{cys-free}$, Q409C&C481A and Q409C&C505T respectively. Voltage commands as in Fig.3.4.2. **E** and **F**:time course of inhibition by 100 and 200 μM Cd^{2+} respectively on Q409C&C505T mutant channel. The solid lines are fit to the equation $y = exp(-\tau/t)$. The value of τ for 100 and 200 μM Cd^{2+} was 4097 s and 801 s respectively. **G**: Bar diagram comparing average inhibition by 100 and 200 μM Cd^{2+} in constructs containing a different number of endogenous cysteines C481 and C505 and exogenous 409C. The representation at the top of each bar shows the cysteines present in each subunit. The grey bars are effects after 200 μM Cd^{2+} and the blacks are after 100 μM. Data are shown as mean$\pm$SD.*

In order to understand the molecular mechanisms leading to Cd^{2+} inhibition in mutant channel Q409C we engineered the tandem constructs $Q409C+C505T_{tandem}$ and $Q409C\&C505T+Q409C_{tandem}$. In the tandem construct $Q409C+C505T_{tandem}$, only two subunits have a cysteine residue at positions 409 and 505. This construct did not give rise to functional channels and therefore we could not record any cGMP activated current. The tandem construct $Q409C\&C505T+Q409C_{tandem}$ has a cysteine residue at position 409 in all the four subunits, but the native C505 is in only two subunits.

In the tandem construct $Q409C\&C505T+w.t_{tandem}$ Cd^{2+} inhibition was drastically reduced and was comparable to that observed in the CNGA1 channels. In this construct, the four native C481 are present, and the observed small Cd^{2+} inhibition indicates a minor role of the native C481 in the inhibition. In contrast, in the tandem $Q409C\&C505T+Q409C_{tandem}$ Cd^{2+} inhibition was very similar to that observed in mutant channel Q409C.

Fig.3.4.6.G compares inhibition by 200 μM Cd^{2+} in the closed state (grey bars) in different constructs: the largest inhibition (84.48 ± 14 %, N = 5) was observed in mutant channel Q409C, where the exogenous cysteine at position 409 is present in all four subunits. A very similar inhibition (79.2 ± 6.6 %, N = 4) was observed in the tandem construct $Q409C\&C505T+Q409C_{tandem}$ where the native C505 was replaced with a threonine in two subunits. In the double mutants Q409C&C481A and Q409C&C505T, Cd^{2+} inhibition following an exposure of 5 minutes was reduced to 59.6 ± 6.4 % (N=4) and to 41 ± 3.2

% (N = 4) respectively(black bars) but it was almost complete for exposures longer than 15 minutes. Cd^{2+} inhibition was very small (2.3 ± 2.1 %, N = 4) in the tandem construct Q409C&C505T+w.t$_{tandem}$ where only two subunits have an exogenous cysteine at position 409. A similar negligible Cd^{2+} inhibition (9.4 ± 6 %, N = 7) was observed in the CNGA1 channel. Cd^{2+} inhibition is significantly slower in the double mutants Q409C&C481A and Q409C&C505 and was abolished but in the tandem construct Q409C&C505T+w.t$_{tandem}$.

These results show that Cd^{2+} inhibition in mutant channel Q409C cannot be ascribed to Cd^{2+} coordination between the exogenous cysteine and one native cysteine in the same subunit as in mutant channel A414C. Therefore it is possible that inhibition in mutant channel Q409C is mediated also by Cd^{2+} coordination to cysteines of different subunits. Taken together the results shown in Fig.3.4.6 indicate that Cd^{2+} inhibition in the closed state observed in mutant channel Q409C is caused not only by the coordination of one or more Cd^{2+} ions with 409C and C481 and C505 of the same subunit but also with 409C of other subunits. In mutant channel Q409C$_{cys-free}$, Cd^{2+} ions do not cause any inhibition because of the absence of the two cysteines at position 481 and 505.

Discussion:

In the present manuscript we have investigated the relative distance between specific residues in the C-linker of CNGA1 channels. These interactions were analyzed by introducing cysteines into selected positions and by studying the effect of thiol specific reagents such as Cd^{2+} and different MTS cross-linkers (Loo and Clarke, 2001). We found that mutant channels Q409C and A414C are irreversibly inhibited in the closed state by 200 μM Cd^{2+} added at the intracellular side of the membrane. In contrast, in the presence of 1 mM cGMP, these two channels are not inhibited by Cd^{2+} ions, but the mutant channel Q409C is powerfully inhibited by the cross-linker reagent M-2-M. In what follows we will discuss the molecular mechanisms underlying these effects and the architecture of the C-linker and CNB domain in CNGA1 channels.

Cd^{2+} and M-2-M inhibition in mutant channels Q409C and A414C

In the closed state 200 μM Cd^{2+} powerfully inhibited mutant channels Q409C and A414C (Fig.3.4.1.B & 4A). Inhibition of mutant channel A414C was not affected by the replacement of C481 with an alanine, but was abolished when C505 was replaced with a threonine (Fig.3.4.4), indicating that Cd^{2+} inhibition can be ascribed to its coordination with A414C to C505. Cd^{2+} inhibition was also abolished in the tandem construct A414C&C505T+w.t$_{tandem}$ where each subunit had only one cysteine of the pair at position 414 and 505. Therefore, Cd^{2+} inhibition can be ascribed to its coordination with C505 and with 414C of the same subunit.

In contrast, Cd^{2+} inhibition in the closed state in mutant channel Q409C cannot be ascribed to a simple mechanism as for mutant channel A414C. As shown in Fig.3.4.5 Cd^{2+} inhibition was reduced but not abolished in double mutant channels Q409C&C481A and Q409C&C505T (Fig.3.4.5). The comparison of Cd^{2+} inhibition in different constructs, shown in Fig.3.4.6, suggested the possibility that inhibition is also mediated by its coordination with cysteines in different subunits. Taken together, all these results suggest that Cd^{2+} inhibition in mutant channel Q409C is mediated by the coordination of

409C with native C481, C505 and with 409C of different subunits.

In the open state Cd^{2+} inhibition was not observed either in Q409C or in A414C mutant channels. In the open state, the cross-linker reagent M-2-M (Loo and Clarke, 2001) powerfully inhibited the mutant channel Q409C but not the mutant channel A414C (Fig.3.4.4.B). M-2-M inhibition was abolished in the double mutant channelQ409C&C505T and in the tandem construct Q409C&C505T+ w.t$_{tandem}$. These results indicate that M-2-M inhibition in the open state is mediated by the cross-linkage between 409C and C505 of the same subunit.

These results show that in the closed state the residue at position 414 is at a distance between 4 and 10 Å from C505 of the same subunit, so that one Cd^{2+} ion can coordinate C505 and 414C of the same subunit. In the open state, C505 moves to a distance between 10.5 and 12.2 Å toward residue Q409 of the same subunit so that M-2-M - but not Cd^{2+}- can cross-link them; C505 has been previously proved to be accessible to MTSEA in the closed state but not in the open state (Sun et al., 1996; Brown et al., 1998; Matulef et al., 1999); C481 moves toward A461 during channel opening (Islas and Zagotta, 2006). All these results indicate a complex molecular rearrangement occurring in the CNB domain and C-linker during gating.

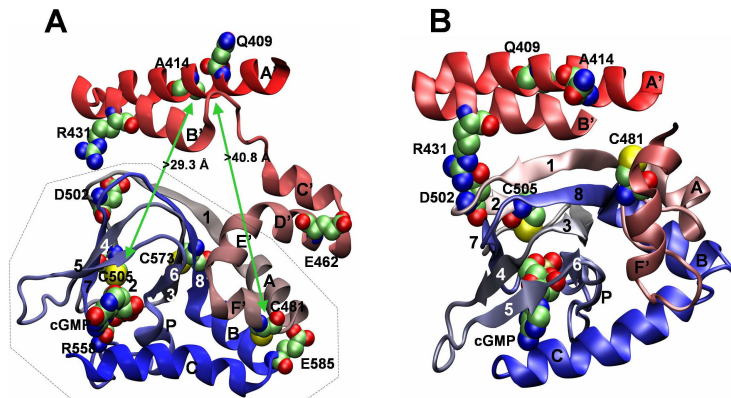### Possible 3-D structure of the C-linker and cyclic nucleotide binding domain

Figure 3.4.7: *Possible structures of the C-linker. A: homology model of the CNGA1 subunit using HCN2 (1Q3E) as a template. Helices are labelled alphabetically, strands are labelled numerically. The model shows that C505 and C481 are very far from either Q409 or A414. In contrast, R431 and D502 are close to each other and form a salt bridge, which is present also in the template and is very well conserved in the CNGA1-4 family. Structural models were built using the Modeller 6.2 program (Sali and Blundell, 1993). B: Homology model restrained according to the experimental observations, where A414 and Q409 are near C481 and C505 as shown in the present manuscript.*

HCN2 and CNGA1 channels share a sequence identity of 35 % in the CNB domain and C-linker region and could be expected to have the same 3D architecture. Indeed R590 and E617 forming a salt bridge in HCN2 channels (Zagotta et al 2003) and the homologous R431 and D502 in CNGA1 channels interact almost identically. In addition, amino acids which were indicated to be important for the HCN2 function, like K472, E502 and D542 (Craven and Zagotta, 2004) are very well conserved in the CNGA1-4 family. Nonetheless, an homology model of the C-linker and CNB domain of the CNGA1 channel based on the HCN2 template (see Fig.3.4.7.A) fail to explain the experimental results here described: in fact, in this homology model, the distance between the C_α of C481 and Q409 is longer than 40.8 Å and the distance between the C_α of C505 and A414 is more than 29.3 Å: these distances are not in agreement with the estimates obtained by the present investigation.

The 3D structure of the CNB domains from six different proteins is available in the Protein Data Bank (Berman et al., 2000): the CNB domain of CAP (Passner et al., 2000), KAP0 (Wu et al., 2004b), 1RL3 (Wu et al., 2004a), KAP3 (Diller et al., 2001), HCN2 (Zagotta et al., 2003), M. loti CNB domain mutant MlotiK1 (Clayton et al., 2004). These proteins share a sequence homology of 40 % to 60 % and the folding of their CNB domains is almost identical, but the overall protein architecture is very different. These considerations indicate that the folding of individual CNB domain is likely to be conserved among all or most of CNB proteins but the assembly of different subunits may be different. Therefore, differences between the 3D structure of HCN2 and CNGA1 channels are likely to reside in the structure of the C-linker domain and/or in the orientation of the single CNB domain subunits. Indeed, as shown in Fig.3.4.7.B, a rotation of the CNB domain around D502 towards the C-linker, can displace C481 and C505 near Q409 and A414 so to satisfy the obtained experimental constraints. The exact molecular rearrangements underlying the transition from the closed to the open state will be determined by the combination of future structural and electrophysiological experiments.

Acknowledgements:

References:

Anselmi,C., P.Carloni, and V.Torre. 2007. Origin of functional diversity among tetrameric voltage-gated channels. *Proteins* **66**:136-146.

Becchetti,A. and K.Gamel. 1999. The properties of cysteine mutants in the pore region of cyclic-nucleotide-gated channels. *Pflugers Arch* **438**:587-596.

Becchetti,A. and P.Roncaglia. 2000. Cyclic nucleotide-gated channels: intra- and extracellular accessibility to Cd^{2+} of substituted cysteine residues within the P-loop. *Pflugers Arch* **440**:556-565.

Berman,H.M., J.Westbrook, Z.Feng, G.Gilliland, T.N.Bhat, H.Weissig, I.N.Shindyalov, and P.E.Bourne. 2000. The Protein Data Bank. *Nucleic Acids Res* **28**:235-242.

Biel,M., X.Zong, F.A.Ludwing, A.Sautter, and F.Hofmann. 1999. Structure and function of cyclic nucleotide-gated channels. *Rev Physiol Biochem Pharmacol* **135**:151-171.

Bradley,J., S.Frings, K.W.Yau, and R.Reed. 2001. Nomenclature for ion channel subunits. *Science* 294:2095-2096.

Brown,R.L., S.D.Snow, and T.L.Haley. 1998. Movement of gating machinery during activation of rod cyclic nucleotide-gated channels. *Biophys J* **75**:825-833.

Chen,T.Y., M.Illing, L.L.Molday, Y.T.Hsu, K.W.Yau, and R.S.Molday. 1994. Subunit 2 (or beta) of retinal rod cGMP-gated cation channel is a component of the 240-kDa channel-associated protein and mediates Ca^{2+}-calmodulin modulation. *Proc Natl Acad Sci USA* **91**:11757-11761.

Chikayama,E., A.Kurotani, Y.Kuroda, and S.Yokoyama. 2004. ProteoMix: an integrated and flexible system for interactively analyzing large numbers of protein sequences. *Bioinformatic* **20**:2836-2838.

Clayton,G.M., W.R.Silverman, L.Heginbotham, and J.H.Morais-Cabral. 2004. Structural basis of ligand activation in a cyclic nucleotide regulated potassium channel. *Cell* **119**:615-627.

Craven,K.B. and W.N.Zagotta. 2004. Salt bridges and gating in the COOH-terminal region of HCN2 and CNGA1 channels. *J Gen Physiol* **124**:663-677.

Craven,K.B. and W.N.Zagotta. 2006. CNG and HCN channels: two peas, one pod. *Annu Rev Physiol* 68:375-401.

Diller,T.C., Madhusudan, N.H.Xuong, and S.S.Taylor. 2001. Molecular basis for regulatory subunit diversity in cAMP-dependent protein kinase: crystal structure of the type II beta regulatory subunit. *Structure* **9**:73-82.

Fesenko,E.E., S.S.Kolesnikov, and A.L.Lyubarsky. 1985. Induction by cyclic GMP of cationic conductance in plasma membrane of retinal rod outer segment. *Nature* **313**:310-313.

Giorgetti,A., A.V.Nair, P.Codega, V.Torre, and P.Carloni. 2005. Structural basis of gating of CNG channels. *FEBS Lett* **579**:1968-1972.

Hofmann,F., M.Biel, and U.B.Kaupp. 2005. International Union of Pharmacology. LI. Nomenclature and structure-function relationships of cyclic nucleotide-regulated channels. *Pharmacol Rev* **57**:455-462.

Islas,L.D. and W.N.Zagotta. 2006. Short-range molecular rearrangements in ion channels detected by tryptophan quenching of bimane fluorescence. *J Gen Physiol* **128**:337-346.

Kaupp,U.B., T.Nidome, T.Tanabe, S.Terada, W.Bonigk, W.Stuhmer, N.J.Cook, K.Kangawa, H.Matsuo, T.Hirose, T.Miyata, and S.Numa. 1989. Primary structure and functional expression from complementary DNA of the rod photoreceptor cyclic GMP-gated channel. Nature **342**:762-766. Kaupp,U.B. and R.Seifert. 2002. Cyclic nucleotide gated channels. *Physiol Rev* **82**:769-824.

Korschen,H.G., M.Illing, R.Seifert, F.Sesti, A.Willams, S.Gotzes, C.Colville, F.Mller, A.Dos, and M.Godde. 1995. A 240 kDa protein represents the complete beta subunit of the cyclic nucleotide-gated channel from rod photoreceptor. *Neuron* **15**:627-636.

Loo,T.W. and D.M.Clarke. 2001. Determining the dimensions of the drug-binding domain of human P-glycoprotein using thiol cross-linking compounds as molecular rulers. *J Biol Chem* **276**:36877-36880.

Matulef,K., G.E.Flynn, and W.N.Zagotta. 1999. Molecular rearrangements in the ligand-binding domain of cyclic nucleotide-gated channels. *Neuron* **24**:443-452.

Menini,A. 1990. Currents carried by monovalent cations through cyclic GMP-activated channels in excised patches from salamander rods. *J Physiol* **424**:167-185.

Nair,A.V., M.Mazzolini, P.Codega, A.Giorgetti, and V.Torre. 2006. Locking CNGA1 channels in the open and closed state. *Biophys J* **90**:3599-3607.

Nakamura,T. and G.H.Gold. 1987. A cyclic nucleotide-gated conductance in olfactory receptor cilia.

Nature 325:442-444.

Nizzari,M., F.Sesti, M.T.Giraudo, C.Virginio, A.Cattaneo, and V.Torre. 1993. Single-channel properties of cloned cGMP-activated channels from retinal rods. *Proc R Soc Lond* **254**:69-74.

Passner,J.M., S.C.Schultz, and T.A.Steitz. 2000. Modeling the cAMP-induced allosteric transition using the crystal structure of CAP-cAMP at 2.1 A resolution. *J Mol Biol* **304**:847-859.

Picco,C. and A.Menini. 1993. The permeability of the cGMP-activated channel to organic cations in retinal rods of the tiger salamander. *J Physiol* **460**:741-758.

Ren,X., D.A.Nicoll, and K.D.Philipson. 2006. Helix packing of the cardiac Na^+-Ca^{2+} exchanger: proximity of transmembrane segments 1, 2, and 6. *J Biol Chem* **281**:22808-22814.

Rothberg,B., K.Shin, P.Phale, and G.Yellen. 2002. Voltage-controlled gating at the intracellular entrance to a hyperpolarization-activated cation channel. *J Gen Physiol* **119**:83-91.

Sali,A. and T.L.Blundell. 1993. Comparative protein modelling by satisfaction of spatial restraints. J Mol Biol 234:779-815.

Sesti,F., E.Eismann, U.B.Kaupp, M.Nizzari, and V.Torre. 1995. The multi-ion nature of the cGMP-gated channel from vertebrate rods. *J Physiol* **487** (Pt 1):17-36.

Shammat,I.M. and S.E.Gordon. 1999. Stoichiometry and Arrangement of Subunits in Rod Cyclic Nucleotide-Gated Channels. *Neuron* **23**:809-819.

Sun,Z.P., M.H.Akabas, E.H.Goulding, A.Karlin, and S.A.Siegelbaum. 1996. Exposure of residues in the cyclic nucleotide-gated channel pore: P region structure and function in gating. *Neuron* **16**:141-149.

Wu,J., S.Brown, N.H.Xuong, and S.S.Taylor. 2004a. RIalpha subunit of PKA: a cAMP-free structure reveals a hydrophobic capping mechanism for docking cAMP into site B. *Structure* **12**:1057-1065.

Wu,J., J.M.Jones, X.Nguyen-Huu, L.F.Ten Eyck, and S.S.Taylor. 2004b. Crystal structures of RIalpha subunit of cyclic adenosine 5'-monophosphate (cAMP)-dependent protein kinase complexed with (Rp)-adenosine 3',5'-cyclic monophosphothioate and (Sp)-adenosine 3',5'-cyclic monophosphothioate, the phosphothioate analogues of cAMP. *Biochemistry* 43:6620-6629.

Zagotta,W.N., N.Olivier, K.Black, E.Young, R.Olson, and E.Gouaux. 2003. Structural basis for modulation and agonist specificity of HCN pacemakers channels. *Nature* **425**:200-205.

Zagotta,W.N. and S.A.Siegelbaum. 1996. Structure and function of cyclic nucleotide-gated channels. *Annu Rev Neurosci* **19**:235-263.

Zheng,J., M.C.Trudeau, and W.N.Zagotta. 2002. Rod cyclic nucleotide gated channels have a stoichiometry of three CNGA1 subunits and one CNGB1 subunit.*Neuron* **36**:891-896.

Zhong,H., L.L.Molday, R.S.Molday, and K.W.Yau. 2002. The heteromeric cyclic nucleotide-gated channel adopts a 3A:1B stoichiometry. *Nature* **420**:193-198.

Zimmerman,A.L. and D.A.Baylor. 1986. Cyclic GMP-sensitive conductance of retinal rods consists of

aqueous pores. *Nature* **321**:70-72.

Zimmerman,A.L., G.Yamanaka, F.Eckstein, D.A.Baylor, and L.Stryer. 1985. Interaction of Hydrolysis-resistant Analogs of Cyclic GMP with the Phosphodiesterase and Light - sensitive Channel of Retinal Rod Outer Segments. *Proc Natl Acad Sci USA* **82**:8813-8817.

Conformational rearrangements in the S6 domain during gating in CNGA1 channels

Monica Mazzolini[1], **Anil V. Nair**[1], Alejandro Giorgetti[*] and Vincent Torre[#]

International School for Advanced Studies

via Beirut 2-4 I-34014 Trieste, Italy

[1] *These authors equally contributed to the work*

[*]*present address:* Biocomputing Department of Biochemical Sciences University of Rome "La Sapienza" P.le Aldo Moro, 5 00185, Rome

[#]**Corresponding author:** Vincent Torre

Scuola Superiore di Studi Avanzati (SISSA)

Area Science Park, SS 14 Km 163.5, Edificio Q1,

34012 Basovizza (TS), Italy

Tel/Fax: +39-040-3756513

e-mail: torre@sissa.it;

Condensed Title: S6 during gating of CNGA1 channels

Key words: gating; ionic channels; CNGA1 channels; Cd inhibition; pore; S6 domain

Abstract:

Conformational changes occurring during channel gating in the S6 domain of bovine CNGA1 channels were investigated. All residues from Phe375 to Val424 were mutated one by one to a cysteine in the CNGA1 background and at selected locations also in the CNGA1$_{cys-free}$ background. Modifications induced by intracellular Cd^{2+} or cross-linkers of different length in the presence and absence of 1 mM cGMP were studied. No Cd^{2+} inhibition was observed in mutant channels from F375C to I390C, with the exception of mutant channel F380C which was inhibited in the closed state and potentiated in the open state. In mutant channel V391C Cd^{2+} ions inhibited reversibly CNGA1 channels with a half inhibition of 32 and 600 nM in the open and closed state respectively. Cd^{2+} did not block in the open state any of the mutant channels from N400C to I412C. In the closed state Cd^{2+} ions inhibited mutant channels A406C and Q409C but not when cysteine was introduced in the CNGA1$_{cys-free}$ background. However the cross-linker reagent M-4-M inhibited in the closed - and not in the open - state mutant channels A406C$_{cys-free}$ and Q409C $_{cys-free}$. Cd^{2+} ions inhibited in the open state mutant channels D413C and Y418C constructed both in CNGA1 and CNGA1$_{cys-free}$ background. Our results suggest that: i - for residues from Phe375 to approximately Asn406, the 3D structure of the KcsA is a good model for the spatial orientation of the S6 domains of the CNGA1 channel in the closed state; ii- in the open state residues from Val391 to Asn406 in homologous subunits move far apart as expected from the gating in K^+ channels; iii- in contrast, residues from Asp413 to Tyr418 in homologous subunits becomes closer in the open state.

Introduction:

Sensory transduction in vertebrate photoreceptors and in olfactory sensory neurons is mediated by cyclic nucleotide gated (CNG) Channels (Craven and Zagotta, 2006; Kaupp and Seifert, 2002; Biel et al., 1999; Zagotta and Siegelbaum, 1996; Kaupp et al., 1989; Nakamura and Gold, 1987; Fesenko et al., 1985; Zimmerman et al., 1985). CNG channels form a tetrameric assembly of several homologous subunits(Craven and Zagotta, 2006; Zheng et al., 2002; Zhong et al., 2002; Shammat and Gordon, 1999; Korschen et al., 1995; Chen et al., 1994), usually referred to as CNGA1-CNGA4, CNGB1 and CNGB3 (Bradley et al., 2001). The primary amino acid sequence of CNGA1 channel from bovine rods is composed of 690 residues (Kaupp et al., 1989) each subunit encoding for a cyclic nucleotide-binding (CNB) domain composed of about 125 amino acids in the cytoplasmic C terminal end (Zagotta and Siegelbaum, 1996; Kaupp et al., 1989). The amino acid sequence of CNG and K^+ channels share a significant homology (Biel et al., 1999; Zagotta and Siegelbaum, 1996) and it has been hypothesized that CNG and K^+ channels share the same 3D topology and gating mechanism. The 3D structure of several K^+ channels has been solved recently: the KcsA in the closed state (Doyle et al., 1998), the MthK in the open state(Jiang et al., 2002a; Jiang et al., 2002b), the KirBac 1.1 (Kuo et al., 2003) and the mammalian Kv1.2 (Long et al., 2005). In all these K^+ channels the pore domain includes four identical subunits comprising two transmembrane helices, S5 and S6 (TM1 and TM2 in KcsA and MthK channels) and a loop forming the filter region and an additional small helix, not spanning the lipid membrane referred as the P-helix. In K^+ channels, the major structural difference on passing from the closed to the open conformation is the bending by 30° of the S6 helix towards the lipid phase, around an alanine hinge (Jiang et al., 2002a; Jiang et al., 2002b)

The analysis of residue accessibility in the pore of CNG channels, based on Cysteine Scanning Mutagenesis (CSM) (Karlin and Akabas, 1998; Krovetz et al., 1997; Benitah et al., 1996; Kurtz et al., 1995; Akabas et al., 1992), has shown that CNG and K^+ channels share the same gross topology (Becchetti et al., 1999). A similar analysis performed in the S6 domain of CNGA1 channels from Thr389 to Ser399 (Flynn and Zagotta, 2003; Flynn and Zagotta, 2001) suggested that also in CNG channels the S6 domain has a helical configuration, possibly crossing at a hypothetical constriction, located between residue Val391 and Ser399. On the basis of their results Flynn & Zagotta (2003) proposed that the closed and open conformations of the CNGA1 channels are similar to the KcsA and MthK 3D structure respectively. A more recent report based on a similar CSM and the analysis of effects of the oxidizing agent CuP on the dose response to cGMP concluded that residues from Gln417 to Val424 in neighbouring subunits become closer in the open state and are far from each other in the closed state (Hua and Gordon, 2005). Therefore homologous residues from Thr389 to Ser399 in different subunits are closer to each other in the closed state and become far apart in the open state, but the opposite conclusion was drawn for residues from Gln417 to Val424.

These CSM analysis were performed in a CNGA1 background were all native cysteines were removed (Matulef et al., 1999), which will be referred as $CNGA1_{cys-free}$ channel. When an exogenous cysteine is introduced in the $CNGA1_{cys-free}$ channel any effect caused by compounds reacting with thiol groups can be safely assumed to be mediated by the exogenous cysteines. The use of CSM using the $CNGA1_{cys-free}$ channel is appropriate to draw conclusions on the structure of the CNGA1 channel only if the molecular structure of CNGA1 and $CNGA1_{cys-free}$ channel are the same or very similar. A recent comparison of CNGA1 and $CNGA1_{cys-free}$ channels has evidentiated several differences and has shown that homologous residues at position 406 in the $CNGA1_{cys-free}$ are approximately 3-4 Å more distant than in the CNGA1 channel (Mazzolini et al 2007, submitted). Therefore CSM based on the use of $CNGA1_{cys-free}$ background does not necessarily provide correct information on the 3D structure and chemical interactions occurring in the CNGA1 channel.

CNG and K^+ channels have a significant homology also with the family of Hyperpolarization - Activated and Cyclic Nucleotide - gated channels (HCN)(Anselmi et al., 2007) composed by four main isoforms called HCN1, HCN2, HCN3 and HCN4 (Hofmann et al., 2005). All these channels open when the membrane potential is hyperpolarized and their activation properties can be modulated to some extent by cyclic nucleotides. The 3-D structure of murine HCN2 C-linker and CNB domains has been recently solved (Zagotta et al., 2003). The sequence alignment of these domains in HCN2 and bovine CNGA1 channels indicates a sequence identity of 32 %. If degree of sequence identity suggests a common 3D architecture among HCN2 and CNG channels some other observations argue differently. At the moment the 3D structure of CNB domains from several different proteins is available in Protein Data Bank (Berman et al., 2000). These proteins share a sequence homology of 40%-60% and the folding of their CNB domain is almost identical, but the overall protein architecture is very different. Therefore it is not obvious whether the C-linker of the HCN2 channel has the same 3D structure of the C-linker of CNGA1 channels either in the open or closed configuration.

The purpose of the present manuscript is to obtain experimental information on the spatial rearrangement of amino acids in the S6 helix and in the initial portion of the C-linker up to Val424 during channel gating. In the present investigation we have repeated a CSM of the entire S6 domain from

Phe375 to Val424 introducing cysteines both in the CNGA1 and CNGA1$_{cys-free}$ channels with the specific aim to examine whether the KcsA and the MthK channels are good models for the closed and open structure of the CNGA1 channel respectively. The 50 residues from Phe375 to Val424 include the entire S6 domain and the initial segment of the C-linker, covering and extending previous analysis of the same domains (Hua and Gordon, 2005; Flynn and Zagotta, 2003; Flynn and Zagotta, 2001; Johnson and Zagotta, 2001). The CSM of these 50 residues was complete in the CNGA1 background and cysteines were introduced in selected positions of the CNGA1$_{cys-free}$. The modifications induced by intracellular Cd^{2+} (Rothberg et al., 2003; Mazzolini et al., 2002; Rothberg et al., 2002) were analyzed in all these mutant channels in the open and closed state, and the effect of other sulfhydryl reagents, such as MTSET and MTS cross-linkers (Loo and Clarke, 2001) was analyzed on selected mutants.

Materials and Methods:

Molecular Biology

The clone of the BROD CNGA1 channel, consisting of 690 residues, was mutated using the QuickChange Site-Directed Mutagenesis kit (Stratagene). CNGA1 and different mutant RNAs were synthesized in vitro by using the mCAP RNA Capping kit (Stratagene), and were subsequently sequenced with the DNA sequencer LI-COR (4000L), to verify that the sequence was correct. Cysteines were introduced in the stretch from Phe375 to Val424 in the CNGA1 channel.

Oocyte preparation and chemicals

The CNGA1 or mutant channel cRNAs were injected into *Xenopus laevis* oocytes ("Rettili" Dr. Rainer Schneider via Corridoni, 3 - 21100 Varese - Italy). Oocytes were prepared as previously described (Nizzari et al., 1993). Injected eggs were maintained at 19°C in a Barth solution supplemented with 50 μg/ml gentamycin sulphate and containing (in mM): 88 NaCl, 1 KCl, 0.82 MgSO$_4$, 0.33 Ca(NO$_3$)$_2$, 0.41 CaCl$_2$, 2.4 NaHCO$_3$, 5 TRIS-HCl, pH 7.4 (buffered with NaOH). During the experiments, oocytes were kept in a Ringer solution containing (in mM): 150 NaCl, 2.5 KCl, 1 CaCl$_2$, 1.6 MgCl$_2$, 10 HEPES-NaOH, pH 7.4 (buffered with NaOH). The MTS compounds were purchased from Toronto Research Chemicals (Ontario, Canada). All the other chemicals were from Sigma Chemicals (St. Louis, MO, USA).

Recording apparatus

cGMP-gated currents from excised patches were recorded 1-5 days after RNA injection with a patch-clamp amplifier (Axopatch 200B, Axon Instruments Inc., Foster City, CA, USA) at room temperature (20-24°C). The perfusion system was as previously described (Sesti et al., 1995) and allowed a complete solution change in less than 1 s. Borosilicate glass pipettes had resistances of 3-10 MΩ in symmetrical standard solution. The current traces used for obtaining steady-state current-voltage relations were the difference between currents in the presence and absence of cGMP. The patch potential was usually stepped from 0 to $\pm$ 60 mV. Currents were low-pass filtered at 2 kHz and acquired on-line at 5 kHz. Clampex 8.0, Clampfit and Matlab were used for data acquisition and analysis.

Application of sulfhydryl-specific reagents

To test the effect of sulfhydryl-specific reagents on the CNG current, Cd^{2+}, MTSEA, MTSET, MTSPT, MTSPtrEA and cross-linkers of the MTS-X-MTS family were applied from the intra cellular side of the membrane. In the inside-out patch-clamp configuration, soon after patch excision, the cytoplasmic face of the plasma membrane was perfused with the same solution filling the pipette to measure the leak current and then by adding 1 mM cGMP to it to measure the current through the activated channel. The Cd^{2+} effect was tested by perfusing the inner side of the patch with a standard solution without EDTA (to avoid partial Cd^{2+} chelation), supplemented with a $CdCl_2$ concentration ranging from 10 nM to 1 mM for variable exposure times ranging from 10 seconds to 5 minutes. The effect of MTS reagents was tested at a concentration of 2.5 mM 100 μM for MTSEA MTSET, MTSPT and MTS-PtrEA in standard solution with EDTA. Cross-linker compounds were dissolved in dimethyl sulfoxide (DMSO) and diluted in standard solution to a final concentration of 100 μM. The final concentration of DMSO was 0.1%. We checked that this concentration of DMSO did not affect the cGMP activated current. Solutions containing cross-linker compounds were prepared immediately before the application (typically <5 min) to prevent degradation, as these reagents dissociate rapidly in aqueous solution. They were not used for more then 45 minutes after dissolving in aqueous solution. To study the effect of the probe in the closed state, patches were exposed to the appropriate reagent in the absence of cGMP. After washout, cGMP was applied to measure the residual current. To study the effect in the open state, sulfhydryl-specific reagents were applied in the presence of 1 mM cGMP. All effects of sulfhydryl reagents here described were obtained after washing out reagents and in the presence of a steady cGMP gated current.

MTS reagents, MTS cross-linkers and Cd^{2+} modify cysteine mutants by different mechanisms and the comparison of their effect are used as a tool for the investigation of conformational changes during channel gating. One molecule of MTSEA, MTSET, MTSPT or MTS-PtrEA forms a covalent bond with the thiol group of a single cysteine. (Karlin and Akabas, 1998; Akabas et al., 1992) The MTS cross-linkers bears reactive S atoms at both ends thus forms covalent bond with two cysteines from different subunits (Loo and Clarke, 2001) while one Cd^{2+} ion usually binds to two or even more cysteines (Loussouarn et al., 2000; Holmgren et al., 1998; Benitah et al., 1996). Inspection of the 3D structure of metallothioneins deposited in the Protein Data Bank indicates that distances between the C_α of two cysteines coordinating the same cadmium ion ranges between 5 and 10 Å(Giorgetti et al., 2005; Maroney, 1999; Ermler et al., 1998; Krovetz et al., 1997). Given thermal fluctuations of side chains and of backbone C , the distance between the C_α of two cysteines able to coordinate one Cd^{2+} ion varies between 8 and 12 Å(Careaga and Falke, 1992; Krovetz et al., 1997; Ermler et al., 1998; Maroney, 1999).

Determination of Cd^{2+} action on exogenous cysteines

As already observed, Cd^{2+} ions have multiple effects on the CNGA1 channel (Becchetti & Roncaglia, 2000): micromolar amounts of Cd^{2+} potentiate the CNGA1 channel reversibly. This potentiation is similar to that observed in the presence of Ni^{2+} ions, known to be mediated by His420 in the C-linker (Gordon and Zagotta, 1995c). At higher concentrations, between 10 and 100 μM, Cd^{2+} ions block in a reversible and voltage dependent way the CNGA1 channel presumably by binding to Glu363 in the pore region (Sesti et al., 1995; Root and MacKinnon, 1993). Fig.3.5.1.A illustrates the effect of 10 and

100 μM Cd^{2+} on the CNGA1 channel and provides a rationale for identifying Cd^{2+} effects caused by its binding to exogenous cysteines. Brief voltage pulses at -100 and +100 mV were alternated, while changing the medium bathing the intracellular side of the membrane patch. Exposures to 10 and 100 μM Cd^{2+} in the absence of cGMP did not cause any significant alteration of the cGMP activated current measured after removing Cd^{2+} ions and adding cGMP. As shown in Fig.3.5.1.A and B, when Cd^{2+} ions were added in the presence of 1 mM cGMP, the cGMP activated current was reduced in a voltage dependent way, but remained almost unaltered at negative voltages such as -80 or -100 mV (see also Becchetti & Roncaglia, 2000).
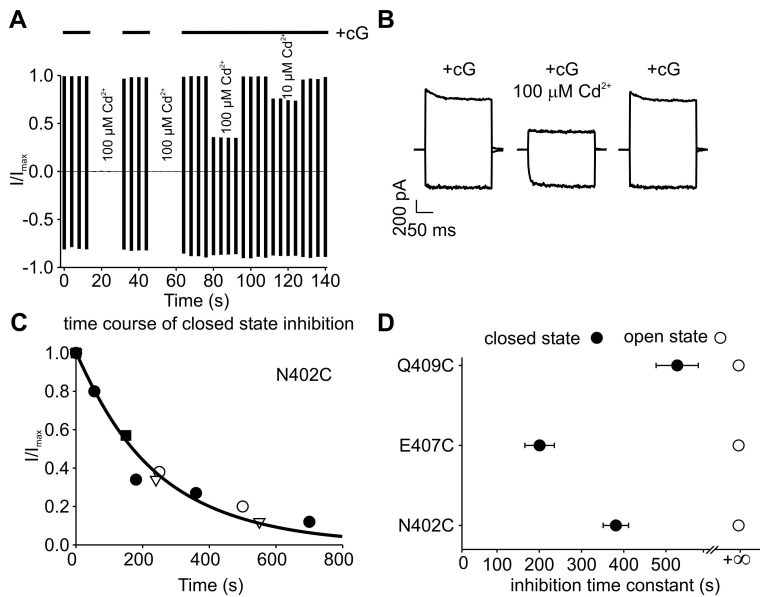

Figure 3.5.1: *The effect of Cd^{2+} on the CNGA1A: Normalized amplitude (I/I_{max}) of the cGMP activated current at ±100 mV in the presence of 10 and 100 μM Cd^{2+}. The thick horizontal bars indicate 1mM cGMP addition. The end points of the vertical bars indicate the normalized current measured at ±100 mV. I_{max} is the maximal current evoked by 1mM cGMP at ±100 mV in the absence of Cd^{2+}. B: Current recordings at membrane voltages ±100 mV of the current activated by 1mM cGMP. C: The rate constant of inhibition of mutant N402C by Cd^{2+} in the closed state. The thick solid line is the best fit to the data with equation $y = exp(-\tau/t)$ where τ is the time constant of inhibition. D: The rate constants of current inhibition by Cd^{2+} for N402C, E407C and Q409C.*

Identical results were obtained with a cysteine free CNGA1 channel (data not shown), kindly provided to us by William Zagotta (Matulef et al 1999). Cd^{2+} caused a voltage dependent block of the cGMP activated current of the cysteine free CNGA1 channel, which was entirely reversible upon Cd^{2+} removal from the bathing medium. As the effect of 10 and 100 μM Cd $^{2+}$ ions on the CNGA1 and its cysteine free construct was the same, exogenous cysteines were introduced in the CNGA1 channel.

These observations provide a rational to distinguish the action of Cd^{2+} ions mediated by the binding to exogenously introduced cysteines: any significant inhibition (larger than 15 %) observed after Cd^{2+} removal from the bathing medium is caused by a binding to exogenous cysteines. Inhibition of the cGMP current observed in the presence of Cd^{2+} at very negative voltages (such as -80 and -100 mV) is also ascribed to an action on exogenous cysteines. The first criterium will be used to establish the state dependency of Cd^{2+} inhibition and the second criterium will be used to determine rate constants of inhibition and recovery from inhibition (Fig.3.5.3).

Determination of time course of Cd^{2+} inhibition

The time course of Cd^{2+} inhibition of selected mutant channels (N402, E407C, Q409C and A414C) was determined by applying 100 and 200 μM of the reagent in the closed state (i.e. in the absence of cGMP) for variable time periods and by measuring the current observed after Cd removal in the presence of 1 mM cGMP. Fig.3.5.1.C show data collected from four patches containing the mutant channel N402C

exposed for variable times to 100 μM Cd^{2+}. Data were normalized to the cGMP current activated at + 60 mV before Cd^{2+} treatment. The solid line through the experimental points was obtained from the equation y = $exp(-\tau/t)$ where τ is the time constant of Cd^{2+} inhibition. The time constant of Cd^{2+} inhibition in the closed state was 250 $\pm$ 12, 183 $\pm$ 15, 394.1 $\pm$ 18 and 188 s for mutant channels N402C, E407C, Q409C and A414C respectively. Therefore we analysed determined Cd^{2+} inhibition by measuring the residual cGMP activated current after exposure to 100 μM for 7 minutes. Cross-linker compounds were dissolved in dimethyl sulfoxide (DMSO) and diluted in standard solution to a final concentration of 100 μM. The final concentration of DMSO was 0.1%. We checked that this concentration of DMSO did not affect the cGMP activated current. Solutions containing cross-linker compounds were prepared immediately before the application (typically <5 min) to prevent degradation, as these reagents dissociate rapidly in aqueous solution. They were never used for more then 45 minutes after dissolving in aqueous solution. The cross-linkers of different length were used to determine the distance between exogenously introduced cysteines (Ren et al., 2006; Loo and Clarke, 2001).

Estimation of the distance between C_α of coordinating cysteines

The distance between the C_α of cysteines coordinating Cd^{2+} ions or cross-linkers such as M-2-M and M-4-M was estimated by inspection of the 3D structure of proteins contained in the Protein Data Bank (PDB) and by molecular dynamical simulations, as described in Mazzolini et al 2007. If Cd^{2+} inhibits the channel by coordinating to two cysteines, the distance between the C_α of coordinating cysteines is ≤ 10.5 Å. If channel inhibition is observed with M-2-M but not Cd^{2+} then the distance between the C_α of coordinating cysteines is between 10 and 13 Å. Similarly, if the inhibition is caused by M-4-M and not by Cd^{2+} and M-2-M, the distance of the C_α of coordinating cysteines is between 12 and 14.5 Å.

Results:

The structures of the KcsA (Zhou et al., 2001; Doyle et al., 1998) and MthK channels (Jiang et al., 2002a; Jiang et al., 2002b) are possible templates for the closed and open state of the S6 domain respectively (Flynn and Zagotta, 2003). Fig.3.5.2.A illustrates the sequence alignment between residues from proline 84 to histidine 124 of the KcsA channel and from Pro367 to Met419 of the CNGA1 channel. Residues of the KcsA channel form an helix (indicated by the blue bar in A) from Gly89 to the final His124. The structure of the KcsA terminates about 15 residues before the termination of the considered stretch of residues in the CNGA1 channel.

The S6 domains of the KcsA channel form an inverted tepee (Doyle et al., 1998) with an angle of about 30° relative to the central axis perpendicular to the membrane and channel pore (see a side view and a top view shown in D and G respectively). According to the sequence alignment shown in Fig.3.5.2.A and the homology modeling, the distance between opposite C_α of Val391, Gly395 and Ser399 of the CNGA1 is expected to be around 11, 9 and 13 Å respectively. Fig.3.5.2.B illustrates the sequence alignment between residues from proline 67 to leucine 98 of the MthK channel and the corresponding residues of the CNGA1 channel. The orientation in space of the initial portion of the S6 domains of the MthK channel is similar to that of KcsA channel, but helices bend towards the lipid phase by about 30° (see a side and a top view in E and F respectively) around Gly83 - indicated by a green ball in

panels D and F - forming the hinge - labeled in yellow in panels A,B and C -. According to the sequence alignment of Fig.3.5.2.B and the homology modeling the distance between opposite C_α of Val391 and Gly395 of the CNGA1 is expected to be around 24 and 27 Å respectively.

If the KcsA channel and MthK channel are appropriate templates for the closed and open state of CNGA1 channels, residues downstream the hinge - such as Val391 and Gly395 - will significantly change their 3D location. This possibility will be tested by analyzing whether Cd^{2+} modification in cysteine mutant channels, such as V391C and G395C is state dependent.
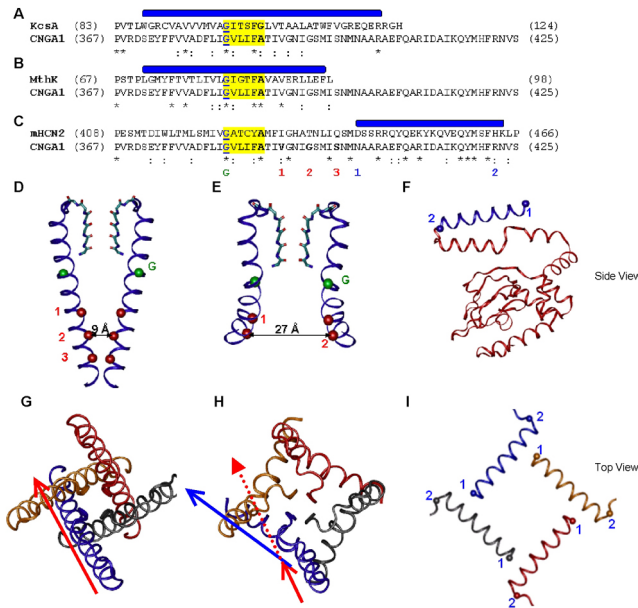

Figure 3.5.2: *Sequence alignments between the S6 domain of CNGA1 and three putative templates: **A:** with the KcsA (K^+ channel from Streptomyces lividans) a possible template for the closed configuration, **B:** with the MthK (K^+ channel from Methanobacterium thermoautotrophicum) a possible template for the open configuration; **C:** with the C-linker of mHCN2 (hyperpolarization activated cyclic nucleotide gated channel isoform 2) a possible template for the open configuration of the C-terminal portion of the S6 domain. Blue regions show known α-helices in the templates. Asterisks and colons indicate identities and conservative mutations respectively. Yellow indicates the hinge of K channels composed by a glycine (underlined residues and indicated in green in A to E) and five residues downstream up to a glycine or an alanine (shown in bold in A, B and C). 1,2 and 3 in red indicate residues V391, G395 and S399. 1 and 2 in blue indicate the beginning and end of the first α helix (A')of the C-linker of the mHCN2 channel. **D, E and F:** side views of the crystal structure of the KcsA, MthK and C-linker of the mHCN2 channel respectively. Residues indicated by red, green and blue symbols in A, B and C are indicated in D, E and F in the same way. In D and E only two opposing subunits are shown. In F only one subunit is shown. **G, H and I:** top views of the three crystal structures. Only the α helices of the four subunits are shown. The direction of the helices of the KcsA channel in a plane parallel to the membrane is shown in red. The direction of the final portion of α helices of the MthK channel in a plane parallel to the membrane is shown in blue. Observe the lateral bending in E and the anticlockwise rotation by about 30° in H of the MthK channel relative to the 3D structure of KcsA channel.*

Fig.3.5.2.C illustrates the sequence alignment between residues from Pro408 to Pro466 of the HCN2 channel and the corresponding residues of the CNGA1 channel. The 3D structure of the C-linker of the mHCN2 channel has been solved in the presence of a cyclic nucleotide (cAMP and/or cGMP) bound to its binding domain. We have shown that the 3D structure of the C-linker of mHCN2 and of the CNGA1 channels are not identical (Mazzolini et al 2007), but the two channels could share several architectural features, such as an helical structure with some kinks connecting the S6 transmembrane helices to the CNB domain. Indeed, the N-terminal segment, from Asp443 to Lys463 of the mHCN2 channel and the

N-terminal part of C-linker region (residues from Asn402 to Ser425) of CNGA1 the channel could be similarly organized as alpha helices, possibly with different spatial orientations. Indeed, in this region there is a high sequence identity (7/24 identical residues), complemented with several conservative mutations (5/24 see Fig.3.5.2.C), between HCN2 and CNGA1 channels.

A comparison of the 3D structure of the KcsA and MthK channels indicate not only a bending towards the lipid phase of lower portion of the terminal α helices (best seen comparing the side views shown in panels D and E) but a concomitant anticlockwise rotation when seen from the top as shown in panels G and H respectively. As indicated by the red and blue arrows, the terminal portion of the α helices not only bends towards the lipid phase but also rotates anticlockwise by about 30° when observed from the top.

The mRNA of wild type and mutant channels were injected in *Xenopus laevis* oocytes and the electrophysiological properties of these channels were analyzed in excised membrane patches in the inside-out configuration. Currents flowing through CNG channels were measured under voltage-clamp conditions, while the composition of the medium bathing the intracellular side of the membrane was changed. The experiments here described were performed in the CNGA1 channel containing endogenous cysteines. Cysteines were also introduced at selected locations of the CNGA1$_{cys-free}$ channel (Matulef et al., 1999)

Cd^{2+} inhibition in mutant V391C

If the KcsA structure is a good template for the closed state and the MthK structure for the open state, a strong state dependent Cd^{2+} inhibition in mutant channels V391C, G395C and S399C is expected.
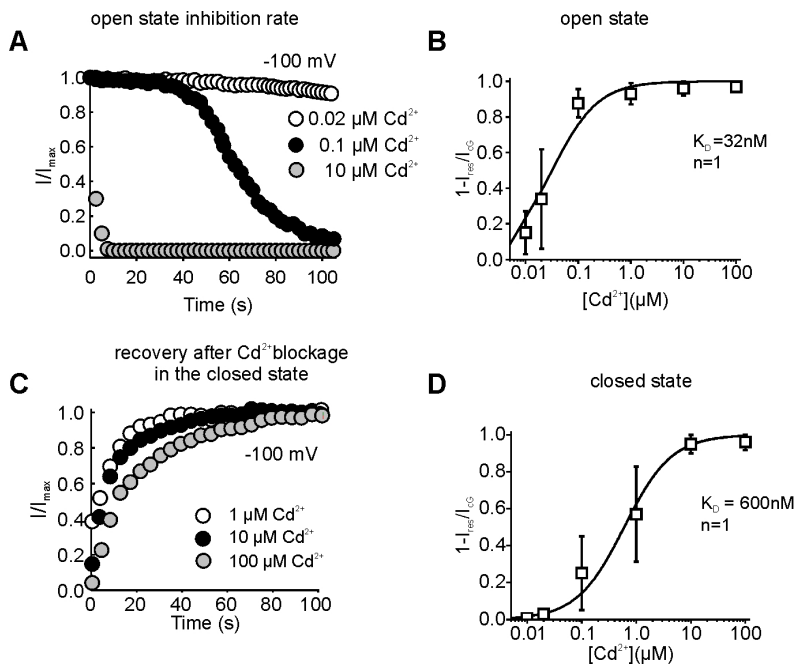

Figure 3.5.3: *Cd^{2+} inhibition on mutant channel V391C. A: Time course of inhibition by 0.02, 0.1 and 10 μM intracellular Cd^{2+} in the presence of 1 mM cGMP. B: stoichiometry of Cd^{2+} inhibition in the presence of 1 mM cGMP. Solid line through the experimental points obtained from the equation $I_{[Cd^{2+}]}/I_{[cG]} = ([Cd^{2+}]/K_{1/2})^n/(1+ [Cd^{2+}]/K_{1/2})^n$, where $[Cd^{2+}]$ is the Cd^{2+} concentration and $K_{1/2}$ is the dissociation constant with the values of $n = 1$ and $K_{1/2} = 32$ nM. C: Time course of current recovery in the presence of 1 mM cGMP after exposure for 20 seconds to 1, 10 and 100 μM intracellular Cd^{2+} in the absence of cGMP. D: stoichiometry of Cd^{2+} inhibition in the absence of cGMP. The solid line through the experimental points is obtained from the same equation with the values of $n = 1$ and $K_{1/2} = 600$ nM.*

When 10 or 100 μM Cd $^{2+}$ was added to the medium bathing the intracellular side of the membrane

in the presence of 1 mM cGMP, the cGMP activated current in mutant channel V391C at -100 mV was quickly suppressed, in contrast with what observed in the CNGA1 channel (see Fig.3.5.1.A and B). This powerful inhibition at very negative voltage indicates a binding to the exogenous cysteines. Cd^{2+} inhibition in mutant channel V391C was reversible and therefore it was possible to study the inhibition rate of different amounts of Cd^{2+} ions in the same patch. As shown in Fig.3.5.3.A Cd^{2+} concentrations of 10 μM inhibited the cGMP activated current with a rate comparable with that of the solution change, occurring in 1 or 2 seconds. A lower Cd^{2+} concentration of 100 nM substantially inhibited the cGMP current but within some seconds. The stoichiometry of Cd^{2+} inhibition, shown in Fig.3.5.2.B, indicates a half inhibition $K_{1/2}$ in the open state, i.e. in the presence of 1 mM cGMP of 32 $\pm$ 15 nM.

Cd^{2+} inhibition in the closed state, was determined by measuring the inhibition of the cGMP activated current immediately after the concomitant Cd^{2+} removal and addition of 1 mM cGMP. As shown in Fig.3.5.3.D exposures to a solution containing 50 or less nM Cd^{2+} for 30 or 60 seconds in the absence of cGMP did not cause any significant inhibition of the cGMP activated current. A closed state inhibition was observed when Cd $^{2+}$ concentration was increased above 0.1 μM. A complete inhibition of the cGMP activated current in the closed state was observed in the presence of 10 and 100 μM Cd^{2+}. The stoichiometry of Cd^{2+} inhibition, shown in Fig.3.5.3.D, indicates a half inhibition $K_{1/2}$ of 600 $\pm$ 34 nM in the closed state. The data of Fig.3.5.3 indicates that Cd^{2+} ions inhibited reversibly the mutant channel V391 both in the closed and open state, but that the half inhibition $K_{1/2}$ is higher in the closed state, indicating a slightly stronger inhibition in the open state.

Cd^{2+} effect on mutant channels from F375C to S399C

Fig.3.5.4 illustrates a summary of the effect of 100 μM Cd^{2+} in the presence and absence of 1 mM cGMP on channel mutants from F375C to S399C. A clear inhibition by Cd^{2+} was observed only in mutant channel V391C with a half inhibition of 600 and 32 nM in the closed and open state respectively. A partial block in the closed state was observed also in mutant channel F380C (Nair et al 2006).
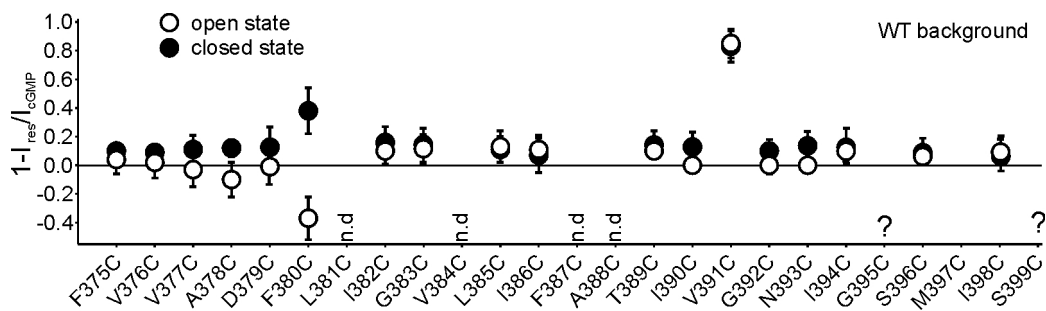
Figure 3.5.4: Cd^{2+} *modification of mutant channels in the S6 segment from F375C to S399C:* fractional change induced by 100 μM Cd^{2+}. The effect of 100 μM Cd^{2+} added for 5 minutes in the absence (black circles) and in the presence of 1 mM cGMP (white circles).

In mutant channel G395C the cGMP activated current was usually small and often only single channel openings could be observed. The open probability in saturating cGMP (1 and 5 mM cGMP) was estimated to be smaller than 0.1 and therefore channels are most of the time in the closed state. Therefore the state dependence of Cd^{2+} modification could not be determined.

The analysis of the effect of sulfhydryl reagents on mutant channel S399C was difficult as the cGMP activated current often but not always declined spontaneously, as already observed (Flynn and Zagotta, 2001). The run down was variable: in 12 out of 28 patches the run down was small and in the remaining patches the cGMP activated current declined within some minutes (from 7 to 15 minutes) to a steady level between 20 and 25 % of the initial current. Given this experimental variability we could not quantify inhibition induced by sulfhydryl reagents in mutant S399C.

As shown in Fig.3.5.4, sulfhydryl reagents did not have any significant effect on cysteine mutants from F375C to I390C, with the exception of mutant channel F380C, which was potentiated by 100 μM Cd^{2+} in the open state and inhibited in the closed state (Nair et al., 2006). Given the moderate effect of sulfhydryl reagents on mutant channels from F375C to S399C the CSM was performed only in the CNGA1 background.

Cd^{2+} inhibition in mutant channels from N400C to Q409C

The analysis of state dependent effects of Cd^{2+} ions on cysteine mutants will be used to identify changes of relative distances among exogenous cysteines occuring during channel activation (Rothberg et al., 2003; Mazzolini et al., 2002; Rothberg et al., 2002; Becchetti and Roncaglia, 2000). Residues from Ala403 to His420 have been already investigated by Johnson & Zagotta (2001). Johnson & Zagotta (2001) mutated one by one all residues into a histidine and analyzed the effect of micromolar amounts of intracellular Ni^{2+} on these mutant channels constructed from a CNGA1 channel in which all endogenous cysteines were mutated and His420 was replaced by a glutamine. In the presence of a saturating cGMP concentration, 1 μM Ni^{2+} caused a small block of the cGMP activated current in mutant channels Q409H and D413H and a potentiation in mutant channel K416H and in the CNGA1 with histidine at position 420. These results strongly suggest that in the open state residues from position 400 to 420 are arranged in an α helix configuration. Ni^{2+} potentiation in the CNGA1 channel has been ascribed to the binding of Ni^{2+} to His420 in different subunits (Gordon and Zagotta, 1995a; Gordon and Zagotta, 1995b; Gordon and Zagotta, 1995c) Channel mutants from N400C to V424C were analyzed. With the exception of mutant channels R411C, N423C and V424C, they were all functional and a cGMP activated current with amplitude and properties similar to those observed in the CNGA1was measured. These mutant channels - with the exception of mutant channel D413C - had an apparent normal gating, as judged by the absence of inactivation and normal I/V relations. The dependence of the cGMP-activated current on cGMP concentration and ionic selectivity of these mutant channels were not investigated in detail. Many of these mutant channels were powerfully and irreversibly inhibited by the addition to the medium bathing the intracellular side of the membrane patch of 100 μM Cd^{2+}. Fig.3.5.5.A-D illustrates the effect of 100 μM Cd^{2+} in the open and closed state on channel mutants N402C, A403C, A406C and Q409C. In the closed state Cd^{2+} ions inhibited powerfully mutant channels N402A, A403C, A406C and Q409C inhibition was not removed or reduced by washing the patch with 0.2 mM EDTA for several minutes (typically 5) and therefore inhibition was assumed to be irreversible.

None of these mutant channels was inhibited by Cd^{2+} ions in the open state. In some experiments the patch containing the mutant channel was first exposed to Cd^{2+} ions in the presence of 1 mM cGMP and when the cGMP activated current fully recovered, the patch was subsequently exposed to Cd^{2+} but in the absence of cGMP. Cd^{2+} inhibition did not depend whether the patch was previously exposed to
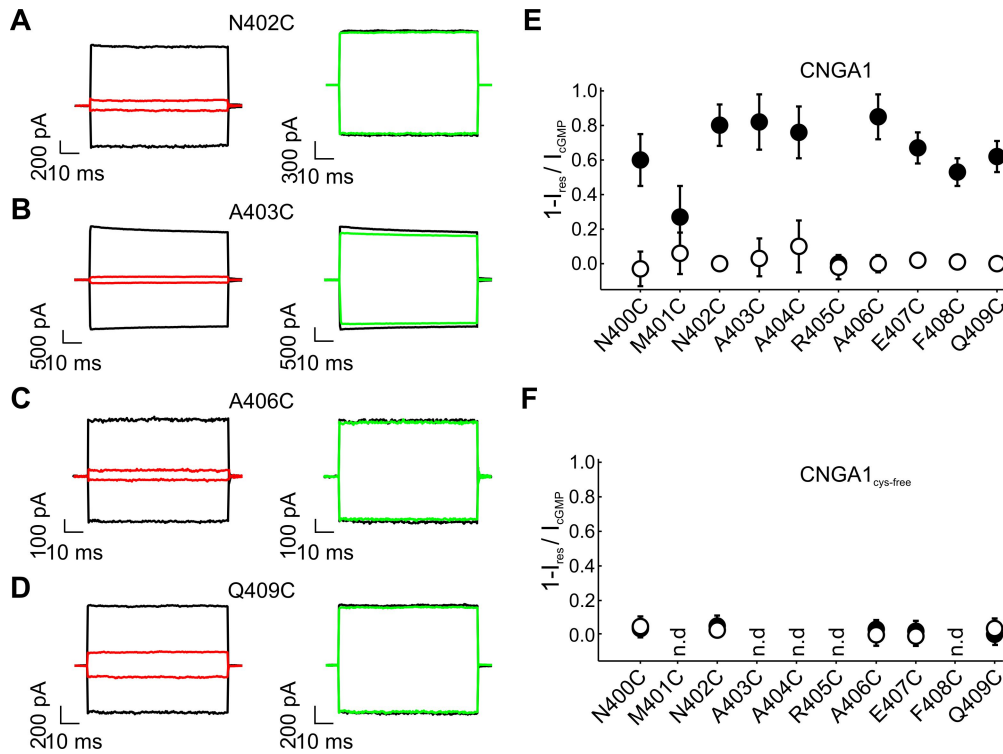
Cd^{2+} in the presence of 1 mM cGMP.

Figure 3.5.5: *The effect of cross-linkers on cysteine free mutants. **A, B:** M-4-M effect in $A406C_{cys-free}$ and $Q409C_{cys-free}$ respectively in the open (right panels) and closed (right panels) states. Blue traces are the effect after the cross-linker application and cyan traces are after the open state application. Black are before the application of cross-linker. All traces are obtained with a holding potential of ± 60 mV. The effect of different cross-linking and other MTS reagents on mutant channels $A406C_{cys-free}$ and $Q409C_{cys-free}$. The black bars show the effect of MTS reagents applied in the closed state; grey show after the open state. Values are shown as mean ± SD.*

In order to explore the molecular mechanism responsible for the Cd^{2+} inhibition of mutant channels illustrated in Fig.3.5.5.E, we have introduced cysteine at specific locations also in the $CNGA1_{cys-free}$ channel (Matulef et al., 1999) where all endogenous cysteines were replaced with amino acids not bearing a S atom and therefore not able to form S-S bonds with thiol reagents. We have analyzed the effect of 100 μM Cd^{2+} ions in mutant channels $N402C_{cys-free}$, $A406C_{cys-free}$ and $Q409C_{cys-free}$ In none of these mutant channels - constructed in a CNGA1 background without any endogenous cysteines - Cd^{2+} ions produced any significant inhibition. None of these mutant channels was modified by 100 μM Cd^{2+}. Fig.3.5.5.F summarizes the effect of 100 μM Cd^{2+} ions on some mutant channels constructed in $CNGA1_{cys-free}$ background.

This different blocking effect of Cd^{2+} ions can be produced by two different mechanisms or by their combination. Cd^{2+} inhibition of the cysteine mutant in the CNGA1 background illustrated in Fig.3.5.5.A can originate by Cd^{2+} coordination to the exogenous cysteine with endogenous cysteines and particularly with Cys481 and/or Cys505 (Mechanism 1) which are part of the C-linker domain (Brown et al., 1998). An alternative explanation is that the 3D structure of $CNGA1_{cys-free}$ channels differs by some Å from that of CNGA1 channels (Mechanism 2), so that Cd^{2+} can coordinate exogenous cysteines introduced in the CNGA1 channels but not in the $CNGA1_{cys-free}$ channels (Mazzolini et al 2007 unpublished data). In order to resolve this issue we studied in detail mutant channel N402C,

A406C and Q409C by performing two series of experiments. In the first series of experiments we analysed Cd^{2+} inhibition in cysteine mutant channels where the two endogenous cysteines 481C and 505C were replaced by residues not reacting with S atoms, such as alanine or threonine. If in these experiments Cd^{2+} inhibition is drastically reduced or eliminated Mechanism 1 will be validated. In the second series of experiments the effect of cross-linkers of different length in mutant channels $N402C_{cys-free}$, $A406C_{cys-free}$ and $Q409C_{cys-free}$ was examined. The recently synthesized MTS cross-linkers (Loo and Clarke, 2001) have a thiol group at both ends with a linker of variable length. For example, the compounds M-2-M, M-4-M and M-6-M have a linker of 5.2, 6.5 and 7.8 Å respectively (Fig.3.3.1 of Mazzolini et al 2007, unpublished data). The existence of MTS cross-linkers able to block mutant channels irreversibly in the closed state will support Mechanism 2.

The effect of MTS cross-linkers on mutant channels $A406C_{cys-free}$ and $Q409C_{cys-free}$

Cd^{2+} ions in the absence of cGMP powerfully inhibited mutant channels A406C and Q409C but not mutant channel $A406C_{cys-free}$ and $Q409C_{cys-free}$ (see Fig.3.5.5.E). In order to investigate the molecular mechanisms causing this different effect by Cd^{2+} ions we investigated inhibition by different thiol cross-linkers of M-X-M family with an increasing length of the linker. 100 μM of the cross-linker M-2-M, did not block mutant channel $A406C_{cys-free}$(n= 6) and $Q409C_{cys-free}$ neither in the open nor in the closed state. In contrast, the same concentration of the reagent M-4-M (n= 7) with a linker of 7.8 Å powerfully inhibited both mutant channels $A406C_{cys-free}$ and $Q409C_{cys-free}$ in the closed state but not in the open state, as shown in Fig.3.5.6.A and B respectively.
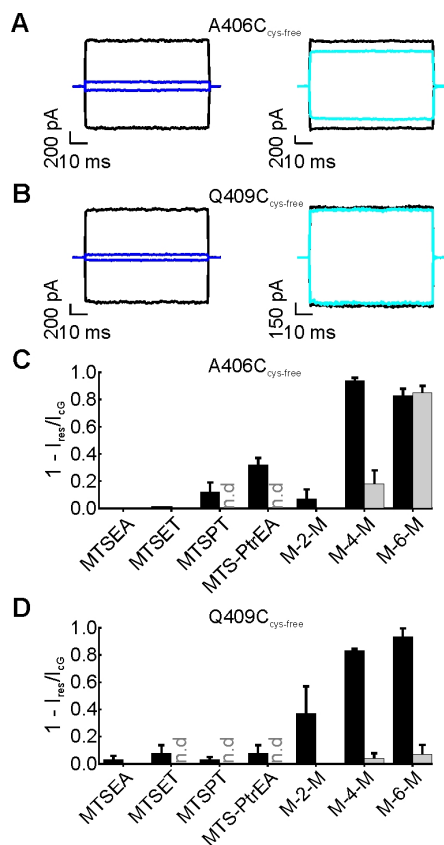
Figure 3.5.6: *The effect of cross-linkers on cysteine free mutants. A, B: M-4-M effect in $A406C_{cys-free}$ and $Q409C_{cys-free}$ respectively in the open (right panels) and closed (right panels) states. Blue traces are the effect after the cross-linker application and cyan traces are after the open state application. Black are before the application of cross-linker. All traces are obtained with a holding potential of ± 60 mV. The effect of different cross-linking and other MTS reagents on mutant channels $A406C_{cys-free}$ and $Q409C_{cys-free}$. The black bars show the effect of MTS reagents applied in the closed state; grey show after the open state. Values are shown as mean ± SD.*

The observed inhibition of mutant channels $A406C_{cys-free}$ and $Q409C_{cys-free}$ by cross-linkers

could be caused by a simple steric occlusion and not by the cross-linking of the two exogenous cysteines. Therefore we have compared the blocking effect of 100 μM of different MTS compounds such as MTSEA, MTSET, MTSPT and MTSPtrEA (see Fig.3.5.6.C) on the mutant channels A406C$_{cys-free}$ and Q409C$_{cys-free}$. As reported by Mazzolini et al 2007 none of these large MTS compounds block significantly both mutant channels A406C$_{cys-free}$ and Q409C$_{cys-free}$. These results indicate that the absence of Cd^{2+} inhibition in mutant channel A406C$_{cys-free}$ is ascribed to the fact that the 3D structure of the CNGA1 and CNGA1$_{cys-free}$ is different and in particular residues at position 406 of the CNGA1$_{cys-free}$ are at a reciprocal distance not compatible with Cd^{2+} coordination but compatible with the coordination of the cross-linker M-4-M (Mazzolini et al 2007).

Inactivation in mutant channels D413C and D413C$_{cys-free}$

As illustrated in Fig.3.5.7 mutant channels D413C and D413C$_{cys-free}$ responded to cGMP with a progressive decline of the cGMP activated current, reminiscent of inactivation observed in some mutant channels in the proe region. Indeed when repetitive voltage pulses were elicited and 1 mM cGMP was rapidly added to the solution bathing the intracellular side of the membrane patch, the cGMP activated current quickly increased, but it started to declined within some seconds (see panels A and B). The CGMP activated current in the mutant channel D413C declined with a time constant varying between 40 and 60 seconds and within 2 or 3 minutes reached a value which was approximately 40 % of what initially observed. The decline of the cGMP activated current was observed also in mutant channel D413C$_{cys-free}$ where it was slightly faster and larger: indeed in mutant channel the cGMP activated current declined to about 20 % of the value measured immediately after the addition of cGMP.
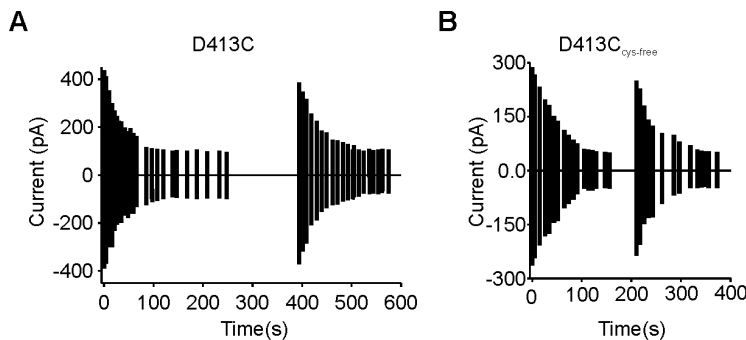
Figure 3.5.7: *The reversible current decline of mutant channels D413C and D413C$_{cys-free}$. A, B: The vertical bars indicate the current elucidated at $\pm$ 60 mV in the presence of 1mM cGMP. By removing cGMP from the solution bathing the intracellular side of the membrane patch for at least 2 minutes, a cGMP activated current with the same amplitude as originally observed could be measured, for both mutant channels D413C and D413C$_{cys-free}$.*

The decline of the cGMP activated current was reversible: indeed by removing cGMP from the solution bathing the intracellular side of the membrane patch for at least 2 minutes, a cGMP activated current with the same amplitude as originally observed could be measured, for both mutant channels D413C and D413C$_{cys-free}$ as shown in Fig.3.5.7. The time dependent decline of the cGMP activated observed in the two mutant channels D413C and D413C$_{cys-free}$ was never observed in any cysteine mutant channels constructed in the S6 and C-linker region from L381 to V424 and is reminiscent of what observed in mutant channels when Glu363 in the pore region was mutated into alanine.

One possibility for this current decline could be that, in the open state D413 form an inter-subunit salt bridge with R411. This salt bridge may be important for stabilizing the open state. Mutating D413 to a cysteine disrupt this salt bridge formation, which results in the time dependent current decline.

Cd^{2+} *inhibition in mutant channels from 410C to V424C*

Mutant channels from 410C to V424C, with the exception of R411C, N423C and V424C were all functional and a cGMP activated current with amplitude and properties similar to those observed in the CNGA1was measured. Fig.3.5.7.A illustrates the effect of 100 μM Cd^{2+} in the open and closed state on channel mutants D413C, A414C, Q417C and 418C. Cd^{2+} ions inhibited powerfully mutant channels A414C and Q417C in the closed state, but in the open state, i. e. in the presence of 1 mM cGMP. The action of Cd^{2+} ions on mutant channel D413C was tested when the cGMP activated current was fully inactivated (see Fig.3.5.7). In the open state, Cd^{2+} ions inhibited mutant channels D413C and 418C. The mutant channel H420C (see Fig.3.5.8.E) was not affected by Cd^{2+} ions in the presence of 1 mM cGMP and was poorly inhibited when was exposed to Cd^{2+} in the absence of cGMP.
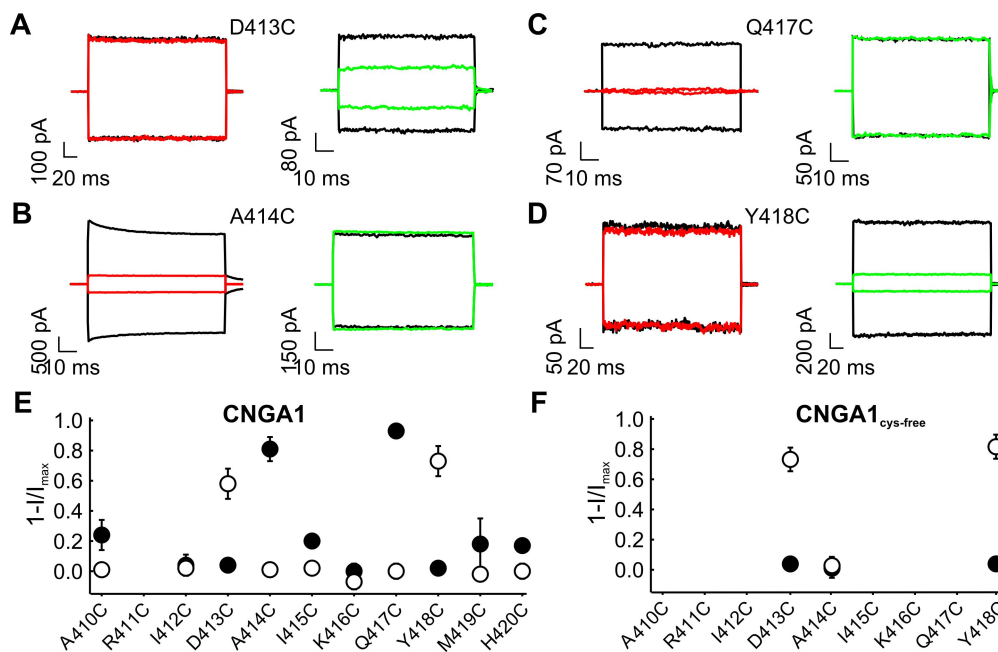

Figure 3.5.8: *Cd^{2+} inhibition in the open state of mutant channels from A410C to H420C. A, B, C, D: Cd^{2+} inhibition in channel mutants D413C, A414C, Q417C and Y418C respectively in open (green) and closed (red) state. Black traces are the current obtained before applying Cd^{2+}. The traces are obtained with a holding potential of $\pm$ 60 mV. In D413C Cd^{2+} was applied after the cGMP dependent current decline was complete. **E:** Summary of collected data of Cd^{2+} inhibition from A400C to H420C in CNGA1 background in the closed (black symbols) and open (white symbols) states. **F:** same as in E but the mutants are constructed in the cysteine free background.*

Cd^{2+} inhibition observed in the closed state in mutant channels A414C and Q417C was not observed when cysteines were introduced in the $CNGA1_{cys-free}$ background (see Fig.3.5.8.F). In contrast, Cd^{2+} inhibition in the open state was also observed in mutant channels $D413C_{cys-free}$ and $Y418C_{cys-free}$ in agreement with what previously reported by Hua & Gordon (2005). As Cd^{2+} inhibition in the open but not in the closed state was observed in mutant channels D413C and Y418D and also in $D413C_{cys-free}$ and $Y418C_{cys-free}$ it is possible to conclude that homologous residues in different subunits in position 413 and 418 move closer in the open state.

In contrast, the understanding of molecular mechanisms underlying the closed state Cd^{2+} inhibition observed in mutant channels A414C and Q417C but not in mutant channels $A414C_{cys-free}$ and

Q417C$_{cys-free}$ requires further experiments.

Role of Cys481 and Cys505 in Cd^{2+} inhibition

We investigated the molecular mechanism of the irreversible Cd^{2+} inhibition observed in the closed state illustrated in Figs.3.5.5 and 8 in mutant channels N402C, A406C, Q409C, A414C and in Q417C by removing native cysteines Cys481 and Cys505.

Membrane patches were exposed for 5 minutes to 100 μM Cd^{2+} ions in the absence of cGMP and the current recorded after Cd^{2+} removal and in the presence of a saturating cGMP concentration was measured. In each panel of Fig.3.5.9 Cd^{2+} inhibition in mutant channels N402C, A406C, Q409C, A414C and in Q417C are compared when C481 and C505 were replaced respectively with an alanine and a threonine.

In some mutant channels (Q409C&C505T and Q409C&C481A) exposure to 100 μM Cd^{2+} resulted in a partial inhibition varying between 30 and 70 %. In these mutant channels, membrane patches were exposed to 100 μM Cd^{2+} for a longer time in order to fully observe Cd^{2+} inhibition. As shown in Fig.3.5.9.A Cd^{2+} inhibition in mutant channel N402C was not observed in the triple mutant channel N402C&C481A&C505T. In contrast, as shown in Fig.3.5.9.B, Cd^{2+} inhibition observed in mutant channel A406C was also observed in the triple mutant channel A406C&C481A&C505T and the time course of Cd^{2+} inhibition in both mutant channels was very similar.

Cd^{2+} inhibition in mutant channel Q409C was slower: indeed 100 μM Cd^{2+} ions inhibited mutant channels with a time constant of about 394 s and of about 812 s and 1018 s in the double mutants Q409C&C505T and Q409C&C481A respectively.
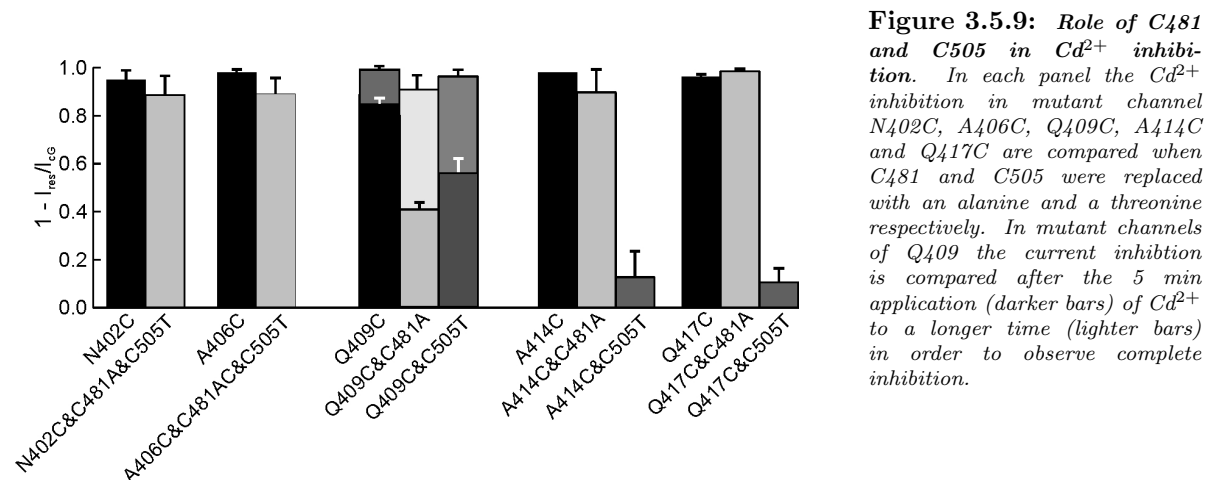
Figure 3.5.9: *Role of C481 and C505 in Cd^{2+} inhibition. In each panel the Cd^{2+} inhibition in mutant channel N402C, A406C, Q409C, A414C and Q417C are compared when C481 and C505 were replaced with an alanine and a threonine respectively. In mutant channels of Q409 the current inhibtion is compared after the 5 min application (darker bars) of Cd^{2+} to a longer time (lighter bars) in order to observe complete inhibition.*

As shown in Fig.3.5.9.D and E, Cd^{2+} inhibition in mutant channels A414C and Q417C was eliminated in the double mutants A414C&C505T and Q417C&C505T but not in the double mutants A414C&C481A and Q417C&C481A.

These results indicate that Cd^{2+} inhibition in the closed state observed in mutant channels N402C and A406C is only weakly dependent on the presence of endogenous cysteines in position 481 and 505.

In contrast in mutant channel Q409C Cd^{2+} inhibition is highly dependent on native cysteines C481 and C505. In both mutant channels A414C and Q417C Cd^{2+} inhibition was insensitive to the presence of a cysteine in position 481, but was significantly reduced when native C505 was replaced with a threonine.

Discussion:

Our results provide new experimental information on the 3D structure of the S6 domain and pave the way to the understanding of molecular mechanisms underlying gating in CNGA1 channels. Let us now discuss in more detail the experimental results and their implications for channel gating.

CSM in the CNGA1 and in the CNGA1$_{cys-free}$

The interpretation of CSM experiments using thiol reagents with a CNGA1$_{cys-free}$ channel is certainly much simpler than when cysteines are introduced in the CNGA1 channel, where 7 native cysteines are present in each subunit. CNGA1 and CNGA1$_{cys-free}$ channels have same ionic selectivity, same I/V relations and are similarly inhibited by a variety of compounds, from divalent cations to tetracaine. However some quantitative differences have been found (Mazzolini et al 2007): the dose response to cGMP is shifted towards lower cGMP concentration in the CNGA1$_{cys-free}$ channel by about 10 times (Matulef et al., 1999), Cd^{2+} inhibition at positive potential is stronger in the CNGA1 channel and inhibition by TEA at negative voltages is higher in the CNGA1cy-free channel. In the closed state homologous residues at position 406 of the CNGA1$_{cys-free}$ channels are 3∼4 Å more distant than in the CNGA1 channel (Mazzolini et al 2007). Therefore the 3D structure of the CNGA1$_{cys-free}$ channels is similar but not identical to that of the CNGA1 channel. For these reasons we have performed a CSM in the CNGA1 background and not in the CNGA1$_{cys-free}$ background. When thiol reagents did not produce a significant effect on cysteine mutants, as on many of those from F375C to S399C (see Fig.3.5.4), the outcome of the experiment was clear and no further investigation was necessary. When Cd^{2+} ions caused a permanent modification of a cysteine mutant, it was necessary to determine whether the effect was entirely mediated by binding to exogenous cysteines or was also caused by binding to some nearby endogenous cysteines. In several mutant channels Cd^{2+} blockage, observed in the closed state (see Figs 3.5.5 and 8) was eliminated when endogenous Cys505 and/or Cys481 were substituted with a threonine and an alanine respectively.

Cd^{2+} action

The present investigation of conformational changes in the S6 domain is primarily based on the analysis of the action of 100 μM Cd^{2+} after its removal from the bathing medium. Indeed as shown in Fig.3.5.1 and in agreement with Becchetti & Roncaglia (2000) exposure for 5 minutes or so of 100 μM Cd^{2+} ions produce a negligible irreversible inhibition of the cGMP activated current in the CNGA1 channel. Therefore any irreversible inhibition larger than 30 % - and any irreversible potentiation - can be reliably ascribed to Cd^{2+} binding to exogenous cysteines.

Methane thio sulfonate reagents, such as MTSEA and MTSEThave been often used to probe the accessibility of channel pores (Flynn and Zagotta, 2003; Flynn and Zagotta, 2001; Liu and Siegelbaum, 2000; Becchetti et al., 1999; Krovetz et al., 1997; Benitah et al., 1996; Sun et al., 1996; Kurtz et al., 1995;

Akabas et al., 1992) and the pattern of their inhibition is usually very similar to that observed with Cd^{2+} ions (Becchetti and Roncaglia, 2000). The recently synthesized MTS-X-MTS cross-linkers have a reactive S at both ends and can covalently bind to two cysteines. Indeed Cd^{2+} ions and MTS reagents block the channel pore by obtruding it. Differences of their blocking efficacy have been usually ascribed to their different radius (Karlin and Akabas, 1998): indeed Cd^{2+}, having a smaller radius, can reach the S atoms of slightly buried cysteines. When Cd^{2+} ions and MTS reagents are used to probe conformational changes outside the channel pore, they can provide rather different results as their binding mechanism is different. One Cd^{2+} ion coordinates to several cysteines and therefore can block the channel, not by obtruding its pore, but by locking the channel in the closed state. As MTS reagents bind to cysteines in a one-to-one ratio, their binding to exogenous cysteines may not lead to channel inhibition, as in the case of several mutant channels from N400C to V424C. Therefore Cd^{2+} modification can reveal changes of proximity of exogenous cysteines introduced in the gating machinery. At certain residues the distance between homologous exogenous cysteines in different subunits is too large for Cd^{2+} coordination and the the newly synthetised MTS-X-MTS reagents (Loo and Clarke, 2001) were used. These reagents can cross-link S atoms at a larger distance, since they have a handle of different length separating reactive S atoms. For these reasons the present investigation of conformational changes underlying gating in CNGA1 channels combines the analysis of the effect of Cd^{2+}, MTS-X-MTS and MTS compounds.

Comparison of Cd^{2+} action on cysteine mutants and Ni^{2+} on histidine mutants

Micromolar amounts of Ni^{2+} potentiate the CNGA1 channel in the open state (Gordon and Zagotta, 1995c) but not in mutant channel H420Q. The analysis of subunit interactions suggested that potentiation was mediated by the binding of Ni^{2+} to His420 of neighboring subunits (Gordon and Zagotta, 1995a,b,c) Johnson & Zagotta (2001) mutated one by one all residues from Ala403 to Met419 to a histidine and analyzed the effect of micromolar amounts of intracellular Ni^{2+}. In the presence of a saturating cGMP concentration, 1 μM Ni^{2+} caused a small block of the cGMP activated current in mutant channels Q409H and D413H, a complete inhibition in mutant channel Q417H, and a potentiation in mutant channels K416H and in the CNGA1. The data of Fig.3.5.8 show that in the presence of 1 mM cGMP, Cd^{2+} ions inhibited to some extent in the open state mutant channel D413C and Y418C but not Q409C. Therefore, with the exception of residue at position 409, the effect by Cd^{2+} on cysteine mutants is rather similar to the effect by Ni^{2+} on histidine mutants.

State dependent Cd^{2+} and MTS-MTS inhibition

The present investigation has identified several mutant channels exhibiting a state dependent inhibition by Cd^{2+} and by the longer cross-linker reagent M-4-M. Cd^{2+} inhibition in mutant channel V491C was more powerful in the open (a $K_{1/2}$ of about 32 nM) than in the closed state ($K_{1/2}$ of about 600 nM) (see Fig.3.5.3). In agreement with previous investigations we conclude that that homologous residues in position 391 in different subunits slightly move apart in the open state. We could not determine the state dependent Cd^{2+} inhibition of mutant channels G395C and S399C. We could measure in mutant channel G395C only single channel openings, even in the presence of saturating cGMP concentrations, larger than 5 mM. The estimated open single channel probability was less than 0.1 and therefore channels of mutant G395C were most of the time in the closed state either in the presence or absence of 5mM cGMP and therefore the state dependent inhibition of Cd^{2+} ions could not be measured.

In mutant channels S399C often the cGMP activated current had a spontaneous run down and therefore we could determine reliably whether the current decline observed upon the addition of Cd^{2+} ions to the bathing medium occurred spontaneously or it was caused by the thiol reagent.

Mutant channels A406C and Q409C are irreversibly inhibited by Cd^{2+} in the closed but not in the open state. When cysteines are introduced in position 406 and 409 in the $CNGA1_{cys-free}$ background no Cd^{2+} inhibition was observed, but M-4-M (see Fig.3.5.6) irreversibly inhibited both mutant channels $A406C_{cys-free}$ and $Q409C_{cys-free}$ in the closed but not in the open state. Taken together these results indicate that homologous residues in position 406 and 409 in different subunits move apart in the open state and are closer in the closed state.

Mutant channels D413C and Y418C were inhibited by Cd^{2+} ions in the open state but not in the closed state (Fig.3.5.8). A similar result was observed for mutant channels also for $D413C_{cys-free}$ and $Y418C_{cys-free}$. Therefore in agreement with Hua & Gordon (2005) we conclude that homologous residues at different subunits in position 413 and 418 move closer in the open state.

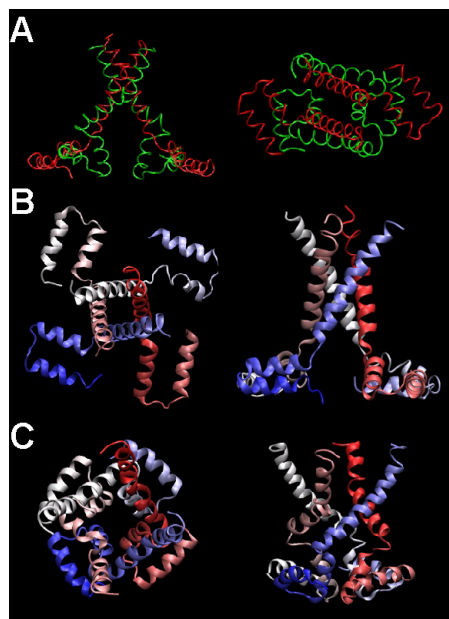**The structure of the S6 domain and initial portion of the C-linker in the closed and open state**

Figure 3.5.10: *Possible 3D arrangement of the residues in the C-linker. A: The residues Asn400 to Gln 409 are near in the closed state (red) than in the open (green) and residues from Asp413 to Tyr418 are near in the open state. B: Shows the top and side view of the C-linker in the closed state. C: The top and side view in the open state.*

On the basis of the results presented in the present manuscript, we propose that residues from Phe375 to Ser399 have an alpha helix conformation with a spatial arrangement referred as an inverted tee-pee (Doyle et al 1998) as expected from the homology with all other ionic channels whose 3D structure has been solved. The relative distance between homologous residues in position 391 does not change significantly in the open and closed state, as Cd^{2+} ions can inhibit mutant channels V391C both in the open and closed state (see Fig.3.5.3), although with a larger affinity in the open state. The apparent higher Cd^{2+} affinity in the open state can be a consequence of a rotation of the S6 helices occurring during channel gating (Nair et al 2006) or by other molecular rearrangements occurring during gating around residues in position 391.

As mutant channels A406C and Q409C are irreversibly inhibited by Cd^{2+} in the closed but not in the open state and mutant channels A406C$_{cys-free}$ and Q409C$_{cys-free}$ are inhibited by M-4-M with the same state dependency, residues from positions 406 and 409 in different subunits are near each other in the closed state but move apart in the open state. A different behaviour was observed for mutant channels D413C and Y418C and for mutant channels D413C $_{cys-free}$ and Y418C $_{cys-free}$ which are inhibited by Cd^{2+} ions in the open but not in the closed state, in agreement with Hua & Gordon (2005).

These experimental observations can be rationalized assuming that residues from Asn400 to His420 have an alpha helix conformation but with a kink between Gln409 and Asp413 so that residues from Asn400 to Gln409 are near in the closed state (see red in Fig.3.5.10.A) and residues from Asp413 to Tyr418 are near in the open state (see green in Fig.3.5.10.A). Fig.3.5.10.B and C illustrate possible 3D arrangements of residues in the closed and open state in the region connecting the S6 helices to the upper portion of the C-linker. These conclusions are in agreement with the model proposed by Giorgetti et al 2005 for residues from Phe375 to approximately Gln409 and with the model proposed by Hua & Gordon (2005) for residues from Gln409 to His420.

Acknowledgment

References

Akabas,M.H., D.A.Stauffer, M.Xu, and A.Karlin. 1992. Acetylcoline receptor channel structure probed in cysteine-substitution mutants. *Science* **258**:307-310.

Anselmi,C., P.Carloni, and V.Torre. 2007. Origin of functional diversity among tetrameric voltage-gated channels. *Proteins* **66**:136-146.

Becchetti,A., K.Gamel, and V.Torre. 1999. Cyclic Nucleotide-gated Channels Pore topology studied through the Accessibility of Reporter Cysteins. *J Gen Physiol* **114**:377-392.

Becchetti,A. and P.Roncaglia. 2000. Cyclic nucleotide-gated channels: intra- and extracellular accessibility to Cd^{2+} of substituted cysteine residues within the P-loop. *Pflugers Arch***440**:556-565.

Benitah,J.P., G.F.Tomaselli, and E.Marban. 1996. Adiacent pore-lining residues within sodium channels identified by paired cysteine mutagenesis. *Proc Natl Acad Sci USA* **93**:7373-7396.

Berman,H.M., J.Westbrook, Z.Feng, G.Gilliland, T.N.Bhat, H.Weissig, I.N.Shindyalov, and P.E.Bourne. 2000. The Protein Data Bank. *Nucleic Acids Res* **28**:235-242.

Biel,M., X.Zong, F.A.Ludwing, A.Sautter, and F.Hofmann. 1999. Structure and function of cyclic nucleotide-gated channels. *Rev Physiol Biochem Pharmacol* **135**:151-171.

Bradley,J., S.Frings, K.W.Yau, and R.Reed. 2001. Nomenclature for ion channel subunits. *Science* **294**:2095-2096.

Brown,R.L., S.D.Snow, and T.L.Haley. 1998. Movement of gating machinery during activation of rod cyclic nucleotide-gated channels. *Biophys J* **75**:825-833.

Chen,T.Y., M.Illing, L.L.Molday, Y.T.Hsu, K.W.Yau, and R.S.Molday. 1994. Subunit 2 (or beta) of retinal rod cGMP-gated cation channel is a component of the 240-kDa channel-associated protein and mediates Ca(2+)-calmodulin modulation. *Proc Natl Acad Sci USA* **91**:11757-11761.

Craven,K.B. and W.N.Zagotta. 2006. CNG and HCN channels: two peas, one pod. *Annu Rev Physiol* **68**:375-401.

Doyle,D.A., J.M.Cabral, R.A.Pfuetzner, A.Kuo, J.M.Gulbis, S.L.Cohen, B.T.Chait, and R.MacKinnon. 1998. The structure of the potassium channel: Molecular basis of K^+ conduction and selectivity. *Science* **280**:69-77.

Ermler,U., W.Grabarse, S.Shima, M.Goubeaud, and R.Thauer. 1998. Active sites of transition metals enzymes with a focus on nickel. *Curr Op Struct Biol* **8**:749-758.

Fesenko,E.E., S.S.Kolesnikov, and A.L.Lyubarsky. 1985. Induction by cyclic GMP of cationic conductance in plasma membrane of retinal rod outer segment. *Nature* **313**:310-313.

Flynn,G.E. and W.N.Zagotta. 2001. Conformational changes in S6 Coupled to the opening of Cyclic neuclotide - gated channels. *Neuron* **30**:689-698.

Flynn,G.E. and W.N.Zagotta. 2003. A Cysteine scan of the inner Vestibule of Cyclic Nucleotide gated channels Reveals Architecture and Rearrangement of the Pore. *J Gen Physiol* **121**:563-582.

Giorgetti,A., A.V.Nair, P.Codega, V.Torre, and P.Carloni. 2005. Structural basis of gating of CNG channels. *FEBS Lett* **579**:1968-1972.

Gordon,S.E. and W.N.Zagotta. 1995a. A histidine residue associated with the gate of the cyclic nucleotide-activated channels in rod photoreceptors. *Neuron* **14**:177-183.

Gordon,S.E. and W.N.Zagotta. 1995b. Localization of regions affecting an allosteric transition in cyclic nucleotide-activated channels. *Neuron* **14**:857-864.

Gordon,S.E. and W.N.Zagotta. 1995c. Subunit interactions in coordination of Ni^{2+} in cyclic nucleotide-gated channels. *Proc Natl Acad Sci U S A* **92**:10222-10226.

Hofmann,F., M.Biel, and U.B.Kaupp. 2005. International Union of Pharmacology. LI. Nomenclature and structure-function relationships of cyclic nucleotide-regulated channels. *Pharmacol Rev* **57**:455-462.

Holmgren,M., K.S.Shin, and G.Yellen. 1998. The activation gate of a voltage-gated K^+ channel can be trapped in the open state by an intersubunit metal bridge. *Neuron* **21**:617-621.

Hua,L. and S.E.Gordon. 2005. Functional interactions between A' helices in the C-linker of open CNG channels. *J Gen Physiol* **125**:335-344.

Jiang,Y., A.Lee, J.Chen, M.Cadene, B.T.Chait, and R.MacKinnon. 2002a. Crystal structure and mechanism of calcium gated pottassium channel. *Nature* **417**:515-522.

Jiang,Y., A.Lee, J.Chen, M.Cadene, B.T.Chait, and R.MacKinnon. 2002b. The open pore conformation of pottassium channels. *Nature* **417**:523-526.

Johnson,J.P. and W.N.Zagotta. 2001. Rotational movement during cyclic nucleotide-gated channel opening. *Nature* **412**:917-921.

Karlin,A. and M.H.Akabas. 1998. Substituted-cysteine accessibility method. *Methods Enzymol* **293**:123-145.

Kaupp,U.B., T.Niidome, T.Tanabe, S.Terada, W.Bonigk, W.Stuhmer, N.J.Cook, K.Kangawa, H.Matsuo, T.Hirose, T.Miyata, and S.Numa. 1989. Primary structure and functional expression from complementary DNA of the rod photoreceptor cyclic GMP-gated channel. *Nature* **342**:762-766.

Kaupp,U.B. and R.Seifert. 2002. Cyclic nucleotide gated channels. *Physiol Rev* **82**:769-824.

Korschen,H.G., M.Illing, R.Seifert, F.Sesti, A.Willams, S.Gotzes, C.Colville, F.Mller, A.Dos, and M.Godde. 1995. A 240 kDa protein represents the complete beta subunit of the cyclic nucleotide-gated channel from rod photoreceptor. *Neuron* **15**:627-636.

Krovetz,H., H.VanDongen, and A.VanDongen. 1997. Atomic distances estimates from disulfides and high-affinity metal-binding sites in a K^+ channel. *Biophys J* **72**:117-126.

Kuo,A., J.M.Gulbis, J.Antcliff, T.Rahman, E.Lowe, J.Zimmer, J.Cuthbertson, F.M.Ashcroft, T.Ezaki, and D.A.Doyle. 2003. Crystal structure of the potassium Channel KirBac1.1 in the closed state. *Science* **3000**:1922-1926.

Kurtz,L.L., H.Zuhlke, J.Zhang, and R.Joho. 1995. Side-chain accessibilities in the pore of a K^+ channel probed by sulfhydryl-specific reagents after cysteine-scanning mutagenesis. *Biophys J* **68**:900-905.

Liu,J. and S.A.Siegelbaum. 2000. Change of pore helix conformational state upon opening of cyclic nucleotide gated channels. *Neuron* **28**:899-909.

Long,S.B., E.B.Campbell, and R.MacKinnon. 2005. Crystal structure of a mammalian voltage-dependent Shaker family K^+ channel. *Science* **309**:897-903.

Loo,T.W. and D.M.Clarke. 2001. Determining the dimensions of the drug-binding domain of human P-glycoprotein using thiol cross-linking compounds as molecular rulers. *J Biol Chem* **276**:36877-36880.

Loussouarn,G., E.N.Makhina, T.Rose, and C.G.Nichols. 2000. Structure and dynamic of the pore of inwardly rectifying KATP channels. *J Biol Chem***275**:1137-1144.

Maroney,M.J. 1999. Structure/function relationships in nickel metallobiochemistry. *Curr Opin Chem Biol* **3**:188-199.

Matulef,K., G.E.Flynn, and W.N.Zagotta. 1999. Molecular rearrangements in the ligand-binding domain of cyclic nucleotide-gated channels. *Neuron* **24**:443-452.

Mazzolini,M., M.Punta, and V.Torre. 2002. Movement of the C-helix during the gating of cyclic nucleotide gated channels. *Biophys J* **83**:3283-3295.

Nair,A.V., M.Mazzolini, P.Codega, A.Giorgetti, and V.Torre. 2006. Locking CNGA1 channels in the open and closed state. *Biophys J* **90**:3599-3607.

Nakamura,T. and G.H.Gold. 1987. A cyclic nucleotide-gated conductance in olfactory receptor cilia. *Nature* **325**:442-444.

Nizzari,M., F.Sesti, M.T.Giraudo, C.Virginio, A.Cattaneo, and V.Torre. 1993. Single-channel properties of cloned cGMP-activated channels from retinal rods. *Proc R Soc Lond* **254**:69-74.

Ren,X., D.A.Nicoll, and K.D.Philipson. 2006. Helix packing of the cardiac Na^+-Ca^{2+} exchanger: proximity of transmembrane segments 1, 2, and 6. *J Biol Chem* **281**:22808-22814.

Root,M.J. and R.MacKinnon. 1993. Identification of an external divalent binding site in the pore of a cGMP-activated channel. *Neuron* **11**:459-466.

Rothberg,B., K.Shin, P.Phale, and G.Yellen. 2002. Voltage-controlled gating at the intracellular entrance to a hyperpolarization-activated cation channel. *J Gen Physiol* **119**:83-91.

Rothberg,B., K.Shin, and G.Yellen. 2003. Movements near the gate of a hyperpolarization-activated cation channel. *J Gen Physiol* **122**:501-510.

Sesti,F., E.Eismann, U.B.Kaupp, M.Nizzari, and V.Torre. 1995. The multi-ion nature of the cGMP-gated channel from vertebrate rods. *J Physiol* **487** (Pt 1):17-36.

Shammat,I.M. and S.E.Gordon. 1999. Stoichiometry and Arrangement of Subunits in Rod Cyclic Nucleotide-Gated Channels. *Neuron* **23**:809-819.

Sun,Z.P., M.H.Akabas, E.H.Goulding, A.Karlin, and S.A.Siegelbaum. 1996. Exposure of residues in the cyclic nucleotide-gated channel pore: P region structure and function in gating. *Neuron* **16**:141-149.

Zagotta,W.N., N.B.Olivier, K.D.Black, E.C.Young, R.Olson, and E.Gouaux. 2003. Structural basis for modulation and agonist specificity of HCN pacemaker channels. *Nature* **425**:200-205.

Zagotta,W.N. and S.A.Siegelbaum. 1996. Structure and function of cyclic nucleotide-gated channels. *Annu Rev Neurosci* **19**:235-263.

Zheng,J., M.C.Trudeau, and W.N.Zagotta. 2002. Rod cyclic nucleotide gated channels have a stoichiometry of three CNGA1 subunits and one CNGB1 subunit. *Neuron* **36**:891-896.

Zhong,H., L.L.Molday, R.S.Molday, and K.W.Yau. 2002. The heteromeric cyclic nucleotide-gated channel adopts a 3A:1B stoichiometry. *Nature* **420**:193-198.

Zhou,Y., J.H.Morais-Cabral, A.Kaufman, and R.MacKinnon. 2001. Chemistry of ion coordination and hydration revealed by a K^+ channel-Fab complex at 2.0 Å resolution . *Nature* **414**:43-48.

Zimmerman,A.L., G.Yamanaka, F.Eckstein, D.A.Baylor, and L.Stryer. 1985. Interaction of Hydrolysis-resistant Analogs of Cyclic GMP with the Phosphodiesterase and Light - sensitive Channel of Retinal Rod Outer Segments. *Proc Natl Acad Sci USA* **82**:8813-8817.

3.6 Conclusions

The cyclic nucleotide-gated channel is believed to share a similar over all 3-D architecture with voltage gated K^+ channels. The KcsA structure has been suggested to be a good template for the over all architecture of CNG in the closed state and MthK in the open state. If this is the situation then the residues down stream S6 helix are supposed to undergo a large translation in space while passing from closed to open conformation. With the current experimental results I conclude that KcsA is a good model of CNG in the closed state. But the MthK cannot be considered as a good model for the open state, because the relative distance between the homologous residues at position 391 from different subunits does not change considerably the position in space. The residues from N400 to Q409 are near in the closed state and move far in the open state. The residues from D413 to Y418 are near in the open state. The result shows that the residues from N400 to H420 has an alpha helical structure with a kink between Q409 and D413 residue.

The crystal structure of bacterial NaK channel has been solved in 2006. The sequence of the selectivity filter of this channel resembles that of CNG channels as D66 in NaK is equivalent to E363 in CNG. The NaK channel has a notable structural difference with KcsA, the K^+ channel. Unlike a K^+ channel selectivity filter, which contains four equivalent K^+-binding sites, the selectivity filter of the NaK channel preserves the two cation–binding sites equivalent to sites 3 and 4 of a K^+ channel, whereas the region corresponding to sites 1 and 2 of a K^+ channel becomes a vestibule in which ions can diffuse but not bind specifically. Another notable difference is that, the N-terminal M0 helix which is parallel to the membrane in NaK is absent in KcsA. The four M0 helices form a cuff that encircles the inner helix bundle crossing, and seem to be positioned to affect the opening and closing of the pore. The sequence similarity of the pore region of CNG and NaK makes the latter as a possible best available template at the moment. Several residues which are important for the functioning of HCN channel
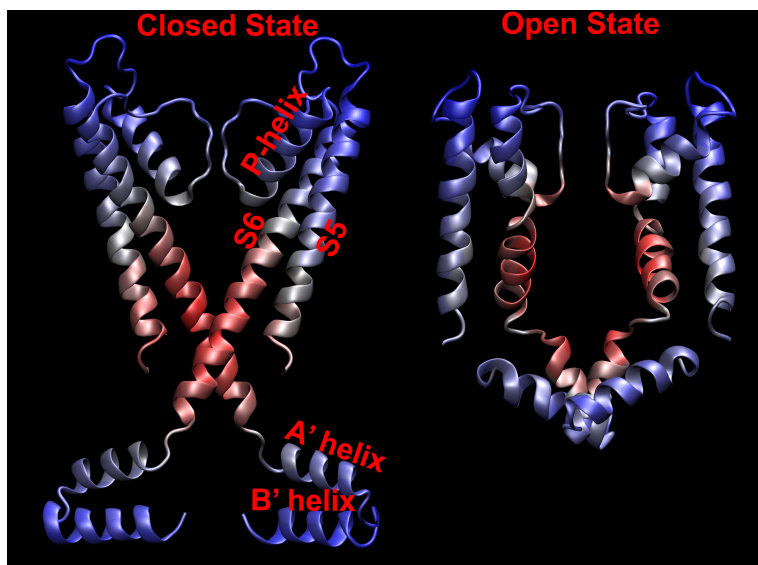
Figure 3.6.1: *Cartoon model of Closed and Open State: The closed model of S5 and S6 was done by using KcsA as a template and the C–linker region by using HCN2. The model of the open state was done by using MthK and HCN2 as a template for the S5 and S6 region and the C-linker region respectively. When the channel opens, the A' and B' helices moves in a plane parallel to the membrane bringing B' from different subunit close to each other. This movement eventually pushes A' almost perpendicular to the membrane. A possible mechanism in which the channel opens could be that, the rotation of S6 about its helical axis moves the P-helix which is coupled to S6. This movement of P-helix flips the pore-filter and the channel opens.*

are conserved also in CNG. The HCN2 and CNGA1 channels share a sequence identity of 35 % in the CNB domain and C-linker region and could be expected to have the same 3D architecture. The HCN2 CNBD crystal structure has been solved. Nevertheless the homology model of CNG using HCN as a

template fails to explain the proximity between several residues, as shown in the fourth section of the results. A rotation of the homology model with HCN of the CNBD around D502 residue could satisfy the experimental results obtained.

During the extensive cysteine scanning an interesting observation was the mutation F380C. In the closed state F380C was able to form a disulfide bond with endogenous C314 and this locked the channel in the closed conformation. F380C was also able to form a disulfide bond in the open state with C314 and locking the channel in the open state. These results are concurrent with an anticlockwise rotation of the S6 - helix about its helical axis, when viewed from the extracellular side. This anticlockwise rotation, by a suitable coupling between the P-helix and S6 causes a small displacement of residues that are forming the narrowest portion of the pore, leading to channel opening. This conclusion is highly coherent with the idea that the gate of CNG channel is situated in the pore itself (Becchetti et al., 1999; Sesti et al., 1995; Bucossi et al., 1996; Fodor et al., 1997b).

The CNGA1 subunit has 7 endogenous cysteines. While doing SCAM analysis it is highly probable that the exogenously introduced cysteines interact with the endogenous ones and bias the conclusion. A cys-free version of CNGA1 channel is extensively used to avoid this non-specific interaction. I have extensively compared the physiological properties of this cys-free version of CNGA1 and the homologous CNGA1 channel. This study shows that though cysteine free proteins can be a very helpful tool in investigating and understanding the structure but it cannot be considered to have the same 3D structure of the CNGA1 channel.

Bibliography

Accardi, A. and Miller, C. Secondary active transport mediated by a prokaryotic homologue of ClC Cl$^-$ channels. *Nature*, 427:803–807, *2004.*

Ahern, C.A. and Horn, R. Stirring up controversy with a voltage sensor paddle. *Trends Neurosci*, 27: 303–307, *2004.*

Akabas, M.H.; Stauffer, D.A.; Xu, M. and Karlin, A. Acetylcoline receptor channel structure probed in cysteine–substitution mutants. *Science*, 258:307–310, *1992.*

Altenhofen, W.; Ludwig, J.; Eismann, E.; Kraus, W.; Bonigk, W. and Kaupp, U.B. Control of ligand specificity in cyclic nucleotide–gated channels from rod photoreceptors and olfactory epithelium. *Proc Natl Acad Sci. U. S. A*, 88:9868–9872, *1991.*

Armstrong, C.M. Interaction of tetraethylammonium ion derivatives with the potassium channels of giant axons. *J. Gen. Physiol*, 58:413–437, *1971.*

Armstrong, C.M. Sodium channels and gating currents. *Physiol Rev*, 61:644–683, *1981.*

Armstrong, C.M. Life among the axons. *Annu Rev Physiol*, 69:1–18, *2007.*

Armstrong, C.M. and Binstock, L. Anomalous rectification in the squid giant axon injected with tetraethylammonium chloride. *J. Gen. Physiol*, 48:859–872, *1965.*

Armstrong, C.M. and Hille, B. Voltage–gated ion channels and electrical excitability. *Neuron*, 20: 371–380, *1998.*

Arshavsky, V.Y.; Lamb, T.D. and Jr, N.E.Pugh. G Proteins and Phototransduction. *Ann. Rev. Physiol*, 64:153–187, *2002.*

Becchetti, A.; Gamel, K. and Torre, V. Cyclic Nucleotide–gated Channels Pore topology studied through the Accessibility of Reporter Cysteins. *J. Gen. Physiol*, 114:377–392, *1999.*

Benndorf, K.; Koopmann, R. and U. B. Kaupp, E.Eismannamd . Gating by cyclic GMP and voltage in the α subunit of the cyclic GMP-gated channel from rod photoreceptors. *J. Gen. Physiol*, 114: 477–489, *1999.*

Berghard, A.; Buck, L.B. and Liman, R. Evidence for distinct signaling mechanisms in two mammalian olfactory sense organs. *Proc. Natl. Acad. Sci. U S A*, 93:2365–2369, *1996.*

Bezanilla, F. The voltage–sensor structure in a voltage–gated channel. *Trends. Biochem. Sci*, 30: 166–168, *2005*.

Bezanilla, F. and Armstrong, C.M. Negative conductance caused by entry of sodium and cesium ions into the potassium channels of squid axons. *J. Gen. Physiol*, 60(5):588–608, *1972*.

Bezanilla, F. and Armstrong, C.M. Inactivation of the sodium channel. I. Sodium current experiments. *J. Gen. Physiol*, 70:549–566, *1977*.

Biel, M.; Zong, X.; Ludwing, F.A.; Sautter, A. and Hofmann, F. Structure and function of cyclic nucleotide–gated channels. *Rev. Physiol. Biochem. Pharmacol*, 135:151–171, *1999*.

Bonigk, W.; Bradley, J.; Muller, F.; Sesti, F.; Boekhoff, I.; Ronnett, G.V.; Kaupp, U.B. and Frings, S. The native rat olfactory cyclic nucleotide–gated channel is composed of three distinct subunits. *J.Neurosci*, 19:5332–5347, *1999*.

Bonigk, W.; Muller, F.; Middendorff, R.; Weyand, I. and Kaupp, U.B. Two alternatively spliced forms of the cGMP–gated channel alpha–subunit from cone photoreceptor are expressed in the chick pineal organ. *J Neurosci*, 16:7458–7468, *1996*.

Bradley, J.; Frings, S.; Yau, K.W. and Reed, R. Nomenclature for ion channel subunits. *Science*, 294: 2095–2096, *2001*.

Broillet, M.C. A single intracellular cysteine residue is responsible for the activation of the olfactory cyclic nucleotide-gated channel by NO. *J. Biol. Chem*, 275:15135–15141, *2000*.

Broillet, M.C. and Firestein, S. Direct activation of the olfactory cyclic nucleotide–gated channel through modification of sulfhydryl groups by NO compounds. *Neuron*, 16:377–385, *1996*.

Broillet, M.C. and Firestein, S. Beta subunits of the olfactory cyclic nucleotide–gated channel form a nitric oxide activated Ca^{2+} channel. *Neuron*, 18:951–958, *1997*.

Brown, R.L.; Gramling, R.; Bert, R.J. and Karpen, J.W. Cyclic GMP contact points within the 63–kDa subunit and a 240–kDa associated protein of retinal rod cGMP–activated channels. *Biochemistry*, 34: 8365–8370, *1995*.

Brown, R.L.; Haley, T.L. and Snow, S.D. Irreversible activation of cyclic nucleotide–gated ion channels by sulfhydryl–reactive derivatives of cyclic GMP. *Biochemistry*, 39:432–441, *2000*.

Brown, R.L.; Haley, T.L.; West, K.A. and Crabb, J.W. Pseudechetoxin: a peptide blocker of cyclic nucleotide–gated ion channels. *Proc Natl Acad Sci U. S. A*, 96:754–759, *1999*.

Buck, L.B. The molecular architecture of odor and pheromone sensing in mammals. *Cell*, 100:611–618, *2000*.

Bucossi, G.; Eismann, E.; Sesti, F.; Nizzari, M.; Seri, M.; Kaupp, U.B. and Torre, V. Time–dependent current decline in cyclic GMP–gated bovine channels caused by point mutations in the pore region expressed in Xenopus oocytes. *J. Physiol. (Lond.)*, 493:409–418, *1996*.

Bucossi, G.; Nizzari, M. and Torre, V. Single–channel properties of ionic channels gated by cyclic nucleotides. *Biophys. J.*, 72:1165–1181, *1997*.

Capovilla, M.; Caretta, A.; Cervetto, L. and Torre, V. Ionic movements through light-sensitive channels of toad rods. *J Physiol*, 343:295–310, *1983*.

Catterall, W.A. From ionic currents to molecular mechanisms: the structure and function of voltage–gated sodium channels. *Neuron*, 26:13–25, *2000*a.

Catterall, W.A. Structure and regulation of voltage–gated Ca^{2+} channels. *Annu Rev Cell Dev Biol*, 16: 521–555, *2000*b.

Catterall, W.A.; Goldin, A.L. and Waxman, S.G. International Union of Pharmacology. *XLVII*. Nomenclature and structure–function relationships of voltage–gated sodium channels. *Pharmacol Rev*, 57:397–409, *2005*a.

Catterall, W.A.; Perez-Reyes, E.; Snutch, T.P. and Striessnig, J. International Union of Pharmacology. *XLVIII*. Nomenclature and structure–function relationships of voltage–gated calcium channels. *Pharmacol Rev*, 57:411–425, *2005*b.

Chanda, B.; Asamoah, O.K.; Blunck, R.; Roux, B. and Bezanilla, F. Gating charge displacement in voltage–gated ion channels involves limited transmembrane movement. *Nature*, 436:852–856, *2005*.

Chang, Q.; Hoefs, S.; Kemp, A.W.van der ; Topala, C.N.; Bindels, R.J. and Hoenderop, J.G. The beta–glucuronidase klotho hydrolyzes and activates the TRPV5 channel. *Science*, 310:490–493, *2005*.

Chen, T.Y.; Illing, M.; Molday, L.L.; Hsu, Y.T.; Yau, K.W. and Molday, R.S. Subunit 2 (or beta) of retinal rod cGMP–gated cation channel is a component of the 240–kDa channel–associated protein and mediates Ca^{2+}–calmodulin modulation. *Proc. Natl. Acad. Sci. U S A*, 91:11757–11761, *1994*.

Chen, T.Y.; Peng, Y.W.; Dhallan, R.S.; Ahamed, B.; Reed, R.R. and Yau, K.W. A new subunit of the cyclic nucleotide–gated cation channel in retinal rods. *Nature*, 362:764–767, *1993*.

Chen, T.Y. and Yau, K.W. Direct modulation by Ca^{2+}–calmodulin of cyclic nucleotide-activated channel of rat olfactory receptor neurons. *Nature*, 368:545–548, *1994*.

Chyb, S.; Hevers, W.; Forte, M.; Wolfgang, W.J.; Selinger, Z. and Hardie, R.C. Modulation of the light response by cAMP in Drosophila photoreceptors. *J Neurosci*, 19:8799–8807, *1999*.

Clapham, D.E.; Julius, D.; Montell, C. and Schultz, G. International Union of Pharmacology. *XLIX*. Nomenclature and structure–function relationships of transient receptor potential channels. *Pharmacol Rev*, 57:427–450, *2005*.

Colamartino, G.; Menini, A. and Torre, V. Blockage and permeation of divalent cations through the cyclic GMP–activated channel from tiger salamander retinal rods. *J. Physiol*, 440:189–206, *1991*.

Contreras, J.E. and Holmgren, M. Access of quaternary ammonium blockers to the internal pore of cyclic nucleotide–gated channels: implications for the location of the gate. *J. Gen. Physiol*, 127: 481–494, *2006*.

Crary, J.I.; Dean, D.M.; Nguitragool, W.; Kurshan, P.T. and Zimmerman, A.L. Mechanism of inhibition of cyclic nucleotide–gated ion channels by diacylglycerol. *J. Gen.. Physiol*, 116:755–768, *2000*.

Craven, K.B. and Zagotta, W.N. Salt bridges and gating in the COOH–terminal region of HCN2 and CNGA1 channels. *J. Gen. Physiol*, 124:663–677, *2004*.

Craven, K.B. and Zagotta, W.N. CNG and HCN channels: two peas, one pod. *Annu. Rev. Physiol*, 68: 375–401, *2006*.

Cudeiro, J. and Rivadulla, C. Sight and insight–on the physiological role of nitric oxide in the visual system. *Trends. Neurosci*, 22(3):109–116, *1999*.

Cuello, L.G.; Cortes, D.M. and Perozo, E. Molecular architecture of the K_vAP voltage–dependent K^+ channel in a lipid bilayer. *Science*, 306:491–495, *2004*.

Dhallan, R.S.; Yau, K.W.; Schrader, K.A. and Reed, R.R. Primary structure and functional expression of a cyclic nucleotide–activated channel from olfactory neurons. *Nature*, 347:184–187, *1990*.

Doyle, D.A.; Cabral, J.M.; Pfuetzner, R.A.; Kuo, A.; Gulbis, J.M.; Cohen, S.L.; Chait, B.T. and MacKinnon, R. The structure of the potassium channel: Molecular basis of K^+ conduction and selectivity. *Science*, 280:69–77, *1998*.

Dutzler, R.; Campbell, E.B.; Cadene, M.; Chait, B.T. and Mackinnon, R. X–ray structure of a ClC chloride channel at 3.0 A reveals the molecular basis of anion selectivity. *Nature*, 415:287–294, *2002*.

Eismann, E.; Muller, F.; Heinemann, S.H. and Kaupp, U.B. A single negative charge within the pore region of a cGMP–gated channel controls rectification, Ca^{2+} blockage, and ionic selectivity. *Proc. Natl. Acad. Sci. U S A*, 91:1109–1113, *1994*.

Fain, G.L.; Matthews, H.R.; Cornwall, M.C. and Koutalos, Y. Adaptation in vertebrate photoreceptors. *Physiol Rev*, 81:117–151, *2001*.

Fesenko, E.E.; Kolesnikov, S.S. and Lyubarsky, A.L. Induction by cyclic GMP of cationic conductance in plasma membrane of retinal rod outer segment. *Nature*, 313:310–313, *1985*.

Finn, J.T.; ; Xiong, W.H.; Solessio, E.C. and Yau, K.W. A cGMP-gated cation channel and phototransduction in depolarizing photoreceptors of the lizard parietal eye. *Vision Res*, 38:13531357, *1998*.

Finn, J.T.; Solessio, E.C. and Yau, K.W. A cGMP-gated cation channel in depolarizing photoreceptors of the lizard parietal eye. *Nature*, 385:815–819, *1997*.

Firestein, S. How the olfactory system makes sense of scents. *Nature*, 413:211–218, *2001*.

Flynn, G.E.; Jr, J.P.Johnson and Zagotta, W.N. Cyclic nucleotide–gated channels: shedding light on the opening of a channel pore. *Nat. Rev. Neurosci*, 2:643–651, *2001*.

Flynn, G.E. and Zagotta, W.N. Conformational changes in S6 Coupled to the opening of Cyclic neuclotide – gated channels. *Neuron*, 30:689–698, *2001*.

Fodor, A.A.; Black, K.D. and Zagotta, W.N. Tetracaine reports a conformational change in the pore of cyclic nucleotide–gated channels. *J. Gen. Physiol*, 110:591–600, *1997*a.

Fodor, A.A.; Gordon, S.E. and Zagotta, W.N. Mechanism of tetracaine block of cyclic nucleotide–gated channels. *J. Gen. Physiol*, 109:3–14, *1997*b.

Frings, S.; Lynch, J.W. and Lindemann, B. Properties of cyclic nucleotide–gated channels mediating olfactory transduction. Activation, selectivity, and blockage. *J. Gen. Physiol*, 100:45–67, *1992*.

Ganetsky, B.; Robertson, G.A.; Wilson, G.F.; Trudeau, M.C. and Titus, S.A. The eag family of K^+ channels in Drosophila and mammals. *Ann. NY. Acad. Sci*, 868:356–369, *1999*.

Gavazzo, P.; Picco, C.; Eismann, E.; Kaupp, U.B. and Menini, A. A point mutation in the pore region alters gating, Ca^{2+} blockage, and permeation of olfactory cyclic nucleotide-gated channels. *J. Gen. Physiol*, 116:311–325, *2000*.

Gordon, S.E.; Brautigan, D.L. and Zimmerman, A.L. Protein phosphatases modulate the apparent agonist affinity of the light–regulated ion channel in retinal rods. *Neuron*, 14:739–748, *1992*.

Gordon, S.E.; Downing-Park, J.; Tam, B. and Zimmerman, A.L. Diacylglycerol analogs inhibit the rod cGMP–gated channel by a phosphorylation–independent mechanism. *Biophys. J*, 69(2):409–417, *1995*.

Gordon, S.E.; Oakley, J.C.; Varnum, M.D. and Zagotta, W.N. Altered ligand specificity by protonation in the ligand binding domain of cyclic nucleotide–gated channels. *Biochemistry*, 35:3994–4001, *1996*.

Gordon, S.E.; Varnum, M.D. and Zagotta, W.N. Direct interaction between amino– and carboxyl– terminal domains of cyclic nucleotide–gated channels. *Neuron*, 19:431–441, *1997*.

Gordon, S.E. and Zagotta, W.N. A histidine residue associated with the gate of the cyclic nucleotide– activated channels in rod photoreceptors. *Neuron*, 14:177–183, *1995*a.

Gordon, S.E. and Zagotta, W.N. Localization of regions affecting an allosteric transition in cyclic nucleotide–activated channels. *Neuron*, 14:857–864, *1995*b.

Gordon, S.E. and Zagotta, W.N. Subunit interactions in coordination of Ni^{2+} in cyclic nucleotide–gated channels. *Proc Natl Acad Sci U S A*, 92:10222–10226, *1995*c.

Goulding, E.H.; Ngai, J.; Kramer, R.H.; Colicos, S.; Axel, R.; Siegelbaum, S.A. and Chess, A. Molecular cloning and single–channel properties of the cyclic nucleotide–gated channel from catfish olfactory neurons. *Neuron*, 8:45–58, *1992*.

Goulding, E.H.; Tibbs, G.R.; Liu, D. and Siegelbaum, S.A. Role of H5 domain in determining pore diameter and ion permeation through cyclic nucleotide–gated channels. *Nature*, 364:61–64, *1993*.

Hamill, O.P.; Marty, A.; Neher, E.; Sakmann, B. and Sigworth, F.J. Improved patch–clamp techniques for high–resolution current recording from cells and cell–free membrane patches. *Pflugers Arch*, 391: 85–100, *1981*.

Hanke, W.; Cook, N.J. and Kaupp, U.B. cGMP-dependent channel protein from photoreceptor membranes: single–channel activity of the purified and reconstituted protein. *Proc. Natl. Acad. Sci. U S A*, 391:94–98, *1988*.

Haynes, L.W. Block of the cyclic GMP–gated channel of vertebrate rod and cone photoreceptors by l–cis–diltiazem. *J. Gen. Physiol*, 100:783–801, *1992*.

Haynes, L.W. and Stotz, S.C. Modulation of rod, but not cone, cGMPgated photoreceptor channels by calcium–calmodulin. *Vis. Neurosci*, 14:233–239, *1997*.

He, F.; Seryshev, A.B.; Cowan, C.W. and Wensel, T.G. Multiple zinc binding sites in retinal rod cGMP phosphodiesterase, PDE6alpha beta. *J Biol Chem*, 275:20572–20577, *2000*a.

He, Y.; Ruiz, M.L. and Karpen, J.W. Constraining the subunit order of rod cyclic nucleotide–gated channels reveals a diagonal arrangement of like subunits. *Proc. Natl. Acad. Sci. U S A*, 97:895–900, *2000*b.

Heginbotham, L.; Abramson, T. and MacKinnon, R. A functional connection between the pores of distantly related ion channels as revealed by mutant K^+ channels. *Science*, 258:1152–1155, *1994*.

Heginbotham, L.; Lu, Z.; Abramson, T. and MacKinnon, R. Mutations in the K^+ channel signature sequence. *Biophys. J*, 66:1061–1067, *1992*.

Heinemann, S.H.; Terlau, H.; Stuhmer, W.; Imoto, K. and Numa, S. Calcium channel characteristics conferred on the sodium channel by single mutations. *Nature*, 356:441–443, *1992*.

Higgins, M.K.; Weitz, D.; Warne, T.; Schertler, G.F. and Kaupp, U.B. Molecular architecture of a retinal cGMP–gated channel: the arrangement of the cytoplasmic domains. *EMBO J*, 21:2087–2094, *2002*.

Hill, A.V. The combinations of haemoglobin with oxygen and with carbon monoxide. *I. J. Ph1siol.*, 40: iv–vii, *1910*.

Hille, B. The hydration of sodium ions crossing the nerve membrane. *Proc Natl Acad Sci U S A*, 68: 280–282, *1971*a.

Hille, B. The permeability of the sodium channel to organic cations in myelinated nerve. *J. Gen. Physiol*, 58:599–619, *1971*b.

Hille, B. The receptor for tetrodotoxin and saxitoxin. A structural hypothesis. *Biophys. J*, 15(6): 615–619, *1975*.

Hille, B. *Ion channels of Excitable Membranes*. Sinauer Associates. Inc, Sundarland, Massachusetts, USA, *2001*.

Hodgkin, A.L. The relation between conduction velocity and the electrical resistance outside a nerve fibre. *J Physiol*, 94:560–570, *1939*.

Hodgkin, A.L. and Huxley, A.F. Resting and action potentials in single nerve fibres. *J Physiol*, 104: 176–195, *1945*.

Hodgkin, A.L. and Huxley, A.F. The components of membrane conductance in the giant axon of Loligo. *J Physiol*, 116:473–496, *1952*a.

Hodgkin, A.L. and Huxley, A.F. Currents carried by sodium and potassium ions through the membrane of the giant axon of Loligo. *J Physiol*, 116:449–472, *1952*b.

Hodgkin, A.L. and Huxley, A.F. The dual effect of membrane potential on sodium conductance in the giant axon of Loligo. *J Physiol*, 116:497–506, *1952*c.

Hodgkin, A.L. and Huxley, A.F. A quantitative description of membrane current and its application to conduction and excitation in nerve. *J Physiol*, 117:500–544, *1952*d.

Hodgkin, A.L. and Katz, B. The effect of sodium ions on the electrical activity of the giant axon of the squid. *J Physiol*, 108:37–77, *1949*.

Hoshi, T.; Zagotta, W.N. and Aldrich, R.W. Biophysical and molecular mechanisms of Shaker potassium channel inactivation. *Science*, 250:533–538, *1990*.

Hoshi, T.; Zagotta, W.N. and Aldrich, R.W. Two types of inactivation in Shaker K^+ channels: effects of alterations in the carboxy–terminal region. *Neuron*, 7:547–556, *1991*.

Hsu, Y.T. and Molday, R.S. Modulation of the cGMP–gated channel of rod photoreceptor cells by calmodulin. *Nature*, 361:76–79, *1993*.

Hua, L. and Gordon, S.E. Functional interactions between A′ helices in the C–linker of open CNG channels. *J. Gen. Physiol*, 125:335–344, *2005*.

Ildefonse, M. and Bennett, N. Single–channel study of the cGMP–dependent conductance of retinal rods from incorporation of native vesicles into planar lipid bilayers. *J Membr Biol*, 123:133–147, *1991*.

Islas, L.D. and Zagotta, W.N. Short–range molecular rearrangements in ion channels detected by tryptophan quenching of bimane fluorescence. *J. Gen. Physiol*, 128:337–346, *2006*.

Jan, L.Y. and Jan, Y.N. A superfamily of ion channels. *Nature*, 345:672, *1990*.

Jentsch, T.J.; Steinmeyer, K. and Schwarz, G. Primary structure of Torpedo marmorata chloride channel isolated by expression cloning in Xenopus oocytes. *Nature*, 348:510–514, *1990*.

Jiang, Y.; Lee, A.; Chen, J.; Cadene, M.; Chait, B.T. and MacKinnon, R. Crystal structure and mechanism of calcium gated pottassium channel. *Nature*, 417:515–522, *2002*a.

Jiang, Y.; Lee, A.; Chen, J.; Cadene, M.; Chait, B.T. and MacKinnon, R. The open pore conformation of pottassium channels. *Nature*, 417:523–526, *2002*b.

Jiang, Y.; Ruta, V.; Chen, J.; Lee, A. and Mackinnon, R. The principle of gating charge movement in a voltage–dependent K^+ channel. *Nature*, 423:42–48, *2003*.

Johnson, J.P.Jr. and Zagotta, W.N. Rotational movement during cyclic nucleotide–gated channel opening. *Nature*, 412:917–921, *2001*.

Kaneda, M.; Andrasfalvy, B. and Kaneko, A. Modulation by Zn^{2+} of GABA responses in bipolar cells of the mouse retina. *Vis Neurosci*, 17:273–281, *2000*.

Karpen, J.W.; Brown, R.L.; Stryer, L. and Baylor, D.A. Interactions between divalent cations and the gating machinery of cyclic GMP–activated channels in salamander retinal rods. *J. Gen. Physiol*, 101: 1–25, *1993*.

Kaupp, U.B. Family of cyclic nucleotide gated channels. *Curr. Opin. Neurobiol*, 5:434–442, *1995*.

Kaupp, U.B.; Niidome, T.; Tanabe, T.; Terada, S.; Bonigk, W.; Stuhmer, W.; Cook, N.J.; Kangawa, K.; Matsuo, H.; Hirose, T.; Miyata, T. and Numa, S. Primary structure and functional expression from complementary DNA of the rod photoreceptor cyclic GMP–gated channel. *Nature*, 342:762–766, *1989*.

Kaupp, U.B. and Seifert, R. Cyclic nucleotide gated channels. *Physiol. Rev*, 82:769–824, *2002*.

Keverne, E.B. The Vomeronasal Organ. *science*, 286:716–720, *1999*.

Kleen, S.J. Spontaneous gating of olfactory cyclic–nucleotide–gated channels. *J. Membr. Biol*, 178: 49–54, *2000*.

Koch, K.W. Biochemical mechanism of light adaptation in vertebrate photoreceptors. *Trends Biochem Sci*, 17:307–311, *1992*.

Koch, K.W. and Kaupp, U.B. Cyclic GMP directly regulates a cation conductance in membranes of bovine rods by a cooperative mechanism. *J Biol Chem*, 260:6788–6800, *1985*.

Korschen, H.G.; Illing, M.; Seifert, R.; Sesti, F.; Willams, A.; Gotzes, S.; Colville, C.; Muller, F.; Dose, A. and Godde, M. A 240 kDa protein represents the complete beta subunit of the cyclic nucleotide–gated channel from rod photoreceptor. *Neuron*, 15:627–636, *1995*.

Koshland, D.E.; Nemethy, G. and Filmer, D. Comparosin of the experiemntal binding data and theoretical models in proteins containing subunits. *Biochemistry*, 5:365–385, *1966*.

Koutalos, Y.; Nakatani, K. and Yau, K.W. The cGMP–phosphodiesterase and its contribution to sensitivity regulation in retinal rods. *J. Gen. Physiol*, 106:891–921, *1995*.

Koutalos, Y. and Yau, K.W. Regulation of sensitivity in vertebrate rod photoreceptors by calcium. *Trends Neurosci*, 19:73–81, *1996*.

Kramer, R.H. and Molokanova, E. Modulation of cyclic–nucleotide–gated channels and regulation of vertebrate phototransduction. *J. Exp. Biol*, 204:2921–2931, *2001*.

Kurahashi, T. and Menini, A. Mechanism of odorant adaptation in the olfactory receptor cell. *Nature*, 385:725–729, *1997*.

Laio, A. and Torre, V. Physical Origin of Selectivity in Ionic Channels of Biological Membranes. *Biophys. J*, 76:129–148, *1999*.

Li, J.; Zagotta, W.N. and Lester, H.A. Cyclic nucleotide–gated channels: structural basis of ligand efficacy and allosteric modulation. *Q. Rev. Biophys*, 30:177–193, *1997*.

Liman, E.R. and Buck, L.B. A second subunit of the olfactory cyclic nucleotide–gated channel confers high sensitivity to cAMP. *Neuron*, 13:611–621, *1994*.

Liman, E.R.; Corey, D.P. and Dulac, C. TRP2: a candidate transduction channel for mammalian pheromone sensory signaling. *Proc. Natl. Acad. Sci. U S A*, 96:5791–5796, *1999*.

Liu, D.T.; Tibbs, G.R.; Paoletti, P. and Siegelbaum, S.A. Constraining ligand–binding site stoichiometry suggests that a cyclic nucleotide–gated channel is composed of two functional dimers. *Neuron*, 21: 235–248, *1998*.

Liu, D.T.; Tibbs, G.R. and Siegelbaum, S.A. Subunit stoichiometry of cyclic nucleotide–gated channels and effects of subunit order on channel function. *Neuron*, 16:983–990, *1996*.

Liu, J. and Siegelbaum, S.A. Change of pore helix conformational state upon opening of cyclic nucleotide gated channels. *Neuron*, 28:899–909, *2000*.

Lu, Z. and Ding, L. Blockade of a retinal cGMP–gated channel by polyamines. *J. Gen. Physiol*, 113: 35–43, *1999*.

Ludwig, J.; Margalit, T.; Eismann, E.; Lancet, D. and Kaupp, U.B. Primary structure of cAMP–gated channel from bovine olfactory epithelium. *FEBS Lett*, 270:24–29, *1990*.

Luhring, H.; Hanke, W.; Simmoteit, R. and Kaupp, U.B. Cation selectivity of the cGMP-gated channel of mammalian rod photoreceptors. *Sensory Transduction Life Sciences*, page 169, *1990*.

Mackinnon, R. Structural biology. Voltage sensor meets lipid membrane. *Science*, 306:1304–1305, *2004*.

Matulef, K. and Zagotta, W.N. Cyclic nucleotide–gated ion channels. *Annu. Rev. Cell Dev. Biol*, 19: 23–44, *2003*.

McGeoch, J.E.; McGeoch, M.W. and Guidotti, G. Eye CNG channel is modulated by nicotine. *Biochem Biophys Res Commun*, 214:879–887, *1995*.

McLatchie, L.M. and Matthews, H.R. Voltage–dependent block by L–cis–diltiazem of the cyclic GMP–activated conductance of salamander rods. *Proc Biol Sci*, 247:113–119, *1992*.

Menini, A. Currents carried by monovalent cations through cyclic GMP–activated channels in excised patches from salamander rods. *J. Gen. Physiol*, 424:167–185, *1990*.

Menini, A. Calcium signalling and regulation in olfactory neurons. *Curr Opin Neurobiol*, 9:419–426, *1999*.

Menini, A.; Lagostena, L. and Boccaccio, A. Olfaction: from odorant molecules to the olfactory cortex. *News Physiol Sci*, 19:101–104, *1999*.

Miller, C. An overview of the potassium channel family. *Genome Biol*, 1(4):1, *2000*.

Molday, L.J.; Cook, N.J.; Kaupp, U.B. and Molday, R.S. The cGMP–gated cation channel of bovine rod photoreceptor cells is associated with a 240–kDa protein exhibiting immunochemicalk cross–reactivity with spectrin. *J. Biol. Chem*, 265:18690–18695, *1990*.

Molday, R.S.; Molday, L.L.; Dose, A.; Clark-Lewis, I.; Illing, M.; Cook, N.J.; Eismann, E. and Kaupp, U.B. The cGMP–gated channel of the rod photoreceptor cell characterization and orientation of the amino terminus. *J. Biol. Chem*, 266:21917–21922, *1991*.

Molokanova, E.; Maddox, F.; Luetje, C.W. and Kramer, R.H. Activity–dependent modulation of rod photoreceptor cyclic nucleotide–gated channels mediated by phosphorylation of a specific tyrosine residue. *J Neurosci*, 19:4786–4795, *1999*.

Molokanova, E.; Trivedi, B.; Savchenko, A. and Kramer, R.H. Modulation of rod photoreceptor cyclic nucleotide–gated channels by tyrosine phosphorylation. *J Neurosci*, 17:9068–9076, *1997*.

Monod, J.; Weyman, J. and Changeux, J. On the nature of allosteric transitions: a plausible model. *J. Mol. Biol*, 12:88–118, *1965*.

Nakamura, T. and Gold, G.H. A cyclic nucleotide–gated conductance in olfactory receptor cilia. *Nature*, 325:442–444, *1987*.

Nakatani, K.; Koutalos, Y. and Yau, K.W. Ca^{2+} modulation of the cGMP–gated channel of bullfrog retinal rod photoreceptors. *J Physiol*, 484:69–76, *1995*.

Nakatani, K. and Yau, K.W. Calcium and magnesium fluxes across the plasma membrane of the toad rod outer segment. *J Physiol*, 395:695–729, *1988*.

Nicol, G.D. The calcium channel antagonist, pimozide, blocks the cyclic GMP–activated current in rod photoreceptors. *J Pharmacol Exp Ther*, 265:626–632, *1993*.

Nilius, B. and Droogmans, G. Amazing chloride channels: an overview. *Acta Physiol Scand*, 117: 119–147, *2003*.

Nizzari, M.; Sesti, F.; Giraudo, M.T.; Virginio, C.; Cattaneo, A. and Torre, V. Single–channel properties of cloned cGMP–activated channels from retinal rods. *Proc. R. Soc. Lond*, 254:69–74, *1993*.

Noda, M.; Ikeda, T.; Suzuki, H.; Takeshima, H.; Takahashi, T.; Kuno, M. and Numa, S. Expression of functional sodium channels from cloned cDNA. *Nature*, 322:826–828, *1986*.

Noda, M.; Shimizu, S.; Tanabe, T.; Takai, T.; Kayano, T.; Ikeda, T.; Takahashi, H.; Nakayama, H.; Kanaoka, Y. and Minamino, N. Primary structure of Electrophorus electricus sodium channel deduced from cDNA sequence. *Nature*, 312:121–127, *1984*.

Nunn, B.J. Ionic permeability ratios of the cyclic GMP-activated conductance in the outer segment membrane of salamander rods. *J. Physiol*, 394:17P, *1987*.

Park, C.S. and Mackinnon, R. TDivalent cation selectivity in a cyclic nucleotide-gated ion channel. *Biochemistry*, 34:13328–13333, *1995*.

Picco, C.; Gavazzo, P. and Menini, A. Coexpression of wild-type and mutant olfactory cyclic nucleotide-gated channels: restoration of the native sensitivity to Ca^{2+} and Mg^{2+} blockage. *NeuroReport*, 12: 2363–2367, *2001*.

Picco, C. and Menini, A. The permeability of the cGMP–activated channel to organic cations in retinal rods of the tiger salamander. *J. Physiol*, 460:741–758, *1993*.

Picollo, A. and Pusch, M. Chloride/proton antiporter activity of mammalian CLC proteins ClC–4 and ClC–5. *Nature*, 436:420–423, *2005*.

Picones, A. and Korenbrot, J.I. Permeation and interaction of monovalent cations with the cGMP–gated channel of cone photoreceptors. *J. Gen. Physiol*, 100:647–673, *1992*.

Ramsey, I.S.; Delling, M. and Clapham, D.E. An introduction to TRP channels. *Annu Rev Physiol*, 68: 619–647, *2006*.

Ranganathan, R.; Malicki, D.M. and Zuker, C.S. Signal transduction in Drosophila photoreceptors. *Annu Rev Neurosci*, 18:283–317, *1995*.

Rebrik, T.I. and Korenbrot, J.I. In intact cone photoreceptors, a Ca^{2+}–dependent, diffusible factor modulates the cGMP–gated ion channels differently than in rods. *J. Gen. Physiol*, 112:537–548, *1998*.

Root, M.J. and MacKinnon, R. Identification of an external divalent binding site in the pore of a cGMP–activated channel. *Neuron*, 11:459–466, *1993*.

Root, M.J. and MacKinnon, R. Two identical non interacting sites in an ion channel revealed by proton transfer. *Neuron*, 265:1852–1856, *1994*.

Rosenbaum, T. and Gordon, S.E. Dissecting intersubunit contacts in cyclic nucleotide–gated ion channels. *Neuron*, 33:703–713, *2002*.

Rosenbaum, T.; Islas, L.D.; Carlson, A.E. and Gordon, S.E. Dequalinium: a novel, high–affinity blocker of CNGA1 channels. *J. Gen. Physiol*, 121:37–47, *2003*.

Ruiz, M. and Karpen, J.W. Opening mechanism of a cyclic nucleotide–gated channel based on analysis of single channels locked in each liganded state. *J. Gen. Physiol*, 113:873–895, *1999*.

Ruiz, M.L. and Karpen, J.W. Single cyclic nucleotide–gated channels locked in different ligand–bound states. *Nature*, 389:389–392, *1997*.

Sautter, A.; Zhong, X.; Hofmann, F. and Biel, M. An isoform of the rod photoreceptor cyclic nucleotide–gated channel beta subunit expressed in olfactory neurons. *Proc. Natl. Acad. Sci. U S A*, 95:46964701, *1998*.

Schachtman, D.P. Molecular insights into the structure and function of plant K^+ transport mechanisms. *Biochim. Biophys. Acta*, 1465:127–139, *2000*.

Schild, D. and Restrepo, D. Transduction mechanisms in vertebrate olfactory receptor cells. *Physiol Rev*, 78:429–466, *1998*.

Scott, S.P.; Harrison, R.W.; Weber, I.T. and Tanaka, J.C. Predicted ligand interactions of $3'5'-$ cyclic nucleotide– gated channel binding sites: comparison of retina and olfactory binding site models. *Protein Eng*, 9:333–344, *1996*.

Seifert, R.; Eismann, E.; Ludwig, J.; Baumann, A. and Kaupp, U.B. Molecular determinants of a Ca^{2+}–binding site in the pore of cyclic nucleotide–gated channels: S5/S6 segments control affinity of intrapore glutamates. *EMBO J*, 18:119–130, *1999*.

Sesti, F.; Eismann, E.; Kaupp, U.B.; Nizzari, M. and Torre, V. The multi–ion nature of the cGMP–gated channel from vertebrate rods. *J. Physiol*, 487:17–36, *1995*.

Sesti, F.; Straforini, M.; Lamb, T.D. and Torre, V. Gating, selectivity and blockage of single channels activated by cyclic GMP in retinal rods of the tiger salamander. *J. Physiol*, 474:203–222, *1994*.

Shammat, I.M. and Gordon, S.E. Stoichiometry and Arrangement of Subunits in Rod Cyclic Nucleotide–Gated Channels. *Neuron*, 23:809–819, *1999*.

Shuster, T.A.; Martin, F. and Nagy, A.K. Zinc causes an apparent increase in rhodopsin phosphorylation. *Curr Eye Res*, 15:1019–1024, *1996*.

Sinnarajah, S.; Dessauer, C.W.; Srikumar, D.; Chen, J.; Yuen, J.; Yilma, S.; Dennis, J.C.; Morrison, E.E.; Vodyanoy, V. and Kehrl, J.H. RGS2 regulates signal transduction in olfactory neurons by attenuating activation of adenylyl cyclase III. *Nature*, 409:1051–1055, *2001*.

Sokolova, O.; Kolmakova-Partensky, L. and Grigorieff, N. Three-dimensional structure of a voltage-gated potassium channel at 2.5 nm resolution. *Structure*, 9:215–220, *2001*.

Su, Y.; Dostmann, W.R.; Herberg, F.W.; Durick, K. and Xuong, N.H. Regulatory subunit of protein kinase A: structure of deletion mutant with cAMP binding domains. *Science*, 269:807–813, *1995*.

Sugimoto, Y.; Yatsunami, K.; Tsujimoto, M.; Khorana, H.G. and Ichikawa, A. The amino acid sequence of a glutamic acid-rich protein from bovine retina as deduced from the cDNA sequence. *Proc Natl Acad Sci U. S. A*, 88:3116–3119, *1991*.

Sun, Z.P.; Akabas, M.H.; Goulding, E.H.; Karlin, A. and Siegelbaum, S.A. Exposure of residues in the cyclic nucleotide–gated channel pore: P region structure and function in gating. *Neuron*, 16:141–149, *1996*.

Sunderman, E.R. and Zagotta, W.N. Mechanism of allosteric modulation of rod cyclic nucleotide-gated channels. *J. Gen. Physiol*, 113:601–619, *1999*.

Tanaka, J.C. The effects of protons on $3'$, $5'$ –cGMP–activated currents in photoreceptor patches. *Biophys. J*, 65:2517–2523, *1993*.

Taylor, W.R. and Baylor, D.A. Conductance and kinetics of single cGMP–activated channels in salamander rod outer segments. *J Physiol*, 483:567–582, *1995*.

Tibbs, G.R.; Goulding, E.H. and Siegelbaum, S.A. Allosteric–activation and tuning of ligand efficacy in cyclic–nucleotide–gated channels. *Nature*, 386:612–615, *1997*.

Trivedi, B. and Kramer, R.H. Real–time patch–cram detection of intracellular cGMP reveals long–term suppression of responses to. *Neuron*, 21:895–906, *1998*.

Trudeau, M.C. and Zagotta, W.N. An intersubunit interaction regulates trafficking of rod cyclic nucleotide–gated channels and is disrupted in an inherited form of blindness. *Neuron*, 34:197–207, *2002*a.

Trudeau, M.C. and Zagotta, W.N. Mechanism of calcium/calmodulin inhibition of rod cyclic nucleotide–gated channels. *Proc Natl Acad Sci U. S. A*, 99:8424–8429, *2002*b.

Ugarte, M. and Osborne, N.N. The localization of free zinc varies in rat photoreceptors during light and dark adaptation. *Exp Eye Res*, 69:459–461, *1999*.

Varnum, M.D.; Black, K.D. and Zagotta, W.N. Molecular mechanism for ligand discrimination of cyclic nucleotide–gated channels. *Neuron*, 15:619–625, *1995*.

Varnum, M.D. and Zagotta, W.N. Interdomain interactions underlying activation of cyclic nucleotide–gated channels. *Science*, 278:110–113, *1997*.

Weber, I.T.; Gilliland, G.L.; Harman, J.G. and Peterkofsky, A. Crystal structure of a cyclic AMP-independent mutant of catabolite gene activator protein. *J. Biol. Chem*, 262:5630–5636, *1987*.

Weber, I.T.; Shabb, J.B. and Corbin, J.D. Predicted structures of the cGMP binding domains of the cGMP - dependent protein kinase: a key alanine/threonine difference in evolutionary divergence of cAMP and cGMP. *Biochemistry*, 28:6122–6127, *1989*.

Weiss, J.N. The Hill equation revisited: uses and misuses. *FASEB J*, 11:835–841, *1997*.

Weitz, D.; Ficek, N.; Kremmer, E.; Bauer, P.J. and Kaupp, U.B. Subunit stoichiometry of the CNG channel of rod photoreceptors. *Neuron*, 36:881–889, *2002*.

Weitz, D.; Zoche, M.; Muller, F.; Beyermann, M.; Korschen, H.G.; Kaupp, U.B. and Koch, K.W. Calmodulin controls the rod photoreceptor CNG channel through an unconventional binding site in the N–terminus of the beta–subunit. *EMBO J*, 17:2273–2284, *1998*.

Wes, P.D.; Chevesich, J.; Jeromin, A.; Rosenberg, C.; Stetten, G. and Montell, C. TRPC1, a human homolog of a Drosophila store-operated channel. *Proc Natl Acad Sci U. S. A*, 92:9652–9656, *1995*.

White, M.M. and Miller, C. A voltage-gated anion channel from the electric organ of Torpedo californica. *J Biol Chem*, 254:10161–10166, *1979*.

Wu, S.M.; Qiao, X.; Noebels, J.L. and Yang, X.L. Localization and modulatory actions of zinc in vertebrate retina. *Vision Res*, 33:2611–2616, *1993*.

Yang, J.; Ellinor, P.T.; Sather, W.A.; Zhang, J.F. and Tsien, R.W. Molecular determinants of Ca^{2+} selectivity and ion permeation in L–type Ca^{2+} channels. *Nature*, 366:158–161, *1993*.

Yau, K.W. and Nakatani, K. Cation selectivity of light–sensitive conductance in retinal rods. *Nature*, 309:352–354, *1984*.

Zagotta, W.N.; Hoshi, T. and Aldrich, R.W. Restoration of inactivation in mutants of Shaker potassium channels by a peptide derived from ShB. *Science*, 250:568–571, *1990*.

Zagotta, W.N.; Olivier, N.; Black, K.; Young, E.; Olson, R. and Gouaux, E. Structural basis for modulation and agonist specificity of HCN pacemakers channels. *Nature*, 425:200–205, *2003*.

Zagotta, W.N. and Siegelbaum, S.A. Structure and function of cyclic nucleotide–gated channels. *Annu. Rev. Neurosci*, 19:235–263, *1996*.

Zheng, J.; Trudeau, M.C. and Zagotta, W.N. Rod cyclic nucleotide gated channels have a stoichiometry of three CNGA1 subunits and one CNGB1 subunit. *Neuron*, 36:891–896, *2002*.

Zheng, J. and Zagotta, W.N. Gating rearrangements in cyclic nucleotide–gated channels revealed by patch–clamp fluorometry. *Neuron*, 28:369–374, *2000*.

Zhong, H.; Molday, L.L.; Molday, R.S. and Yau, K.W. The heteromeric cyclic nucleotide–gated channel adopts a 3A:1B stoichiometry. *Nature*, 420:193–198, *2002*.

Zimmerman, A.L. and Baylor, D.A. Cyclic GMP–sensitive conductance of retinal rods consists of aqueous pores. *Nature*, 321:70–72, *1986*.

Zimmerman, A.L. and Baylor, D.A. Cation interactions within the cyclic GMP-activated channel of retinal rods from the tiger salamander. *J. Physiol*, 449:759–783, *1992*.

Zimmerman, A.L.; Yamanaka, G.; Eckstein, F.; Baylor, D.A. and Stryer, L. Interaction of Hydrolysis–resistant Analogs of Cyclic GMP with the Phosphodiesterase and Light – sensitive Channel of Retinal Rod Outer Segments. *Proc. Natl. Acad. Sci. U S A*, 82:8813–8817, *1985*.

Zufall, F. and Firestein, S. Divalent cations block the cyclic nucleotide–gated channel of olfactory receptor neurons. *J Neurophysiol*, 69:1758–1768, *1993*.

Zufall, F.; Firestein, S. and Shepherd, M. Cyclic nucleotide–gated ion channels and sensory transduciton in olfactory receptor neurons. *Ann. Rev. Biophys. Biomol. Struct*, 23:577–607, *1994*.

Zufall, F.; Hatt, H. and Firestein, S. Rapid application and removal of second messengers to cyclic nucleotide-gated channels from olfactory epithellium. *Proc. Natl. Acad. Sci. U S A*, 90:9335–9339, *1993*.

Zufall, F. and Munger, S.D. From odor and pheromone transduction to the organization of the sense of smell. *Trends. Neurosci*, 24:191–193, *2001*.

Acknowledgments

A journey is easier when you travel together. Interdependence is certainly more valuable than independence. This thesis is the result of four years of work whereby I have been accompanied and supported by many people. It is a pleasant aspect that I have now the opportunity to express my gratitude for all of them.

The first person I would like to thank is my supervisor Prof. Vincent Torre, for the most valuable guidance and support. Without his patience, I shouldn't have surpassed some of the crazy moments of my life in Trieste. I would like to thank Monica Mazzolini who taught me the molecular biology part, and in need always helped me with electrophysiology experiments. The one without whose help I shouldn't have understood the basics of electrophysiology is Paolo Codega. All those smoking time, the long discussions where I understood some part of the Italian culture, the language...thank you very much for your valuable friendship. I am thankful to Alejandro Giorgetti who helped me in understanding homology modeling. I would like to thank Claudio Anselmi, who for the past two and half years helped me very much in understanding complex molecular interactions in simple terms. Also I am thankful for his friendship.

Paolino...other than helping me to start with Matlab, who has been a nice listener for three years...near to my seat in Galileo. I still remember his startled face: in that forest house...when some one shouted ... "...ino...that Indian guy jumped out of the balcony..." Lizzy (Elizabeth), who has been a kind friend, good supporter and a nice listener and advisor. Sergio Graziosi...tips in Corel draw...all those drunken Friday evenings...with him, Lizzy...so much of fond memories about Trieste. The walking encyclopedia of Matlab...Waltere...(Walter)...a nice friend...I don't know in the future with whom I will play ping-pong, basket ball, jogging all those treks to Alps...the sleepless night I gave him at croda da lago.. with my drum beat snoring..

Just few words of thanks, cannot end my gratitude...GioPino (Giovanni)...Whenever I was in need of a true friend the one and only one support...who listened and solaced me...the long discussions about photography...life...I have the ever lasting memories about the Christmas time which I spent with your family... that was the time which I could never get back...

Nandini, who like an elder sister gave so much company...which are valid part of my life. My other friends... Sanjeev...all those drunken evenings and the songs of Guide!!, Rajesh, Venkat... Jummi..Sandya, Sripad.. thanks to all of you buddies... specially to those who helped me to realize the weakness in me as a human......

Kamil...with whom I shared the house for three years...all those evenings of listening...All my labmates... Fred, the crazy guy, Alby, the amusement... Jelena, the grappa lady... Elizabeth ... Silvia.. Francesco, Giulietta, Ranken... Daniela (I am sad to say that I am resigning the post as your secretary soon)... Amanda Colombo, the big eyed kind lady..(I am sorry If I did hurt you by making fun sometimes.. not intentional)...Marianna, the lively and funny girl...Matteo, Silvia, Flavia, Roberto, Reza, Libero, Andrea, Simone. The recent addition to Trieste.. Shyju (Mr. Muscolo).. and Shamna.. Jeena madam, Pier davide, Sailesh..so much to carry with me from Trieste. I would like to thank Anna.. who has been a very kind friend.. helped me in need and advised me.....

The one to whom I cannot just say thanks is my Asha.. she is my best asset from trieste.... be with me forever.. Last but not the least.. my parents.. To my mother who is a very good friend of mine...with whom I can talk anything.. My father my brother

Life goes on ... seasons change... life too... but fond memories never...